NTNU

Norwegian University of
Science and Technology

Behaviour of piles in clay subjected to cyclic lateral loading

Andrea Strand Støren

Civil and Environmental Engineering
Submission date: June 2018
Supervisor: Gudmund Reidar Eiksund, IBM
Co-supervisor: Hendrik Sturm, NGI

Norwegian University of Science and Technology
Department of Civil and Environmental Engineering

Preface

This thesis was written during the spring semester of 2018 and is the final part of the master's programme in Civil and Environmental Engineering at the Norwegian University of Science and Technology (NTNU, Trondheim). Hendrik Sturm at the Norwegian Geotechnical Institute (NGI) proposed the topic and the work has been carried out in collaboration with NGI.

Oslo, 2018-06-11

Andrea Støren

Acknowledgment

I would like to thank my supervisor Hendrik Sturm for proposing the topic and for great guidance throughout this semester. I would also like to thank Gudmund Reidar Eiksund and the Geotechnical Division at NTNU.

I am grateful that I got the opportunity to conduct the work of my master thesis at NGI. I would like to thank the staff at the laboratory and the department of Computational Geomechanics for a great work environment and for being so helpful whenever I have needed some assistance in my work. I especially want to acknowledge Tariq Abdu for teaching me how to operate the p-y device and Heidi Debreczeny Wilkinson for her advice concerning MTS.

I would also like to thank my family and my fiancé for being so supportive, motivating me and helping me through stressful periods. Finally, big thanks goes to my friends that I have studied with at NTNU for five great years.

A.S.

Summary and Conclusions

In order to make offshore wind turbines more cost-efficient and competitive in international energy markets, design methods must be improved to reduce uncertainties in load and soil modelling. The current method of modelling the lateral soil response of piles is performed using API p-y curves. This method has some clear limitations and tends to underestimate soil strength and stiffness parameters, resulting in the overly conservative design of offshore wind turbines (NGI, 2016).

NGI and BP America have developed a novel soil testing device that can obtain monotonic and cyclic p-y curves directly from laboratory tests of soil samples. The device, which is denoted p-y apparatus, was originally developed for well conductor fatigue limit state assessment. For that purpose, displacement controlled tests with symmetric cyclic loading were performed. Comparisons with centrifuge tests and field measurements showed reasonably good agreement (Zakeri et al., 2017). The objective of the present study is to investigate the possibility of using the p-y apparatus for serviceability limit state design of offshore wind turbines and other pile-shaped foundations subjected to lateral cyclic loading. A series of load-controlled tests with varying average and cyclic load amplitudes have been conducted. Two different types of clay were tested, reconstituted kaolin clay and intact samples taken at an offshore field in the North Sea. The testing program for each specimen was comprised of a series of non-symmetric cyclic load parcels with varying average and cyclic load amplitudes followed by a monotonic push-over test at the end of each test. In addition, one test was subjected to a random load series for comparison purposes.

In general, the device performs well and is considered to produce plausible results based on the evaluation of the performed tests. The evaluation of the results includes assessment of drainage and comparisons with contour diagrams, direct simple shear test results and centrifuge test results. The observed pile response is generally as expected and can be described with cyclic contour diagrams. An estimate of the soil drainage indicates that the specimens may behave undrained within a cycle, but partially drained over the duration of the test execution. This is supported by the observed response in the test results. In some tests there has been observed a response similar to behaviour typically seen in the case of gapping during testing at larger load amplitudes. Because of the small displacements induced by the applied cyclic loading, this is interpreted as highly disturbed soil in close vicinity to the model pile resulting in behaviour resembling gapping.

In conclusion, the p-y apparatus has shown to produce plausible results when used to perform load controlled tests with non-symmetric cyclic loading and is therefore considered applicable to assess the serviceability of piles subjected to cyclic lateral loading. Not all observations made in the tests can be explained and there still remain some open questions. In order to use the p-y apparatus in actual design projects for assessing the serviceability of laterally loaded piles, it is recommended to perform further tests and as well as complementary finite element analyses using appropriate constitutive soil models. The presented work and the conducted tests may serve as a basis for further investigations.

Contents

List of Figures

List of Tables

Nomenclature

Acronyms

API	American Petroleum Institute
BF	Best Fit
DSS	Direct Simple Shear
FE	Finite Element
FEA	Finite Element Analysis
FLS	Fatique Limit State
I Gain	Integral Gain
LB	Lower Bound
MPT	Multi Purpose Testware
NC	Normally Consolidated
NGI	Norwegian Geotechnical Institute
NTNU	Norwegian University of Science and Technology
OC	Over Consolidated
OCR	Over Consolidation Ratio
OWT	Offshore Wind Turbine
P Gain	Proportional Gain
SLS	Serviceability Limit State
UB	Upper Bound
ULS	Ultimate Limit State

WAS-XL	WAveloads and Soilsupport for eXtra Large monopiles

Greek Letters

α	Roughness factor
γ	Shear strain
γ^e	Elastic component of shear strain
γ^p	Plastic component of shear strain
γ_a	Average component of shear strain
γ_p	Permanent component of shear strain
γ_w	Unit weight of water, taken to be 10 kN/m^3
γ_{cy}	Cyclic component of shear strain
ρ_s	Specific density
σ_c'	Consolidation pressure
σ_{vc}'	Current stress
τ	Shear stress
τ_a	Average component of shear stress
τ_{cy}	Cyclic component of shear stress
ξ_1	Scaling factor
ξ_2	Scaling factor

Lowercase Letters

c_v	Coefficient of consolidation
h	Height of specimen after consolidation
k	Permeability
p	Pressure
p'_c	Preconsolidation pressure
p_a	Average component of pressure
p_u	Ultimate lateral bearing pressure

p_{+3mm}	Lateral resistance
p_{-3mm}	Lateral resistance
p_{cy}	Cyclic component of pressure
s_u	Undrained shear strength of soil
t	Time
t_p	Cycle period
u	Pore pressure
u_{cy}	Cyclic component of pore pressure
u_p	Permanent component of pore pressure
w	Water content
w_l	Liquid limit
w_p	Plastic limit
y	Lateral displacement
y_a	Average component of lateral displacement
y_{cy}	Cyclic component of lateral displacement

Uppercase Letters

D	Diameter of pile element
D_{norm}	Normalized damping
F	Load
G_{max}	Small strain shear modulus
H	Lateral load
I_p	Plasticity index
K_0'	At-rest coefficient
$K_{sec,norm}$	Normalized secant stiffness
$K_{sec,ss,norm}$	Normalized secant stiffness at steady state
K_{sec}	Secant stiffness

M	Oedometer modulus
N	Number of cycles
N_p	Bearing capacity factor
P	Normalized excess pore pressure
T	Normalized time
T_p	Normalized cycle period

Chapter 1

Introduction

1.1 Background and Motivation

The increased knowledge and attention to global warming and environmental problems have led to an extensive focus on alternative sustainable energy sources. Energy production generates around 60% of the total global greenhouse gas emissions (United Nations), and the seventh of UN's sustainable development goals states that everyone should have access to affordable, sustainable and modern energy. Among several targets to reach this goal, increased energy production from renewable sources is emphasized.

Offshore wind has over the past 10 years developed to be a significant renewable energy source. In order to be competitive in international energy markets, installation and foundation costs need to be reduced. This can be accomplished by reducing uncertainties in load and soil modelling and developing more reliable design analyses and testing methods (NGI, 2017).

Figure 1.1 shows typical foundation concepts for offshore wind turbines (OWTs). Monopiles are large diameter cylindrical steel tubes, and are the most used foundation method for offshore wind turbines today. Considering levelized cost of energy, i.e. the lifetime costs relative to the produced energy, monopile foundations seem to be the best alternative for shallow to intermediate water depths (NGI, 2016).

The monopile design methodology is continuously improved with particular focus on stiffness and capacity predictions and it is expected that also foundation serviceability will become more important. Cyclic loading can potentially cause accumulated displacements and

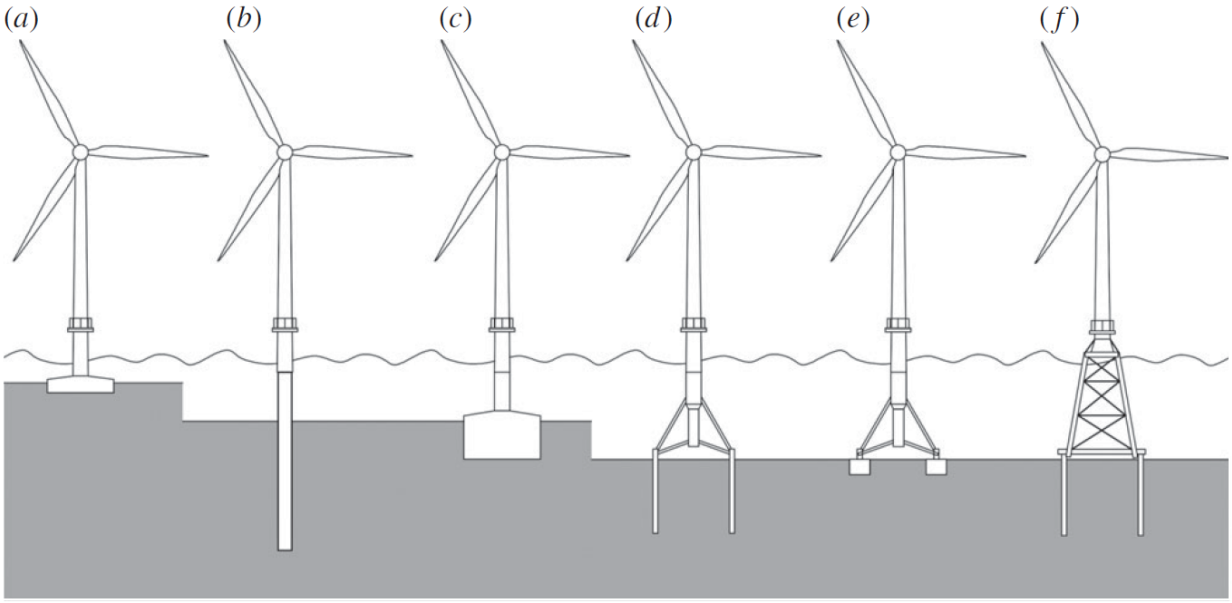

Figure 1.1: Foundation concepts of offshore wind turbines. (a) gravity based foundation, (b) monopile foundation, (c) caisson foundation, (d) multipile foundation, (e) multi caisson foundation and (f) jacket foundation. (Kallehave et al., 2015)

the long-term permanent displacements have to be acceptable. Lateral displacement and accumulated tilt over the lifetime will affect the performance of the offshore wind turbine. This has to be taken into account by the serviceability limit state (SLS) design.

The current design practice of piles, including monopiles, is based on modelling of soil response using p-y springs characterized by lateral load-displacement relationships. Standard p-y curves are developed for ultimate limit state (ULS) design of pile foundations, and the intended loading situation is storm and hurricane loading (Zakeri et al., 2017). This method includes several simplifications and does not consider complex irregular load histories and many of the interaction effects between loads, structure and soil support (NGI, 2017). P-y curves are in particular not suitable for the assessment of foundation stiffness nor SLS design, as this requires a detailed description of the stress-strain response of the soil.

To determine improved p-y relationships for structural fatigue limit state (FLS) design, a new apparatus has been developed. The so-called 'p-y apparatus' is a small scale model test device originally developed to simulate well conductor-soil interaction, aiming to obtain p-y data and hysteretic damping. Corresponding data are retrieved by performing displacement controlled tests with symmetric cyclic loading. Comparisons with centrifuge test results and in-situ measurements confirm the suitability of the p-y apparatus for assessing cyclic p-y backbone curves and corresponding damping values for structural fatigue analysis (Zakeri et al., 2017).

In this study, the goal is to explore the potential of the apparatus further, focusing on SLS assessment of pile foundations for offshore wind turbines. This MSc thesis is a part of an ongoing research project at NGI and Sintef Ocean, WAS-XL (WAve loads and Soil support for eXtra Large monopiles), aiming to improve analyses and testing methods for large diameter monopiles by developing improved modelling and experimental techniques for bottom-mounted offshore wind turbines (NGI, 2018).

1.2 Objectives

In order to investigate the potential to use the device in geotechnical SLS design of OWTs, the main objectives of this study are:

1. Test the p-y apparatus' ability to run load controlled tests and tests with non-symmetric cyclic loading.
2. Evaluate the plausibility of the results.

To achieve this, the main tasks are

1. Prepare clay samples with equal properties using Kaolin.
2. Learn how to operate the device and gain experience by performing displacement controlled tests similar to those performed in Zakeri et al. (2017).
3. Adjust the tuning of the MTS system to load control.
4. Perform load controlled tests with non-symmetric cyclic loading
5. Investigate the possibilities to run tests with irregular load series with the MTS system, and perform a test with an irregular load history.
6. Compare the test results with contour diagrams.
7. Estimate drainage.
8. Compare the test results with DSS and centrifuge test results.
9. Evaluate the plausibility of the results.

1.3 Approach

The work started with learning how to operate the device. To get familiar with the apparatus and gain some experience, four tests were performed and evaluated. During the first weeks kaolin clay was reconstituted and installed for consolidation.

There was performed 12 model tests on the reconstituted kaolin clay using the p-y apparatus. The tests in the lab program were planned consecutively, depending on the results from the performed tests.

The results were evaluated by different approaches, including comparison to laboratory test results, evaluation of drainage and a literature survey in order to explain the findings in the test results.

1.4 Structure of the Report

Chapter 2 gives a brief introduction to cyclic loading, the current design practice and soil behaviour under cyclic loading. Evaluation methods are presented in Chapter 3.

In Chapter 4, there is a description of the p-y apparatus, the material used in the tests, the preparations and preliminary work performed and a description of the test design.

Results are presented in Chapter 5. In Chapter 6 the results are discussed and evaluated using the methods introduced in Chapter 3. Chapter 7 summarizes and concludes the main findings of the thesis and gives recommandations for future work.

Chapter 2

Soil behaviour under cyclic loading

2.1 Cyclic loading

Environmental loads on offshore marine structures are mainly cyclic loading, typically consisting of both a cyclic and an average component. Over an OWT's lifetime, the structure is exposed to cyclic loading of different intensities, frequencies, directions and durations. The primary forces are lateral wind and wave loads, which are best represented by load controlled tests (Andersen, 2015) and often non-symmetric. Therefore, to simulate the actual in-situ loading conditions, the tests in this study are performed load-controlled with cyclic loading including a constant or varying average component.

Different modes of cyclic loading are shown in Figure 2.1. In this thesis, cyclic loading with an average component is denoted non-symmetric. The average component is also referred to as the static component. Non-symmetric loading can be either one-way or two-way, depending on the load's amplitude and average component. Cyclic loading without an average component is denoted symmetric.

2.2 Current design practice

In design, cyclic load events are usually represented as simplified load parcels with equal load levels, also referred to as load steps in this thesis. The load parcels are applied in ascending order, resulting in conservative estimates of soil strength and hence capacity (NGI, 2016). Since the actual in-situ loading conditions are irregular with continuously varying average and cyclic load amplitudes, the loads need to be processed before they can be used

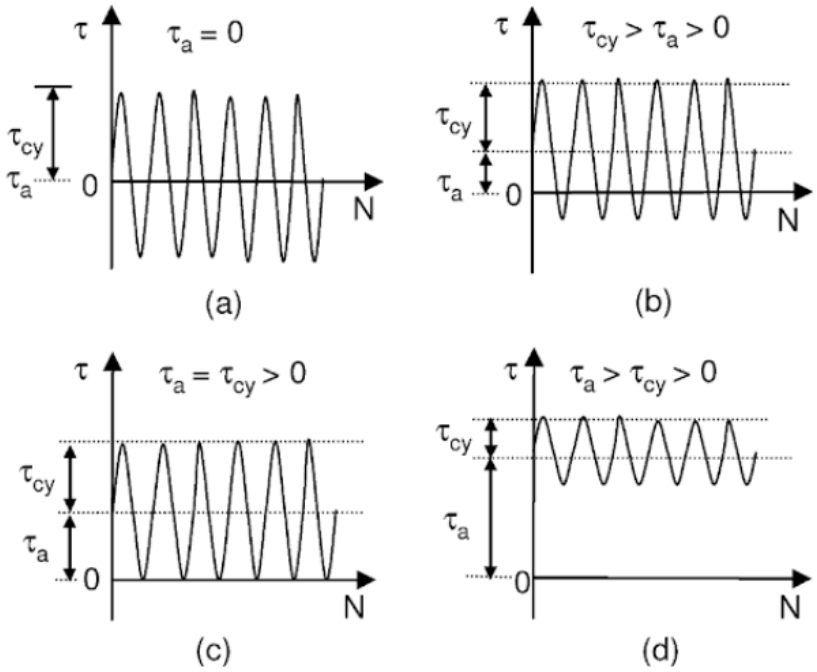

Figure 2.1: Cyclic loading (a) Symmetric, (b) Two-way non-symmetric, (c) and (d) One-way non-symmetric (Randolph and Gourvenec, 2011)

in design. There exists several cycle-counting methods, and the method used in this study is rainflow counting. Rainflow counting method is a cycle-counting method used in fatigue analyses. The method simplifies irregular load histories by counting the number of times cycles of various sizes occur, resulting in load steps with constant loads applied an equivalent number of cycles. The embedded cycle-counting command in MatLab (MathWorks) is utilized, which is based on the guidelines in ASTM Standard E 1049 (2011).

The standard procedure of modelling soil response due to lateral loading is by using p-y curves. The concept is illustrated in Figure 2.2. P-y curves are characterized by the relationship between lateral load and displacement and are dependent on the soil type, strength properties and load characteristics. The industry standard is API p-y curves developed by the American Petroleum Institute (API) for static and cyclic loading. These were intended for ULS design of pile foundations for structures subjected to monotonic or cyclic storm or hurricane loading (Zakeri et al., 2017). Cyclic p-y curves represent fully degraded soil behaviour under large cyclic load amplitudes and do not account for the actual cyclic load histories (NGI, 2018). API p-y curves are in particular not suitable for stiffness dominated analyses and serviceability analyses. The procedure does not regard complex drainage conditions nor the interaction effects between the loads, structure and soil support (NGI, 2016).

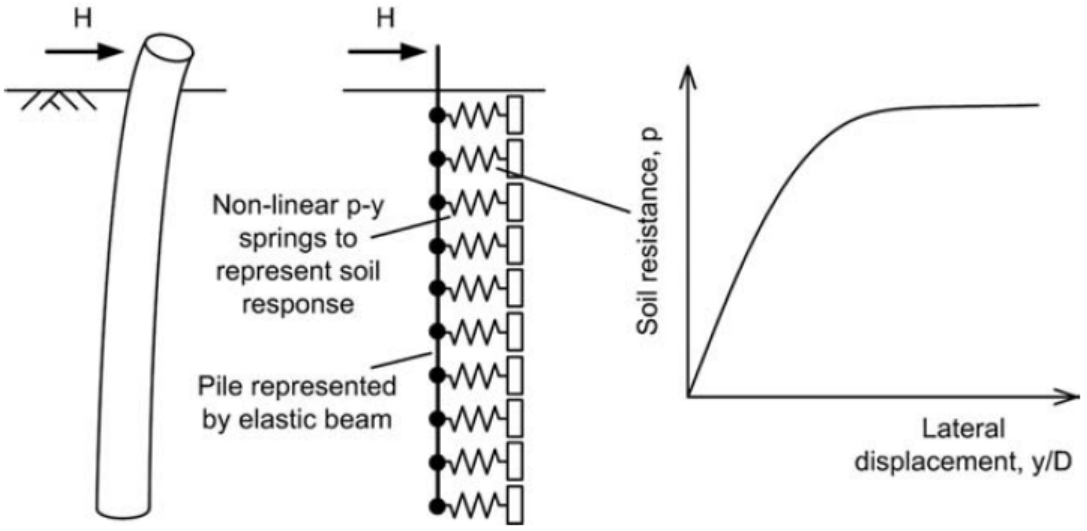

Figure 2.2: Principle of p-y springs (Randolph and Gourvenec, 2011)

2.3 Soil behaviour

Soil behaviour under cyclic loading is considerably different to the response to monotonic loading. Cyclic loading makes the soil structure break down, causing volumetric deformation. Depending on the initial density and stress state, a soil element may densify or loosen if drainage allows. Normally consolidated clays typically contract, meaning that each cycle generates a small densification or a small increase in pore pressure in the soil, depending on the material's permeability (Verruijt, 2012). The generated pore pressures can be divided into a permanent and a cyclic component. The effective stresses in the soil are reduced due to the pore pressure build-up, and this results in increased average, permanent and cyclic shear strains (Andersen, 2015).

Definitions of cyclic, average and permanent shear strains, stresses and pore pressures are illustrated in Figure 2.3 and these terms are used throughout this thesis. In design, the most important components are the permanent pore pressures and the cyclic, average and permanent shear strains. While pore pressure is the preferred parameter for design in sand, cyclic shear strain is normally used to quantify the accumulated effect of cyclic loading in clays (Andersen, 2015). The cyclic shear strain is defined as the single amplitude value illustrated in Figure 2.3 and is the primary parameter in calculations of displacements and soil stiffness (Andersen, 2015). Deformations accumulated under cyclic loading are due to the permanent shear strain generated by dissipation of cyclically induced pore pressures (Randolph and Gourvenec, 2011)

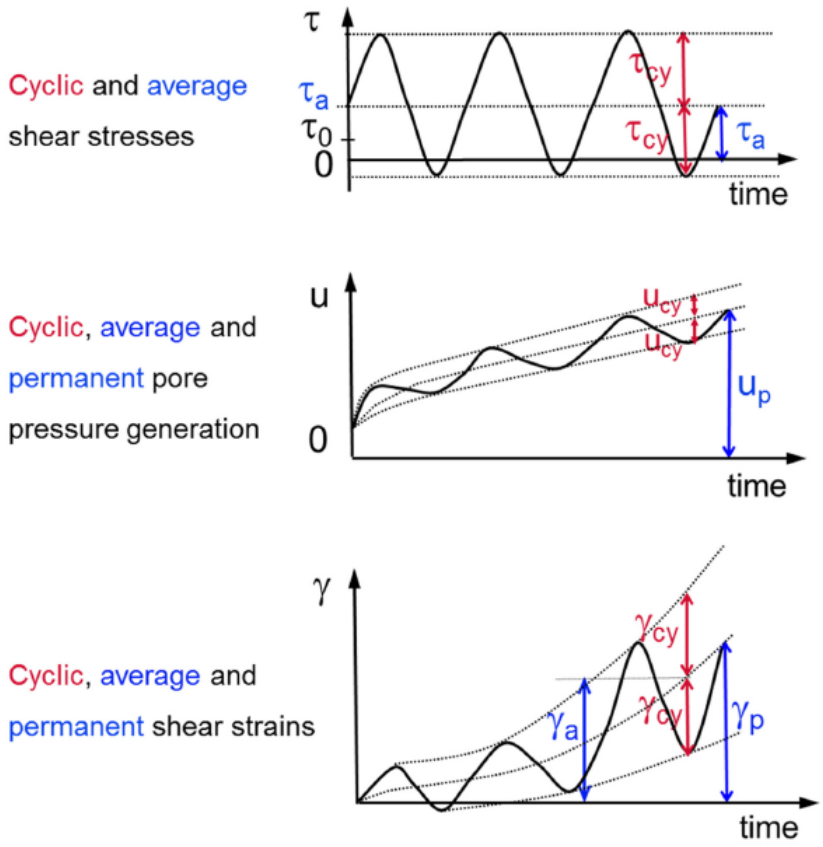

Figure 2.3: Pore pressure and shear strain as functions of time under undrained cyclic loading (Andersen, 2015)

When soils are subjected to cyclic loading, the strain accumulation will either stabilize or go to failure, usually defined as when either the average or cyclic strains reach 15% (Randolph and Gourvenec, 2011). For small load levels, the displacement accumulation rate will stabilize so the displacement remains constant or increase linearly. Subjected to large load levels, the displacement accumulation may increase exponentially and rapidly reach failure. Both large cyclic and large average shear strains can cause failure, depending on the loading conditions. The cyclic shear strength is dependent on the applied loading, the duration of the cyclic event and the stress path (Randolph and Gourvenec, 2011).

Soils are sensitive to the order of cyclic loading. Wind and wave loads are usually continuously varying between severe phases with large load amplitudes and phases with smaller amplitudes. When pore pressures accumulate under cyclic loading, the effective stresses decrease. This leads to a reduction in shear strength and stiffness, often denoted as cyclically degraded soil (NGI, 2017). While large cyclic load amplitudes can cause a degradation of the soil strength and stiffness, the soil may regain its strength and stiffness when subjected to lower cyclic load amplitudes (Sturm, 2017). Hence, the practice of applying the load as

parcels in ascending order simplifies the load history in the most unfavorable way.

2.3.1 Damping

To improve cost-efficiency, OWTs are getting larger and require larger foundations. With increased size, the eigenfrequencies usually decrease and get closer to the primary wave frequencies. This results in a narrow frequency range between the wave loads and eigenfrequency, making the structures more vulnerable to non-linear wave loading (NGI, 2016).

The energy dissipation caused by the cyclic loading is taken into account by the damping properties of soil. Damping is dependent on the average and cyclic loads and number of cycles. Improved understanding of damping is necessary to optimize design of offshore structures. This is especially important considering dynamic amplification near the system's resonant frequencies (Løvholt et al., 2018).

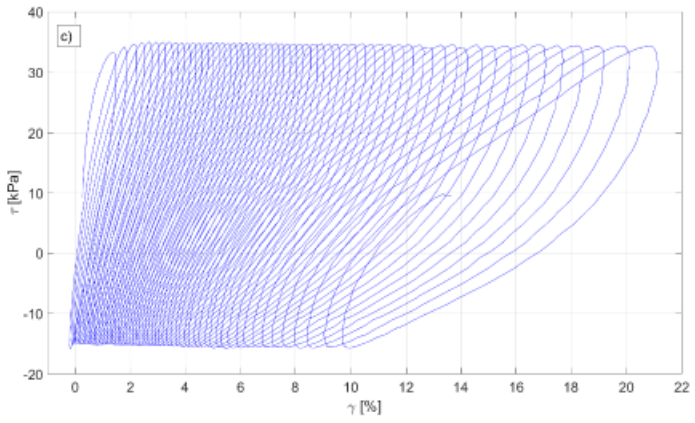

Figure 2.4: DSS test on soil element subjected to non-symmetric loading (Løvholt et al., 2018)

Most existing research on damping have focused on symmetric cyclic loading, but loads on offshore structures are generally non-symmetric and the average shear strain will increase from cycle to cycle. While symmetric loading have nearly closed hysteresis loops, accumulation of average strain under non-symmetric loading will cause open hysteresis loops that combine into a spiral shaped curve, as shown in Figure 2.4. This complicates the calculation of energy loss due to damping (Løvholt et al., 2018).

When soils are subjected cyclic loading generating large strains, the hysteresis loops may change from the classical oval shaped loop to a more s-shaped loop (Zakeri et al., 2017). An example of this behaviour is illustrated in figure 2.5. The figure shows the response to a displacement controlled cyclic test reported by Zakeri et al. (2017) using the p-y apparatus.

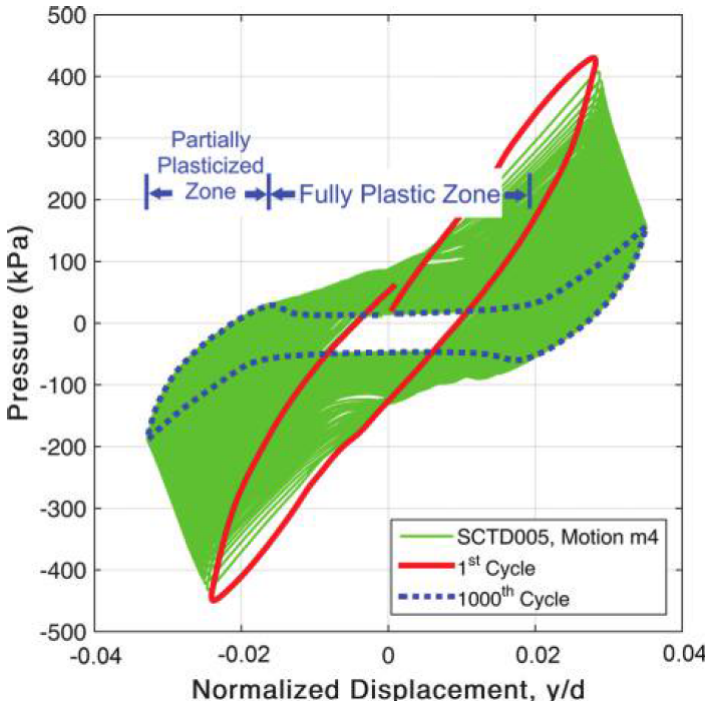

Figure 2.5: Pressure-displacement plot of large strain cyclic loading (Zakeri et al., 2017)

Methods of estimating energy loss under non-symmetric cyclic loading are presented by Løvholt et al. (2018). These are applied in the evaluation of the p-y test results by using the NGI developed program, DLP.

2.3.2 Drainage under cyclic loading

Normally consolidated soils subjected to cyclic loading under partly drained conditions will first accumulate pore pressures before the pore pressures dissipate after a certain number of cycles. The dissipation rate is dependent on the pore pressure gradients. This causes consolidation of the soil and increased soil strength. During the early stages of consolidation, the soil adjactent to the drainage boundary will consolidate, while the soil adjactent to the impervious boundaries will not experience any change in the effective stress (Wilson and Elgohary, 1974).

Drainage within a cycle can be evaluated to assess if drained or undrained conditions can be assumed, based on the cycle period, coefficient of consolidation c_v and representative drainage path length. When piles are subjected to non-symmetric cylic loading, the pore pressures induced by the static component will cause seepage flow in the soil from the compression side and around the pile. The evaluation of drainage performed in this study is based on the method proposed by Zhang et al. (2018) described in Section 3.2.

2.3.3 Lateral capacity of piles in clay

There are two main failure mechanism for laterally loaded piles. At shallow depths, a conical wedge is lifted, as illustrated in figure 2.6. At larger depths, soil moves horisontally around the pile (Randolph and Gourvenec, 2011). The flow-around failure mechanism is shown in figure 2.7.

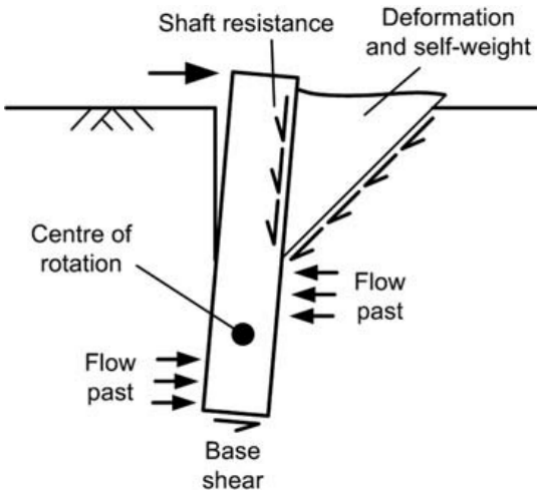

Figure 2.6: Failure mechanism at shallow depths (Randolph and Gourvenec, 2011)

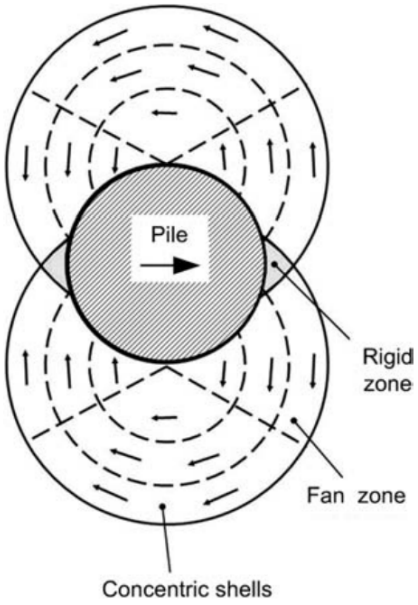

Figure 2.7: Failure mechanism at large depths (Randolph and Gourvenec, 2011)

The ultimate lateral bearing pressure is calculated according to Equation 2.1. The bearing capacity factor N_p is calculated by Equation 2.2 for a suitable roughness factor α. The ultimate resistance of piles with fully smooth interface conditions is calculated with a roughness factor of zero, while a roughness factor of $\alpha = 1$ is assumed for fully rough piles.

$$p_u = N_p s_u \tag{2.1}$$

$$N_p = 9 + 3\alpha \tag{2.2}$$

2.3.4 Set-up effects

During installation of driven piles, the soil is displaced and disturbed. Displacements are mainly horizontal along the pile wall, causing large radial strains. As the soil is displaced, excess pore pressures are generated and effective stresses of the adjactent soil decrease accordingly. With time, the pore pressures will dissipate and the effective stresses increase (Komurka et al., 2003). This process of equalization is called set-up and results in consolidation of the soil close to the pile and consequently an increased pile resistance (Randolph and Gourvenec, 2011).

The p-y apparatus simulates pile-soil interaction by applying lateral cyclic load to the model pile installed in the soil sample. The installation process in described in Section 4.1. A hollow steel tube is used to remove material before the model pile is inserted, but because the model pile is not perfectly in line during insertion, some disturbance of the soil is expected. This may cause increased shear strength in material in close vicinity of the model pile. The small displacements caused by cyclic loading may also trigger a response of re-consolidation or set-up.

Chapter 3

Evaluation methods

3.1 Contour diagrams

Contour diagrams present the cyclic behaviour of soils and relate number of cycles to cyclic and average shear stresses and strains. An illustration of the principle of contour diagrams is shown in Figure 3.1. In contour diagrams, the cyclic and average shear strains are represented as functions of cyclic and average shear stresses and number of cycles. Contour diagrams have been used for many years and are the basis for an established procedure for design of offshore structures (DNV-GL, 2017).

Contour diagrams are based on stress controlled DSS or triaxial tests with different combinations of cyclic and average shear stresses. For a certain number of cycles, there is a contour diagram which defines the combination of cyclic and average shear stresses. Failure is given by the average and cyclic shear strains, as well as the number of cycles to failure. The static shear strength is defined as the intersection between the curves and the horisontal axis. Contour diagrams are valid for undrained stress controlled tests with constant shear stresses (Andersen, 2015).

Contour diagrams for the kaolin clay used for the tests in this study is constructed from stress controlled DSS tests. These diagrams are included in Appendix E.

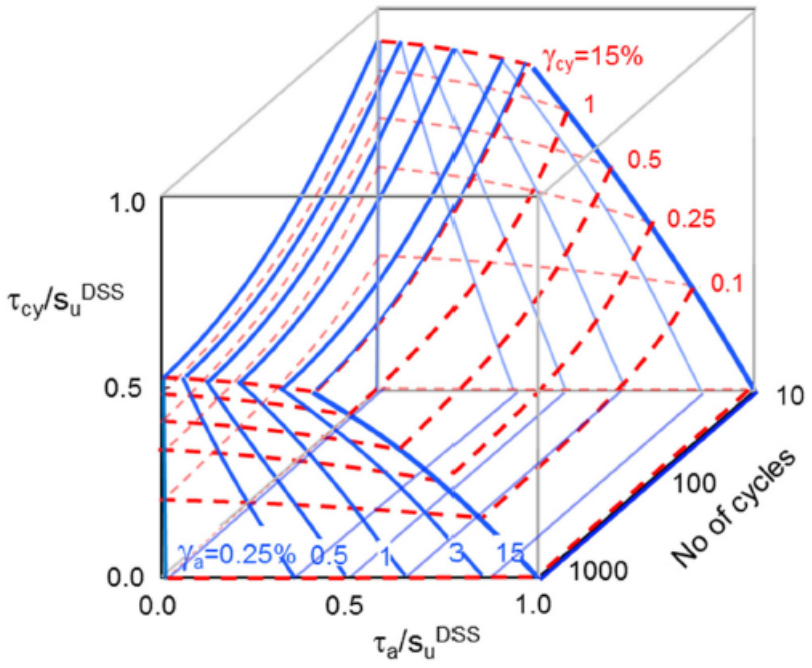

Figure 3.1: 3D representation of contour diagram (Andersen, 2015)

3.2 Evaluation of drainage

Soil strength and stiffness are highly dependent on the drainage conditions. Under fully undrained conditions, pore pressures are built up and no dissipation occurs. If drainage conditions are partly drained, pore pressure generation under cyclic loading and dissipation will take place simultaneously (Andersen, 2015).

A method to simply assess the drainage conditions around a monopile is developed by Zhang et al. (2018). Pure horizontal drainage is assumed. The method is intended for monopiles in sand, but is assumed to give an indication also for the tests on kaolin clay performed in this work.

Figure 3.2 is used for evaluation of drainage under static loading and shows the variation of the normalized excess pore pressure in the loading direction for different values of normalized time T. The normalized time includes whether the conditions can be assumed undrained, partly drained or fully drained. T varies from undrained conditions at T = 0 to drained conditions at T = 12.6.

Figure 3.3 is used for evaluation of drainage under cyclic loading, where $T_p = 0$ indicates undrained, and $T_p = 48.5$ indicates drained conditions within a cycle.

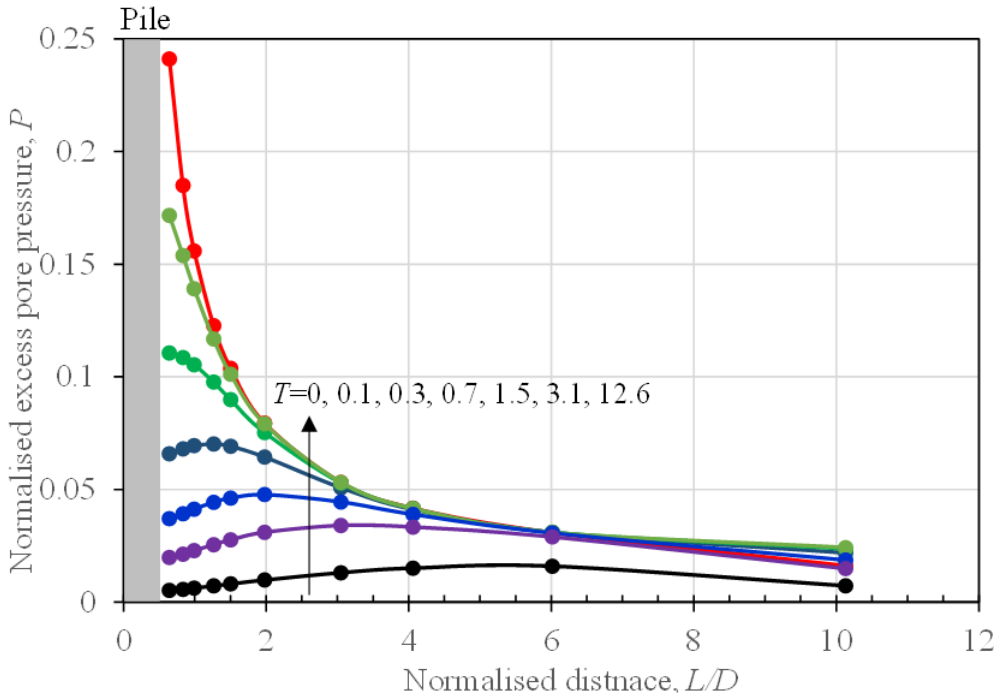

Figure 3.2: Evaluation of drainage under static loading (Zhang et al., 2018)

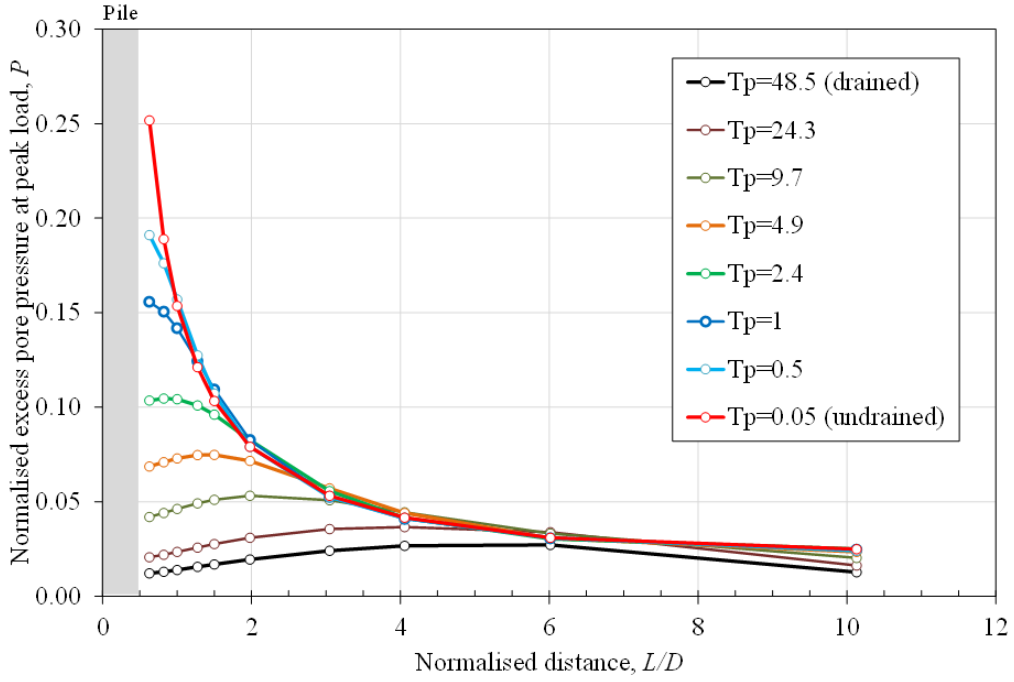

Figure 3.3: Evaluation of drainage under cyclic loading (Zhang et al., 2018)

Normalized excess pore pressure P is given by Equation 3.1, where u is the excess pore pressure and p is the average bearing pressure calculated as the applied force divided by the laterally projected area on the pile slice (Zhang et al., 2018). Normalized time for static and cyclic loading is calculated according to Equations 3.2 and 3.3, where D is the diameter of the pile, c_v is the coefficient of consolidation, t is time and t_p is is the cycle period.

$$P = \frac{u}{p} \tag{3.1}$$

$$T = \frac{tc_v}{D^2} \tag{3.2}$$

$$T_p = \frac{t_p c_v}{D^2} \tag{3.3}$$

3.3 Establishing p-y curves from DSS results

To evaluate the plausibility of the performed p-y tests, the results can be compared with DSS test results using the procedure proposed by Zhang et al. (2017). The concept is based on the analogy between shearing of a DSS test and lateral loading of a pile element, as shown in Figure 3.4. It is assumed that the load-deflection response of a pile element is equivalent to the stress-strain curve of a DSS soil element.

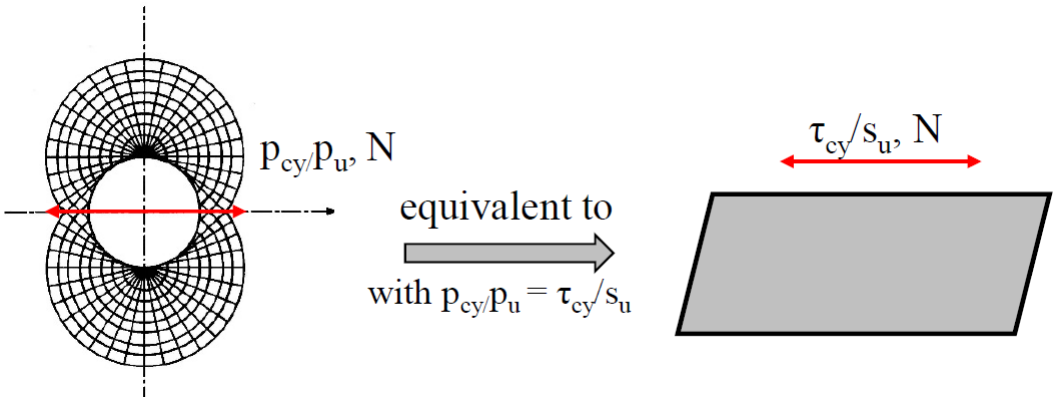

Figure 3.4: Analogy between shearing of a DSS element and lateral loading of a pile element (Zhang et al., 2016)

P-y curves are obtained by scaling stress-strain curves from DSS tests. The framework is illustrated in Figure 3.5. The shear stress mobilisation of a point in a stress-strain curve is equivalent to the lateral bearing pressure with the same mobilisation in a pressure-displacement curve (Eq. 3.4). The corresponding normalized displacement y/D is calculated by scaling the shear strain using Equation 3.5. The scaling coefficient for elastic strains is $\xi_1 = 2.8$ and the coefficient scaling plastic strains ξ_2 is calculated by Equation 3.6, where α is the roughness factor (Zhang et al., 2017). Elastic and plastic shear strains are calculated by Equations 3.7 and 3.8.

The flow-around failure mechanism and equations are described previously in Section 2.3.3. The ultimate lateral bearing pressure p_u is given by Equation 2.1 and the bearing capacity factor in Equation 2.2. By scaling DSS results according to this framework, the p-y test results may be compared and the plausibility of the tests evaluated.

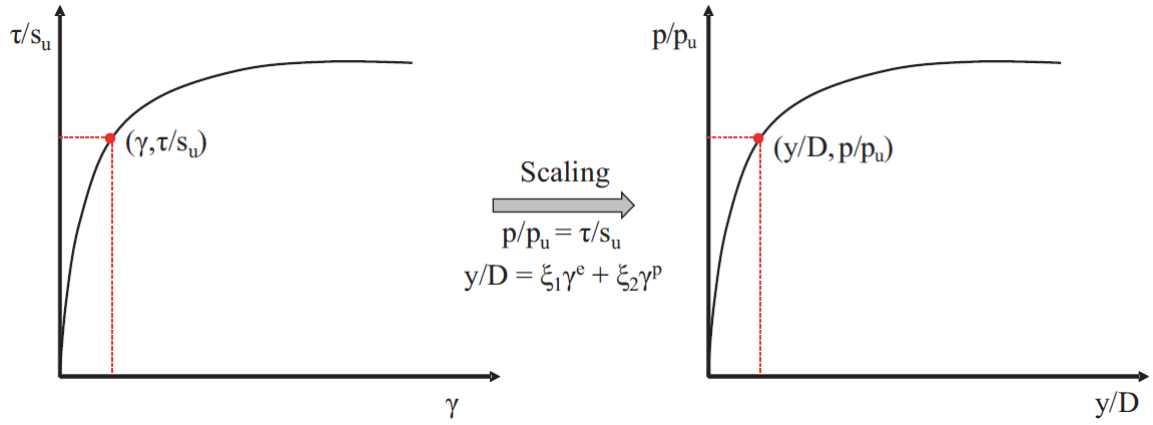

Figure 3.5: Construction of p-y curves from stress-strain curves (Zhang et al., 2016)

$$\frac{\tau}{s_u} = \frac{p}{p_u} \tag{3.4}$$

$$\frac{y}{D} = \xi_1 \gamma^e + \xi_2 \gamma^p \tag{3.5}$$

$$\xi_2 = 1.35 + 0.25\alpha \tag{3.6}$$

$$\gamma^e = \frac{\tau}{G_{max}} \tag{3.7}$$

$$\gamma^p = \gamma - \gamma^e \tag{3.8}$$

3.4 Comparison with centrifuge test results

Test results are compared with centrifuge test results from Zakeri et al. (2015) and Zakeri et al. (2016), which were used for comparison of p-y test results reported in Zakeri et al. (2017). Templates of the diagrams used in the evaluation in Sections 6.1.4 and 6.3 are provided by NGI.

Normalized secant stiffness at steady state is calculated according to Equation 3.9. Values of secant stiffness are taken at the end of each load parcel and a bearing capacity factor of $N_p = 12$ is assumed. Upper bound, lower bound and best fit from centrifuge tests are given by Equations 3.10, 3.11 and 3.12. Normalized damping and secant stiffness are calculated by Equations 3.13 and 3.14.

$$K_{sec,ss,norm} = \frac{K_{sec}}{N_p s_u} \tag{3.9}$$

$$K_{sec,UB} = 0.9(\frac{\Delta y}{D})^{-1.05} \tag{3.10}$$

$$K_{sec,LB} = 0.5(\frac{\Delta y}{D})^{-0.95} \tag{3.11}$$

$$K_{sec,BF} = 0.67(\frac{\Delta y}{D})^{-0.97} \tag{3.12}$$

$$D_{norm} = \frac{D}{67} \tag{3.13}$$

$$K_{sec,norm} = \frac{K_{sec}}{4G_{max}/s_u} \tag{3.14}$$

3.5 OCR correction

Soil strength is dependent on the over consolidation ratio (OCR). OCR is given by Equation 3.15, where p'_c is the preconsolidation stress and σ'_{vc} is the current stress.

$$OCR = \frac{p'_c}{\sigma'_{vc}} \tag{3.15}$$

The effect of OCR varies considerably for different soils. Soils that are contractive in their normally consolidated state, like most clays, will be more influenced by OCR than dense sand and silt that are dilatant already in the normally consolidated state. The effect of OCR also depends on the effective stresses in the normally consolidated state, but this is more important for sands and silts than for clays (Andersen, 2015). If the initial shear strength and OCR is known, shear strength for the given OCR can be scaled according to the diagram in Figure 3.6.

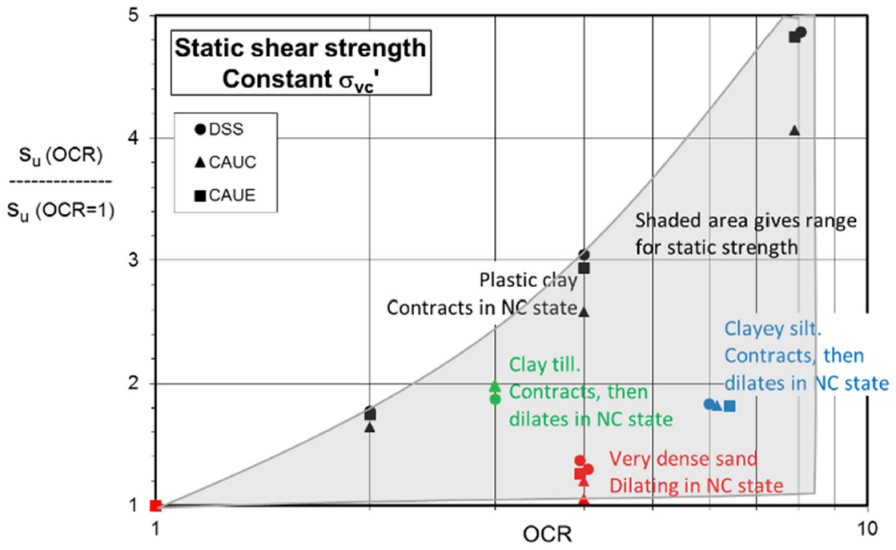

Figure 3.6: Undrained static shear strength as a function of OCR (Andersen, 2015)

Chapter 4

Model tests

Laboratory work is performed at NGI's geotechnical laboratory in Oslo.

4.1 The p-y apparatus

The p-y apparatus was planned, designed and built by NGI for BP America. The device consists of a cylindrical soil chamber containing the soil sample, a steel rod to model the pile foundation and an actuation piston for applying the prescribed load or displacement. The apparatus is shown in Figure 4.1. Pictures, specifications and more detailed drawings are given in Appendix G. Some key dimensions are given in Table 4.1.

Table 4.1: Selected dimensions

Steel rod diameter	10 mm
Inner diameter soil chamber	68 mm
Height of specimen	ca. 100 mm

The soil sample is built into the soil chamber and placed in the apparatus, fastened by a fastening block in front and end supports at the specimen's ends. The inner diameter of the soil chamber is 68 mm and the height of the specimen is approximately 100 mm after it is built into the soil chamber. The end support on the right hand side is free to slide during consolidation and is fixed during cyclic testing. The end support on the left hand side is a fixed reaction support. There is a hole for insertion of the steel rod in both end supports. The diameter of the steel rod is 10 mm. Slides in the end caps make lateral movement of the steel rod possible. Loading from the actuation piston is transferred to the soil specimen by two push/pull rods connected to the steel rod, as illustrated in Figure 4.1(b). When the soil

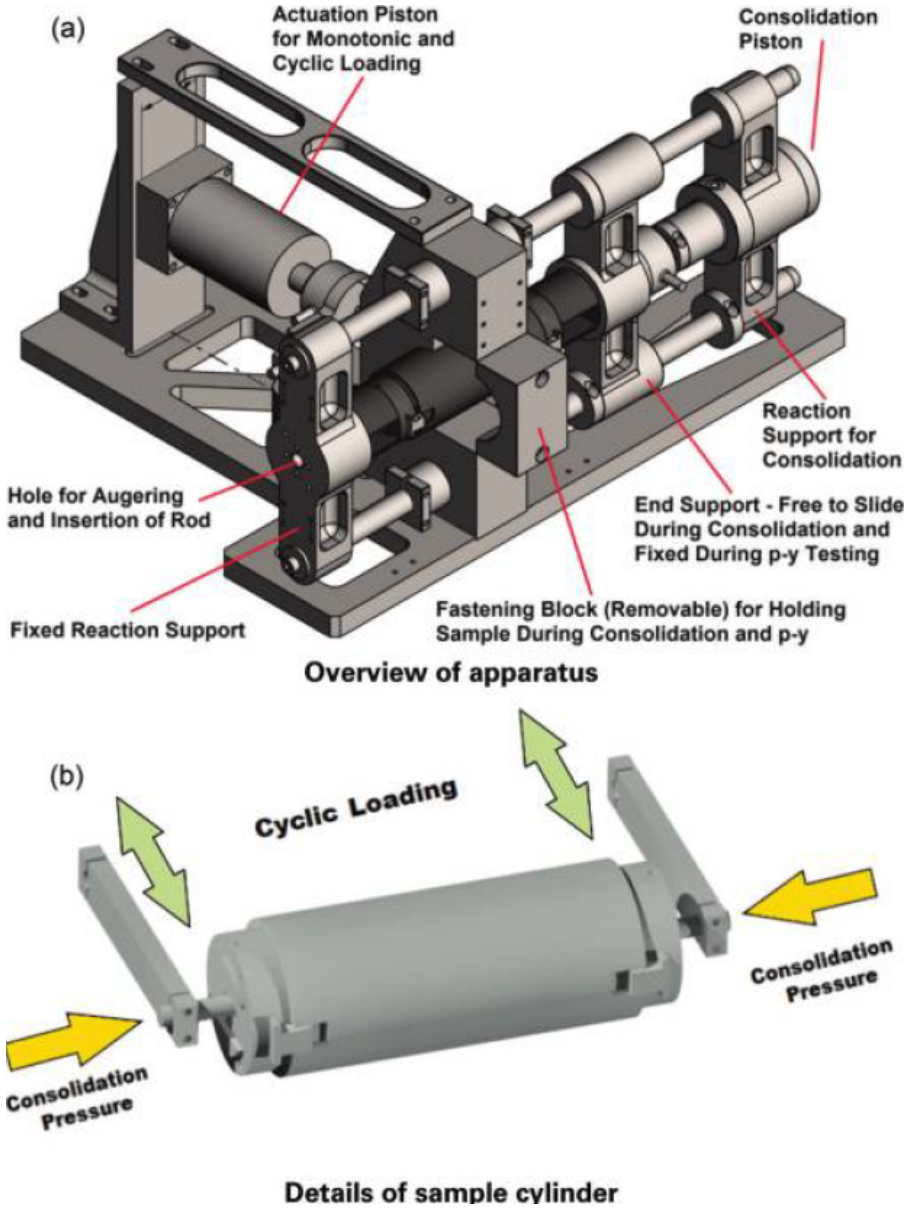

Figure 4.1: (a) Overview of apparatus and (b) details of cylinder (Zakeri et al., 2017)

specimen is installed in the apparatus, both consolidation and cyclic testing can be carried out.

By inserting the steel rod into the soil specimen, the in-situ installation process is mimicked (Zakeri et al., 2017). A hollow steel tube with the same diameter as the model pile is inserted first to remove material and minimize the sample disturbance. Next, the steel rod is carefully installed. The soil specimen is consolidated with the installed steel rod under constant pressure using an air pressure piston.

After consolidation, the apparatus is fixed and cyclic loading can be applied to the specimen using the hydraulic actuator. The end supports are fixed to obtain constant soil height

during testing. The hydraulic system is turned on and warmed up before the apparatus is assembled for tesing. Depending on what test is going to be performed, displacement or load controlled, tuning of the system is performed before or after mounting. During cyclic testing, deformation sensors measure the lateral displacement of the push/pull rods by the steel rod's ends. Also the displacement and load applied by the actuation piston is logged during testing.

4.1.1 Hydraulic actuator

Cyclic loading is applied to the soil specimen using a hydraulic actuator controlled by MTS operating software (MTS Systems Corporations). Both monotonic and cyclic loading may be applied, as well as regular and irregular load histories.

The tests in this lab program were performed using the waveforms ramp and sine. Ramp waveform applies the load or displacement at constant rate, and sinusoidal waveform as sine waves. One test was also performed using the profile command procedure to apply an irregular load history.

Loading can be applied both displacement and load controlled. Using displacement control, the displacement is prescribed and the force response from the soil specimen is measured. In load controlled tests the load is prescribed and the displacement is measured.

The maximum displacement amplitude that can be applied during testing is 4 mm due to the design of the apparatus. If this limit is exceeded, the device will be damaged. Load control is more challenging than displacement control as the displacements are not restrained. By overestimating the material's strength, the prescribed load may cause the material to fail, which will lead to large displacements and damage to the equipment. Load controlled tests are also more sensitive for outer interruptions such as vibrations, and the system may go out of control searching for the prescribed load levels. For this reason, it has been necessary to be present at all times during testing.

Tuning

Tuning of the test system adjusts the accuracy between the command and the response of the actuator. Tuning parameters determine the response and stability of the servo control loop. The command is the prescribed load or displacement, and the feedback is the actual

response of the system to the command. The error is the difference between the command and the feedback. Correct tuning will improve the performance of the test system as the response of the actuator follow the command accurately (MTS Systems Corporations, 2008).

Tuning parameters are greatly dependent on material, control mode and type of loading. Different materials respond differently and tuning has to be adjusted according to material behaviour. What test to be performed, cyclic or monotonic, and choice of control mode, frequency and waveform will effect the test system and tuning parameters.

Tuning of load controlled and displacement controlled tests are carried out differently. The controlling feedback source in displacement control mode is a displacement sensor in the actuator. Tuning can be performed before the installation of the soil sample (MTS Systems Corporations, 2008). In load control mode the load sensor in the actuator is the controlling feedback source. The soil sample has to be installed to perform the tuning of the system.

The main tuning parameter is proportional gain (P Gain). P Gain is proportional to the error signal and scale it to control the system. P Gain adjusts the effect of the error signal on the servovalve, and this regulates the system response. Large values of P Gain increase the input to the servovalve and opens it, so the oil can move faster into the actuator. This makes the system respond faster. Too large values of P Gain will make the system unstable (MTS Systems Corporations, 2008).

Integral gain (I Gain) is the integral of the error signal. I Gain generates increased gain over longer time periods and gradually adjusts the response of the servovalve command. During static or low frequency test programs, I Gain increases the system response. In high-frequency test programs, I Gain helps to maintain the mean level. Too high values may cause oscillation (MTS Systems Corporations, 2008).

Dither amplitude is adjusted to improve the system response on low frequency or low amplitude tests. Dither are small, high-frequency sine waves applied to the servovalve to improve the valve's response to low amplitude signals. Too low dither amplitude is visible as distortions at the maximum and minimum points of the waveform (MTS Systems Corporations, 2008).

4.2 Material

4.2.1 Reconstituted kaolin clay

Model tests in this study are performed on reconstituted Prestige-NY kaolin clay. The material was prepared and consolidated as kaolin clay used in a research project at NGI in 2015, to have access to material data and results from former laboratory tests. The soil to water ratio and the consolidation pressure were determined based on this material in order to use former test results to calculate material parameters. Some key properties used in this study are given in Table 4.2. A detailed description of the procedure and consolidation of the kaolin clay, as well as material parameters are described in Appendix F.

Table 4.2: Properties of kaolin clay

s_u	[kPa]	25.2
σ'_c	[kPa]	120
G_{max}	[MPa]	7.76
$p_{u,N_p=12}$	[kPa]	303
c_v	$[m^2/s]$	0.2e-6

4.2.2 North Sea clay

Tests 11 and 12 were performed on material from an offshore site in the North Sea, from depths 14.2-14.4 and 14.4-14.6 meters. The material is inhomogeneous, with some large grains and cavities of silt and sand, as shown in Figure 4.2. Material parameters are given in Table 4.3.

Table 4.3: Material parameters of North Sea samples

γ'	$[kN/m^3]$	20.1
w	[%]	21.0
I_p	[%]	17.0
OCR	[-]	1.6
σ'_c	[kPa]	143
p'_c	[kPa]	240
s_u	[kPa]	71.6

Figure 4.2: North Sea sample

4.3 P-y testing

4.3.1 Preliminary work

Because the p-y apparatus is newly developed, it has been necessary to use some time to learn how to operate the device and gain some practical experience before starting the lab test program. Four dummy tests were performed during the preparation period in addition to one dummy test performed later to look into the possibilities of applying irregular load histories. The preparation tests were done on Speswhite kaolin clay preconsolidated to 60 kPa. The material was excess samples from earlier projects at NGI. The specimens were consolidated in the apparatus according to Table 4.4.

Three of the dummy tests were performed displacement controlled with symmetric cyclic loading. The results were evaluated and compared to centrifuge data and existing results from previous performed tests reported in Zakeri et al. (2017). Two load controlled dummy tests were also performed. The apparatus has not been used for load controlled tests before, so the two dummy tests were run to see if it was realistic to include load controlled tests in the lab test program. It was necessary to adjust the tuning parameters in order to prepare the MTS system for load control mode before the tests could be performed.

Tuning of the load contolled tests revealed that high values of P Gain, I Gain and dither amplitude were required in order to get the MTS load to follow the MTS load command with satisfactory accuracy. Extreme values to achieve the intended precision would make the system very sensitive and vulnerable for outer disturbance. For the purpose of the work with this thesis, the accuracy resulting from standard tuning of the MTS system was considered acceptable. Overprogramming could be a solution to the poor accuracy, but is not included in this study. The error depends on load level and frequency, and there is not gained enough experience with load control mode tests on the device to correctly adjust the load command for the different load conditions.

4.3.2 Tests

This study includes 12 tests, in addition to five dummy tests. An overview of the performed tests is presented in Table 4.7. A complete overview of all the tests, including the preliminary work, is presented in Appendix A. Nine of the tests were successful, and the rest, complete or parts, were aborted and/or discarded due to various problems.

The material used in tests 1 to 10 was reconstituted kaolin clay. Tests 11 and 12 were performed on North Sea clay. Details about the materials are presented in Section 4.2 and in Appendix F. The specimens were consolidated after mounted in the apparatus with the model pile installed. The consolidation steps are given in Table 4.4.

Table 4.4: Consolidation steps

Material	Step 1	Step 2	Step 3
Kaolin clay	30 kPa	60 kPa	120 kPa
North Sea clay	95 kPa	191 kPa	143 kPa

The kaolin samples were subjected to cyclic loading applied as sequences of load parcels with varying amplitude and average load. Tuning parameters used for testing are given in Table 4.5. Tests were performed load controlled using sine waveform. At the end of all the tests a cycle with displacement amplitude of 3 mm was applied using the ramp procedure. Table 4.6 and Figure 4.3 show the outline of the 3 mm cycle.

Some of the tests were performed over two days. The hydraulic system has to be turned off by night and the apparatus must be dismounted from the hydraulic actuator before turned off to prevent damage to the device. The position of the steel rod at end of testing on the

first day will therefore not be maintained until the next day and may be displaced when the device is dismounted.

Table 4.5: Tuning parameters

Control mode	P Gain	I Gain	Dither amplitude
Displacement	70	7	0.45
Force	95	9.5	0.45

Table 4.6: Outline of 3 mm cycle

Δ t	Start	End
4 s	0 mm	3 mm
8 s	3 mm	-3 mm
8 s	-3 mm	3 mm
4 s	3 mm	0 mm

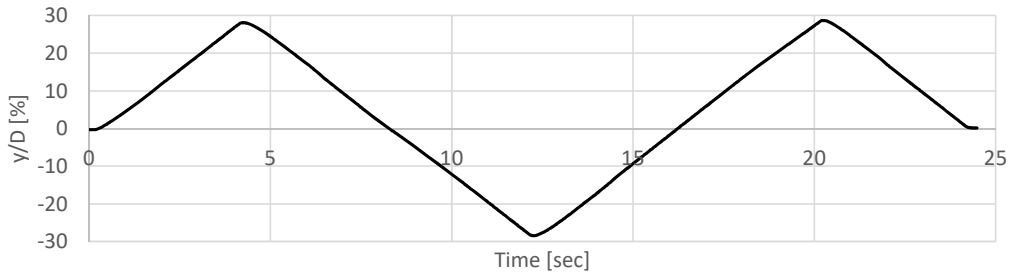

Figure 4.3: Outline of 3 mm cycle

The two North Sea specimens were subjected to a load history generated by Sintef Ocean. In test 11, the 3 hour irregular load history was applied to the specimen. In test 12, the storm history was simplified by rainflow counting and applied as regular load parcels in ascending order. The load history was scaled so a maximum load of 200 N was applied to the specimen. Both tests were completed with three load controlled symmetric cycles with load amplitude 270 N, as well as the displacement controlled 3 mm cycle that has been applied at the end of all the tests. The load amplitude of the 270 N cycle accounts for a load factor of 1.35 applied to the largest load cycle in the load history.

After testing was completed, the specimens were carefully extracted from the sample cylinder and cut into several parts. Water content in both ends and in the middle of the specimen was determined.

Table 4.7: P-y tests

Test	Average [N]	Amplitude [N]	Number of cycles	Frequency [Hz]	Comment
	0	20	500	0.25	
	0	40	500	0.25	
	0	60	500	0.25	
1	0	80	500	0.25	
	0	80	500	0.25	
	0	120	500	0.25	
	0	80	500	0.25	
					Incorrect zero reading. Discarded.
	20	20	500	0.25	
	-20	20	500	0.25	
	40	40	1000	0.25	
2	-40	40	1000	0.25	
	50	50	500	0.25	
	-50	50	500	0.25	
	-50	50	500	0.25	One day after
	-50	50	500	0.25	
	40	20	500	0.25	
	40	40	500	0.25	
3	40	60	500	0.25	
	40	80	500	0.25	
	40	120	500	0.25	
					Loose screws on left side. Discarded.
	40	40	500	0.25	
	40	60	500	0.25	
4	40	80	500	0.25	
	40	60	500	0.25	
	40	40	500	0.25	
	40	40	500	0.25	One day after
	40	40	500	0.25	
	80	40	500	0.25	
	40	40	500	0.25	
5	0	40	500	0.25	
	-40	40	500	0.25	
	-80	40	500	0.25	
	-40	40	500	0.25	
	0	40	500	0.25	
	20	40	500	0.25	
	20	40	200	0.05	
	-20	40	500	0.25	
	-20	40	100	0.05	
	20	40	250	0.25	
6	20	40	50	0.05	
	-20	40	250	0.25	
	-20	40	50	0.05	
	-40	40	500	0.25	
	-40	40	100	0.05	
	40	40	500	0.25	

	40	40	100	0.05	
	20	30	500	0.25	
7	40	30	500	0.25	
	20	30	471	0.25	End of test due to hydraulic interlock.
	20	30	500	0.25	
	40	30	500	0.25	
	20	30	500	0.25	
8	0	30	500	0.25	
	-20	30	500	0.25	
	-40	30	500	0.25	
	-20	30	500	0.25	
	0	30	500	0.25	
	30	15	500	0.25	
	30	30	500	0.25	
9	30	45	500	0.25	
	30	15	500	0.25	
	30	30	500	0.25	
	30	45	500	0.25	
	30	45	500	0.25	
10	30	60	250	0.25	
	30	45	2600	0.25	
11		3h irregular load history			North Sea sample depth 14.2-14.4 m
		3h irregular load history simplified by rainflow counting			North Sea sample depth 14.4-14.6 m
	-33.3	9.2	1339	0.31	
	-32.0	27.6	796	0.31	
	-32.0	46.0	604	0.31	
	-31.8	64.3	351	0.31	
12	-29.7	82.7	176	0.31	
	-27.8	101.1	77	0.31	
	-23.5	119.5	35	0.31	
	-22.4	137.9	12	0.31	
	-22.6	160.9	2	0.31	
	-29.9	170.1	1	0.31	
	-16.9	179.2	1	0.31	

4.4 Raw data

Sensor raw data were logged and written to text-files. The program ModLab developed by NGI were used to do zero-readings, calibrate the sensors and administrate data logging.

During consolidation, the consolidation displacement and force were logged. The file update interval was set to 1 second when adjusting the load, and increased to 30-60 seconds when the displacement was starting to stabilize.

During cyclic testing, the load and displacement measured in the MTS actuator were logged, as well as the deformation measured at the push/pull rods by the ends of the steel rod. The file update interval was 0.01 seconds to achieve sufficient accuracy during cyclic loading. The data were written to a text-file and later corrected for elastic deformations of the system, denoted false deformation.

The steel rod is not rigid and elastically bends during loading, especially when subjected to small displacements. The displacement of the steel rod is measured at the ends of the rod. Because the rod has some elastic deflection during loading, the displacements in the soil specimen are smaller than the measured deflections at the steel rods ends and must be corrected (Zakeri et al., 2017). The calculation of false deformation is based on the applied load, the distance between the deformation sensors and the specimen's height after consolidation. NGI has provided a script that executes this calculation, in addition to reducing the text-files from the laboratory so only the relevant data are stored.

The corrected data sets were divided based on the load parcels in the test using the program DLP developed by NGI. Secant stiffness, cyclic and average normalized displacement, damping and pressure were computed using this program. Pressure subjected to the soil was calculated according to Equation 4.1, where F is the applied load from the hydraulic actuator and A is the affected area calculated by the diameter of the steel rod and height of the specimen after consolidation. The secant stiffness was calculated by Equation 4.2 as illustrated in Figure 4.4. Cyclic and average normalized displacements were calculated according to Equations 4.3 and 4.4. Damping was calculated as described in Løvholt et al. (2018).

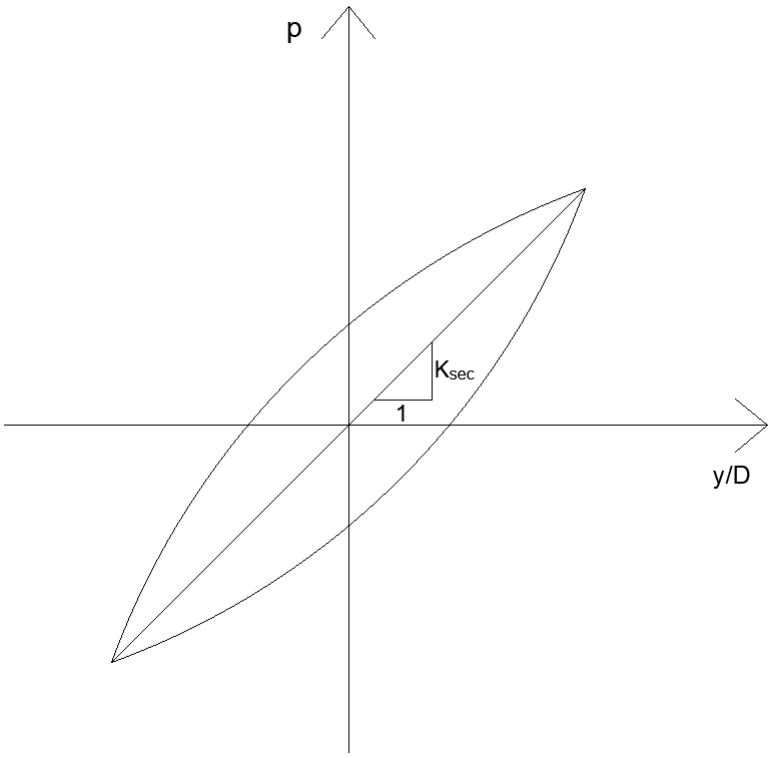

Figure 4.4: Secant stiffness

$$p = \frac{F}{A} = \frac{F}{Dh} \tag{4.1}$$

$$K_{sec} = \frac{\Delta p}{\frac{\Delta y}{D}} \tag{4.2}$$

$$\frac{\Delta y_{cy}}{D} = \frac{1}{2D}(\Delta y_{max} - \Delta y_{min}) \tag{4.3}$$

$$\frac{\Delta y_a}{D} = \frac{1}{2D}(\Delta y_{max} + \Delta y_{min}) \tag{4.4}$$

Chapter 5

Results

Diagrams with all the test results are included in Appendix B and should be referred to by the reader. Some examples are given in the report for illustration. Appendix A provide details of the load steps. Pictures of the specimens are shown in Appendix C and the material's water content after testing is given in Appendix D.

5.1 Tests on kaolin samples

All test results are included in Appendix B.1.

Tests 1, 3 and 7 were aborted due to various problems. Results of test 1 are discarded as the zero reading before testing was incorrect and also wrongly adjusted during the test. Results of test 3 are not included as the device was incorrectly mounted. Test 7 was ended after 3 of 8 planned load parcels as the temperature exceeded the limit and MTS shut down. The results in parcels 1-3 should not be affected by this and are considered reliable.

In test 2, one-way cyclic loading was applied and both the load amplitude and average load varied. Displacements are shown in Figure 5.1. In the first four load steps, the displacement amplitude is nearly constant within each parcel, indicating elastic response. For the remaining load parcels the displacement amplitudes stabilize after some cycles. The displacement amplitude remains nearly unchanged when the average load changes from the positive to negative side of the two first load steps, but increases between the remaining parcels as the load amplitude is repeated or increased. The displacement accumulation stabilizes to linearly increasing during the load parcels. The displacement accumulation rate

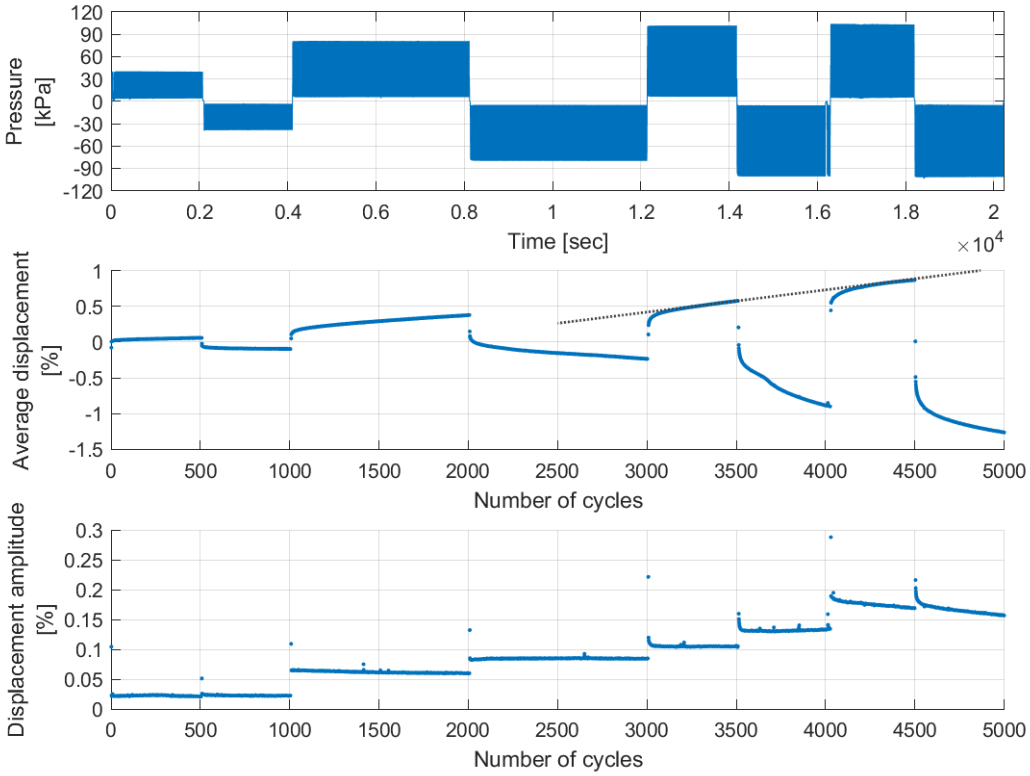

Figure 5.1: Normalized displacements of test 2

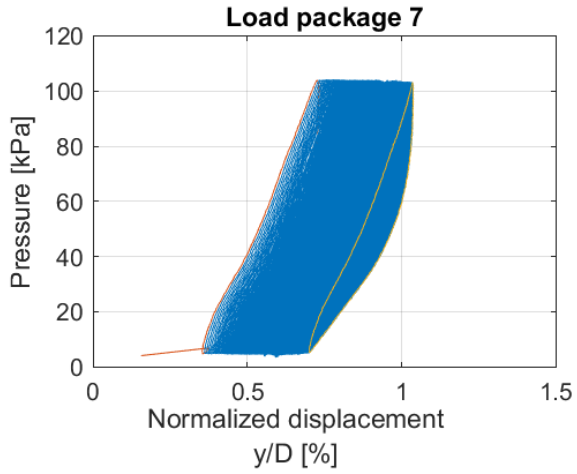

Figure 5.2: Pressure-displacement plot of test 2, parcel 7

increases when the load level increases. The pressure-displacement plot shows the classical oval shaped hysteresis loops for all load steps, as exemplified in figure 5.2.

Load parcels 7 and 8, as well as the 3 mm cycle of test 2 were applied one day after the rest of the test, and had the same load amplitude and average as load steps 5 and 6. As mentioned in Section 4.3.2, the hydraulic system has to be off by night and the apparatus must be dismounted from the hydraulic actuator before turned off. This can potentially affect the position of the steel rod and it is therefore related some uncertainty to the measured aver-

age displacement in load parcels 7 and 8. The average displacement seems to continue from where it left off the last time the same load was applied, as illustrated with the dashed line in Figure 5.1. Displacement accumulation in load step 7 increases with the same rate as in load step 5 the day before. The displacement rate of step 6 varies during the parcel, but seems to be fairly similar also for load steps 6 and 8.

5.1.1 Constant average load

In tests 4, 9 and 10 the load steps were applied with a constant average load while the load amplitude was varied in the different parcels. Test 4 consists of six load steps, where the last load parcel was applied one day after the rest. Displacements are shown in Figure 5.3. Load step 6 had the same load as parcel 5 the day before. The measured displacement amplitude is approximately the same for the two last load steps after stabilization, but there is a large change in average displacement due to disturbance when dismounting of the device between the two steps.

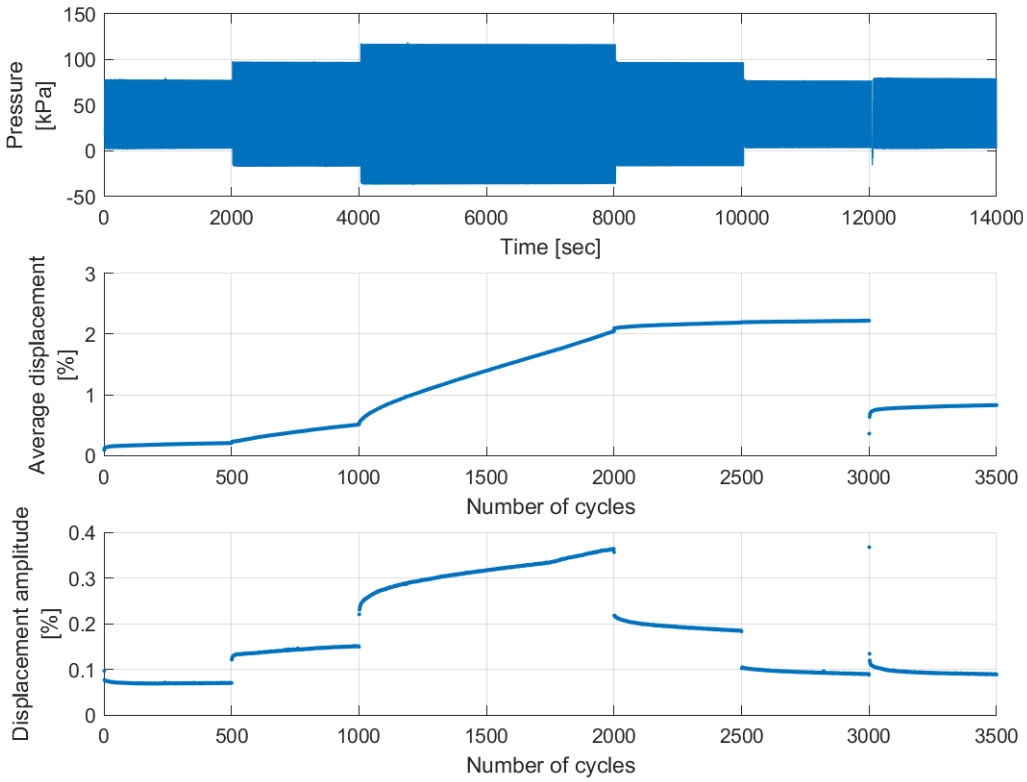

Figure 5.3: Normalized displacements of test 4

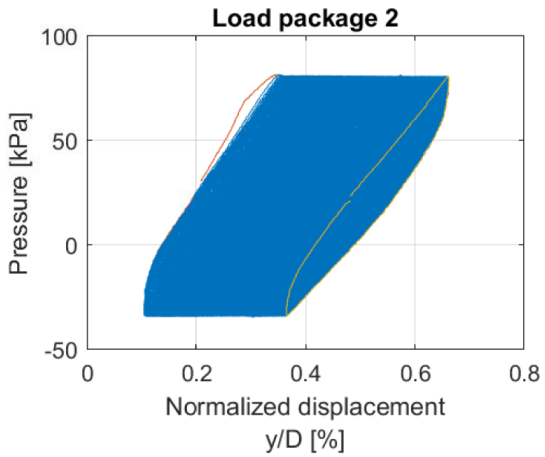

Figure 5.4: Pressure-displacement plot of test 4, load step 2

The pressure-displacement plot shows oval shaped hysteresis loops for all of the load steps, as shown in Figure 5.4. The displacements are gradually increasing, causing open loops combining into the spiral shaped curve as described in Section 2.3.1.

Secant stiffness is calculated from the cyclic load and displacement components, and should be relatively independent of the average load. This behaviour can be seen in both test 4 and 9, as exemplified in Figure 5.5. The secant stiffness decreases when the cyclic load increases for load steps 1 to 3, and increases when the load is reduced in steps 4 and 5. There is also a slight increase in secant stiffness for the last load step. The secant stiffness varies as expected when the load amplitude is changed, and seems to increase towards the end level of the previous similar load parcel when repeated.

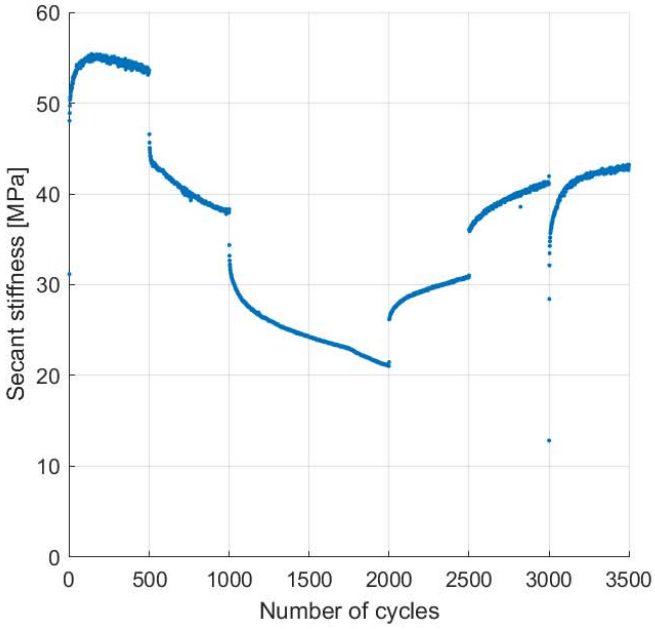

Figure 5.5: Development of secant stiffness during test 4

In test 9, the average load was kept constant while the load amplitude was varied. The load amplitude was increased during load steps 1-3, and then repeated in parcels 4-6 in the same order. The displacement amplitude follows the variation of the load amplitude, as shown in Figure 5.6. The pressure-displacement plots, refer Appendix B.1, show oval hysteresis loops for all load steps. The average displacements of both tests 4 and 9 accumulate during increased loading over the first three load steps, and remain at the same level when unloaded and throughout the rest of the test, except step 6 in test 4 as mentioned previously.

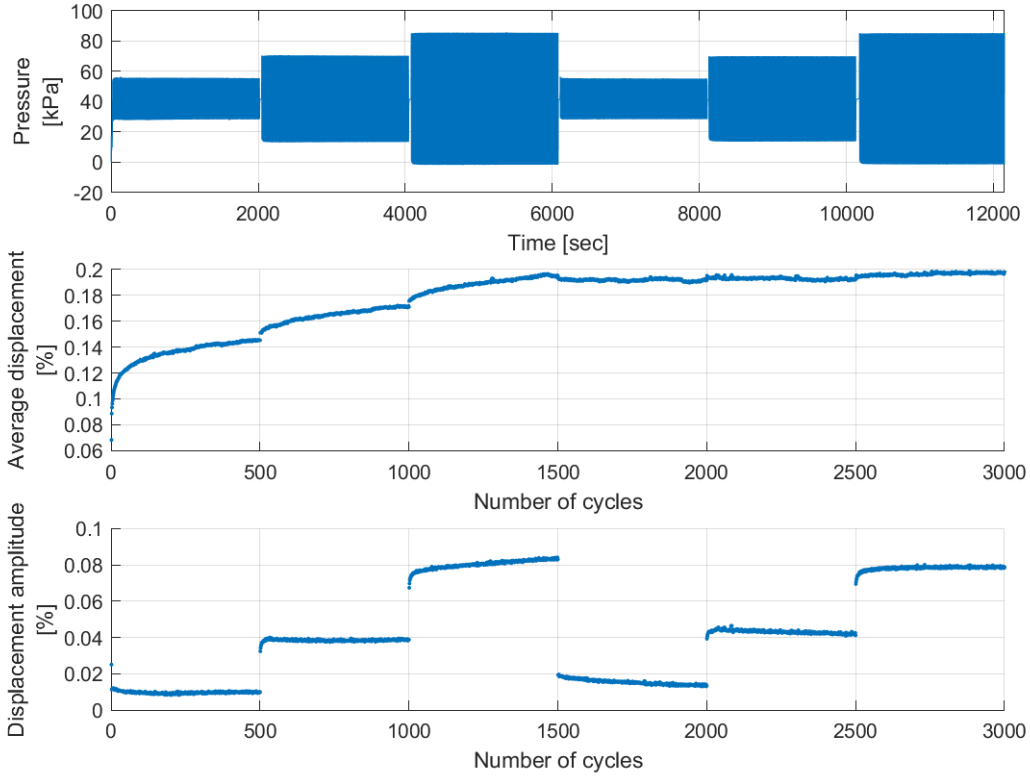

Figure 5.6: Normalized displacements of test 9

Test 10 was designed to investigate displacement accumulation rate based on the observations in test 4. The accumulation rate in step 3 of test 4 was larger than in step 2 due to the increased load level. When the load was reduced in step 4 to the same level as in parcel 2, the average displacement remained constant at the end level of step 3, as shown in Figure 5.3. Since the accumulation rate of the average displacement was larger in step 2 than in step 4, but constant in both, the question arise if the rate in parcel 4 would increase as illustrated by the arrows and dashed lines in Figure 5.7 at the point when the total average displacement in step 4 reach the extended line indicating the accumulation of average displacements during step 2. The aim was to see the difference in displacement accumulation rate. Test 10 was meant to have the same loading conditions as test 4 to investigate this, but to avoid any prob-

lems with gap/remoulded zone, the load amplitude was reduced. Unfortunately, it was not possible to see the tendency in test 4 from the results of test 10. The load level was possibly too low, and the test should preferrably be performed again with increased load levels.

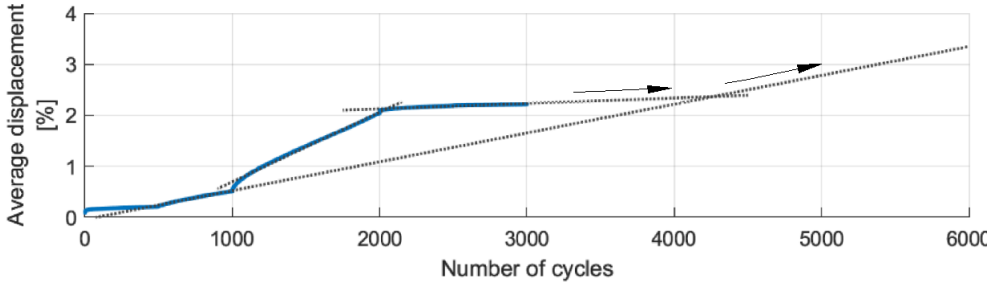

Figure 5.7: Average displacement test 4

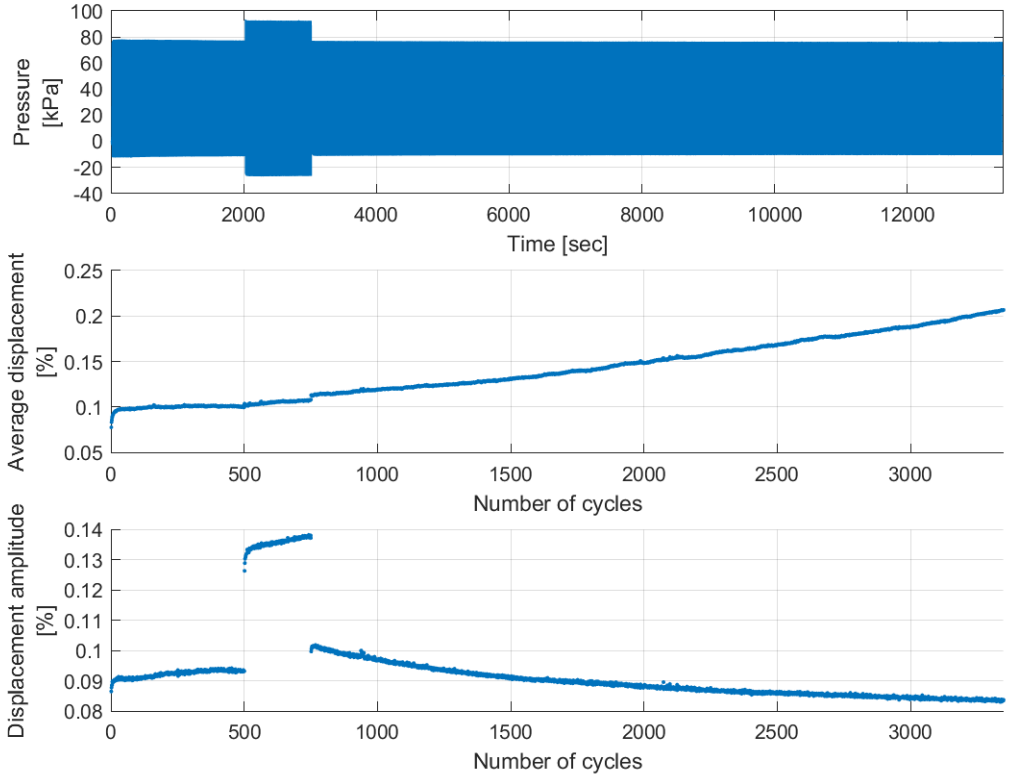

Figure 5.8: Normalized displacements of test 10

While tests 4 and 9 exhibit similar behaviour, the development of average and cyclic displacements of test 10 is different, as shown in Figure 5.8. The average displacement gradually increases with number of cycles during load parcels 2 and 3, and instead of stabilizing, the accumulation rate seems to increase. The displacement amplitude decreases during load step 3. This could indicate installation effects in combination with too small load amplitudes and set-up, and is discussed in Chapter 6. The pressure-displacement plots show oval shaped hysteresis loops. It should be noted that test 10 gives the largest capacity for the 3 mm push over of all the tests. Also, test 10 consolidated one extra day at the last consolidation

step.

5.1.2 Constant load amplitude

In tests 5, 6, 7 and 8 the load parcels were applied with constant load amplitudes and varying average loads. The average and cyclic displacements of test 5 are shown in Figure 5.9. The displacement amplitude in test 5 is approximately constant within each load step and almost the same in all the load steps with different average loads, except for load steps 4 and 8. Parcels 4 and 8 had zero average load and thus symmetric cyclic loading conditions. The average displacements increased rapidly before stabilizing in load steps 4 and 8, and the displacement amplitudes were significantly larger than for the other load steps.

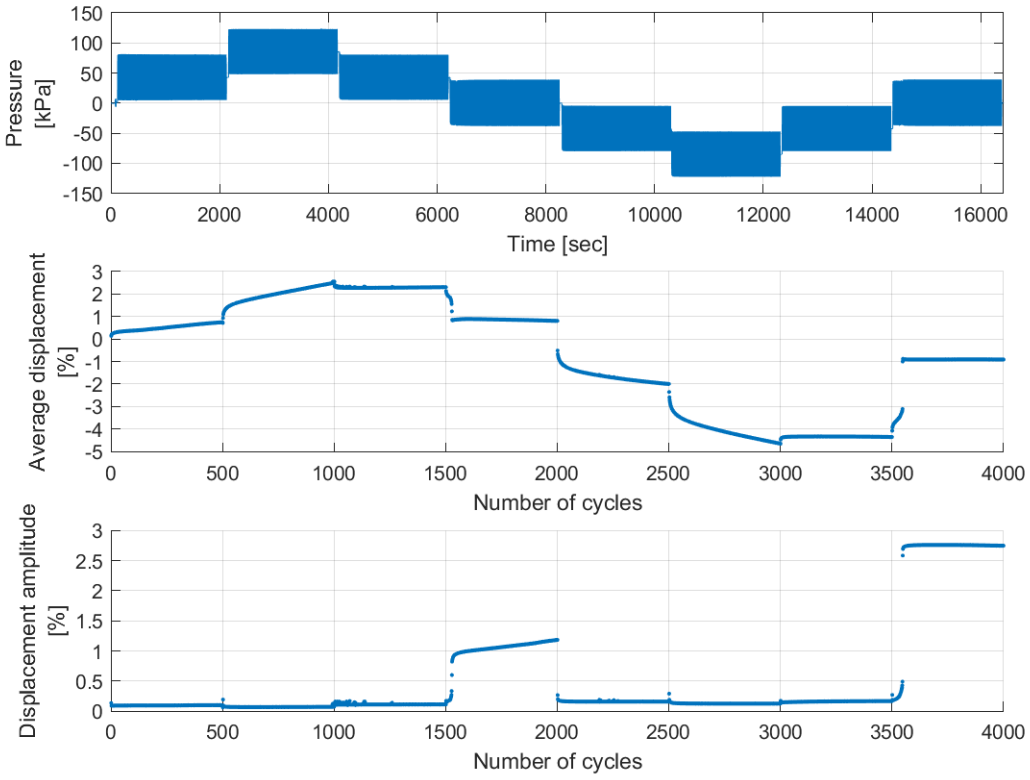

Figure 5.9: Normalized displacements of test 5

The average displacement of load steps 4 and 8 had a rapid change after approximately 20-50 cycles. After the sudden change, the displacement stabilized and remained almost constant for the remaining 450-470 cycles. During steps 4 and 8 the load curve became uneven and the displacement curve of the model pile was almost square, even though the load was applied with the sine waveform. This can be seen in the 20 second time interval from load step 4 shown in Figure 5.10. The secant stiffnesses for load steps 4 and 8 were significantly lower than the secant stiffnesses for the other load parcels, refer Appendix B.1.

Load steps 4 and 8 were the only steps with two-way cyclic loading during test 5. Figure 5.11 shows an example of the pressure-displacement plots where the hysteresis loop changes from the oval loop in the start to a s-shaped loop at the end.

The soft response observed in load parcels 4 and 8 was unexpected, as these were the two steps with the lowest applied load during test 5. The displacements increased suddenly from amplitudes of approximately 0.3% to nearly 3% within 2 cycles. At the same time the load curve became uneven. The displacement increase and pressure in step 8 is shown in Figure 5.12. These observations might indicate that a gap has developed between the model pile and soil and are further discussed in Chapter 6.

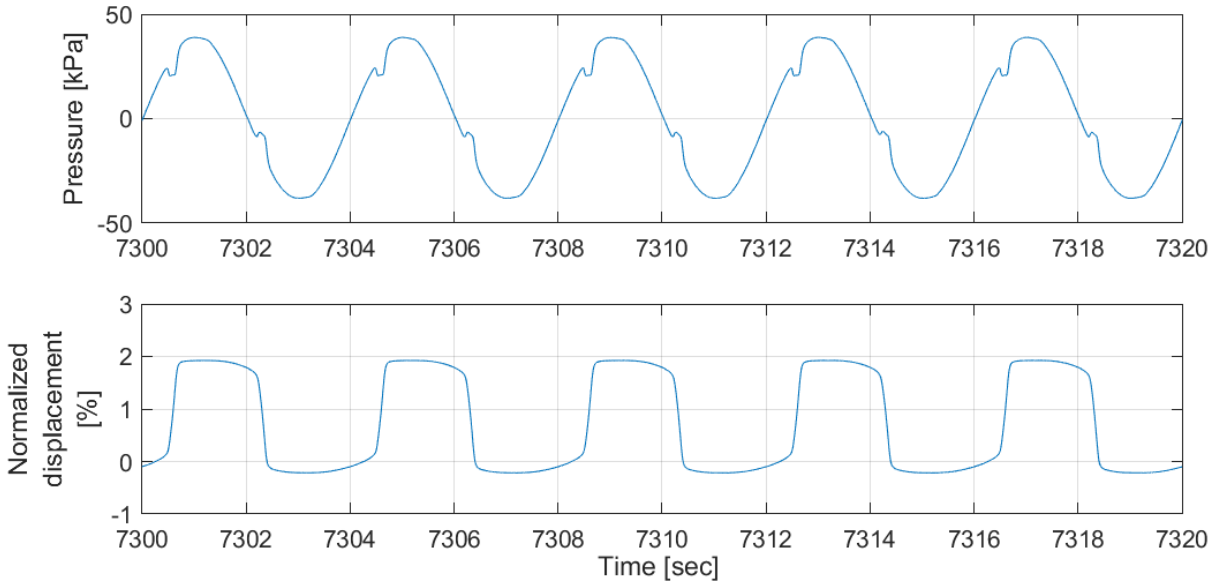

Figure 5.10: Test 5, load parcel 4: Normalized displacement and pressure.

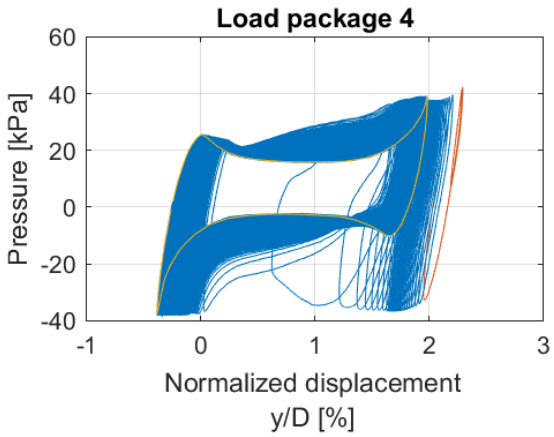

Figure 5.11: Pressure-displacement plot of test 5, load parcel 4

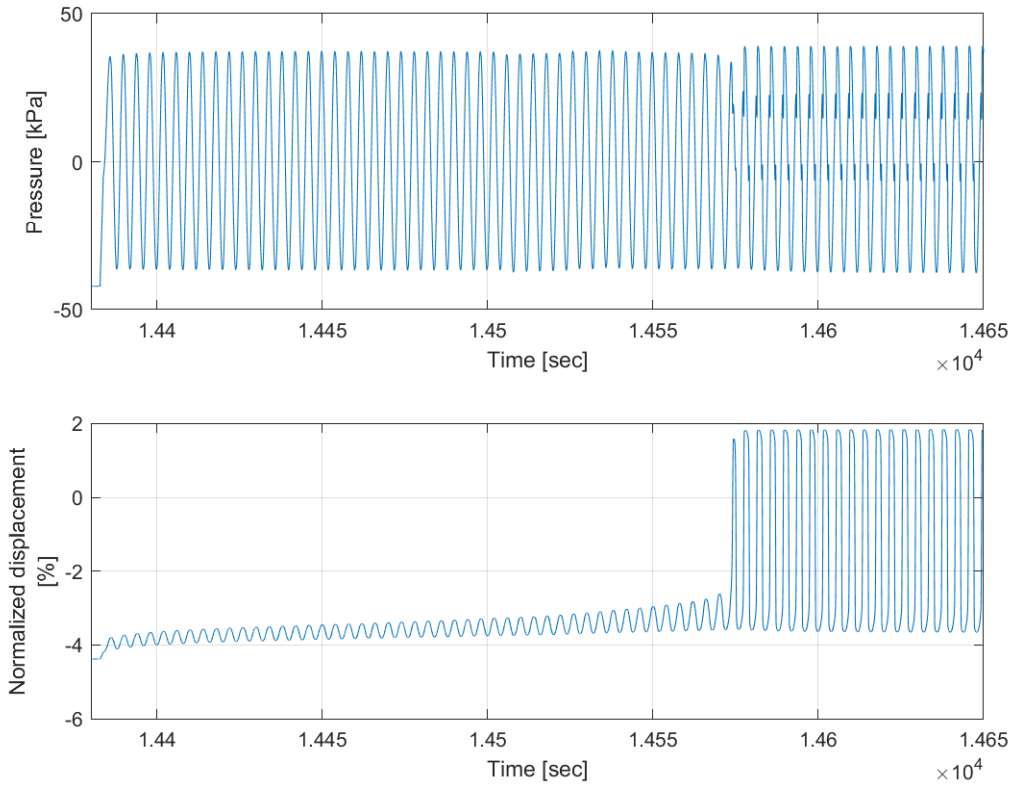

Figure 5.12: Normalized displacement and pressure of test 5, load step 8

Based on the observations in test 5, it was decided to run the same test again at a lower load level, which resulted in tests 7 and 8. Due to overheating of the MTS system, test 7 was automatically aborted at the end of load parcel 3, but the results from the three completed load parcels may be interpreted. Refer to Appendix B.1 for results of test 7. The displacement amplitudes in test 7 are nearly constant within each of the three load steps and remain at approximately the same level over the two first parcels, but increase slightly when the same load level is repeated in parcel 3. The average displacement stabilizes after approximately 50-200 cycles for all load steps, and is then constant or linearly increasing for the remaining cycles. The hysteresis loops are oval.

Test 8 had the same outline of load steps as test 7, and the displacements are presented in Figure 5.13. Displacement amplitudes remain approximately at the same level throughout the test, but increase between load parcels when the same load conditions are repeated. Average displacements seem to stabilize within the first 50-100 cycles of each load step and keep a constant level or linerarly increase or decrease for the the remaining cycles. The pressure-displacement plots show oval hysteresis loops.

Test 7 and parcels 1-3 of test 8 are identical and similar results are therefore expected. The two tests exhibit the same tendencies in behaviour, but differ considerably in achieved se-

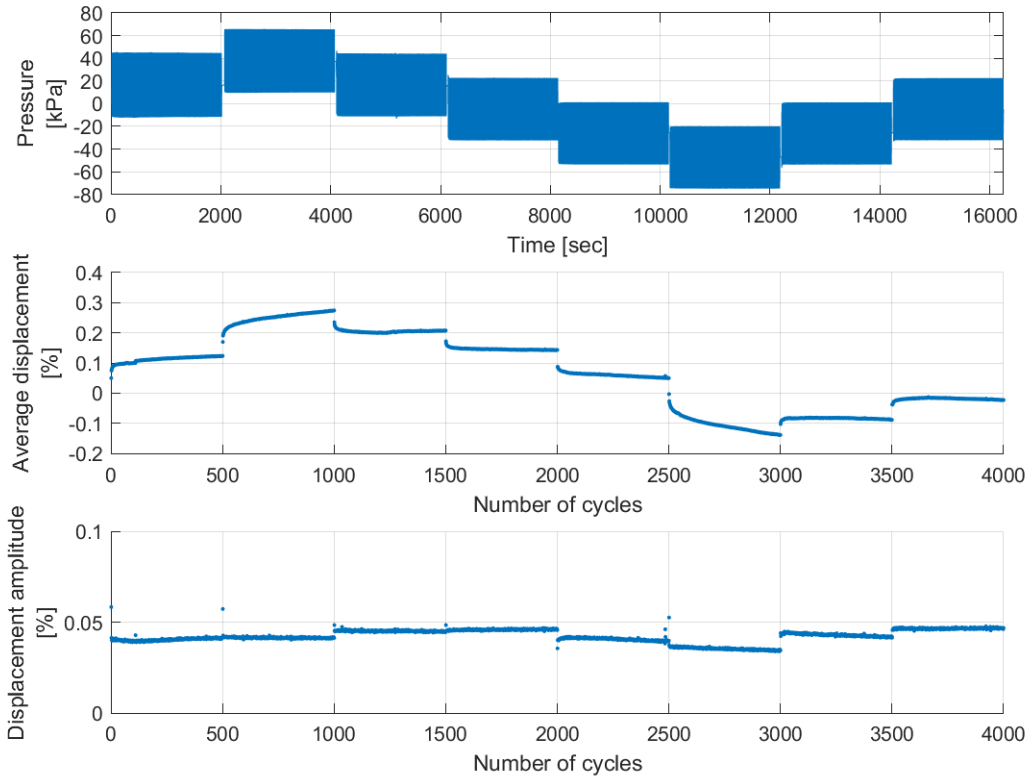

Figure 5.13: Normalized displacements of test 8

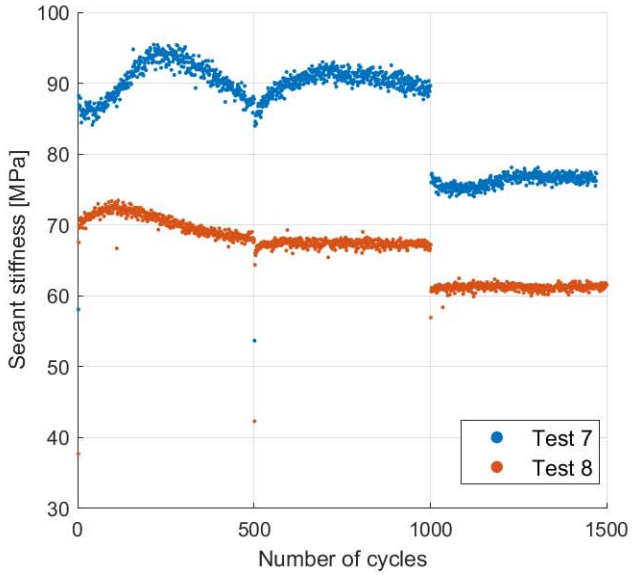

Figure 5.14: Secant stiffness during the first three load steps of tests 7 and 8.

cant stiffness, as seen in Figure 5.14. Secant stiffness of the first three load parcels of test 8 is approximately 60-70 MPa, while the corresponding load parcels of test 7 obtain a secant stiffness of 75-90 MPa. Tendencies are the same, but secant stiffness of test 8 is approximately 20% lower than in test 7. This can be a result of installation effects and is discussed further in chapter 6.

Test 6 was performed with different frequencies to evaluate drainage during testing. Half of the load steps were applied with frequency 0.05 Hz, the rest with 0.25 Hz. Displacements versus time and number of cycles are shown in Figure 5.15. The displacement amplitude is approximately constant within each load parcel, and the same for similar load parcels with the same frequency. The displacement amplitude increases when the frequency decreases from 0.25 Hz to 0.05 Hz. This is most likely a result of better accuracy of the MTS actuator for lower frequencies, as discussed in Section 6.4. The accumulation rate of average displacements relative to number of cycles increase when the frequency is lowered. When inspected in the diagram with average displacement vs. time it seems to be nearly unchanged. The secant stiffness decreases for lower frequency and increased load. No clear indication of drainage is observed.

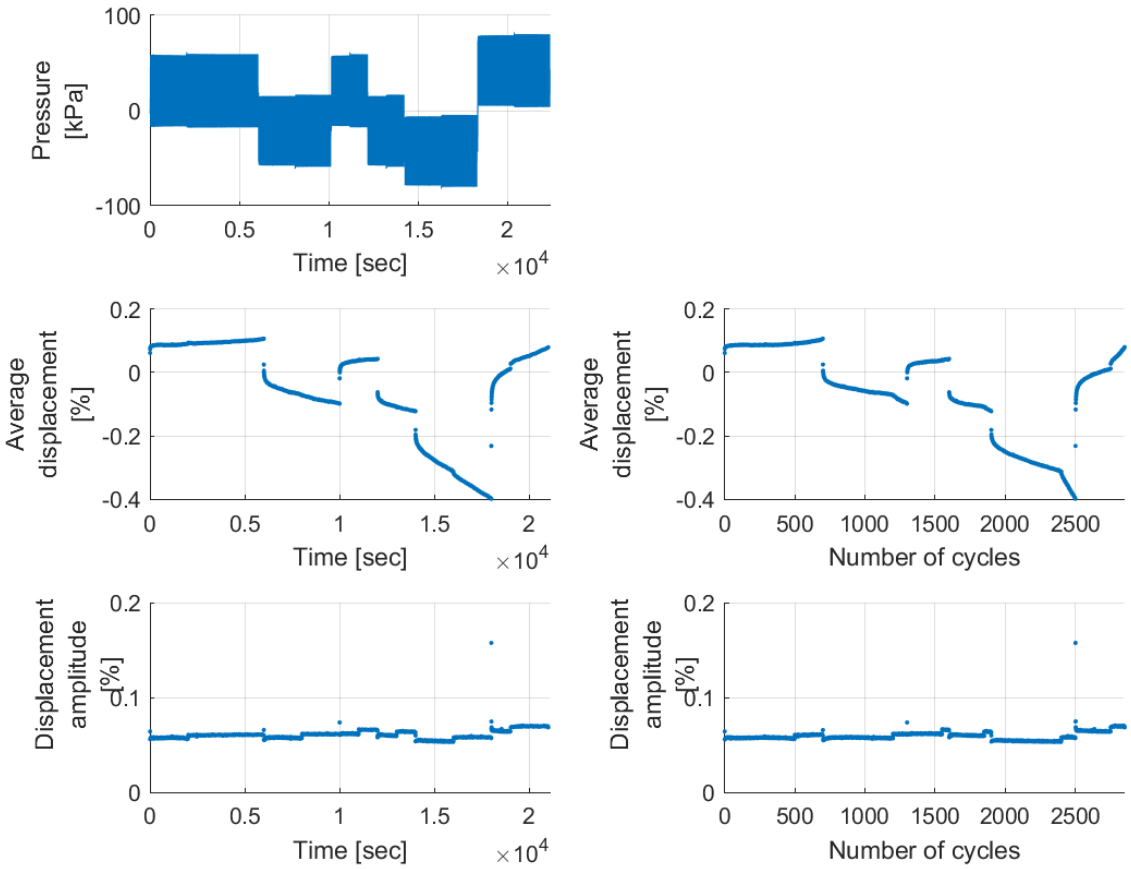

Figure 5.15: Normalized displacements of test 6

5.1.3 General observations

In general, the average displacement accumulates during the first part of the load steps before it stabilizes. After stabilization the accumulation rate is either zero or constant. The pressure-displacement plots are mostly oval shaped and open. The open hysteresis loops combines into a spiral shaped curve, as described in Section 2.3.1. Load step 3 in test 2 is an example of this response, as shown in Figure 5.16. Some of the tests show a more s-shaped hysteresis loop, appearing together with uneven displacement and load curves. This is further discussed in Chapter 6.

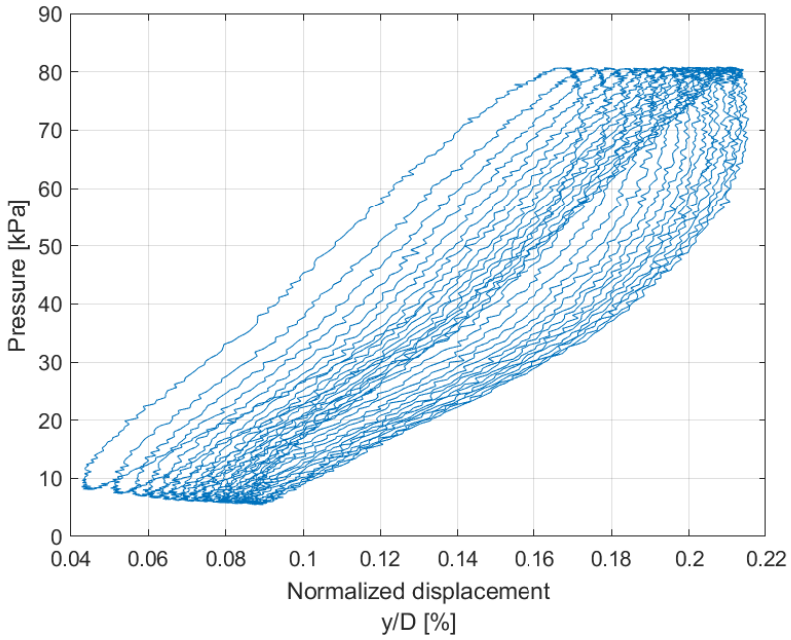

Figure 5.16: Pressure versus displacement during the first cycles of test 2, load step 3

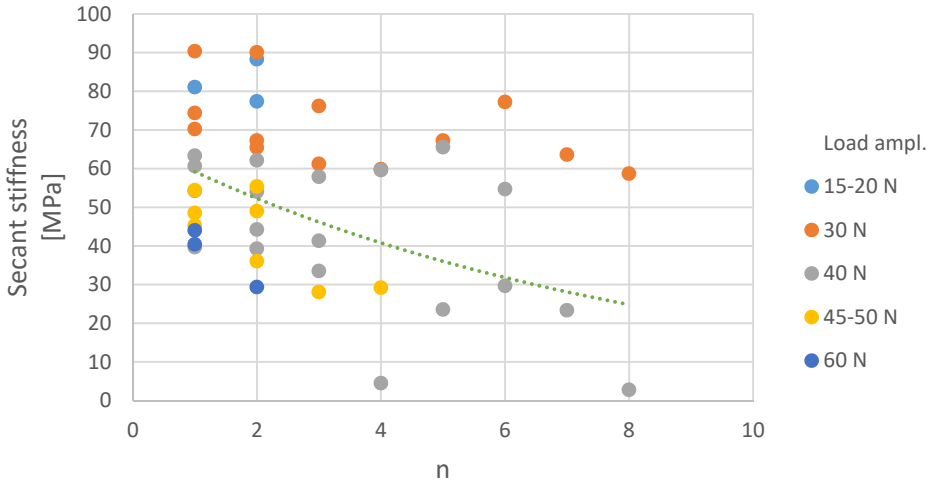

Figure 5.17: Development of secant stiffness

The diagram in Figure 5.17 shows the development in secant stiffness. Load parcels are arranged after load amplitudes, and numbered according to how many similar load parcels that have been applied earlier in the test. For instance in test 4, load steps 1, 5 and 6 have the same load amplitude, and are numbered 1, 2 and 3. The diagram shows as expected that the stiffness is largest for the first load parcel and decreases when repeated. The figure also shows that the secant stiffness decrease with increased load amplitude.

Figures 5.18, 5.19 and 5.20 present results of the 3 mm cycle together with the ultimate lateral bearing pressure p_u. The ultimate capacity is calculated according to Equation 2.1 with a ultimate bearing capacity factor of $N_p = 12$ assuming rough piles. The measured lateral resistance during the 3 mm cycle shows unsymmetric response for all the tests. Stiffer response in the material is seen for the first push over to 3 mm, than in the reverse direction. This is expected as the material first is loaded in the positive direction and therefore degraded when the displacement is applied in the reverse direction.

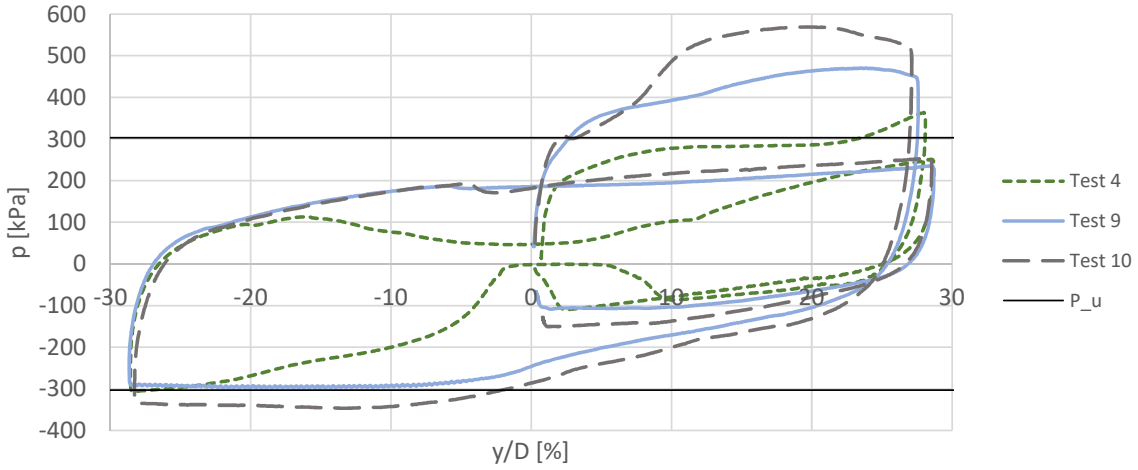

Figure 5.18: 3 mm cycle of tests 4, 9 and 10.

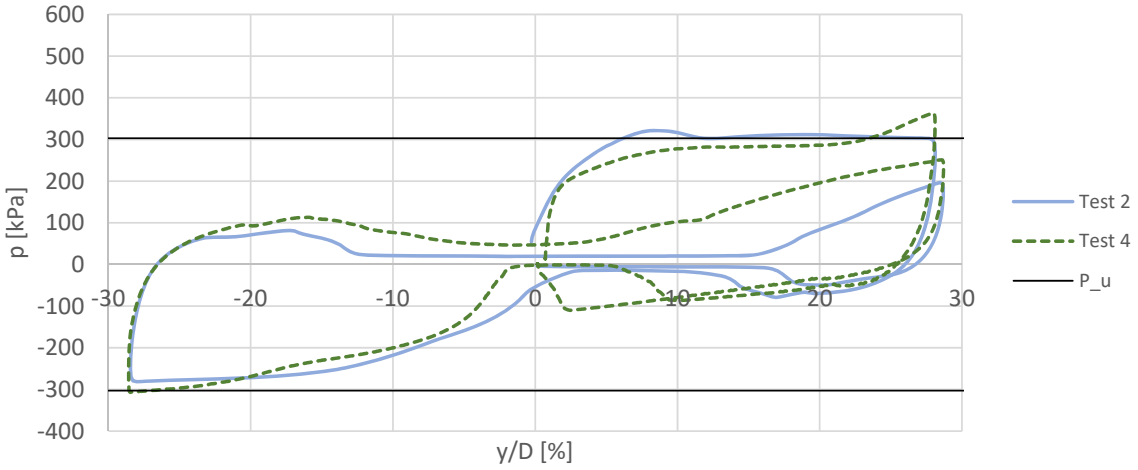

Figure 5.19: 3 mm cycle of tests 2 and 4.

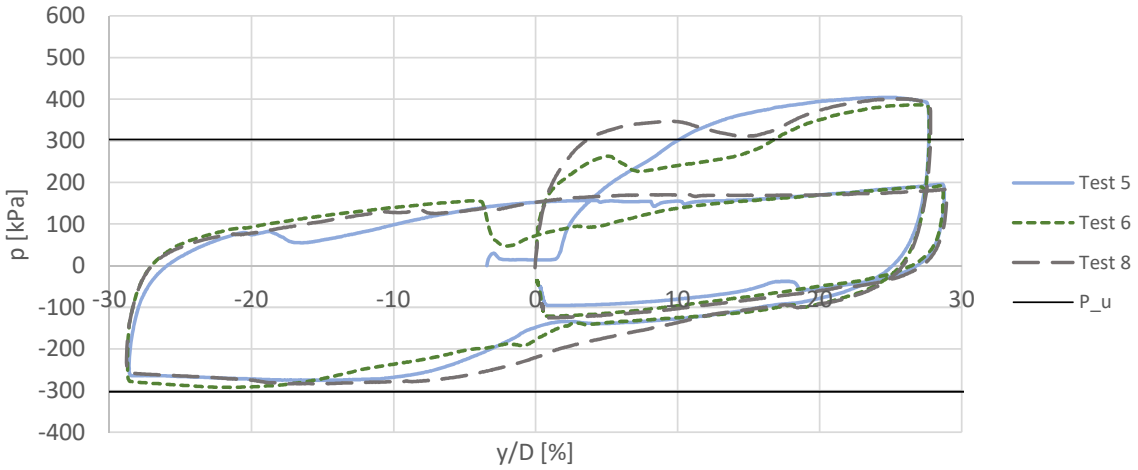

Figure 5.20: 3 mm cycle of tests 5, 6 and 8.

There are large differences in the achieved ultimate resistance between the different tests. As mentioned previously, test 10 reaches the largest capacity during the 3 mm cycle. In Figure 5.18, the 3 mm cycle of tests subjected to a constant average load is presented. Test 4 reaches approximately the value of p_u, while both tests 9 and 10 exceed this value by far.

The lateral resistance of the two tests performed over two days, test 2 and 4, generally keeps within the expected range of measured pressures in the first push over. These tests are shown in Figure 5.19. Note that the pressures, and hence the secant stiffnesses, are considerably reduced near the neutral position of the steel rod for these two tests. Tests 5, 6 and 8 were subjected to cyclic loading with varying average loads and constant load amplitudes. The 3 mm cycle is shown in Figure 5.20. The achieved lateral resistances are beyond the calculated ultimate lateral capacity, but fit better than the results of test 9 and 10.

5.2 Tests on North Sea samples

All test results are included in Appendix B.2.

The results from tests 11 and 12 performed on North Sea samples are presented in Table 5.1. The accumulated displacement is the average displacement at the end of the test. The secant stiffness is calculated from the three cycles of symmetric loading to 270 N. Maximum load is the maximum load measured during the last 3 mm cycle.

A large part of the average displacement accumulates during the first few minutes of the load history. After two minutes, nearly 50% of the total average displacement is accumulated. The first part of test 11 is shown in Figure 5.21.

Table 5.1: Results from tests 11 and 12 on North Sea samples

	Test 11 Irregular load history	Test 12 Rainflow counting
Accumulated displacement	-0.43 %	-0.15 %
Secant stiffness	200 MPa	265 MPa
Maximum load	1849 N	1858 N

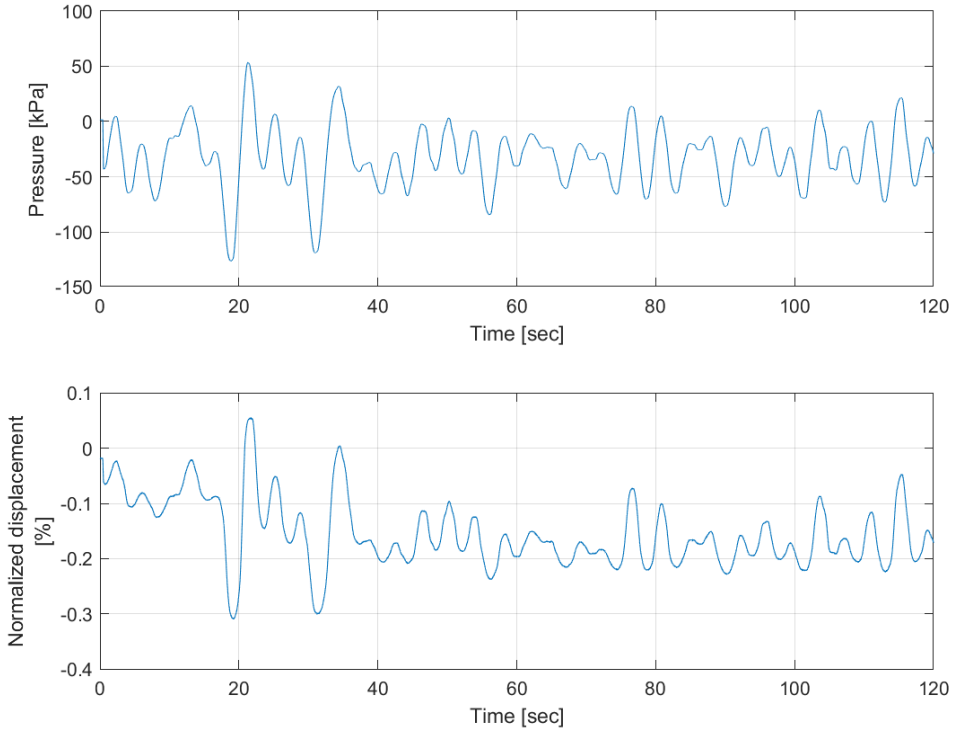

Figure 5.21: First 120 seconds of test 11

The 270 N cycles of tests 11 and 12 are shown in Figure 5.22. Test 11 obtains larger displacements than test 12. As observed in Figure 5.23, the displacements of test 12 follow the applied ramp waveform, while test 11 has a rapid change in displacement around the neutral. Also, small kinks are visible in the pressure curve of test 11. The 3 mm cycle is similar for the two tests and results in approximately the same maximum pressure.

Test 12 has less accumulated displacement and higher secant stiffness than test 11, which contradicts the prior expectations. These results were based on the cyclic load event and 270 N cycles, which both induced small displacements. The capacity measured during the 3 mm cycle is approximately the same for the two tests. This indicates that the unexpected results may be caused by installation effects. The results are further discussed in Chapter 6.

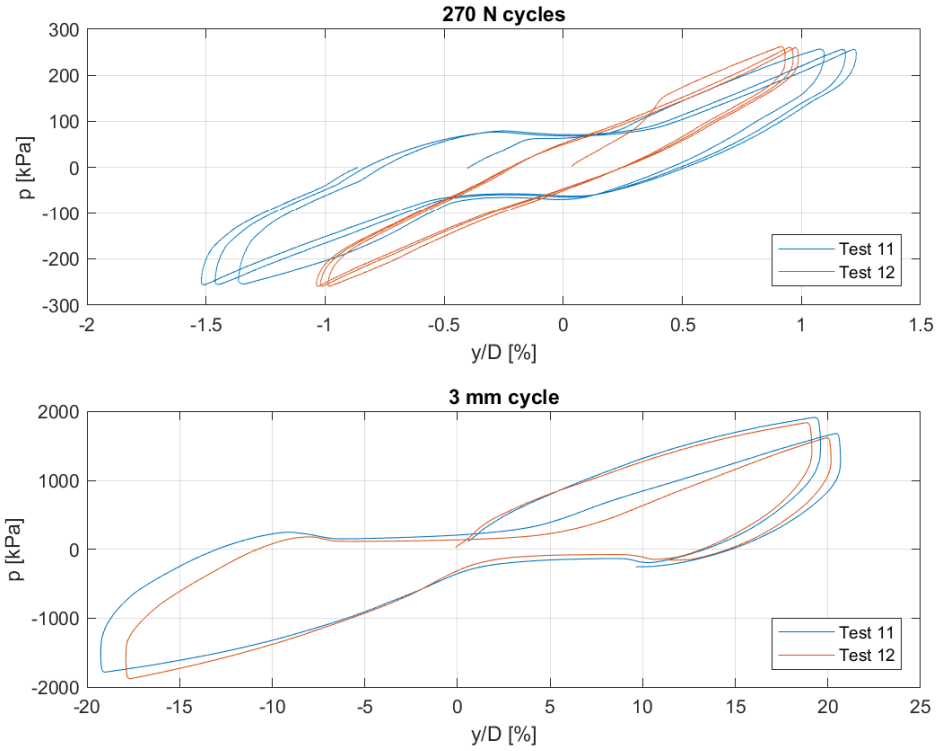

Figure 5.22: 270 N and 3 mm cycles of tests 11 and 12

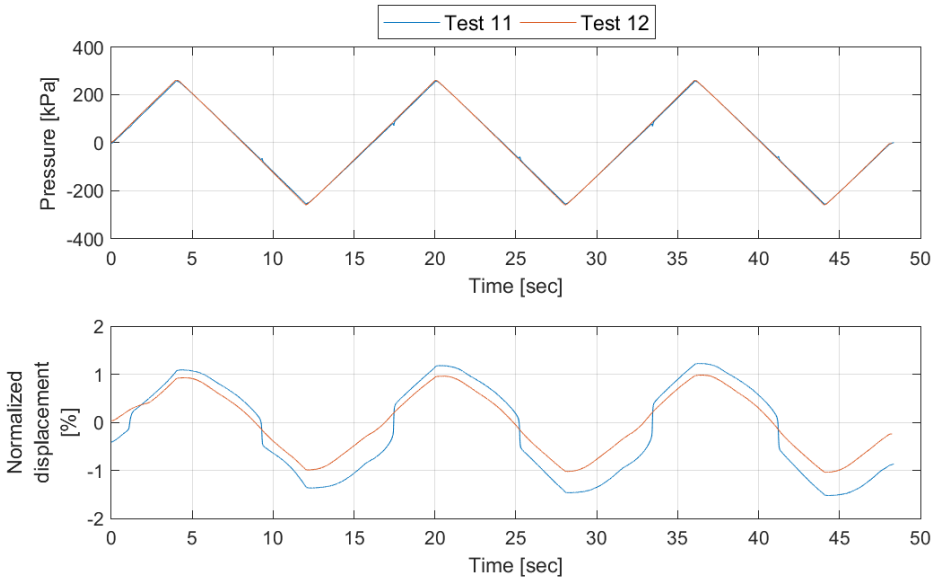

Figure 5.23: 270 N cycles

5.3 Dummy tests

All results from the dummy tests are available in Appendix B.3. During these tests tuning parameters were determined and preparation for load control performed.

Chapter 6

Discussion

6.1 Kaolin specimens

The behaviour seen in the test results is generally as expected according the different loading conditions. Tests 4, 9 and 10 were subjected to cyclic loading with constant average loads. Tests 4 and 9 have similar results. Increased load amplitude causes an increase in both the displacement amplitude and the average displacement. When the load amplitude decreases to a lower load level, the average displacement remains constant at its current level, as seen previously in Figure 5.6. The displacement amplitude follows the variation of the load amplitude between parcels. In test 9, the displacement amplitude keeps approximately constant within each load step after stabilization, while in test 4 it varies considerably. Different behaviour is observed in the results of test 10. The average displacement continues to increase after reducing the load in step 3 and does not seem to stabilize. The displacement amplitude gradually reduces during the same parcel, indicating increased strength. This is discussed further in Sections 6.1.3 and 6.1.5.

Tests 5, 6 and 8 were subjected to cyclic loading with constant load amplitudes. The results show that the displacement amplitudes remain approximately the same when the average load amplitudes change for the different load steps, while the average displacements follow the variation. This behaviour is presented previously in e.g. Figure 5.13. Exceptions to the main tendencies are discussed in Section 6.4.

6.1.1 Comparison with contour diagrams

Cyclic contour diagrams constructed from DSS tests by Carotenuto et al. (2018) on Prestige-NY kaolin clay are presented in Appendix E. The results of the p-y tests generally show the same tendencies as the contour diagrams. The accumulation of displacements is primarily dependent on the applied cyclic load amplitude and number of cycles. The average displacement is governed by the average load. This is the expected response according to the cyclic contour diagrams, which are described in Section 3.1. The nearly horizontal lines of γ_{cy} in the DSS contour diagrams indicate that the cyclic shear strain is nearly independent of the average shear stress level in the small strain range. In Figure 6.1 p-y test results are included in the contour diagrams using the scaling method by Zhang et al. (2017) described in Section 3.3.

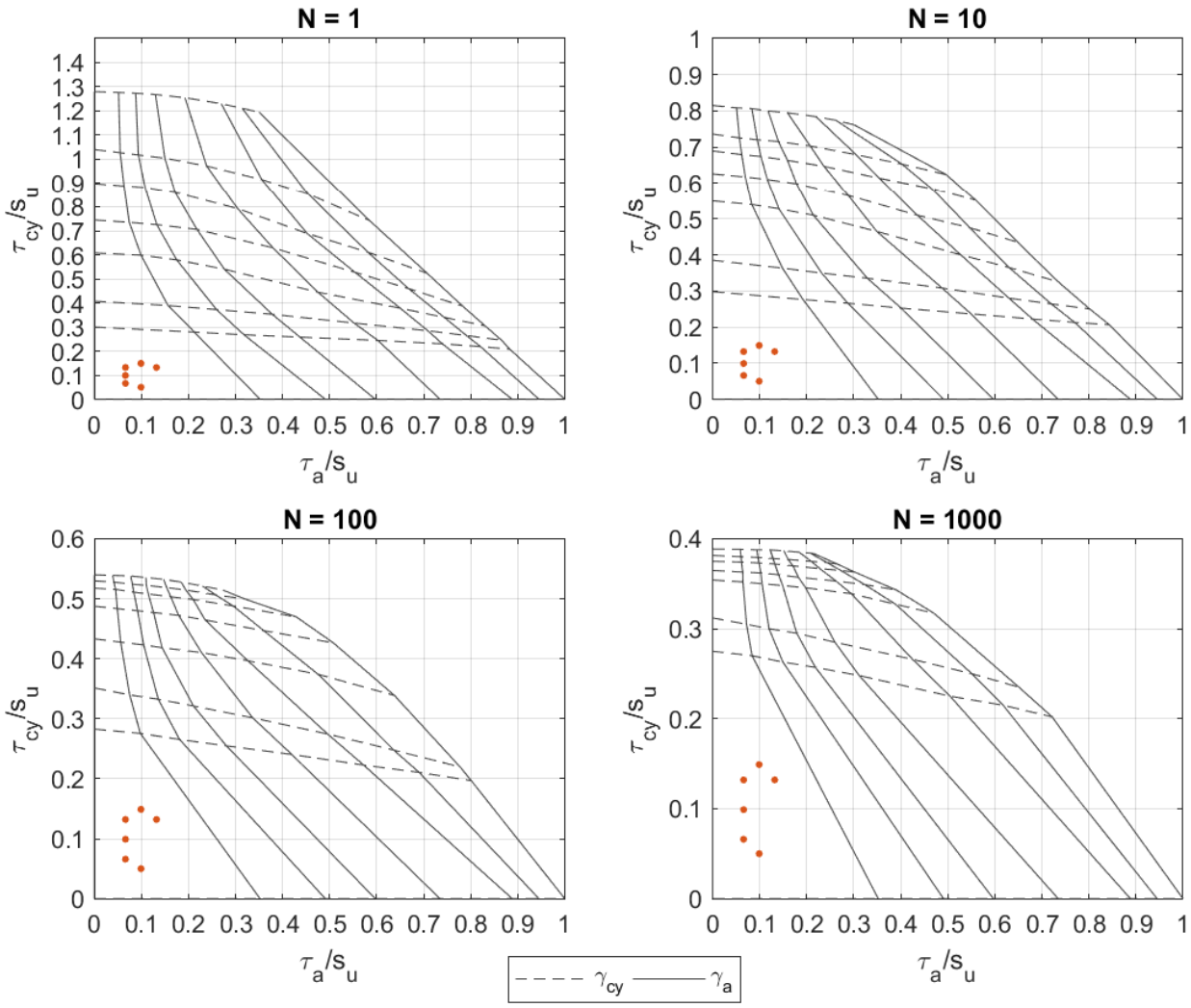

Figure 6.1: Scaled p-y test results in cyclic contour diagrams.
γ_{cy} = 0 - 0.05 - 0.1 - 0.25 - 0.5 - 1.0 - 2.5 - 15%, γ_a = 0 - 0.1 - 0.25 - 0.5 - 1.0 - 2.5 - 5.0 - 15%.

The average and cyclic displacement components after 1, 10, 100 and 1000 cycles are inspected for the first load parcel of all tests. As many of the load steps have less than 1000 cycles, displacements of the last cycle of the parcel is used instead, i.e. cycle 500. In general, displacements have stabilized during the first 200 cycles, so it is considered acceptable to apply the displacements accumulated after 500 cycles.

According to the contour diagrams in Figure 6.1, the expected range of cyclic shear strains for the applied load parcels are $\gamma_{cy} < 0.05\%$. The average shear strains are expected to be in the range of $\gamma_a < 0.1\%$. A simple check reveals that the cyclic and average shear strains of all tests after 1, 10, 100 and 1000(500) cycles in the first load parcel are within this range, except test 5 which has larger average shear strains at both cycle 100 and 500. Strains that are larger than expected from the contour diagrams could be a result of several aspects, e.g. installation effects or time effects such as creep, relaxation or drainage.

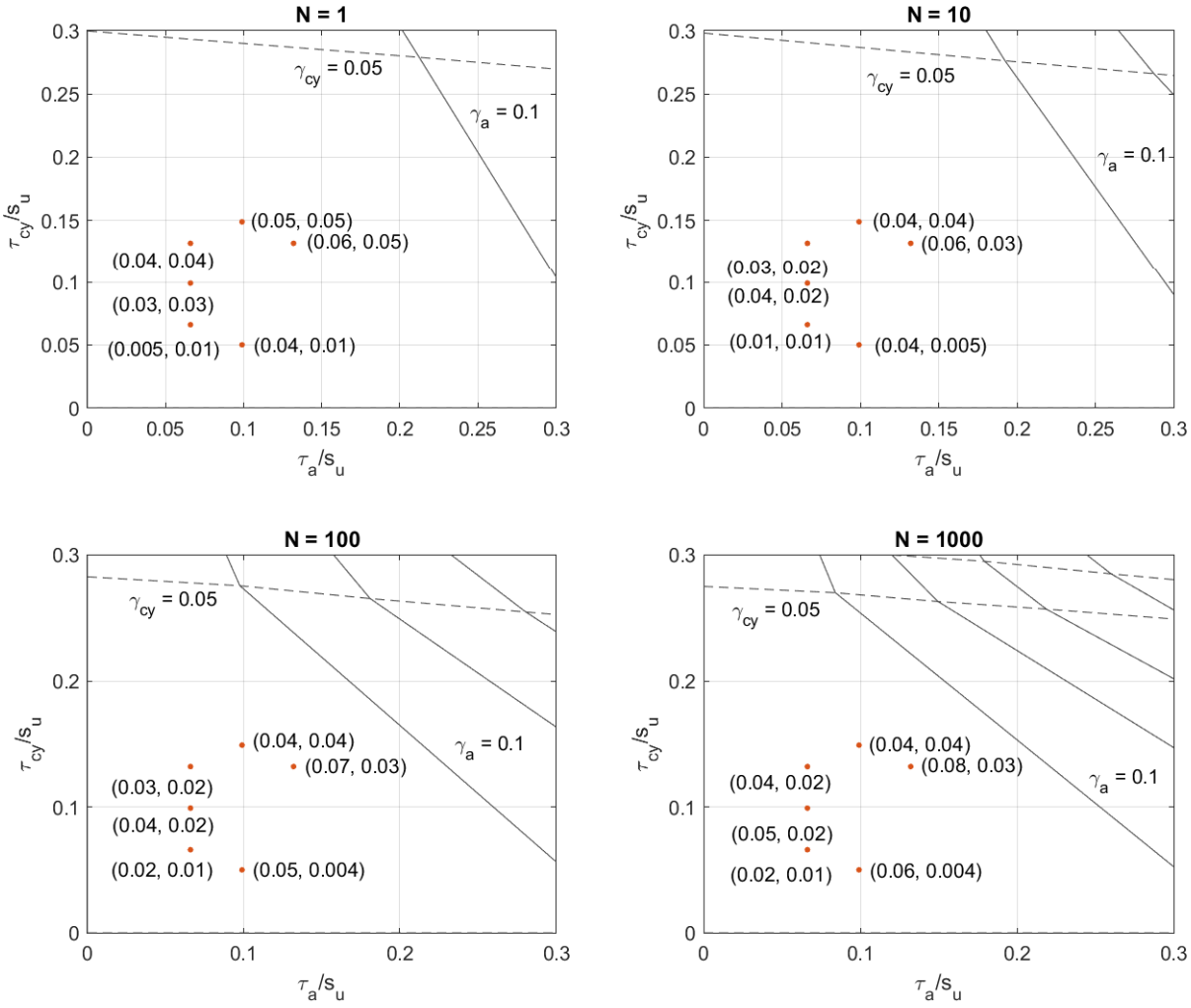

Figure 6.2: Cyclic contour diagrams marked with the shear strains (γ_a, γ_{cy}) of scaled p-y test results

In Figure 6.2, results from the p-y tests are shown in the small strain range of the contour diagrams. Each point of average and cyclic shear stresses are marked with the corresponding average and cyclic shear strains (γ_a, γ_{cy}). Test 5 is not included as the load levels are the same as in test 4, and the strains exceed the estimated range. As seen in the figure, the cyclic shear strains increase as expected with increased cyclic shear stress for all the points. The cyclic shear strain decrease with number of cycles, which is not the typical response for cyclic loading under undrained conditions. As seen in the figure, the average shear strains for most of the tests increase with number of cycles as the average displacements accumulate. Generally the response can be described by the corresponding contour diagrams and the results are therefore considered plausible.

Only the first load parcels are included in Figures 6.1 and 6.2. If other load parcels should be included, accumulated pore pressures would have to be considered. Repeated parcels or load steps with reduced load levels can not be compared to the contour diagrams as conditions of unloading is not taken into account by the diagrams.

6.1.2 Drainage

Drainage is evaluated based on the method proposed by Zhang et al. (2018), as described in Section 3.2. Equations and diagrams used in the calculations are also presented there. Relevant parameters are given in Table 6.1.

Table 6.1: Parameters for drainage estimate

Coefficient of consolidation	c_v	$[m^2/s]$	0.2e-6
Diameter of steel rod	D	[m]	0.01

$$t = \frac{D^2}{c_v} T \tag{6.1}$$

$$t_p = \frac{D^2}{c_v} T_p \tag{6.2}$$

The time intervals the kaolin specimens have to be subjected to static loading for different values of normalized time T are calculated by Equation 6.1. The variation of normalized time is shown previously in Figure 3.2, and includes whether the conditions can be assumed undrained, partly drained or fully drained. Table 6.2 shows the normalized time T together

with the calculated time for the different drainage conditions. To assume drained conditions, the kaolin specimen must be subjected to static loading for minimum 1 hour and 45 minutes according to this method by Zhang et al. (2018).

Similarly, the cycle periods for different normalized loading periods T_p are calculated according to Equation 6.2. The normalized loading periods are shown previously in Figure 3.3, and include whether the conditions can be assumed undrained, partly drained or fully drained within a cycle. Table 6.3 presents the normalized loading period T_p and the corresponding cycle periods for the different drainage conditions. For a cycle period less than 25 seconds, nearly fully undrained conditions can be assumed within a load cycle.

Table 6.2: Time estimates for different drainage conditions under static loading

	Normalized time T	Duration t [hh:mm:ss]
Undrained	0	00:00:00
	0.1	00:00:50
	0.3	00:02:30
	0.7	00:05:50
	1.5	00:12:30
	3.1	00:25:50
Drained	12.6	01:45:00

Table 6.3: Estimatied cycle periods for different drainage conditions

	Normalized loading period T_p	Cycle period t_p [hh:mm:ss]
Undrained	0.05	00:00:25
	0.5	00:04:10
	1.0	00:08:20
	2.4	00:20:00
	4.9	00:40:50
	9.7	01:20:50
	24.3	03:22:30
Drained	48.5	06:44:10

The tests in this study are subjected to non-symmetric cyclic loading, i.e. cyclic loading with a static component. Cycle periods and durations under constant average loads are given in Table 6.4. A typical load parcel has 500 cycles and a duration of approximately 33 minutes. As mentioned previously, the elapsed time sufficient to correctly assume drained conditions under static loading is approximately 1 hour and 45 minutes. Hence, for tests 4, 9 and 10 that were subjected to a constant average load during the entire test, drained conditions can be assumed. For the remaining tests the average load was varied throughout the test. The estimate is therefore based on the duration of the longest load parcel within each test. Based

Table 6.4: Cycle periods and durations under static load

Test	Maximum duration under constant average load [hh:mm:ss]	Maximum cycle period [sec]
2	00:33:20	4
4	03:20:00	4
5	00:33:20	4
6	01:40:00	20
8	00:33:20	4
9	03:20:00	4
10	03:50:00	4

on these time intervals, partly drained conditions can be assumed for the tests with varying average load according to Table 6.2.

The specimen is not sealed when installed in the apparatus and drainage towards the specimen's ends can be expected. As described in Section 2.3.2, non-symmetric cyclic loading may induce pore pressures and seepage flow from the compression side and around the steel rod. If a small gap between the model pile and soil has developed during cyclic loading, water might also drain towards the steel rod.

Cyclic contour diagrams are valid for tests where almost fully undrained conditions within a single cycle can be assumed. Based on the method by Zhang et al. (2018), the cycle period has to be less than 25 seconds to assume undrained conditions, as seen in Table 6.3. In all of the tests, except test 6, the load was applied with a frequency of 0.25 Hz corresponding to a cycle period of 4 seconds. Some load steps in test 6 were applied with frequency 0.05 Hz and thus a 20 second cycle period. Accordingly, undrained conditions within a cycle may be assumed, and contour diagrams can be used for validation of the test results.

6.1.3 Comparison with DSS test results

Results from the p-y tests have been evaluated using the scaling method by Zhang et al. (2017), described in Section 3.3. DSS test results are provided from the report by Carotenuto et al. (2018). Key parameters are given in Table 6.5 and the equations are described in Section 3.3.

Pressure and displacements measured during the first push over in the 3 mm cycle, as well as scaled results from the DSS test, are shown in Figure 6.3. The measured lateral resistances are larger than expected and exceed the ultimate lateral bearing pressure p_u for most of the

Table 6.5: Parameters for comparison with DSS test results

Ultimate bearing capacity factor	N_p	[-]	12
Undrained shear strength	s_u	[kPa]	25
Ultimate lateral bearing pressure	p_u	[kPa]	303
Scaling coefficients	ξ_1	[-]	2.8
	ξ_2	[-]	1.6

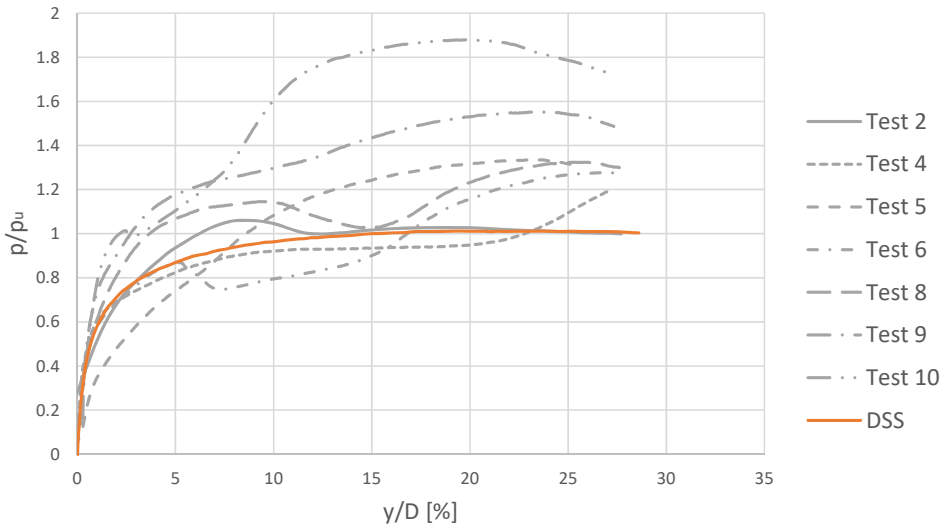

Figure 6.3: Test results of all tests compared to scaled DSS results

tests. The measured values of p/p_u are expected to approximately follow the scaled curve from the DSS test, and not exceed a value of 1.0 during this first push over to 3 mm. The ultimate lateral bearing pressure is calculated according to Equation 2.1. It is dependent on the undrained shear strength and the bearing capacity factor, which varies from 9 for fully smooth to 12 for fully rough interface conditions. Rough piles are assumed and thus the maximum factor of $N_p = 12$ is used in the calculations. Therefore, the interpretation is that the large lateral resistances indicate increased soil strength in zones close the pile. This is further discussed in Section 6.1.5.

The 3 mm cycle is applied after several hours of cyclic loading. The increased strength could be a result of consolidation effects in the affected soil due to the applied average load. As mentioned previously, the static component of non-symmetric cyclic loading may cause an increase in pore pressures and thus seepage flow in the soil. The estimate of drainage in Section 6.1.2 also suggests partly drained or drained conditions for all the tests based on the duration of the applied average load.

In Figure 6.4, the tests with constant average load conducted over one day are plotted together with the DSS results. Both tests 9 and 10 had a constant average load of 30 N. These

two tests gave the largest lateral resistances out of all the tests during the 3 mm cycle, and reached significantly larger resistances than the theoretically calculated ultimate lateral bearing pressure p_u. The outline of loading for test 10 was different compared to the rest of the tests. While most of the tests were conducted with load parcels of 500 cycles, load step 3 of test 10 was continued for 2600 cycles. The displacement accumulation rate is increasing during load step 3, as shown previously in Figure 5.8. In the same figure one can also observe that the displacement amplitude is decreasing during load step 3, indicating an increase in shear strength.

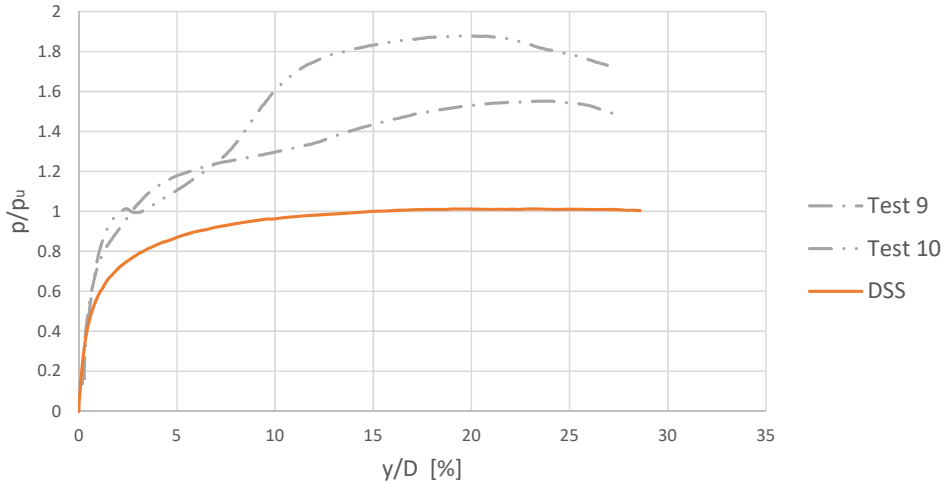

Figure 6.4: Test results of tests subjected to a constant average load compared to scaled DSS results

The tests loaded with constant amplitude and varying average are plotted together with scaled DSS results in Figure 6.5. These tests show a slightly better fit than the tests with constant average load, but the measured lateral resistances are still larger than expected. Test 5 deviates from the rest of the tests for small strains and has a softer respons in the range of normalised displacements below 5%. As described in Chapter 5, test 5 had increased displacements for two of the load steps, and the soft response could be due to cyclic degradation of the soil or development of a gap behind the pile. In Section 6.4, gapping is discussed further.

Tests 2 and 4 were performed over two days and the results of the 3 mm push over are shown in Figure 6.6. In test 2 there was no dominant loading or drainage direction, as the loading direction was changed after each load step. That may be the explanation why the lateral resistance measured in the push over to 3 mm of test 2 shows a much better fit with the DSS test result than the other tests. The pore pressures generated by cyclic loading on the first day are assumed to be fully dissipated before the test continued the second day. In test 2

the results did not suggest any significant remoulding or gap during cyclic loading, so the specimen is assumed to be intact when testing resumes.

Also in test 4 the results coincide much better with the DSS results, but that questiones the explanation to the high resistances reached in several of the other tests. If the high lateral resistances were due to consolidation effects, one would expect to see similar results also for test 4 which was subjected to a constant average load, even if the 3 mm cycle was applied one day after cyclic loading.

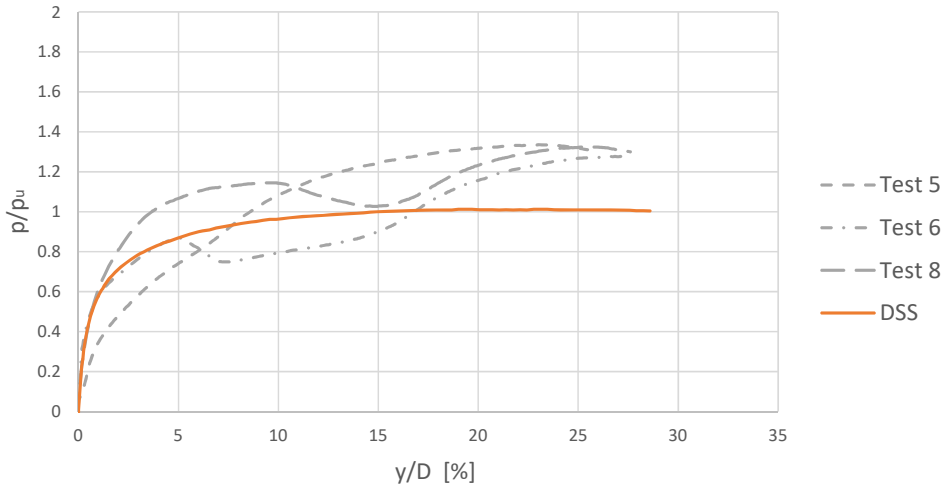

Figure 6.5: Test results of tests subjected to a constant load amplitude compared to scaled DSS results

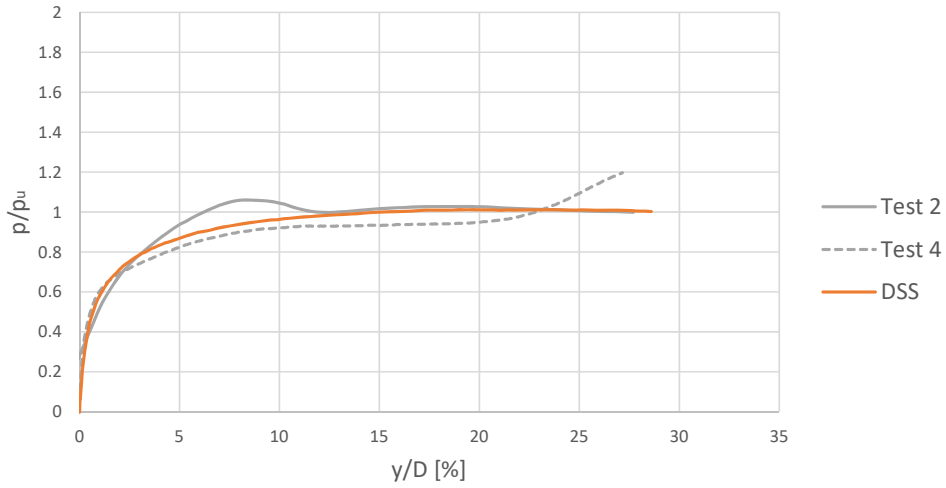

Figure 6.6: Test results of tests performed over two days compared to scaled DSS results

In the diagrams of the 3 mm cycle in Figures 5.18, 5.19 and 5.20, one can observe that the response is not symmetric for the positive and negative displacements. This is expected as the soil will already be degraded due to the first 3 mm push over when the reverse displacement is applied. Figure 6.7 shows pressure and displacement measured in the 3 mm cycle from 0 to -3 mm together with the same DSS test results. The measured resistances are expected to

be below the ultimate resistance indicated by the DSS results, as the DSS test represents the initial push over on intact material. For the same reason, the initial parts of the resistance curves show a softer response than the DSS result.

Pressures presented in Figure 6.7 show as expected a softer response than for the first part presented in Figure 6.3, but several of the tests reach or exceed the ultimate lateral bearing pressure also in the negative displacement push over, indicating that the undrained shear strength has increased also here.

Figure 6.8 shows pressure and displacement during the 3 mm cycle of tests 9 and 10 from 0 to -3 mm. Tests 5, 6 and 8 are shown in Figure 6.9 and tests 2 and 4 are shown in Figure 6.10.

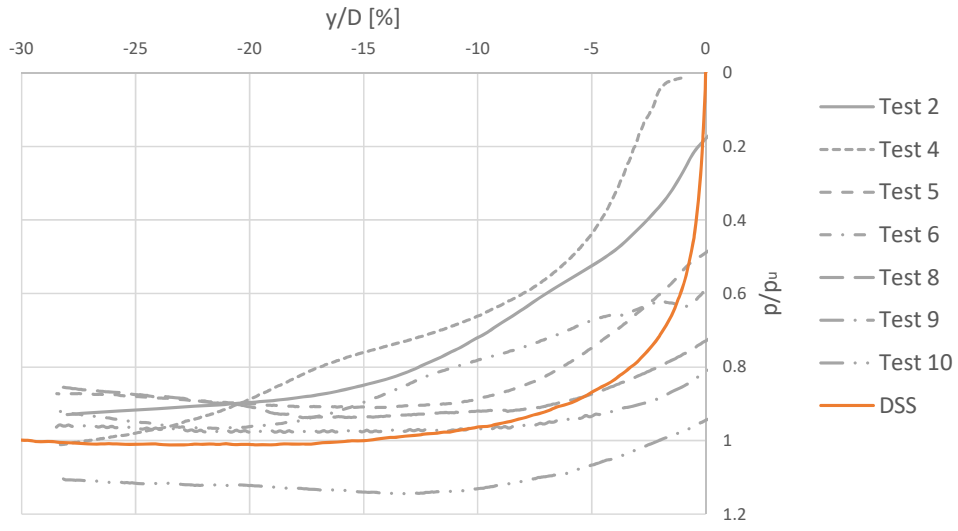

Figure 6.7: Test results of all tests compared to scaled DSS results

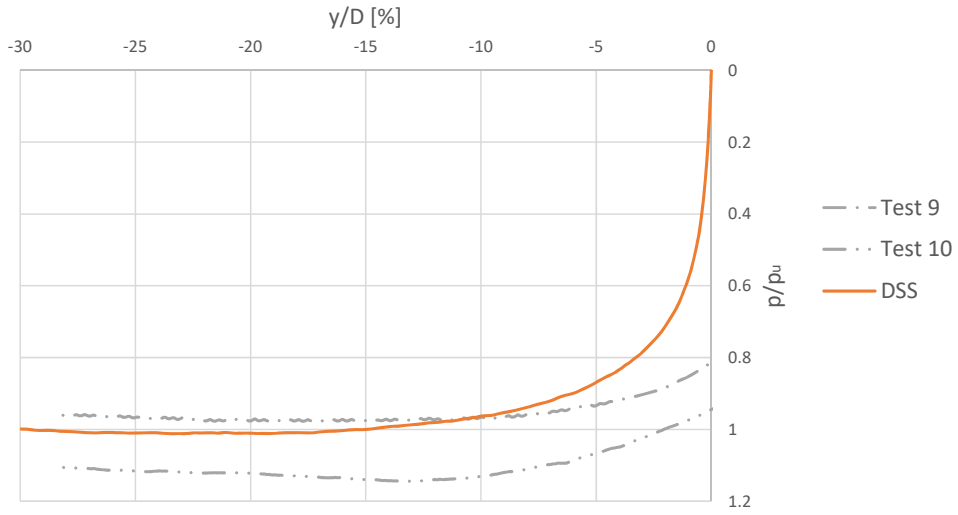

Figure 6.8: Test results of tests subjected to a constant average load compared to scaled DSS results

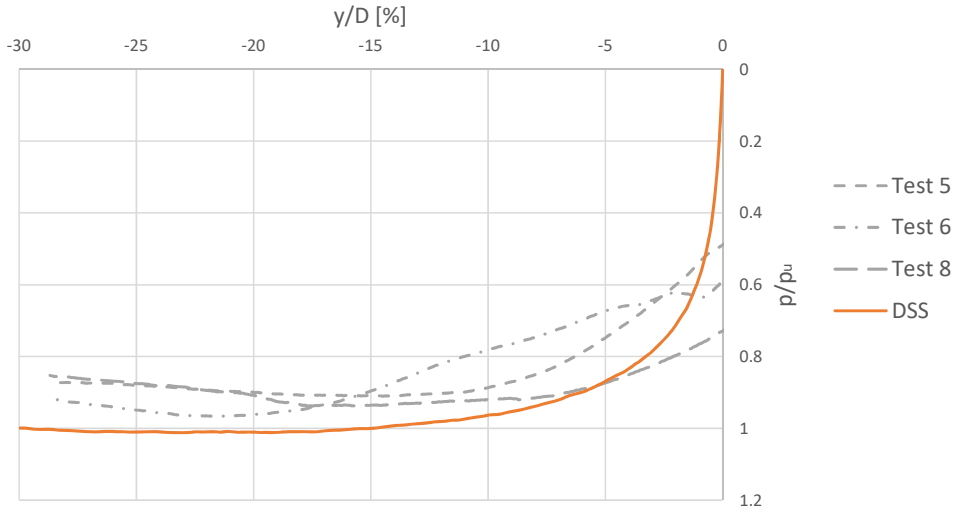

Figure 6.9: Test results of tests subjected to a constant load amplitude compared to scaled DSS results

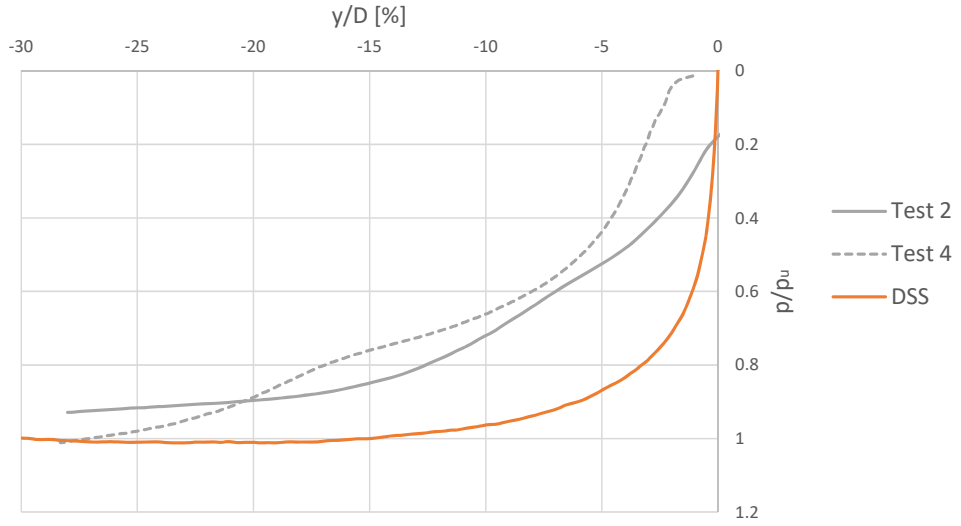

Figure 6.10: Test results of tests performed over two days compared to scaled DSS results

In former tests performed with the p-y device, the ratio between lateral resistances measured during the first and second amplitude, calculated according to Equation 6.3, has been 130% in average. Former DSS tests have shown a ratio of 120% in average. Table 6.6 shows the measured lateral resistances at the first and second amplitude for the tests in this study. The ratio calculated for tests 2 and 4 is 116% in average, approximately at the same level as shown in former DSS tests. Test 5, 6 and 8 were subjected to cyclic loading with varying average load. These tests have a ratio of 130-140%, approximately the same ratio as the former p-y tests. Test 9 and 10 were loaded with cyclic loading with a constant static component, and these two tests have the largest ratio of lateral resistances measured during the two displacement amplitudes, approximately 160% in average.

When testing the kaolin specimens, constant average loads were always applied in the positive direction, and varying average loads were consistently first applied in the positive direction. The ratios in Table 6.6 supports the assumption that constant average loads generate a significant increase in shear strength in the compression zone of the specimens. This is further evaluated by performing an OCR correction in Section 6.1.5.

$$Ratio = \frac{p_{+3mm}}{p_{-3mm}} \tag{6.3}$$

Table 6.6: Measured lateral resistance during the 3 mm cycle

Test	+3mm [kPa]	-3mm [kPa]	Ratio
2	321	281	114%
4	363	307	118%
5	404	276	146%
6	387	293	132%
8	401	284	141%
9	470	298	158%
10	569	347	164%

6.1.4 Comparison with centrifuge test results

An overview with results from all the tests compared to centrifuge test data is presented in Figures 6.11, 6.12 and 6.13. Details and equations are described in Section 3.4. Relevant parameters are given in table 6.7.

Table 6.7: Parameters for comparison with centrifuge test results

Ultimate bearing capacity factor	N_p	[-]	12
Undrained shear strength	s_u	[kPa]	25
Small strain shear modulus	G_{max}	[MPa]	7.76

Figure 6.11 shows the normalized secant stiffness at steady state, $K_{sec,ss,norm}$, which is normalized by the ultimate bearing capacity factor and undrained shear strength. The two outlying points of test 5 are load steps 4 and 8. The secant stiffnesses of the tests are overall lower compared to the centrifuge test results.

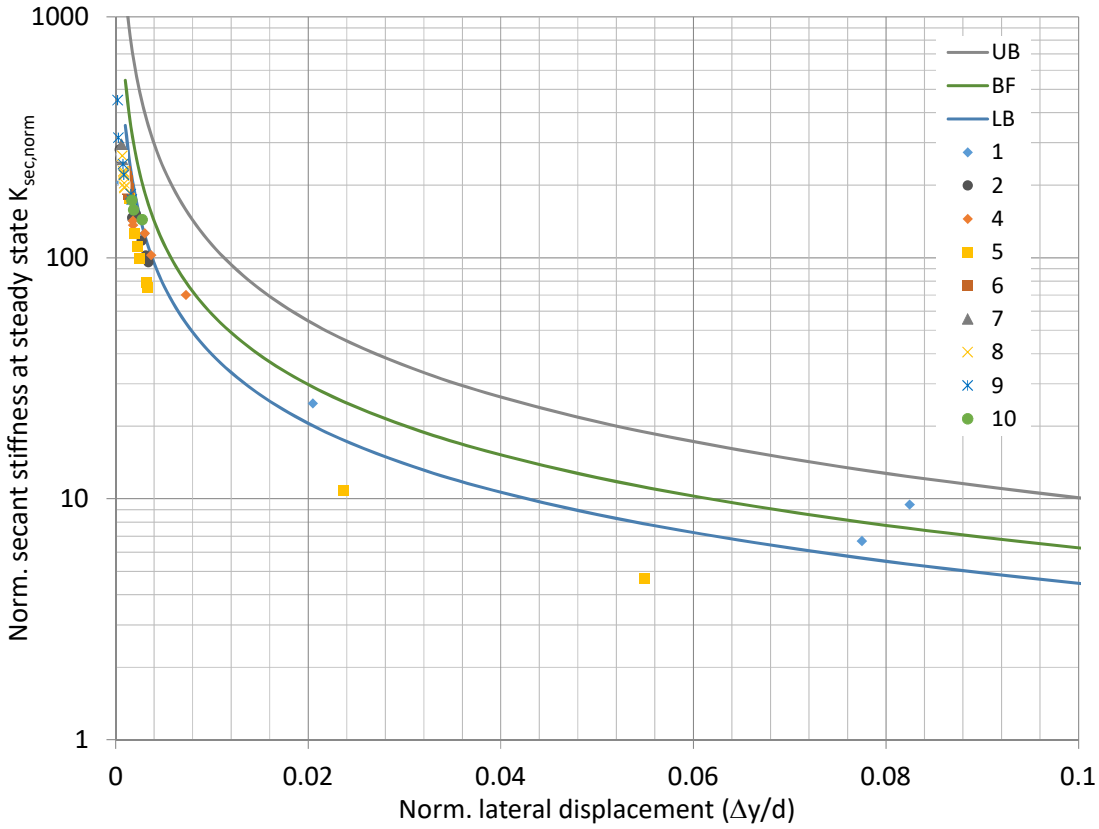

Figure 6.11: Normalized secant stiffness at steady state. The upper and lower bound (UB and LB) and best fit (BF) is based on centrifuge data by Zakeri et al. (2017)

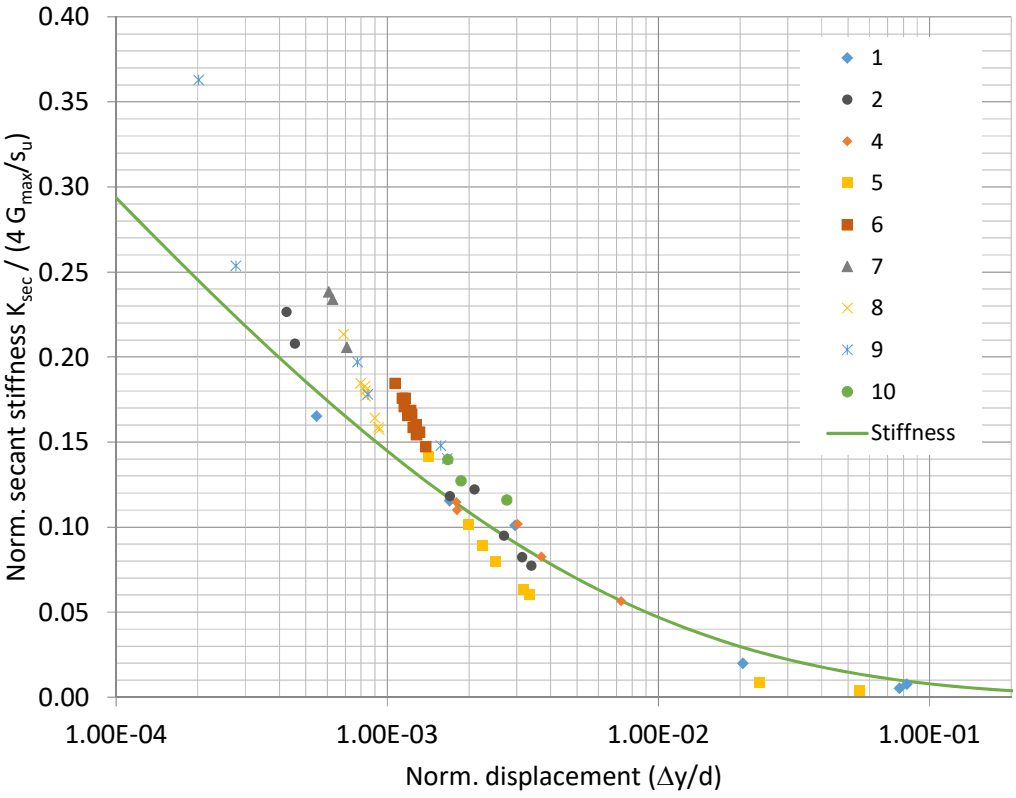

Figure 6.12: Secant stiffness normalized by small strain shear modulus and undrained shear strength

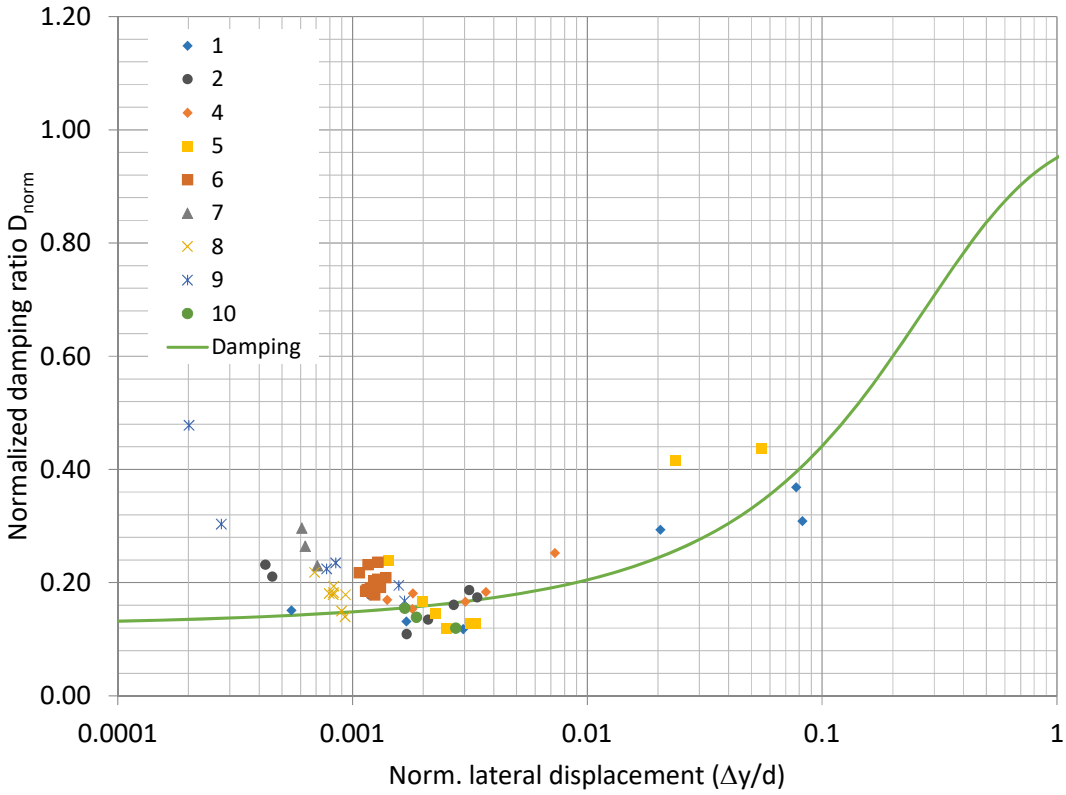

Figure 6.13: Normalized damping ratio

Figure 6.12 shows the secant stiffness normalized by the small strain shear modulus and the undrained shear strength, $K_{sec,norm}$. The values coincide reasonably well with the stiffness trendline provided from NGI internal reports, but show a slightly different tendency. The stiffnesses are larger than the trendline for the smallest displacements. The normalized damping ratio D_{norm} is shown in Figure 6.13. The test results generally coincide reasonably well with the centrifuge test results from Zakeri et al. (2017), with some exceptions. The results that fit the least are from load parcels were the applied loads are repeated or reduced.

6.1.5 OCR correction

Each specimen was subjected to load controlled cyclic loading. The cyclic events ended at zero load before the displacement controlled 3 mm cycle was applied. The results indicate that the shear strength has increased in parts of the material.

Especially tests with a constant average load reached high lateral resistances during the 3 mm cycle, suggesting that the average component of the cyclic loading contributes to the strength increase as discussed previously in this chapter. The material also in the opposite direction of the average load exceeded the expected resistances.

Table 6.8: Parameters for OCR correction

Ultimate bearing capacity factor	N_p	[-]	12
Undrained shear strength for OCR=1	$s_{u,OCR=1}$	[kPa]	25
Consolidation pressure	σ'_c	[kPa]	120
At rest coefficient after consolidation	K'_0	[-]	0.5
Pressure due to average load	p'_a	[kPa]	30

An OCR correction is performed based on the method described in Section 3.5. Relevant parameters in the calculations are provided in Table 6.8. Figure 6.14 shows the cross section of the specimen in the soil chamber with the installed steel rod. The arrow indicates the direction of the average component of the cyclic loading, which is distributed over the longitudinal area of the steel rod, calculated according to Equation 4.1. The included failure mechanism is the same as shown in Section 2.3.3 taken from Randolph and Gourvenec (2011). The horizontal axis starts at the model pile wall, and indicates the distance from the pile wall relative to the steel rod's diameter. The distribution of pressure from the applied average load is indicated in the figure. The applied load is distributed over a gradually increasing width with increased distance to the model pile. Hence, the stresses in the soil due to the average load are reduced with increased distance from the steel rod, similar to a stress distribution under a surface load, as illustrated in figure 6.15.

The material in close vicinity to the steel rod is assumed to be remoulded and have cyclically degraded strength and stiffness. The increase in shear strength due to the average load varies with the distance from the steel rod and corresponds to the pressure distribution of the load throughout the specimen. The zone particulary affected by the average load where the undrained shear strength is assumed to be significantly increased, is the compression zone in a distance below 50% of the steel rod diameter.

$$OCR = \frac{K'_0\sigma'_c + p_a}{K'_0\sigma'_c} \tag{6.4}$$

Results from tests 9 and 10 have been OCR corrected according to the method proposed by Andersen (2015), introduced in Section 3.5. OCR is calculated according to Equation 6.4, where p_a is the applied average pressure in the affected material, σ'_c is the consolidation pressure of 120 kPa and K'_0 the at rest coefficient. The first term in the equation is the effective horizontal pressure after consolidation before cyclic loading is applied.

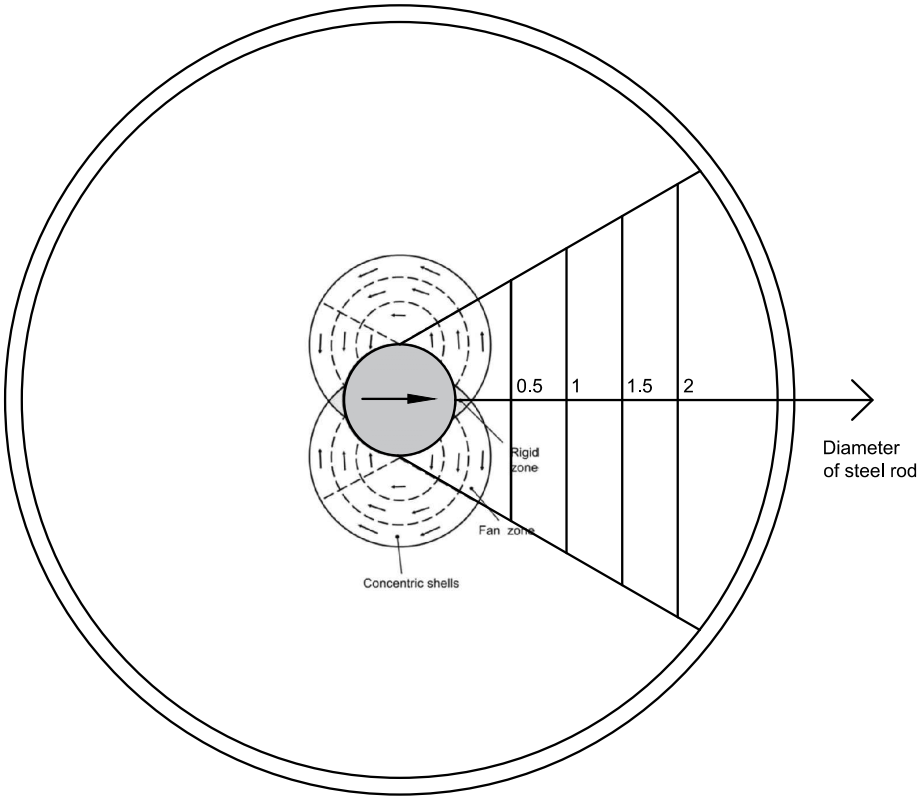

Figure 6.14: Pressure distribution in specimen

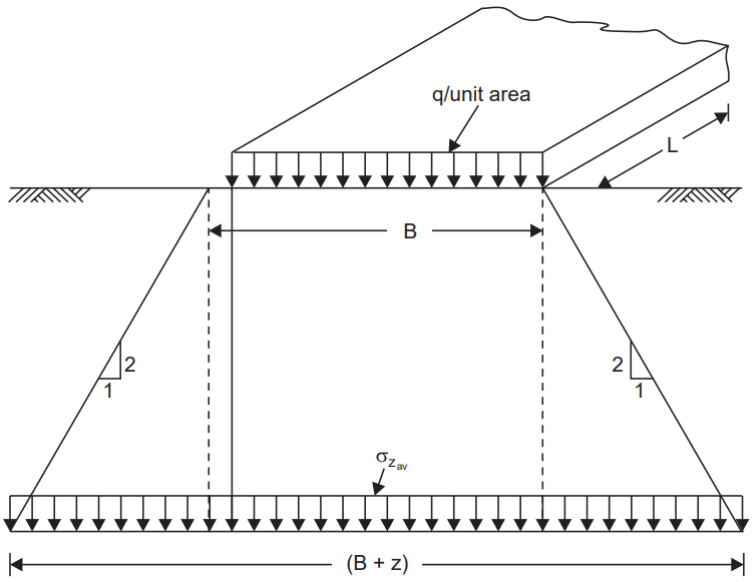

Figure 6.15: Stress distribution (Venkatramaiah, 2006)

The average pressure applied to tests 9 and 10 was 30 kPa. The material with the largest increase of shear strength at the compression side is assumed to be in a distance below 50% of the pile's diameter from the steel rod. The average pressure applied in this zone is estimated to be around 25 kPa. If K_0' is assumed to be 0.5 after consolidation, OCR is calculated to be 1.4. By using the diagram in Figure 3.6, the ratio between undrained shear strength

with OCR=1.4 and OCR=1 is approximately 1.3. Based on this, the undrained shear strength is estimated to approximately 33 kPa for tests 9 and 10.

Figure 6.16 shows the first push over of the 3 mm cycle of tests 9 and 10 together with the DSS test results. The ultimate lateral bearing pressure p_u is calculated according to Equation 2.1 both with the original s_u and the OCR-corrected. The curves for tests 9 and 10 coincides much better with the DSS test results when corrected for OCR due to the average component of the applied cyclic loading.

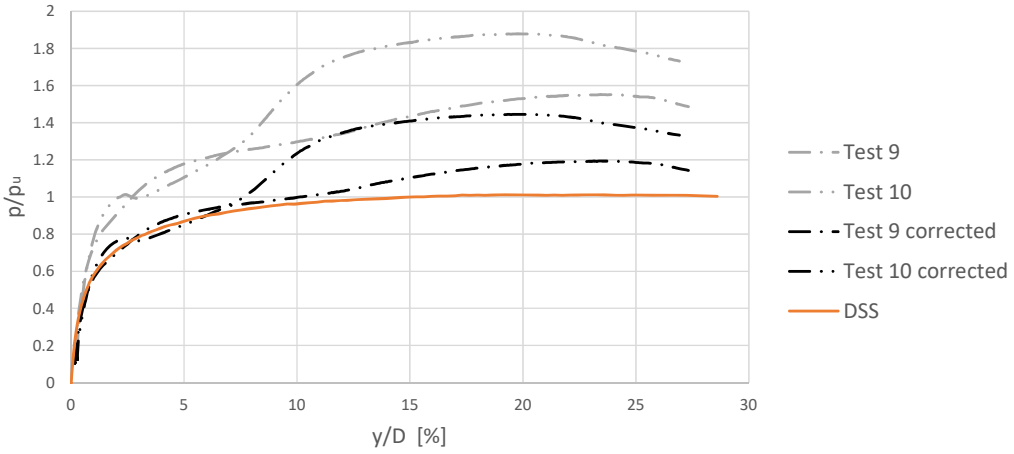

Figure 6.16: DSS test results and test 9 and 10 with OCR-corrected s_u

6.2 North Sea specimens

As described in Chapter 2, the usual methods of simplifying irregular load histories, generally tend to overestimate fatigue damage and result in conservative estimates. The two tests with clay from the North Sea were performed to investigate this. An irregular load history was applied to test 11, and the specimen of test 12 was subjected to an idealized load history comprising a sequence of cyclic load parcels with constant cyclic amplitude based on the same load history. The expectation was to see less accumulated displacement and potentially also higher capacity when subjected to irregular loading compared to load parcels. Results from the two tests did not coincide with literature and prior expectations. Test 12 exhibit less accumulated displacement and larger stiffness than test 11.

Pressure-displacement plots of the 270 N and 3 mm cycles have previously been shown in Section 5.2. The soil response to the 3 mm cycle deviates from the response of kaolin clay reported in Section 5.1.3. The 3 mm cycle causes nearly symmetric response, and the large difference in lateral resistances measured at the three amplitudes is not seen. This is most

likely due to that the specimen remains intact through the entire 3 mm cycle.

While the response to the 3 mm cycle is almost identical for the two tests, different behaviour is observed in the 270 N cycles. Figure 5.23 in Section 5.2 shows the 270 N cycles for tests 11 and 12. The load curve of test 11 is uneven around 80 N, as shown clearer in Figure 6.17. The normalized displacement of test 12 follows the ramp shape of the applied load, but test 11 have a rapid change in displacement near the neutral position. The rapid movement appear at the same time as the load curve kinks.

This behaviour may suggest that there has developed a gap between the steel rod and the material which can explain the soft response to the irregular load history observed in test 11. The unexpected results could also be a consequence of the inhomogeneous material or due to installation effects.

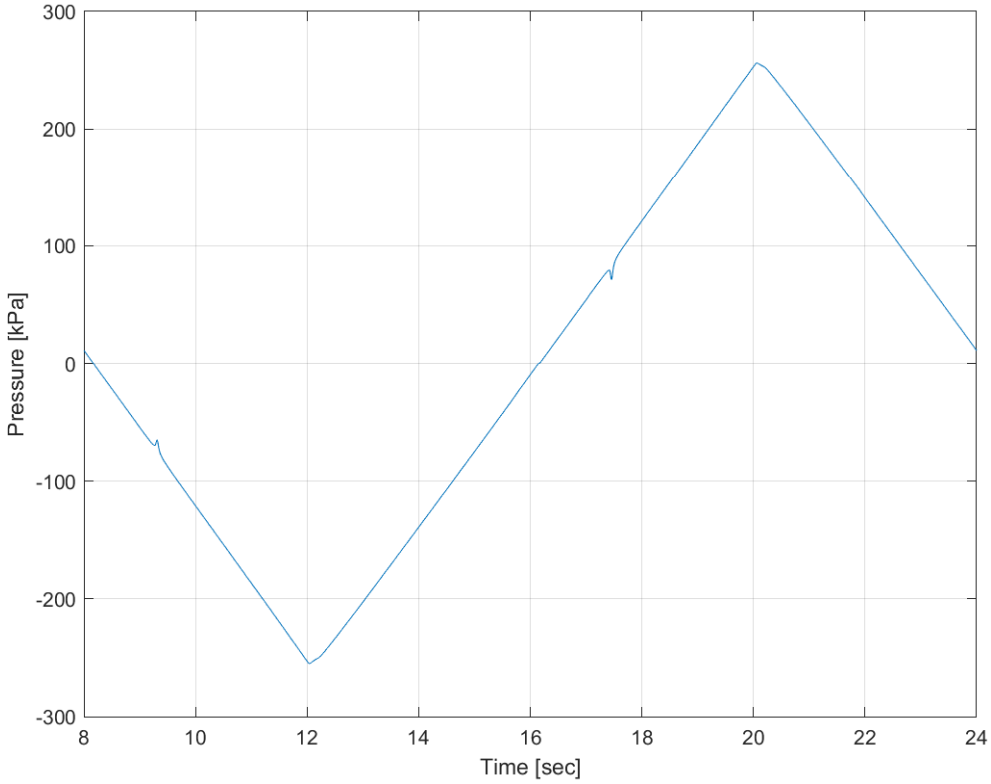

Figure 6.17: 270 N cycle test 11

Installing the model pile in the offshore clay specimens proved to be difficult. Removal of material with the hollow steel tube had to be done from both sides before the steel rod could be insterted. The material was inhomogeneous with some larger grains and cavities of sand. Inhomogeneity and the problems during installation might contribute to the unexpected results of tests 11 and 12. The difference in results is seen in the accumulated displacements during the tests and in the 270 N cycles, which generated normalized displacements below

2%. The response to the 3 mm cycle is approximately the same for the two tests. The difference is seen only for small displacements, indicating that the main cause is installation effects.

As seen in Figure 5.22, the normalized displacement goes to approximately 2 mm and not 3 mm as it should. In tests 11 and 12, the 3 mm and 270 N cycles were included in the load procedure at the end of the irregular load history, and started immediately after the generated storm was completed. In tests 1-10 the 3 mm cycle was programmed manually, so there was a small break before the test was continued. While the hydraulic actuator have acceptable accuracy during the load history and 270 N cycles, it underachives considerably to the 3 mm amplitudes of tests 11 and 12, resulting in amplitudes closer to 2 mm than 3 mm. This is presumably caused by the sudden change from load control to displacement control, or the rapid increase in displacements from below 1% during testing to the commanded 30%. As described in Chapter 4, the hydraulic system must be warmed up before testing. As the loading during the three hours of testing caused only small displacements, the system was might not "prepared" for the sudden change in both control mode and increased displacement levels.

6.3 Dummy tests

Test results of both displacement and load controlled dummy tests are compared with data from centrifuge tests as introduced in Chapter 3. Because the material parameters are unknown for the dummy tests, the undrained shear strength was estimated to be approximately 23 kPa. The objective of the dummy tests was to reproduce the trend and not the actual values of the centrifuge test results, as the material properties are unknown.

Results from the dummy tests are presented in Figures 6.18, 6.19 and 6.20. Figure 6.18 show the normalized secant stiffness at steady state. The results seem to fit reasonably well with the tendency seen in the centrifuge test results, apart from a few exceptions. The results that fit the least are from load parcels were the applied force/displacement is reduced. Also in Figures 6.19 and 6.20 the results from the dummy tests generally seem to match the main tendencies of the centrifuge test results.

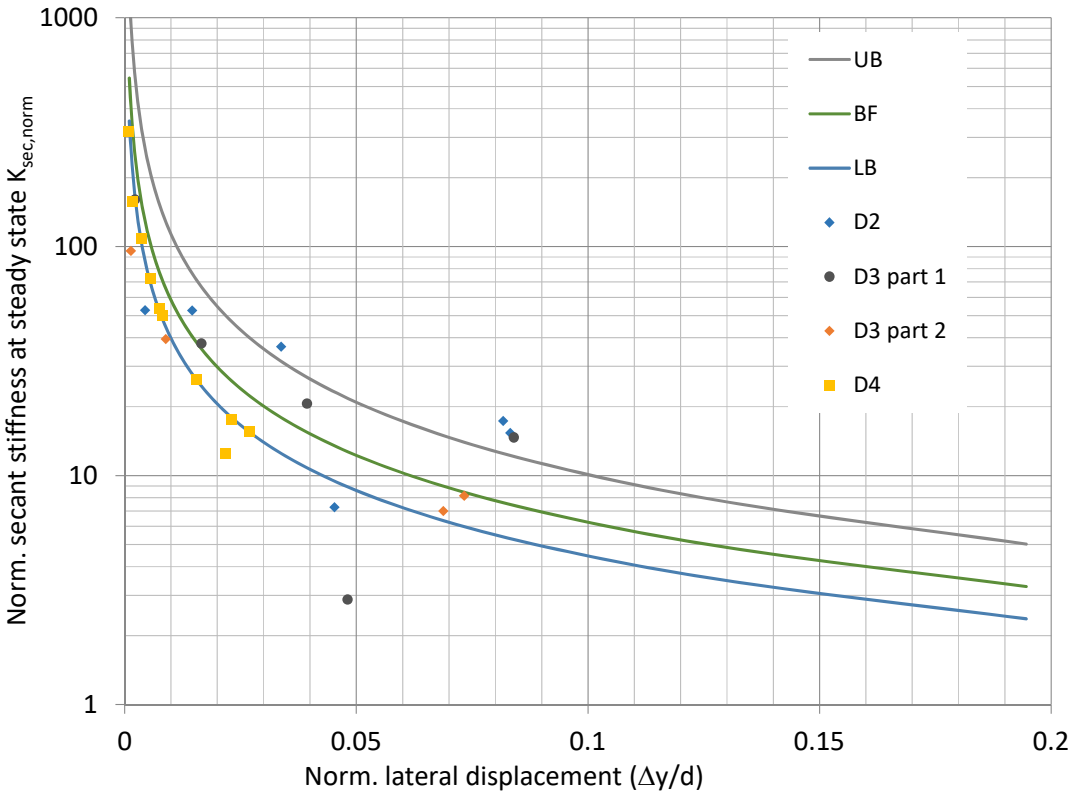

Figure 6.18: Normalized secant stiffness at steady state. The upper and lower bound (UB and LB) and best fit (BF) is based on centrifuge data by Zakeri et al. (2017)

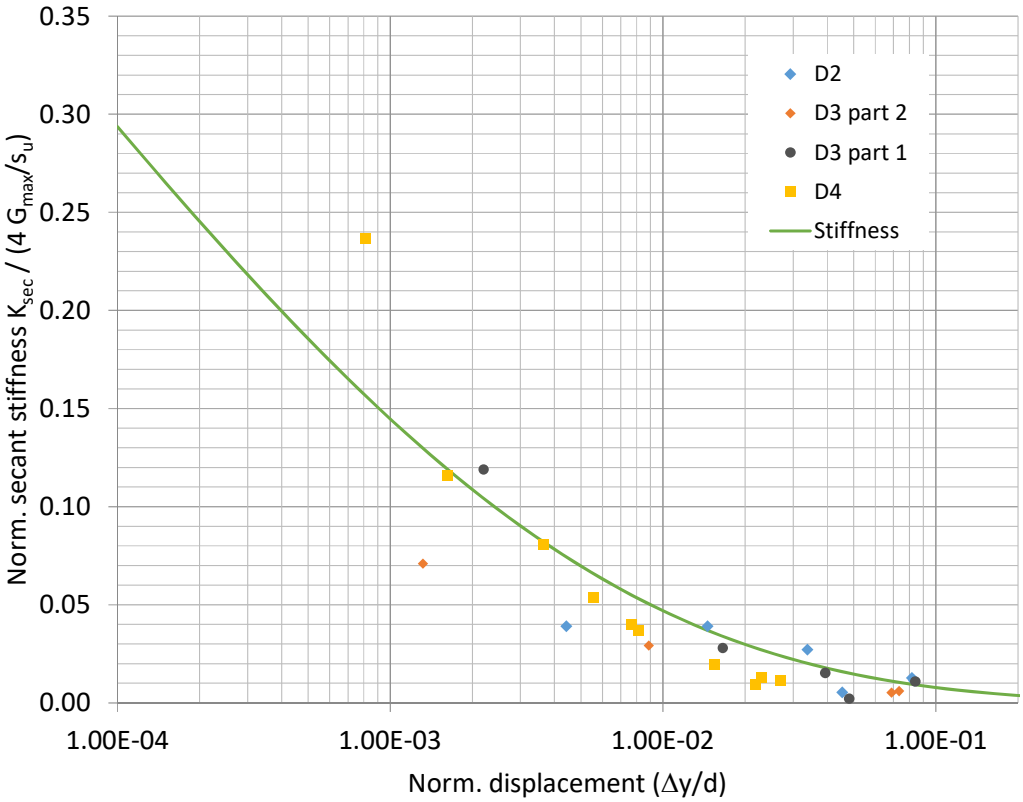

Figure 6.19: Secant stiffness normalized by small strain shear modulus and undrained shear strength

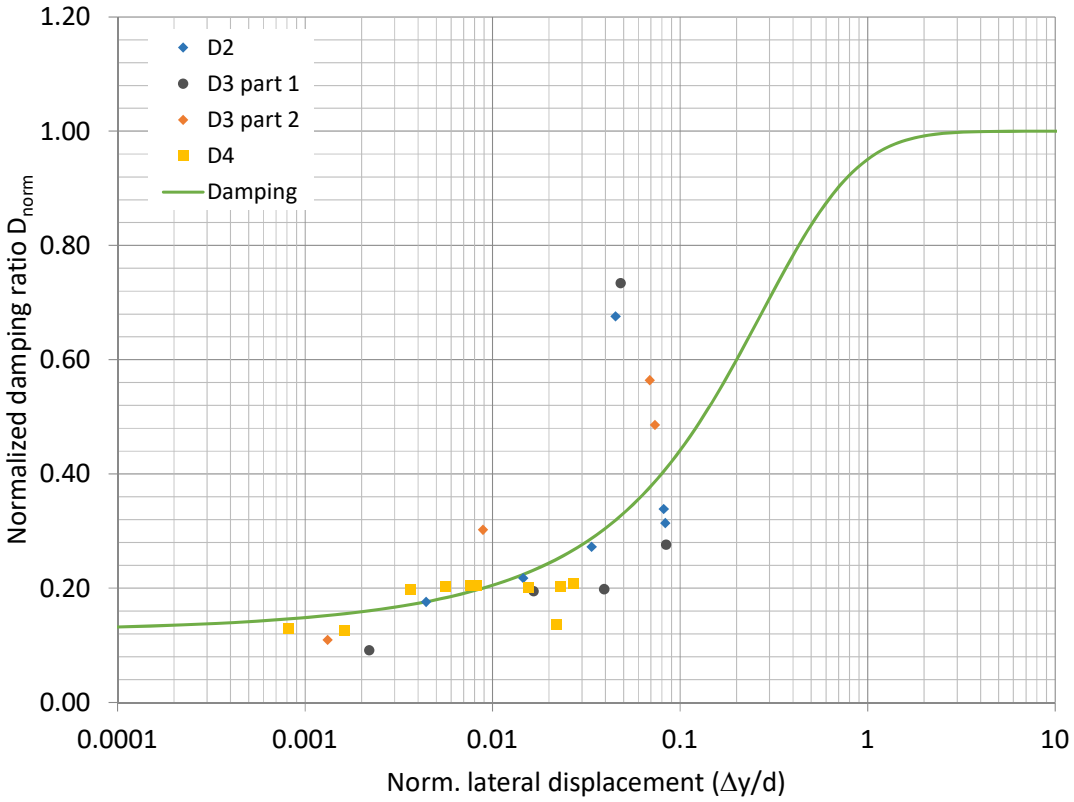

Figure 6.20: Normalized damping ratio

6.4 General

Overall, the p-y apparatus performs well and most of the tests are successful and produce plausible results. Tests coincide well with the contour diagrams, and tendencies seen in the test results are generally as expected. When the test specimens are loaded with constant amplitude and varying average load, the displacement amplitude remains nearly constant, while the average displacement to a greater extent follow the change in average load. In tests applied with constant average load and varying load amplitude, the displacement amplitude follows the load amplitude's variation, while the average displacement gradually accumulates during the test.

The applied load levels cause relatively small deformations, typically less than 0.5 mm. For the smallest displacements, false deformation can be a significant part of the measured deformations. Elastic deflection of the steel rod is therefore calculated and the results are adjusted accordingly.

The testing procedure is sensitive for installaton effects as a small-scale model test is performed. The steel rod is inserted manually and should ideally be installed exactly the same way each time. The kaolin specimens were homogeneous and quite soft, and there were no

problems inserting the steel rod in those specimens. However, disturbance due to the steel rod insertion or small differences in the installation procedure might have an effect. For that reason, the last part of consolidation is done after the specimen is mounted in the apparatus and the steel rod is installed. This will close potential gaps and reduce the effects from installation. Yet, differences in behaviour are observed. The three first load parcels in tests 7 and 8 were identical and therefore expected to produce similar results. There was a considerable difference in the obtained deformation and secant stiffness, as shown previously in Figure 5.14. In future testing, repeated tests should be performed to look closer into installation effects.

When the device is assembled, some tension or pressure in parts connecting the steel rod to the actuator is introduced. This is corrected before the test is started by regulating the position of the MTS actuator, so the MTS load is adjusted back to zero. If not done carefully, this can be a potential source of error in the tests. A correct zero reading of the load sensor before mounting the device is required.

As described in Chapter 5, uneven load curves and a change in the displacement plots were observed during cyclic loading. The displacement during one cycle increased rapidly, stagnated and decreased rapidly, and did not follow the commanded waveform. This could be seen clearly when observing the model pile in the apparatus during testing. When evaluating the results, the irregularities could be seen both in the curves for load and displacement versus time, and in the hysteresis loops in pressure-displacement plots, as presented in Chapther 5. The behaviour was identified in some of the load steps of tests 1, 5, 11 and some of the dummy tests.

Klinkvort (2012) reported similar tendencies in centrifuge tests, and explains it by an elongated hole as illustrated in Figure 6.21. The pile push the soil and a gap is generated behind the pile. When unloaded, the pile moves back toward the initial position in the cavity behind the pile before pushed in the reversed direction. The load levels of the tests reported by Klinkvort (2012) caused significantly larger displacements during cyclic loading than the p-y tests in this study, so the figure is only included as a schematic sketch.

Randolph and Gourvenec (2011) also refers to this behaviour as gapping. A gap is generated behind the pile due to lateral displacement and causes low resistance, especially when the pile passes through its neutral position, as illustated in Figure 6.22. Consequently, a considerable reduction in stiffness is obtained. Particulary for two-way cyclic loading, lateral load

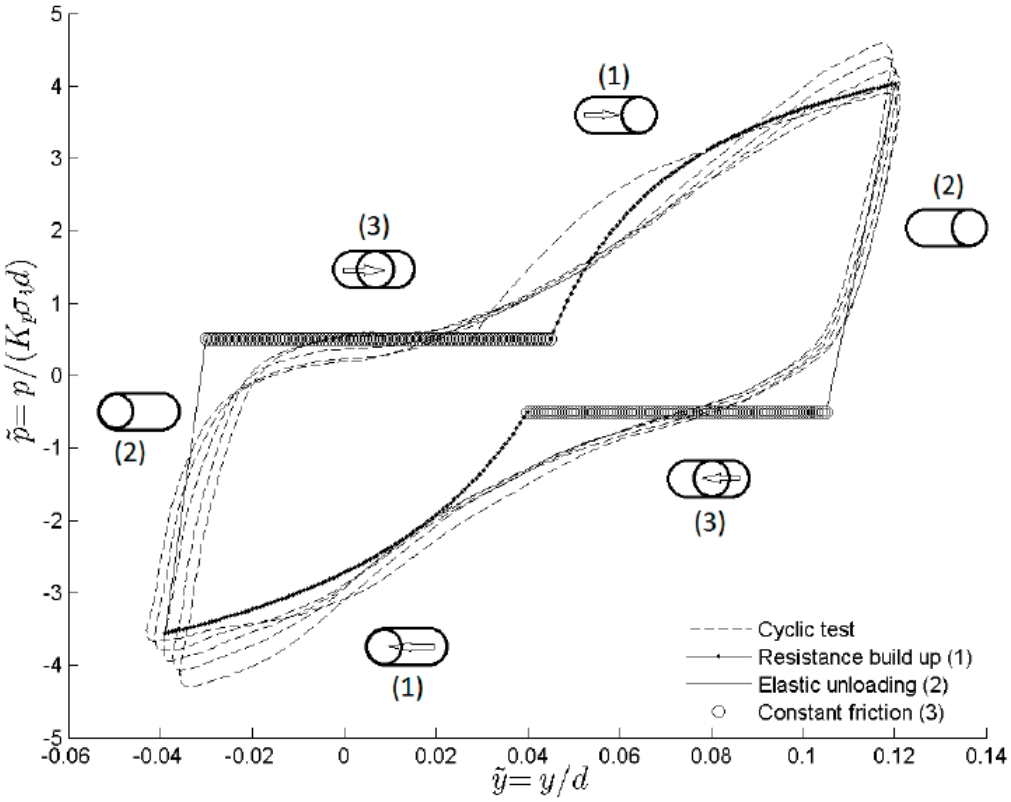

Figure 6.21: Cyclic pile-soil interaction from centrifuge test results (Klinkvort, 2012)

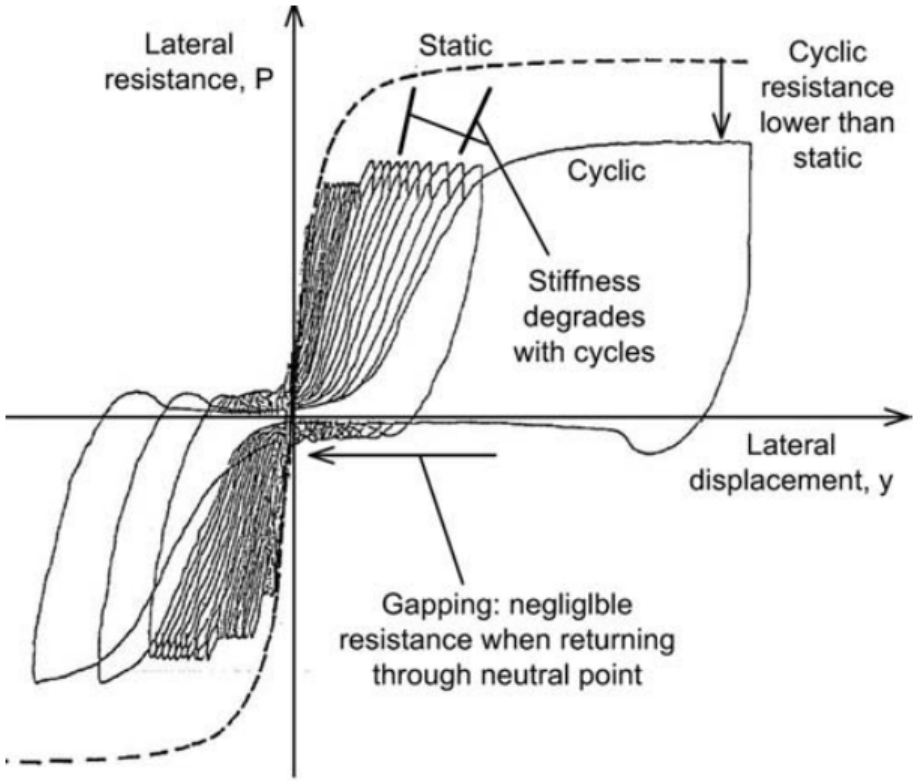

Figure 6.22: Cyclic p-y response after development of a gap (Randolph and Gourvenec, 2011)

transfer may become significantly degraded (Randolph and Gourvenec, 2011).

The described behaviour is clearly recognized in the results of test 5. Parcels 4 and 8 are the only load steps with two-way cyclic loading in test 5 and the secant stiffnesses of these two parcels are significantly lower than seen for other parcels of similar load levels, refer Appendix B.1. Also, the development and shape of the pressure-displacement curves are similar to the example illustrated in Figure 6.22. An example from test 5 is shown previously in Section 5.1.2.

Values of the ultimate lateral soil resistance coefficient are normally considered to vary from $N_p = 9$ for smooth to $N_p = 12$ for rough piles. Calculations in this study have assumed rough piles and $N_p = 12$. As reported by Aubeny et al. (2005), the coefficient can be as low as 8 for partially embedded rough cylinders. In Figure 6.23 the secant stiffness at steady state for test 5 is calculated both with $N_p = 8$ and $N_p = 12$. The response during load step 4 and 8 of test 5 is similar to typical behaviour seen when a gap has developed. In the case of gapping, a coefficient between 8 and 9 might be expected, and as seen in Figure 6.23, the results show a better fit with $N_p = 8$.

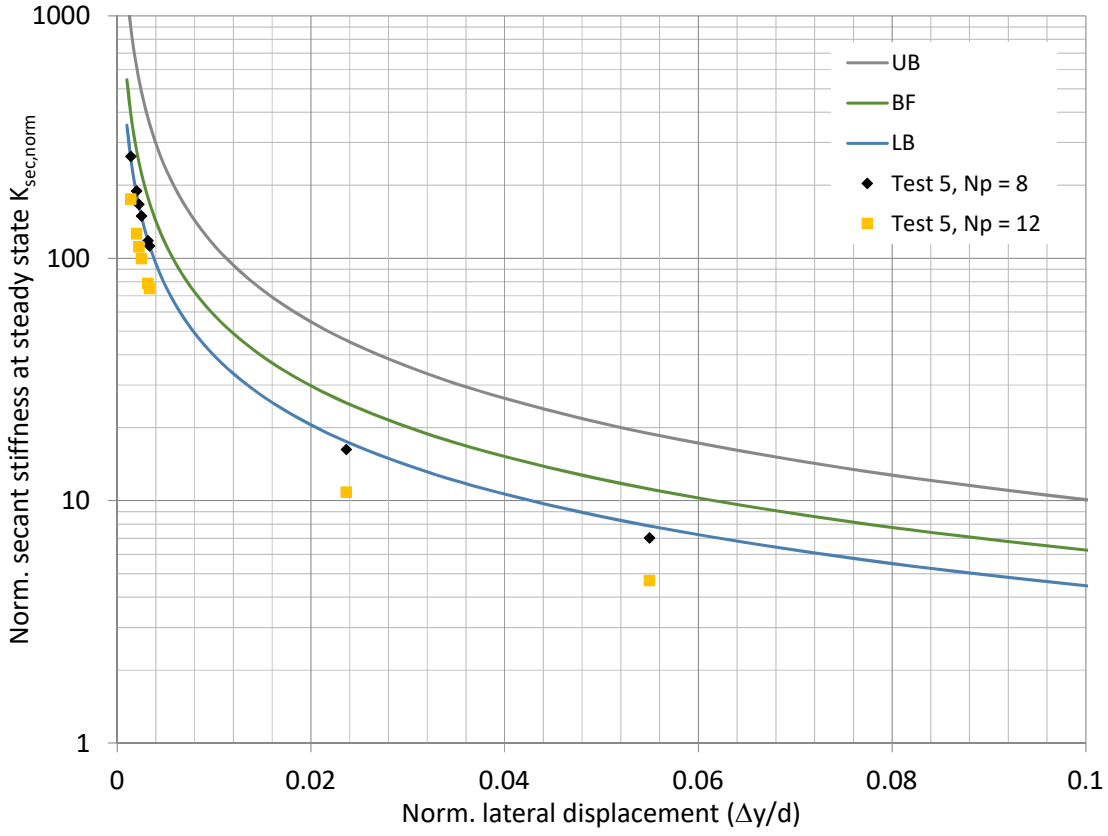

Figure 6.23: Normalized secant stiffness at steady state for test 5, calculated with N_p=12 and N_p=8.

The observed behaviour may accordingly be interpreted as an elongation of the hole in vicinity of the model pile, inducing a gap when the steel rod is pushed back and forth. However, the displacements are very small. The gap-shaped response seen in the test results is more likely due to significantly disturbed soil adjacent to the model pile. The soft disturbed clay in combination with drainage towards the steel rod due to the static component of the cyclic load, results in a very soft material with the low stiffness. The behaviour seen in the pressure-displacement plots are very similar to those demonstrating gapping, but considering the small displacements, the cause is most likely highly disturbed soil.

To prevent this response, it seems that high load levels should be avoided and a reduction in load level from one parcel to the next should be moderate. Further testing could investigate which load intervals may trigger a gap-shaped load-displacement pile response. This response should be avoided in the case where an undrained flow-around failure mecanism shall be simulated in the p-y apparatus. This may require modifications to the testing procedure.

In-situ, gaps are mainly occuring in shallow soil layers under drained conditions. At greater depths, the soil reponse softens by remoulding, but the development of a gap is prevented by the weight of the above soil and the undrained conditions (Randolph and Gourvenec, 2011). In this study, testing is performed under constant soil height. Because the specimen is not sealed, partially drained conditions are assumed. There could be a reduction in axial stresses during testing under constant soil height due to relaxation and thus a decreased resistance to gapping. In that case, the problem might be solved by running the tests with constant axial stress. Another possibility is to choose a material with lower coefficient of consolidation to ensure undrained conditions, which also would increase the resistance to gapping.

The MTS system used for the tests in this study is calibrated for displacement control. Test performance and accuracy might be improved by calibrating MTS again and optimize for load control. Tuning for load control proved to be challenging, and sufficient accuracy was not reached even with extreme values of P Gain and I Gain. High tuning values also made the test system very sensitive and unstable. Consequently, standard values were chosen even though desired accuracy could not be achieved with these parameters.

Tuning of load controlled tests have to be performed with the specimen installed and adjusted for different soil behaviour. More comprehensive tuning should ideally be carried out on several intact specimens before running the tests. Dummy tests D3 (part 2) and D4 were

used for tuning, but with the steel rod fixed to avoid sample disturbance. Test performance would improve if more thoroughly tuning of the system could be executed on intact specimens dedicated for tuning to adjust according to actual soil behaviour.

Load commands may also be adjusted to obtain the aimed load levels when sufficient accuracy is not obtained by tuning. By over programming the load levels, desired response of the actuator can be achieved. This was not done for the tests in this work, as the error and how it varies for different load levels and frequencies was unknown beforehand.

The accuracy of the applied load relative to the command is presented in Figure 6.24. In general, the accuracy is better for larger load amplitudes. The error also decreases when the frequency is reduced. Load parcels in test 6 were applied with frequency 0.25 Hz and 0.05 Hz. The average relative error in load amplitudes for load steps in test 6 with frequency 0.25 Hz was 8%, while 5% for frequency 0.05 Hz.

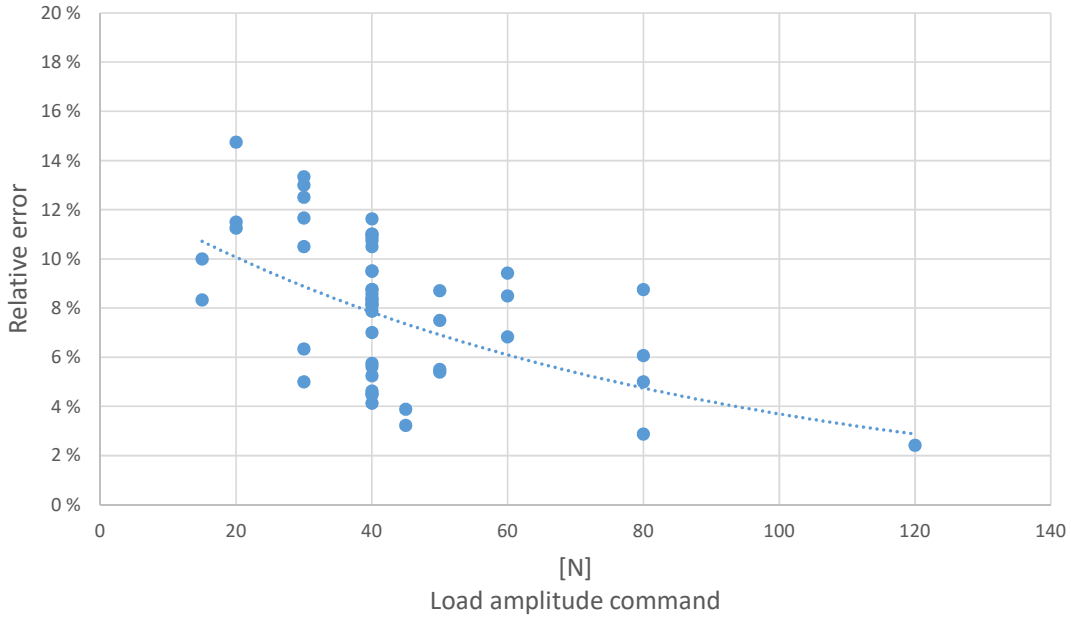

Figure 6.24: Accuracy of load command

The cyclic loading in most of the tests was applied with sine waveform at 0.25 Hz. If further testing concerning design of OWTs shall be performed, the choice of frequency could be reconsidered, as the typical frequencies of wave loads are below 0.1 Hz. Decreased frequencies would also increase the accuracy of the hydraulic actuator.

Chapter 7

Summary and Conclusions

7.1 Summary

The p-y apparatus is a newly developed laboratory-sized model test device and the application possibilities of the apparatus are not yet fully explored. In this study, the application possibilities for SLS design of offshore wind turbines are investigated. For that purpose, a series of load controlled tests subjected to non-symmetric cyclic loading were performed.

As seen in comparison to theoretically calculated ultimate lateral bearing pressure and DSS results, the measured lateral resistance to the monotonic push-over applied at the end of each test, exceeded the expected levels for nearly all of the tests, as discussed in Section 6.1.3. The largest lateral resistances were achieved by the specimens subjected to cyclic loading where the average component was kept constant throughout the test. When results from these tests were corrected for OCR based on the average load component, the response showed a better fit with the DSS results.

Constant average loads were applied in the positive direction and varying average loads were consistently first applied in the positive direction. The ratio of lateral resistance in the first and second displacement amplitude during the 3 mm cycle varied for the different tests, as shown in Table 6.6. Tests performed over two days obtained approximately the same ratio as seen in equivalent DSS tests. Tests with varying average load components obtained the same ratio as seen in former p-y tests. The largest difference between the resistance of the first and reverse displacement amplitude were observed in the tests subjected to a constant average load. The ratios of these tests were considerably higher.

An evaluation of drainage is performed, considering both drainage within a cycle and drainage during the entire test or load parcel with a constant average load component. Undrained conditions within a cycle can be assumed based on the performed assessment. The drainage evaluation due to static loading showed that partially drainage can be assumed for all tests based on the duration the specimens were subjected to a constant average load component during cyclic loading.

Comparisons with DSS results and the ultimate lateral bearing pressure suggest that the test specimens have experienced some consolidation effects during cyclic loading resulting in an increased undrained shear strength, especially in the material close to the steel rod in compression due to the average load component. This is supported by observations in the test results as well as the performed drainage evaluation and OCR correction.

The results of the tests performed over two days contradicts this interpretation. The response of these two tests coincided much better in comparison to the DSS results and did not obtain the high lateral resistances seen in the other tests. This does not support the assumption of consolidation effects. In that case, especially test 4 subjected to a constant average load should achieve the same high resistances as tests 9 and 10, even if the 3 mm cycle were applied on the second day.

Response observed in some of the tests is very similar to the behaviour typically exhibited in the case of gapping. This was observed by increased displacements and reduced stiffness, and was particulary evident in the results of load parcels 4 and 8 of test 5, presented in Section 5.1.2. Because the displacements during cyclic testing have been small for all the tests, it is concluded that the most likely cause of the observed behaviour is highly disturbed soil in close vicinity to the steel rod in combination with excess pore water that has drained towards the center of the specimen. The consequence is very soft material close to the steel rod and thus the behaviour resembling gapping. To prevent this in the future, tests should be performed on less permeable material to ensure undrained conditions during cyclic loading. Tests should also be performed under constant axial pressure rather than constant soil height.

In general, the device performs well and the observed pile response can be described with cyclic contour diagrams. The p-y apparatus has shown to produce plausible results when used to perform load controlled tests with non-symmetric cyclic loading and is therefore considered applicable to assess the serviceability of piles subjected to cyclic lateral loading.

7.2 Conclusions

The main objectives in this MSc thesis were to investigate if the p-y device was able to run load controlled tests with non-symmetric cyclic loading and evaluate the obtained test results.

The first objective is met and a number of load controlled tests with different combinations of average and cyclic load components have been performed. The results are evaluated considering installation effects, drainage and comparisons to DSS and centrifuge test results. The numerous load combinations made interpretation challenging in cases where the results exhibited inconsistent tendencies. The evaluation of the results led to possible explanations of most of the tendencies observed in the tests, but there still remain some open questions. Hence, the second objective is not fully met.

Based on this study, the apparatus is considered to be able to produce plausible results for SLS assessments, but more tests and analyses are required in order to use it in design. A better understanding of the results obtained from p-y tests is necessary. This study will hopefully contribute as an experience basis and give some helpful recommandations for further work.

7.3 Recommendations for Further Work

The next step would be to do some FE-analyses to investigate the behaviour observed in the test results presented in this study. 2D FE analyses to model soil subjected to non-symmetric cyclic loading would be helpful in order to understand the observed response. Also, more complex fully coupled FE analyses should be performed to see if the increased soil strength in the tests can be explained by drainage and consolidation effects due to the average component in the cyclic loading.

To assess the reliability of the restults and evaluate the installation effects, several identical tests should be executed and the compared. As reported in Chapter 5, two identical tests resulted in different average displacement and secant stiffness. Further testing should be performed more systematic and equal tests repeated. This will lead to more reliable results and simpler interpretation.

To evaluate the accuracy of the rainflow counting method and possibly other counting methods representing cyclic load events, there should be performed a model test program on homogeneous samples with irregular load histories and corresponding simplified load sequences.

The tests are recommended to be performed on homogeneous material, preferrably reconstituted clay with a lower coefficient of consolidation than the kaolin clay used in this study. This will ensure undrained conditions during the complete test execution. Tests are recommended to be performed under constant axial pressure, rather than constant soil height.

To have a reference for the material's ultimate lateral resistance, the 3 mm cycle should be applied to a few intact specimens. If time is limited, an alternative is to apply it one day after cyclic loading, as the results in this study demonstrated that a better fit with DSS results was achieved if this was performed.

The accuracy of MTS could be improved by calibrating the system for load control. Thorough tuning is also necessary. A few specimens should be prepared and consolidated to be used solely for tuning, as the specimens have to be installed when tuning for load control mode and the tuning parameters are dependent on the material's behaviour.

Bibliography

Andersen, K. H. (2015). The third ISSMGE McClelland Lecture - Cyclic soil parameters for offshore foundation design.

ASTM Standard E 1049 (2011). Standard practices for cycle counting in fatigue analysis.

Aubeny, C. P., Shi, H., and Murff, J. D. (2005). Collapse loads for a cylinder embedded in trench in cohesive soil.

Carotenuto, P., Carraro, A., Torres, Y. G., Dyvik, R., Andresen, L., and Cassidy, M. (2018). Characterization of Kaolin under undrained cyclic loading [In progress].

DNV-GL (2017). Recommended practice - DNVGL-RP-C212. Offshore soil mechanics and geotechnical engineering.

Kallehave, D., Byrne, B. W., Thilsted, C. L., and Mikkelsen, K. K. (2015). Optimization of monopiles for offshore wind turbines.

Klinkvort, R. (2012). Centrifuge modelling of drained lateral pile-soil response.

Komurka, V. E., Wagner, A. B., and Edil, T. B. (2003). A review of pile set-up.

Løvholt, F., Madshus, C., and Andersen, K. H. (2018). Intrinsic soil damping from cyclic laboratory tests with average strain development [Submitted].

MathWorks. Rainflow counts for fatigue analysis. URL: se.mathworks.com/help/signal/ref/rainflow.html.

MTS Systems Corporations. Testing systems, mechanical testing and sensing solutions. URL: www.mts.com.

MTS Systems Corporations (2008). MTS Series 793 Tuning and Calibration.

NGI (2016). Wave loads and soil support for extra large monopiles.

NGI (2017). Objective, research goals, work flow and main deliverables of WAS-XL: WP-2.

NGI (2018). Was-xl webinar. status on accomplished and upcoming soil testing.

Randolph, M. and Gourvenec, S. (2011). Offshore geotechnical engineering.

Sturm, H. (2017). Design aspects of suction caissons for offshore wind tubine foundations.

United Nations. Affordable and clean energy: why it matters. URL: https://www.un.org/sustainabledevelopment/energy/.

Venkatramaiah, C. (2006). Geotechnical engineering.

Verruijt, A. (2012). Soil mechanics.

Wilson, N. E. and Elgohary, M. M. (1974). Consolidation of soils under cyclic loading.

Zakeri, A., Clukey, E., Kebadze, B., and Jeanjean, P. (2016). Fatigue analysis of offshore well conductors: Part 1 - study overview and evaluation of series 1 centrifuge tests in normally consolidated to lightly over-consolidated kaolin clay.

Zakeri, A., Clukey, E., Kebadze, B., Jeanjean, P., Piercey, G., Templeton, J., Connelly, L., and Aubeny, C. (2015). Recent advances in soil response modeling for well conductor fatigue analysis and development of new approaches.

Zakeri, A., Sturm, H., Dyvik, R., and Jeanjean, P. (2017). Development of novel apparatus to obtain soil resistance-displacement relationship for well conductor fatigue analysis.

Zhang, Y., Andersen, K. H., Jeanjean, P., Mirdamadi, A., Gundersen, A. S., and Jostad, H. P. (2017). A framework for cyclic p-y curves in clay and application to pile design in gom.

Zhang, Y., Andersen, K. H., Klinkvort, R., Jostad, H. P., Sivasithamparam, N., Boylan, N. P., and Langford, T. (2016). Monotonic and cyclic p-y curves for clay based on soil performance observed in laboratory tests.

Zhang, Y., Li, S., and Jostad, H. P. (2018). Drainage conditions around monopiles in sand [Submitted].

Appendix A

Tables of all performed tests

Table A.1: Dummy tests

Test	Amplitude	Number of cycles	Frequency [Hz]		Comment
D1					Displacement controlled
D2	0.0625 mm	1000	0.25	Sinusoidal	Displacement controlled
	0.125 mm	1000	0.25		
	0.25 mm	1000	0.25		
	0.5 mm	1000	0.25		
	0.25 mm	1500	0.25		
	0.125 mm	500	0.25		
D3	0.0625 mm	500	0.25	Sinusoidal	Displacement controlled
	0.125 mm	500	0.25		
	0.25 mm	500	0.25		
	0.5 mm	500	0.25		
	20 N	56	0.25	Ramp	Load controlled
	50 N	70	0.25		
	65 N	100	0.25		
	80 N	100	0.25		
D4	40 N	500	0.25	Ramp	Load controlled
	60 N	300	0.25	Ramp	
	40 N	300	0.25	Ramp	
	60 N	300	0.25	Ramp	
	40 N	100	0.25	Sinusoidal	
	60 N	100	0.25	Sinusoidal	
D5				Irregular load	Load controlled

Table A.2: P-y tests

Test	Average [N]	Amplitude [N]	Number of cycles	Frequency [Hz]	Comment
	0	20	500	0.25	
	0	40	500	0.25	
	0	60	500	0.25	
1	0	80	500	0.25	
	0	80	500	0.25	
	0	120	500	0.25	
	0	80	500	0.25	
					Incorrect zero reading. Discarded.
	20	20	500	0.25	
	-20	20	500	0.25	
	40	40	1000	0.25	
2	-40	40	1000	0.25	
	50	50	500	0.25	
	-50	50	500	0.25	
	-50	50	500	0.25	One day after
	-50	50	500	0.25	
	0 mm	3 mm	1.5		
	40	20	500	0.25	
	40	40	500	0.25	
3	40	60	500	0.25	
	40	80	500	0.25	
	40	120	500	0.25	
					Loose screws on left side. Discarded.
	40	40	500	0.25	
	40	60	500	0.25	
4	40	80	500	0.25	
	40	60	500	0.25	
	40	40	500	0.25	
	40	40	500	0.25	One day after
	0 mm	3 mm	1.5		
	40	40	500	0.25	
	80	40	500	0.25	
	40	40	500	0.25	
5	0	40	500	0.25	
	-40	40	500	0.25	
	-80	40	500	0.25	
	-40	40	500	0.25	
	0	40	500	0.25	
	0 mm	3 mm	1.5		
	20	40	500	0.25	
	20	40	200	0.05	
	-20	40	500	0.25	
	-20	40	100	0.05	
	20	40	250	0.25	
6	20	40	50	0.05	
	-20	40	250	0.25	
	-20	40	50	0.05	

	-40	40	500	0.25	
	-40	40	100	0.05	
	40	40	500	0.25	
	40	40	100	0.05	
	0 mm	3 mm	1.5		
	20	30	500	0.25	
7	40	30	500	0.25	
	20	30	471	0.25	End of test due to hydraulic interlock.
	20	30	500	0.25	
	40	30	500	0.25	
	20	30	500	0.25	
8	0	30	500	0.25	
	-20	30	500	0.25	
	-40	30	500	0.25	
	-20	30	500	0.25	
	0	30	500	0.25	
	0 mm	3 mm	1.5		
	30	15	500	0.25	
	30	30	500	0.25	
9	30	45	500	0.25	
	30	15	500	0.25	
	30	30	500	0.25	
	30	45	500	0.25	
	0 mm	3 mm	1.5		
	30	45	500	0.25	
10	30	60	250	0.25	
	30	45	2600	0.25	
	0 mm	3 mm	1.5		
11		3h irregular load history			North Sea sample
	0 N	270 N	3		
	0 mm	3 mm	1.5		
					depth 14.2-14.4 m
		3h irregular load history simplified by rainflow counting			North Sea sample depth 14.4-14.6 m
	-33.3	9.2	1339	0.31	
	-32.0	27.6	796	0.31	
	-32.0	46.0	604	0.31	
	-31.8	64.3	351	0.31	
12	-29.7	82.7	176	0.31	
	-27.8	101.1	77	0.31	
	-23.5	119.5	35	0.31	
	-22.4	137.9	12	0.31	
	-22.6	160.9	2	0.31	
	-29.9	170.1	1	0.31	
	-16.9	179.2	1	0.31	
	0 N	270 N	3		
	0 mm	3 mm	1.5		

Appendix B

Test results

B.1 Tests on kaolin clay

Test results of tests 2, 4, 5, 6, 7, 8, 9 and 10 are given in this section.

The results of each test are presented in the following order:

- Consolidation force, piston travel
- Pressure, normalized displacements
- Normalized displacements
- Secant stiffness
- 3 mm cycle
- Hysteresis loops in pressure-displacement plots

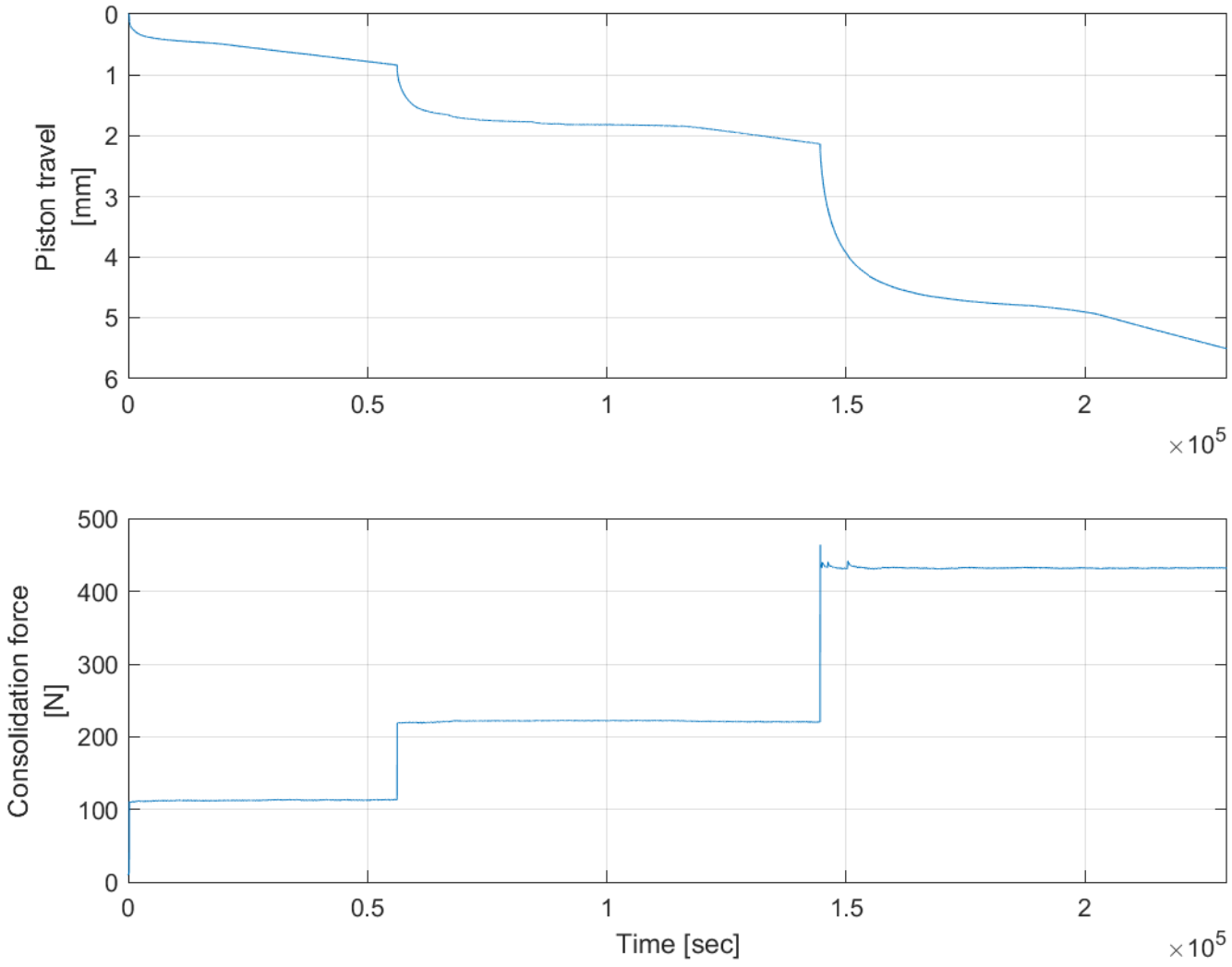
Piston travel [mm]
0
1
2
3
4
5
6
0
0.5
1
1.5
2
×10^5
Consolidation force [N]
500
400
300
200
100
0
0
0.5
1
1.5
2
Time [sec]
×10^5

Test 2

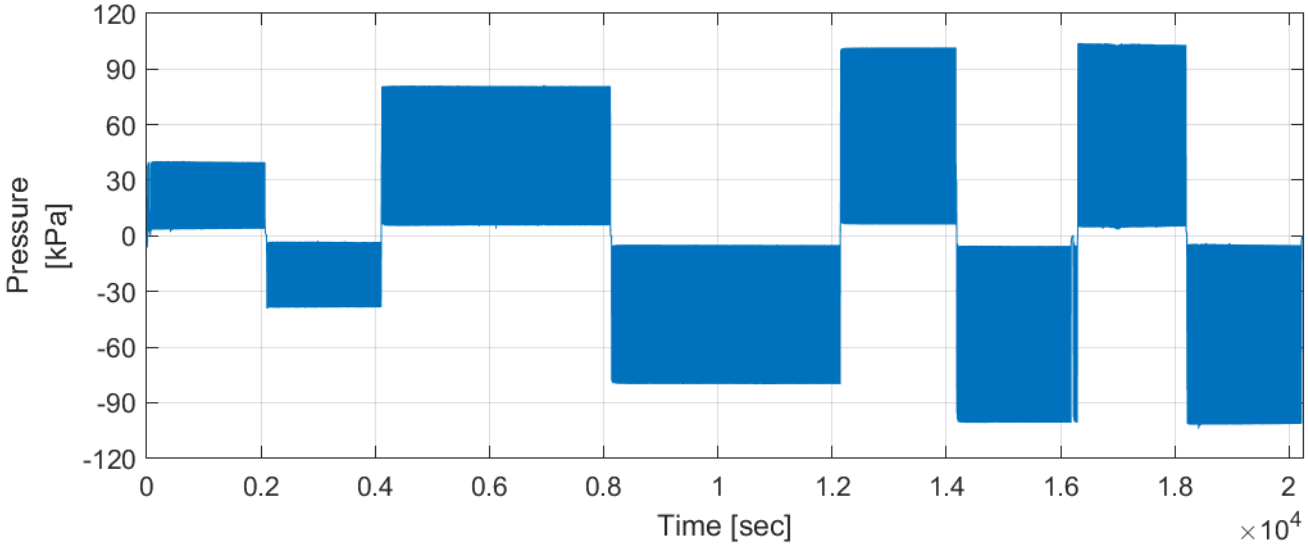
Pressure [kPa]
120
90
60
30
0
-30
-60
-90
-120
0
0.2
0.4
0.6
0.8
1
1.2
1.4
1.6
1.8
2
Time [sec]
×10^4

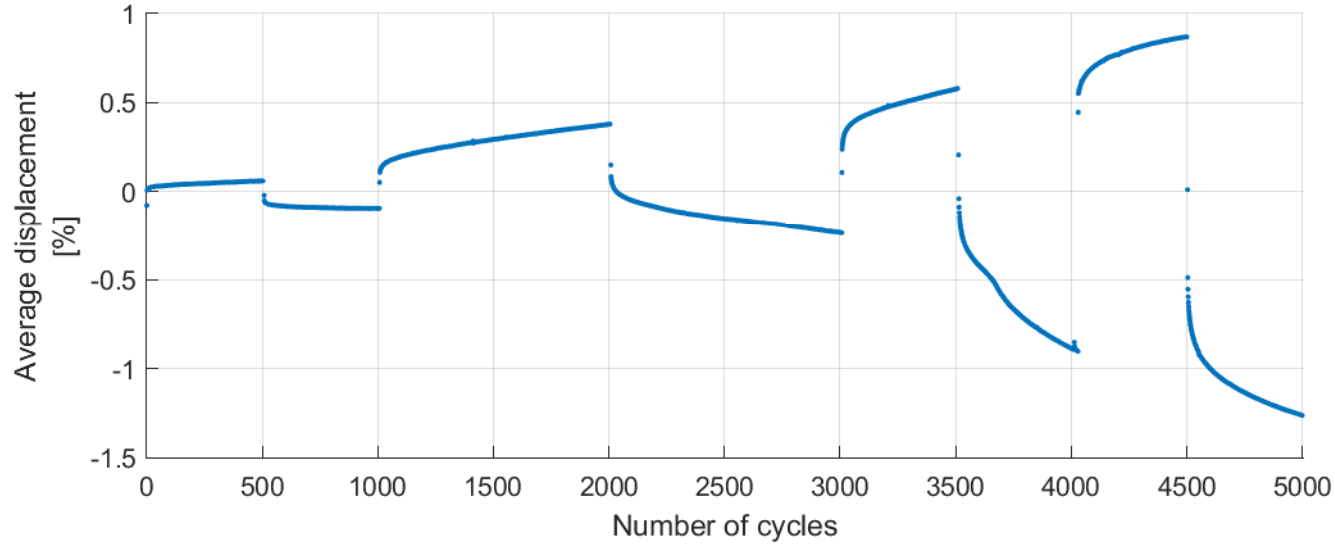
Average displacement [%]
1
0.5
0
-0.5
-1
-1.5
0
500
1000
1500
2000
2500
3000
3500
4000
4500
5000
Number of cycles

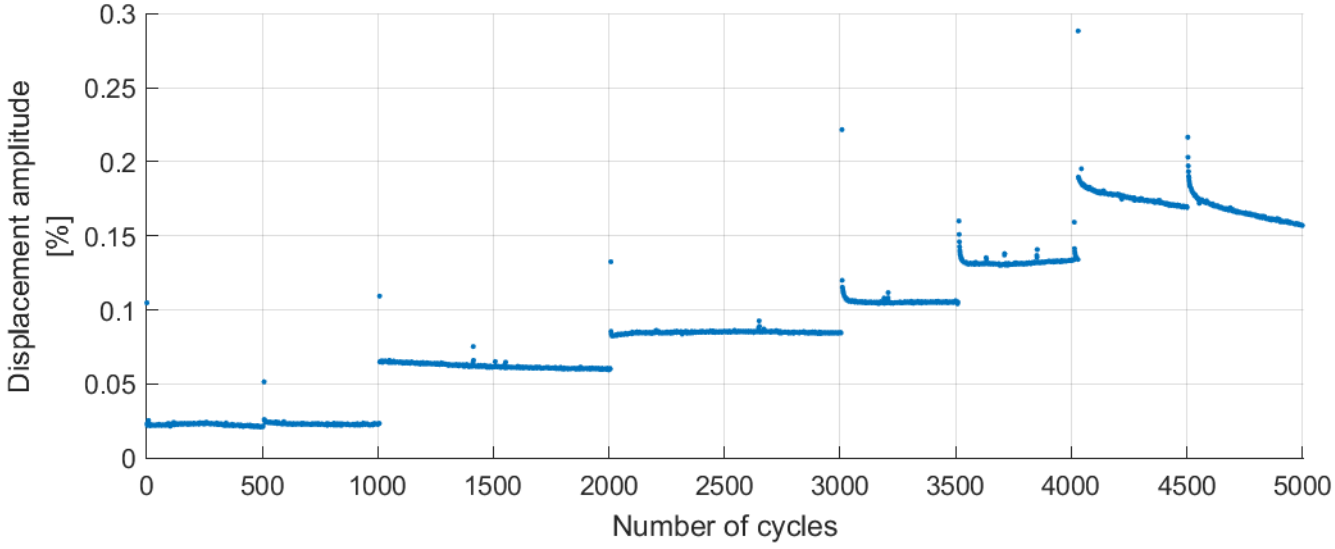
Displacement amplitude [%]
0.3
0.25
0.2
0.15
0.1
0.05
0
0
500
1000
1500
2000
2500
3000
3500
4000
4500
5000
Number of cycles

Test 2

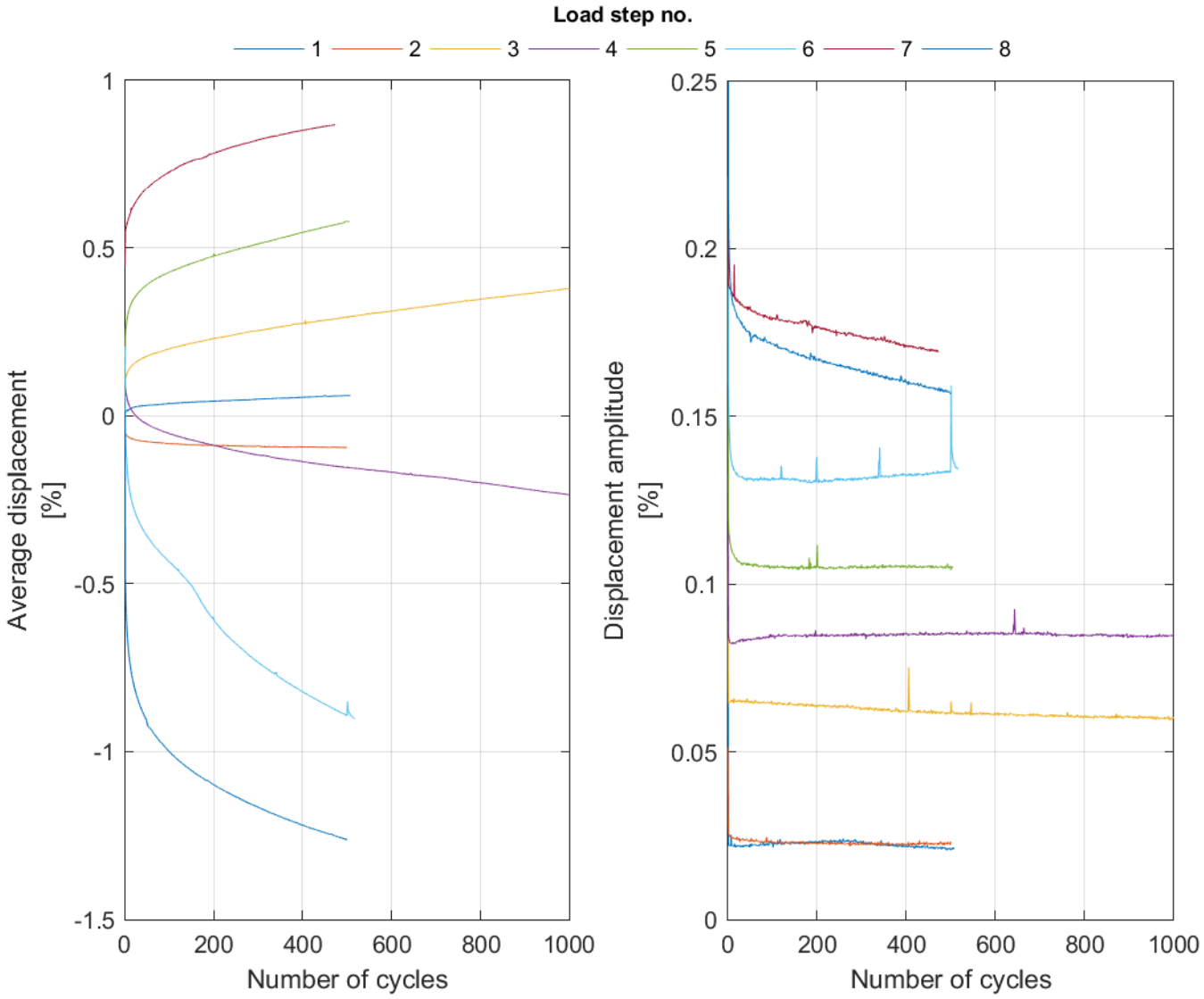
Load step no.
1
2
3
4
5
6
7
8
Average displacement [%]
Number of cycles
Displacement amplitude [%]
Number of cycles

Test 2

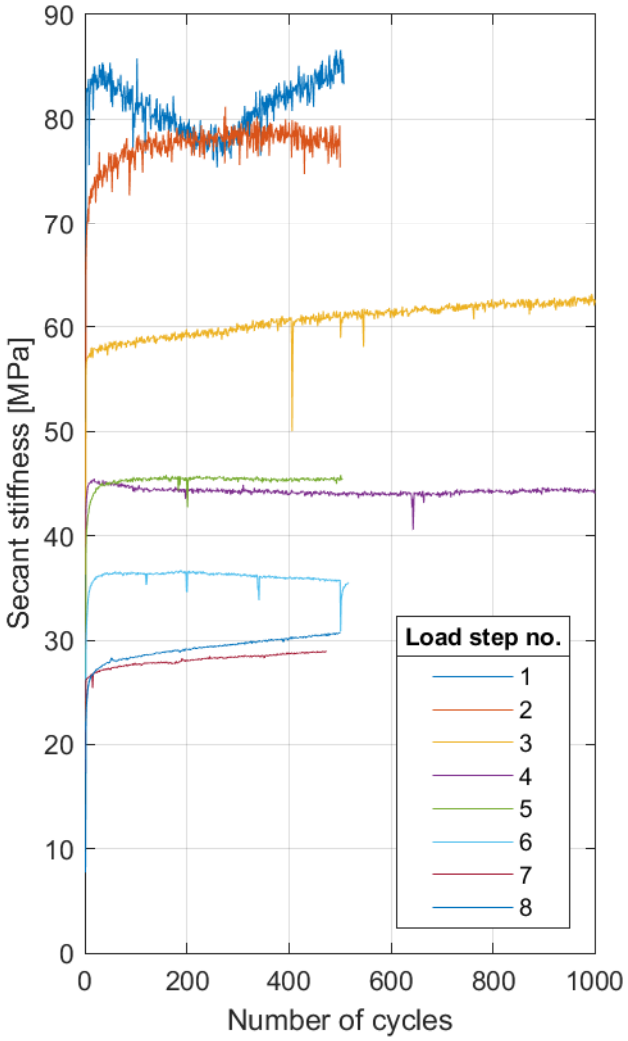
Secant stiffness [MPa]
Number of cycles
Load step no.
1
2
3
4
5
6
7
8

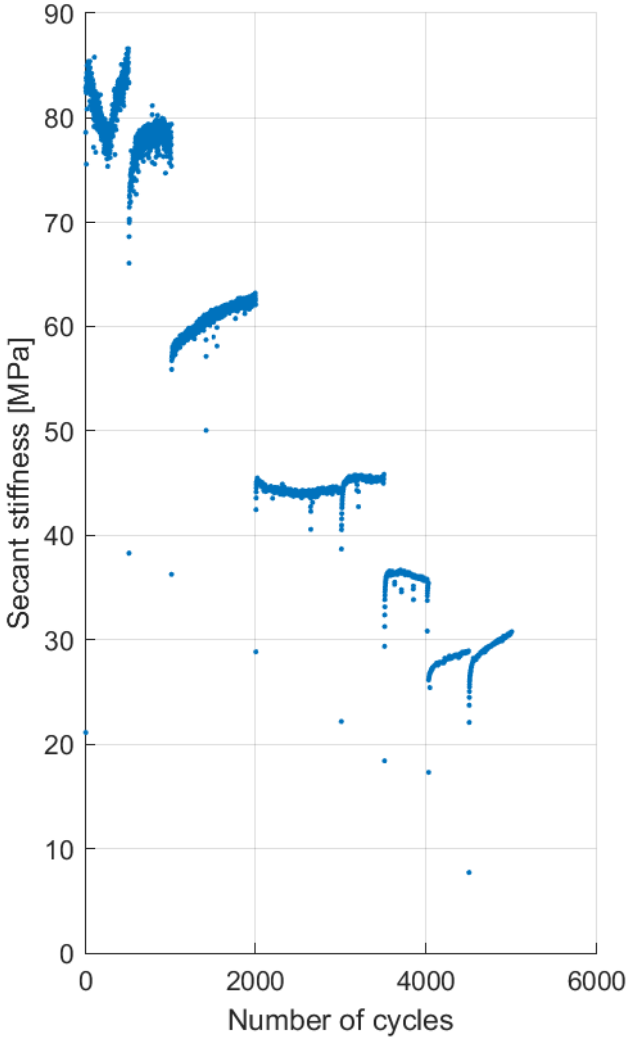
Secant stiffness [MPa]
Number of cycles

Test 2

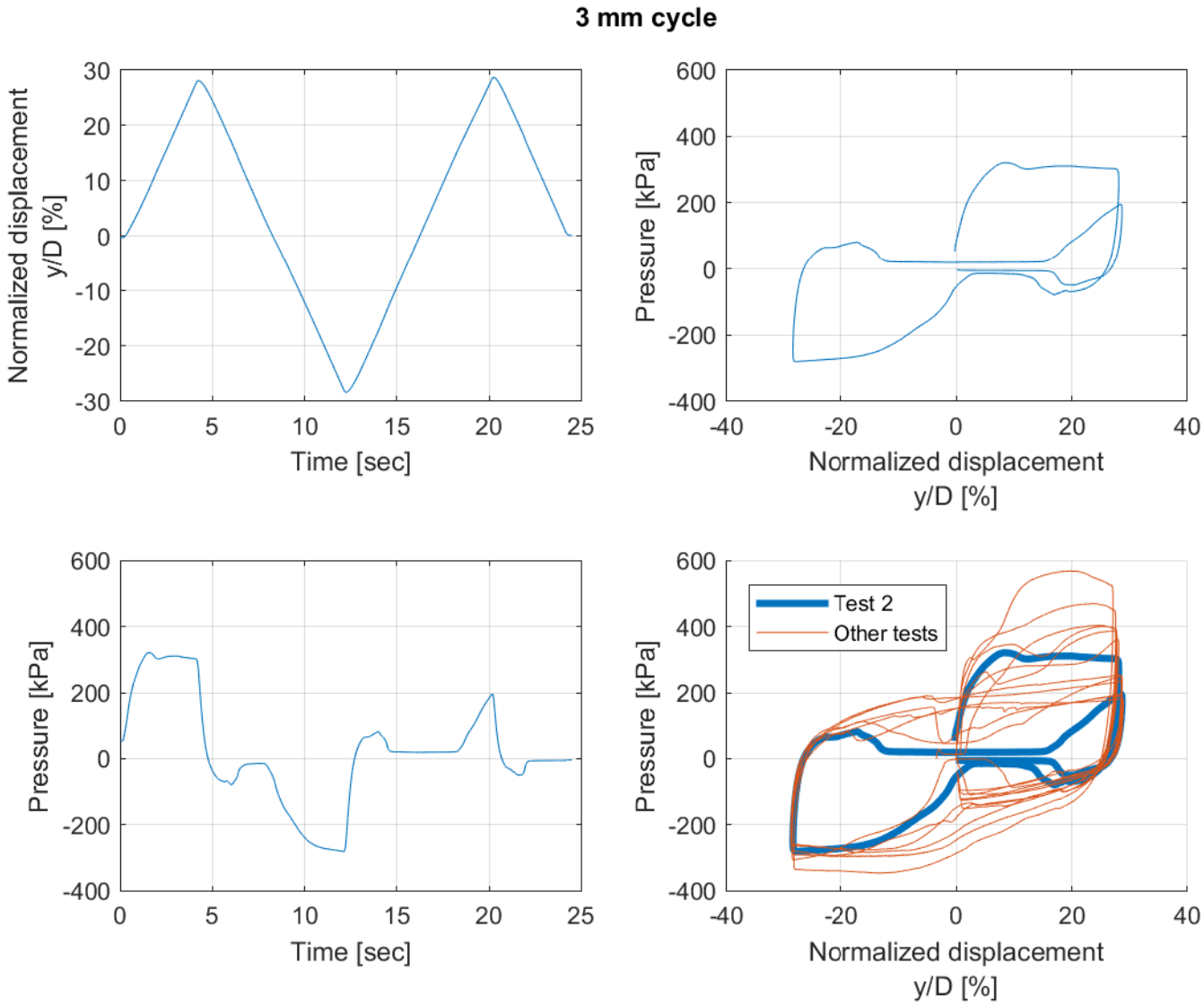
3 mm cycle
Normalized displacement y/D [%]
Time [sec]
Pressure [kPa]
Normalized displacement y/D [%]
Pressure [kPa]
Time [sec]
Test 2
Other tests
Pressure [kPa]
Normalized displacement y/D [%]

Test 2

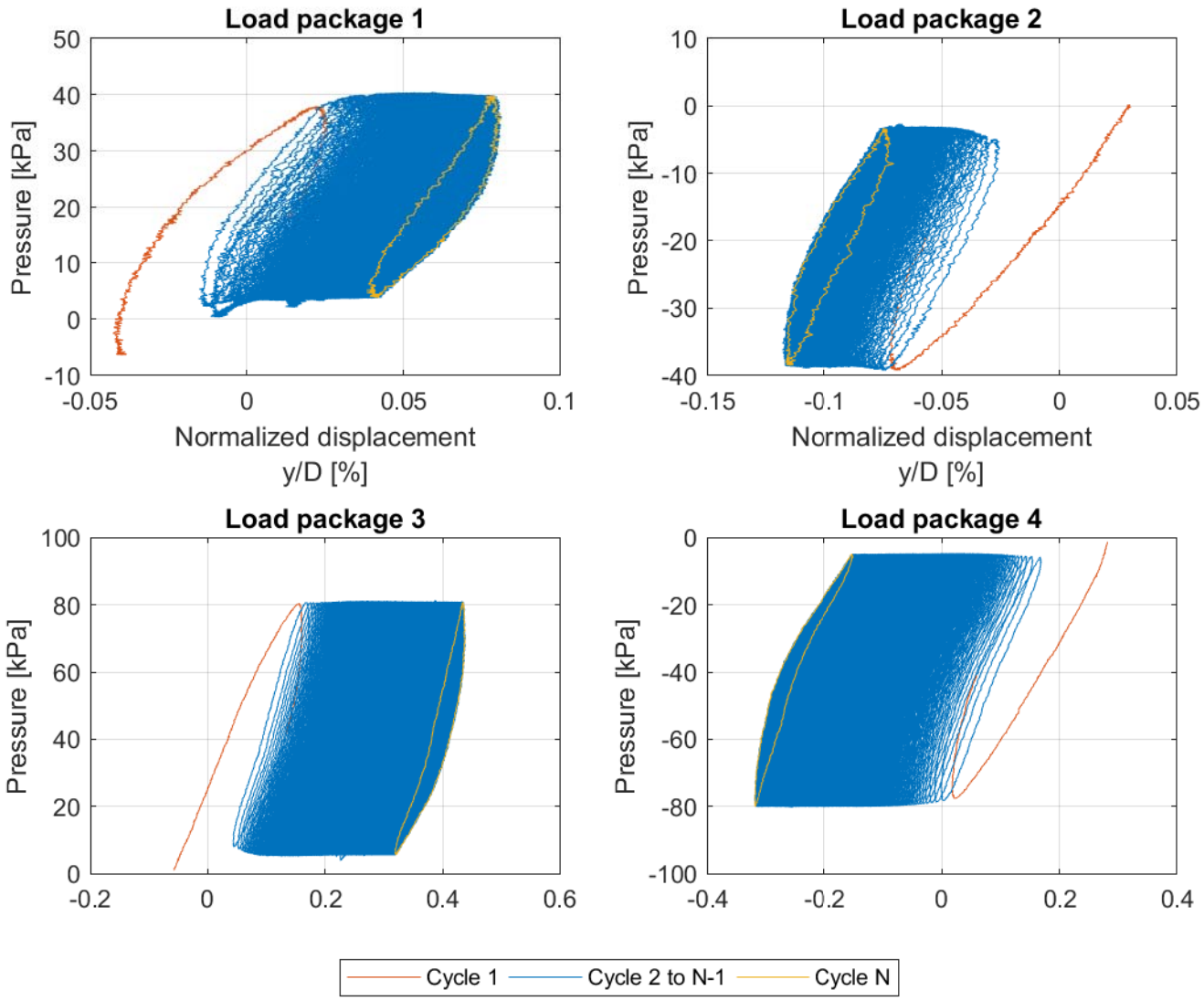
Load package 1
Pressure [kPa]
Normalized displacement
y/D [%]
Load package 2
Pressure [kPa]
Normalized displacement
y/D [%]
Load package 3
Pressure [kPa]
Load package 4
Pressure [kPa]
Cycle 1
Cycle 2 to N-1
Cycle N

Test 2

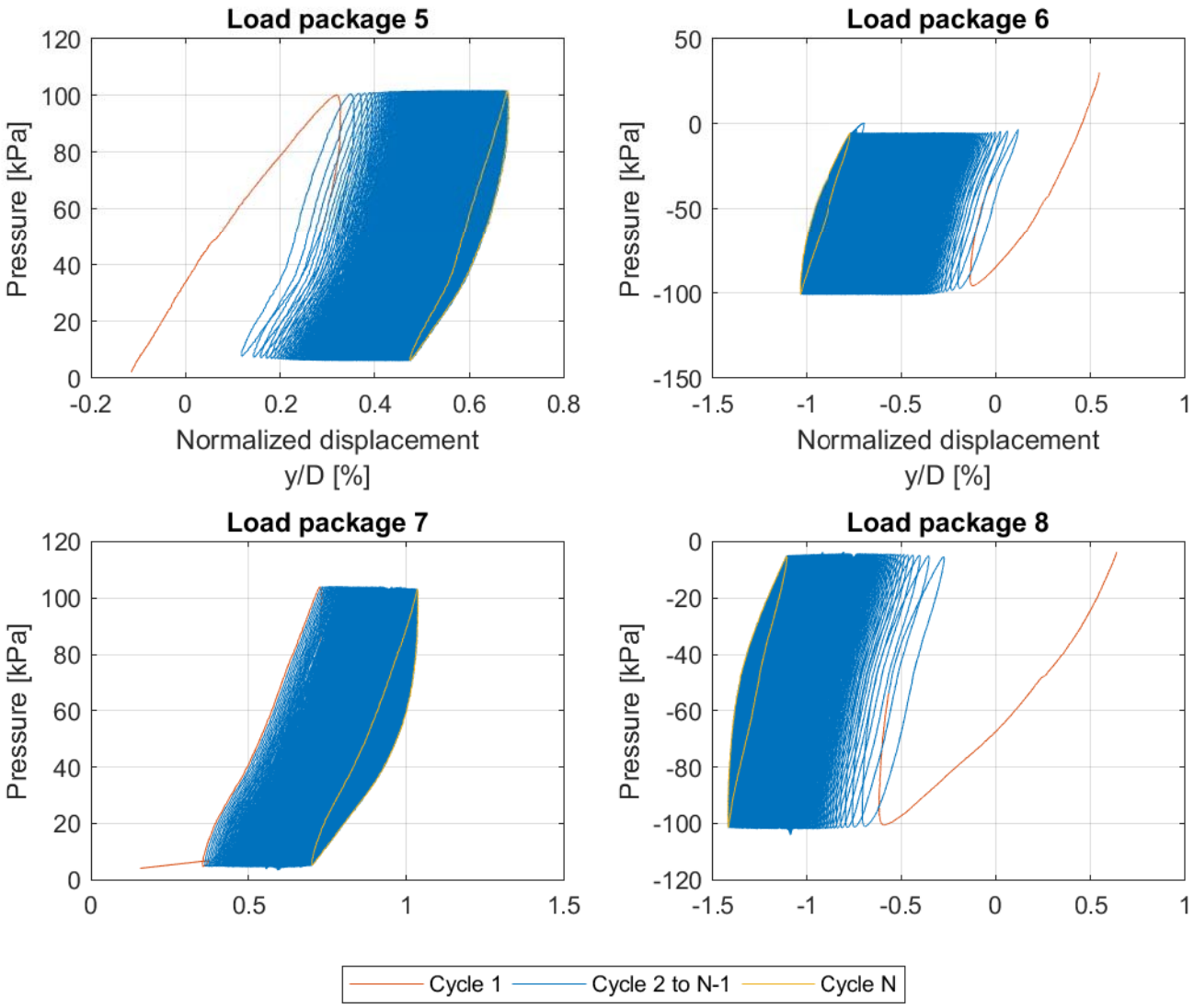
Load package 5
Pressure [kPa]
Normalized displacement
y/D [%]
Load package 6
Pressure [kPa]
Normalized displacement
y/D [%]
Load package 7
Pressure [kPa]
Load package 8
Pressure [kPa]
Cycle 1
Cycle 2 to N-1
Cycle N

Test 2

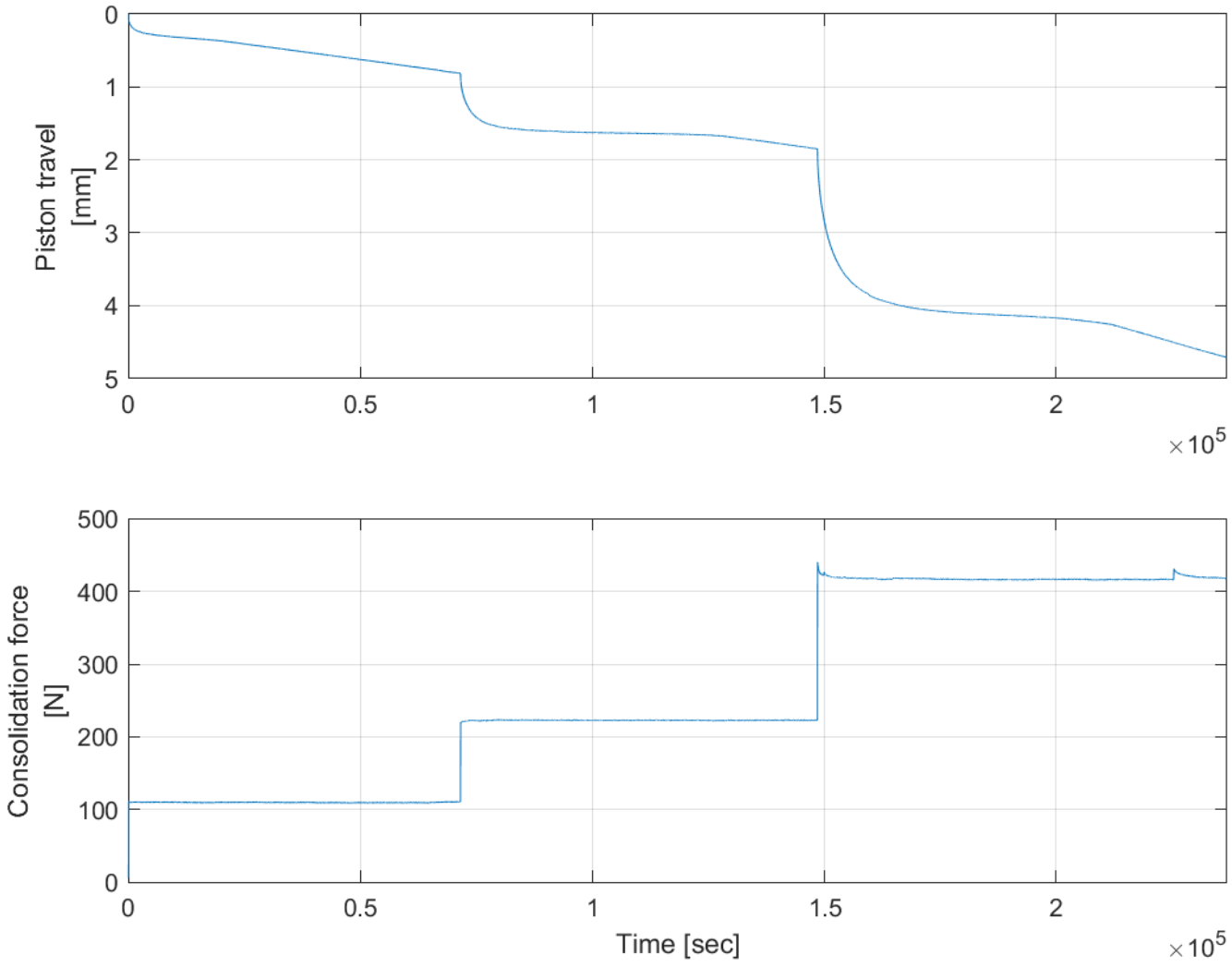
Piston travel
[mm]
0
1
2
3
4
5
0
0.5
1
1.5
2
×10^5
Consolidation force
[N]
500
400
300
200
100
0
0
0.5
1
1.5
2
Time [sec]
×10^5

Test 4

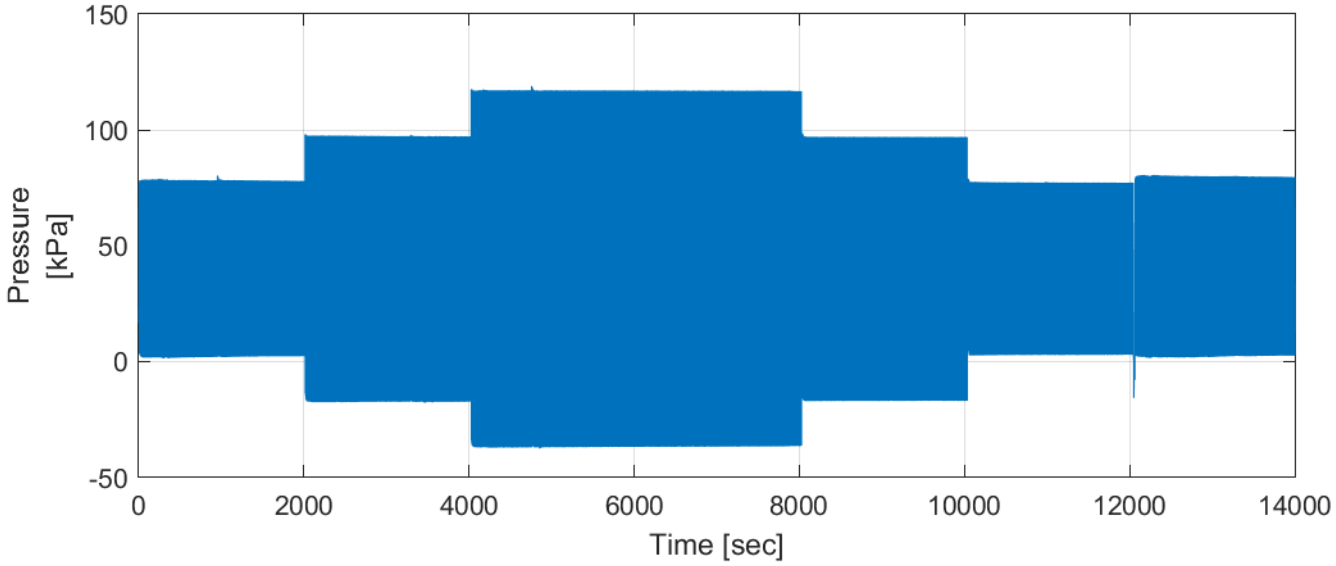
Pressure [kPa]
150
100
50
0
-50
0
2000
4000
6000
8000
10000
12000
14000
Time [sec]

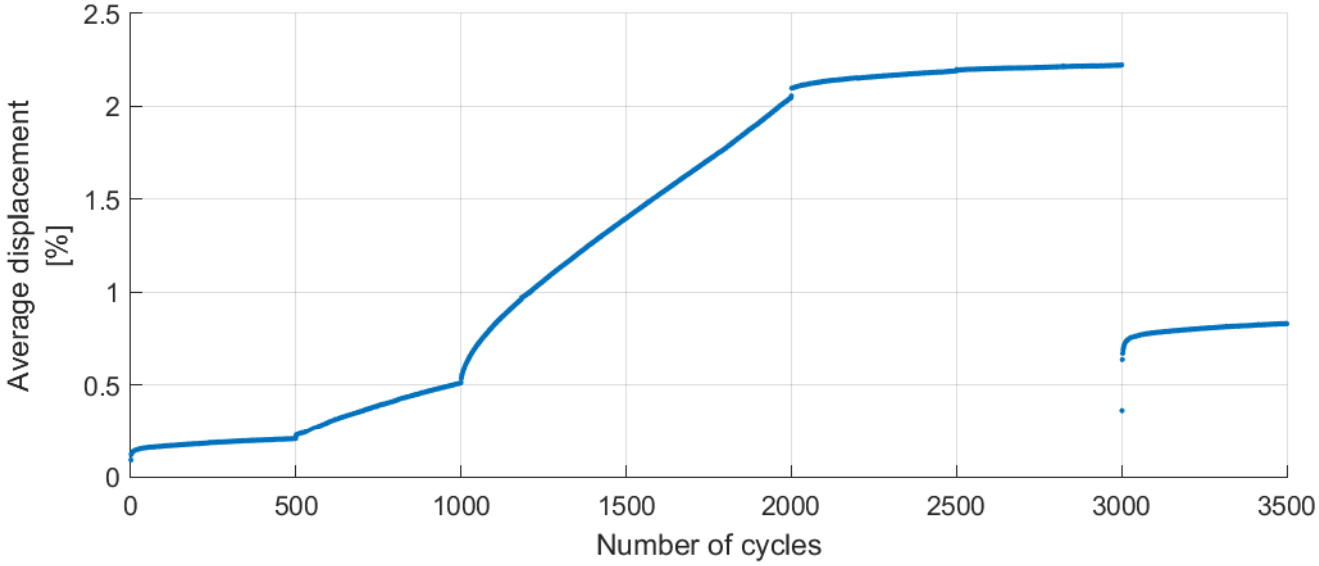
Average displacement [%]
2.5
2
1.5
1
0.5
0
0
500
1000
1500
2000
2500
3000
3500
Number of cycles

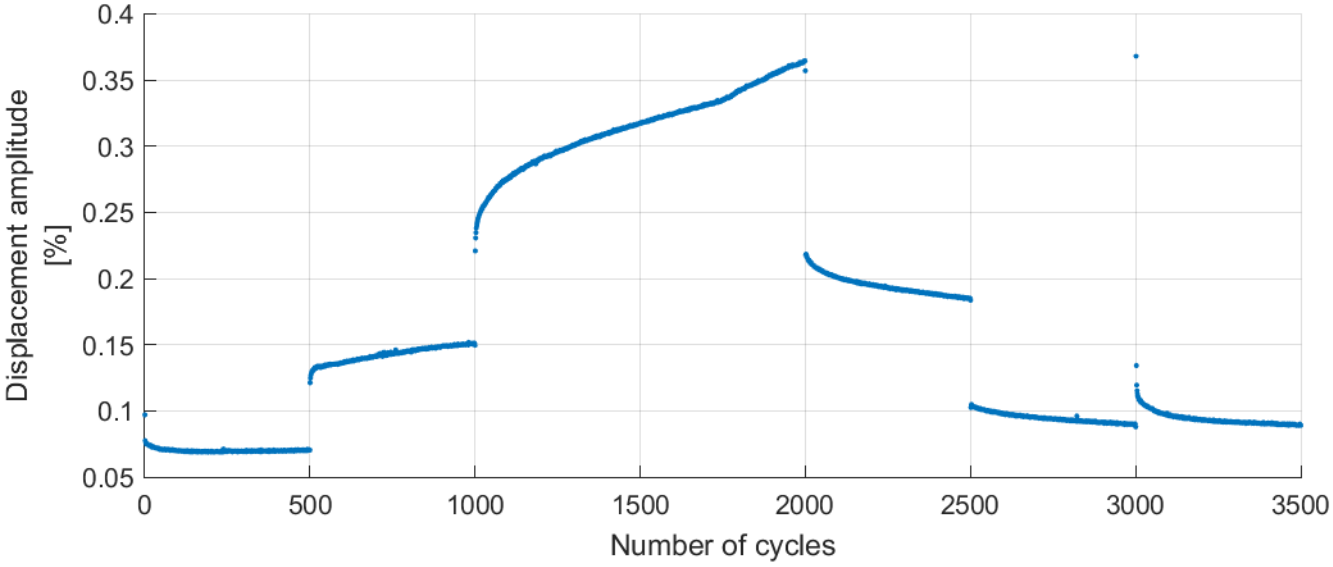
Displacement amplitude [%]
0.4
0.35
0.3
0.25
0.2
0.15
0.1
0.05
0
500
1000
1500
2000
2500
3000
3500
Number of cycles

Test 4

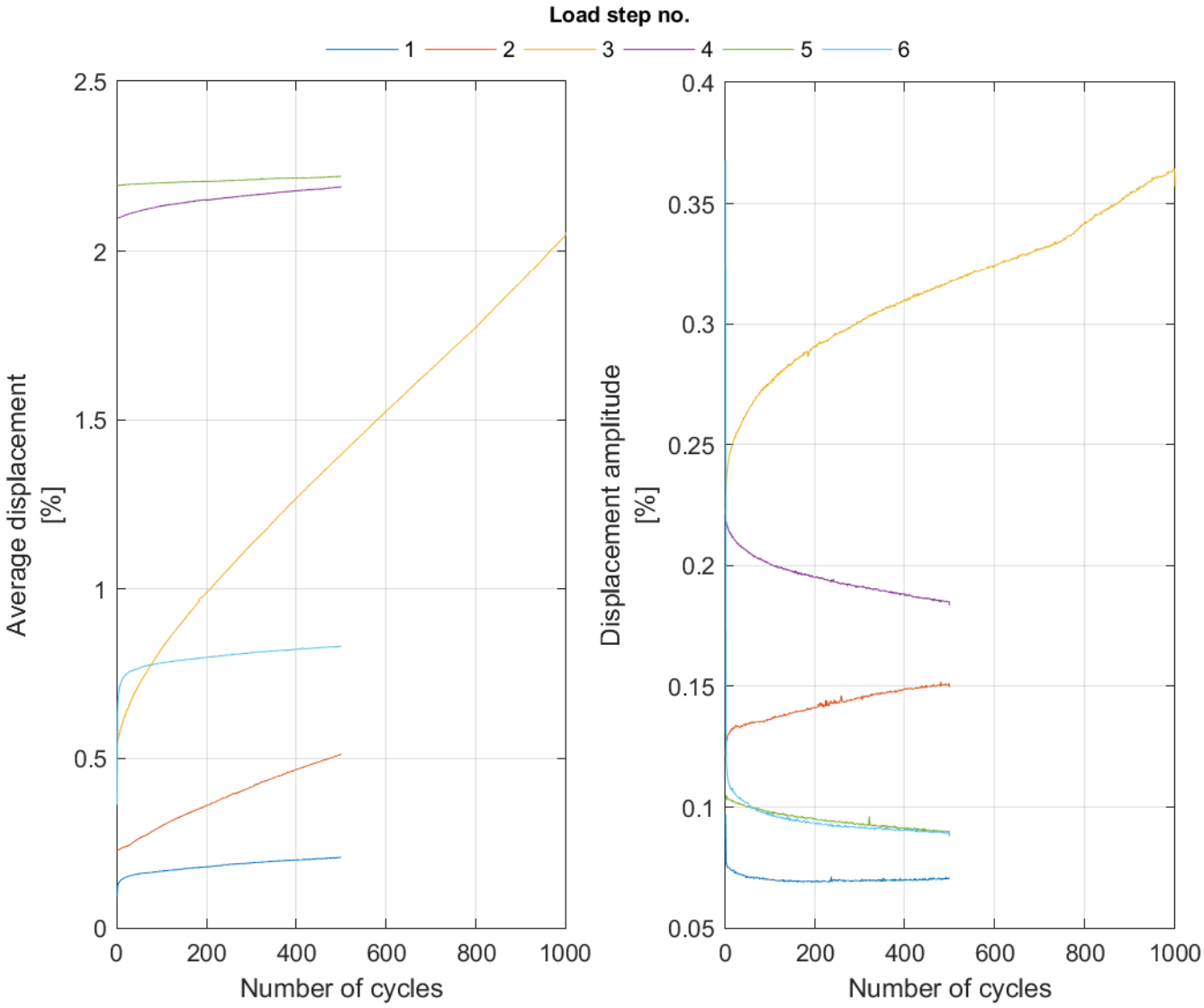
Load step no.
1
2
3
4
5
6
Average displacement [%]
Number of cycles
Displacement amplitude [%]
Number of cycles

Test 4

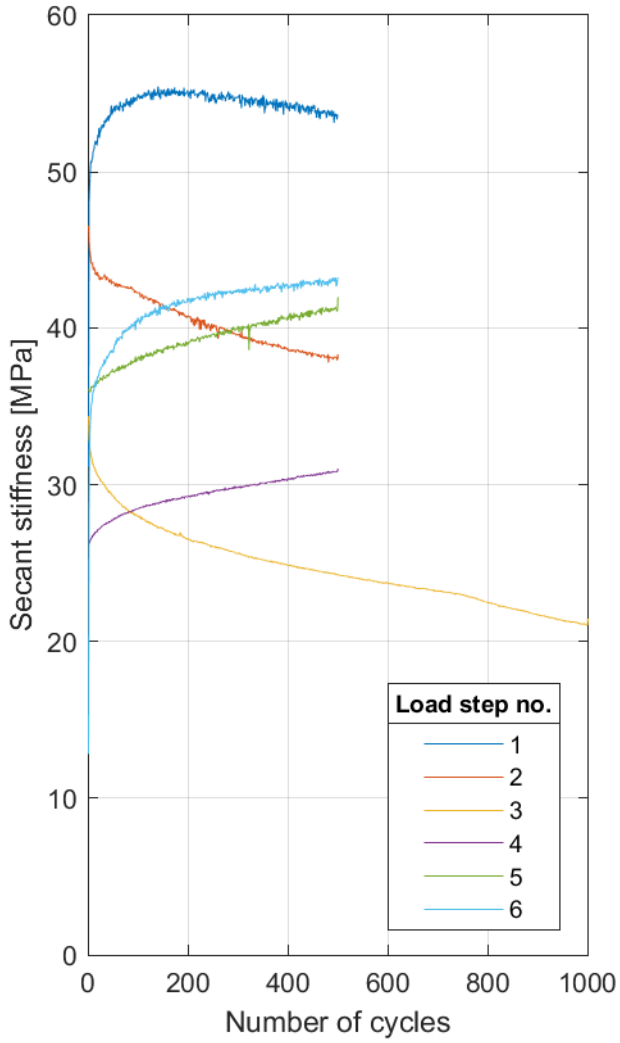
Secant stiffness [MPa]
Number of cycles
Load step no.
1
2
3
4
5
6

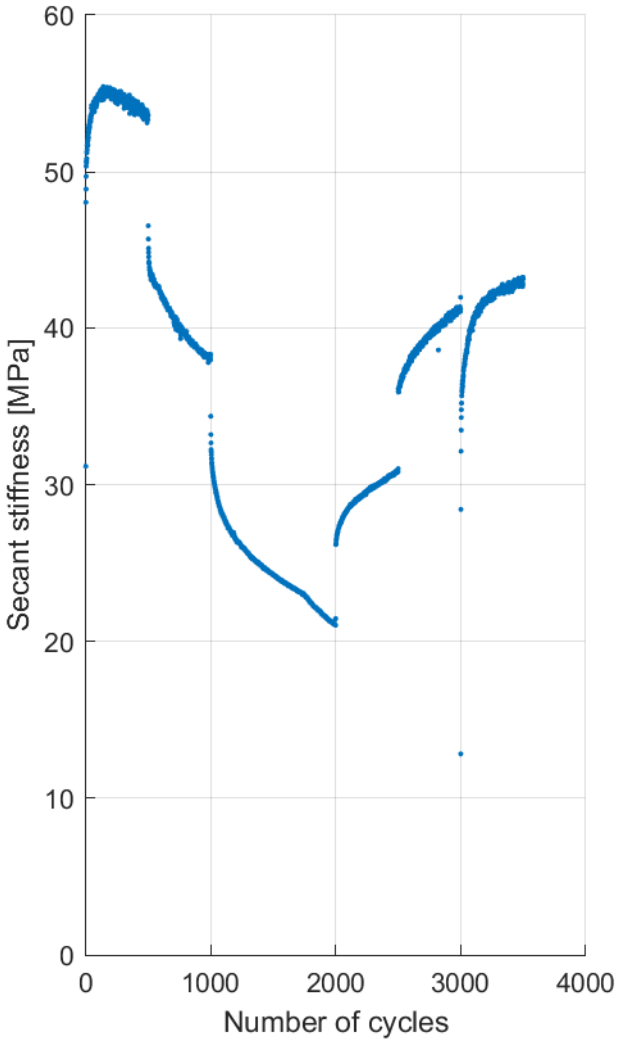
Secant stiffness [MPa]
Number of cycles

Test 4

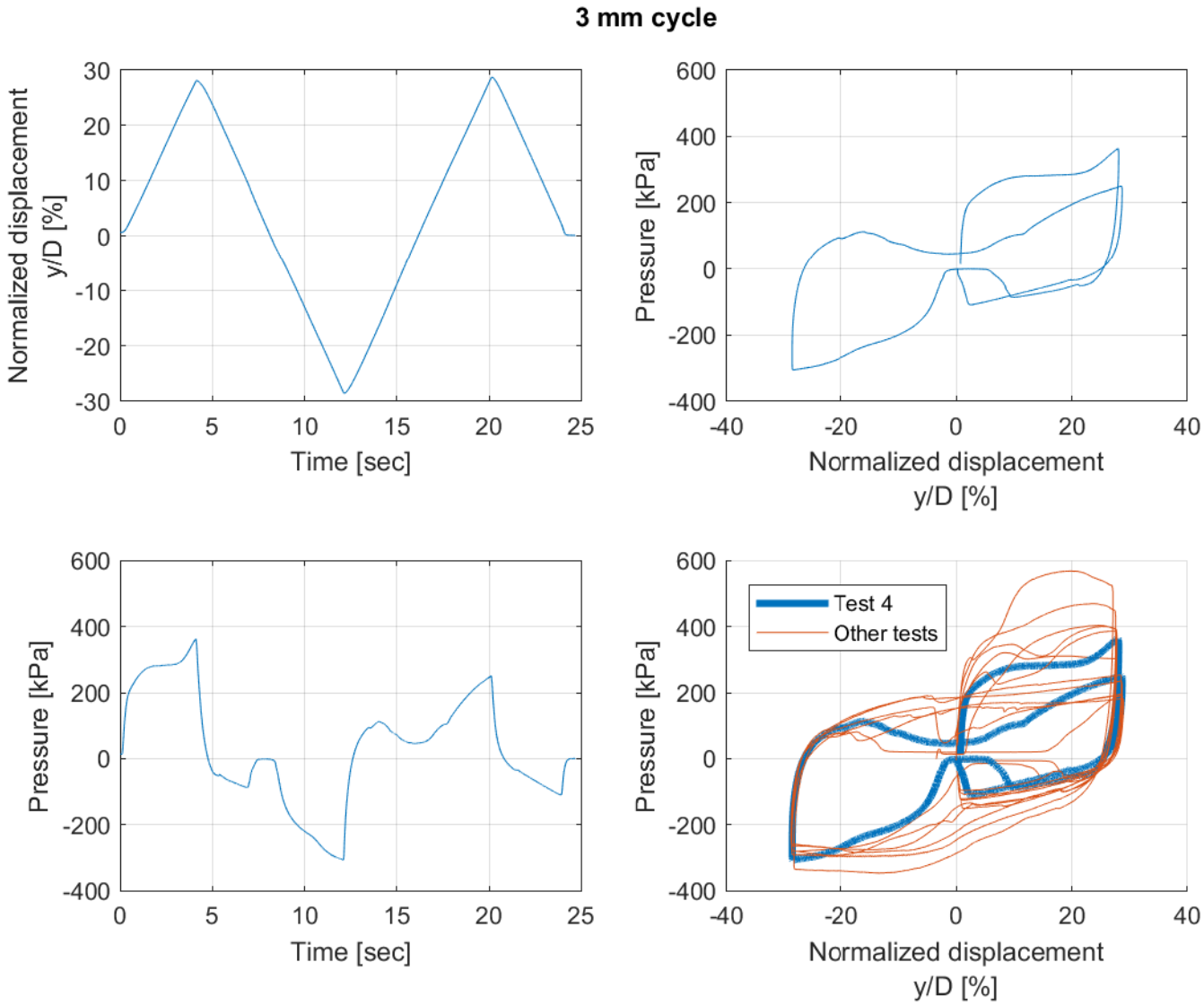
3 mm cycle
Normalized displacement y/D [%]
Time [sec]
Pressure [kPa]
Normalized displacement y/D [%]
Pressure [kPa]
Time [sec]
Test 4
Other tests
Pressure [kPa]
Normalized displacement y/D [%]

Test 4

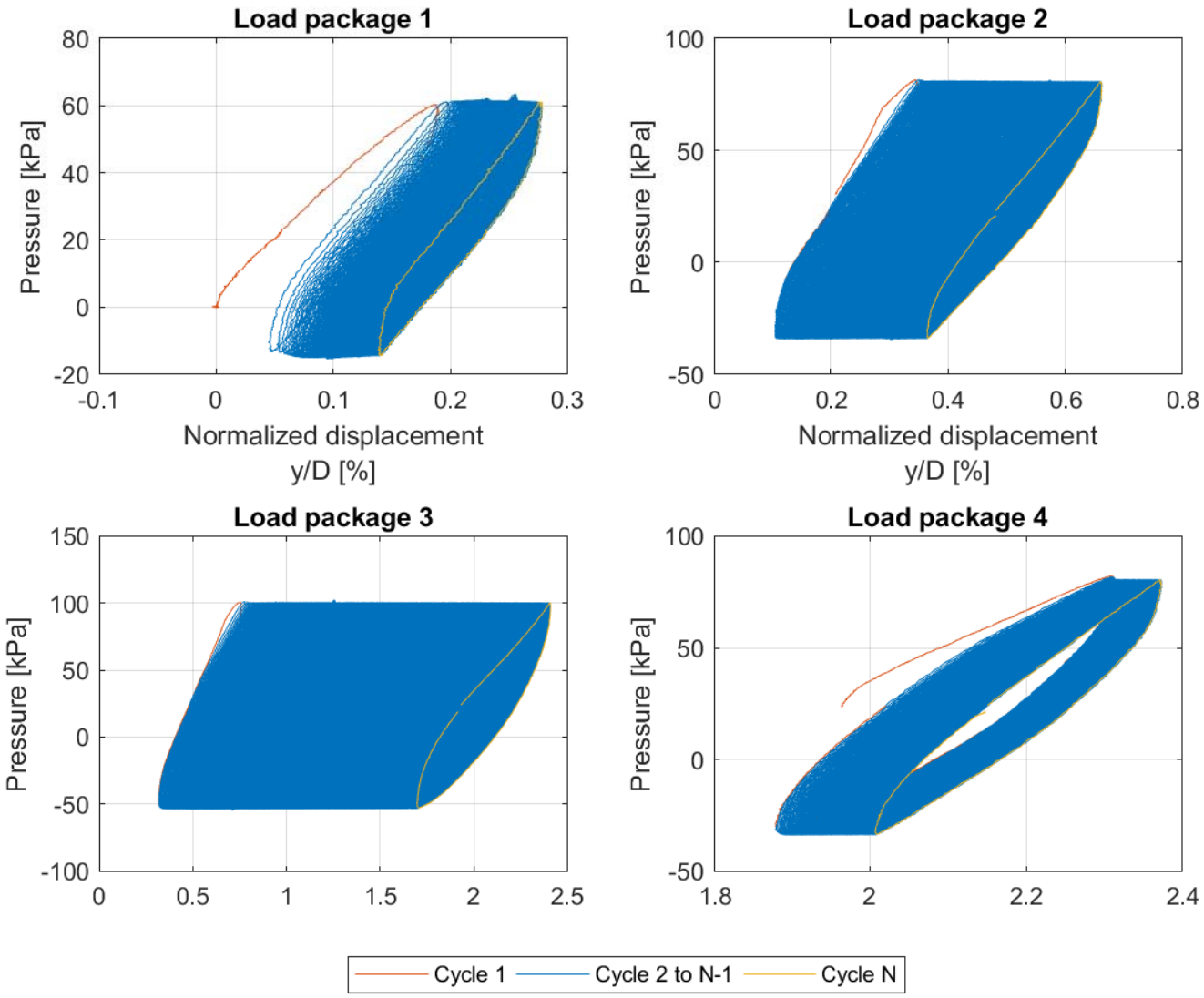
Load package 1
Pressure [kPa]
Normalized displacement
y/D [%]
Load package 2
Pressure [kPa]
Normalized displacement
y/D [%]
Load package 3
Pressure [kPa]
Load package 4
Pressure [kPa]
Cycle 1
Cycle 2 to N-1
Cycle N

Test 4

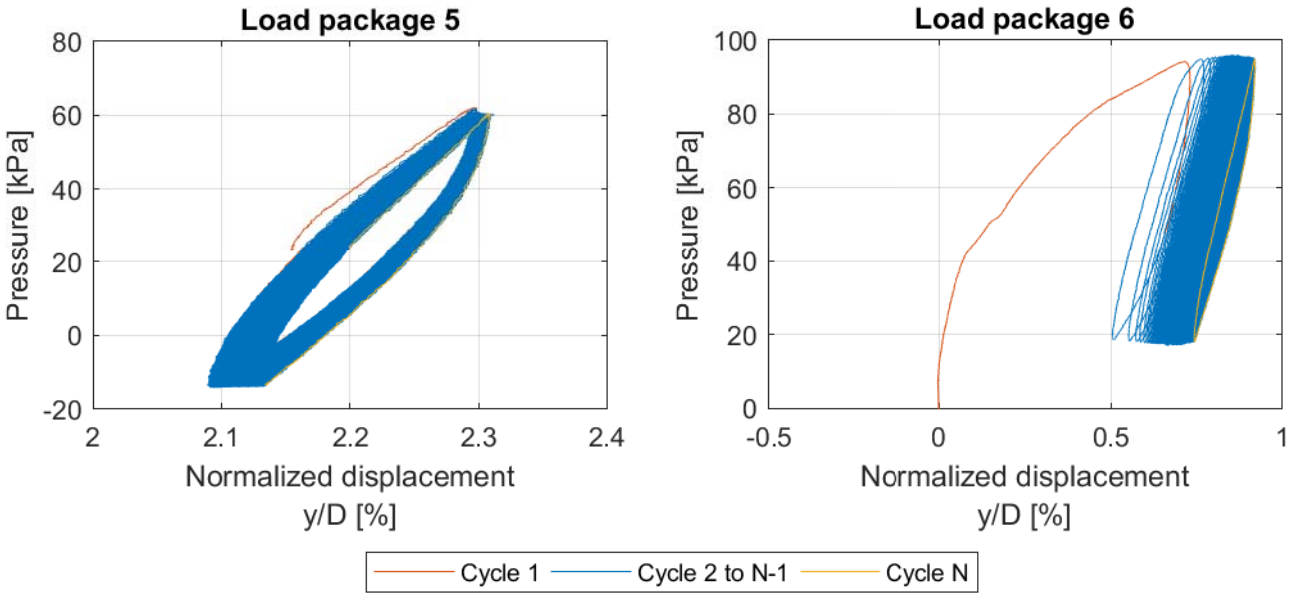
Load package 5
Pressure [kPa]
80
60
40
20
0
-20
2
2.1
2.2
2.3
2.4
Normalized displacement
y/D [%]
Load package 6
Pressure [kPa]
100
80
60
40
20
0
-0.5
0
0.5
1
Normalized displacement
y/D [%]
Cycle 1
Cycle 2 to N-1
Cycle N

Test 4

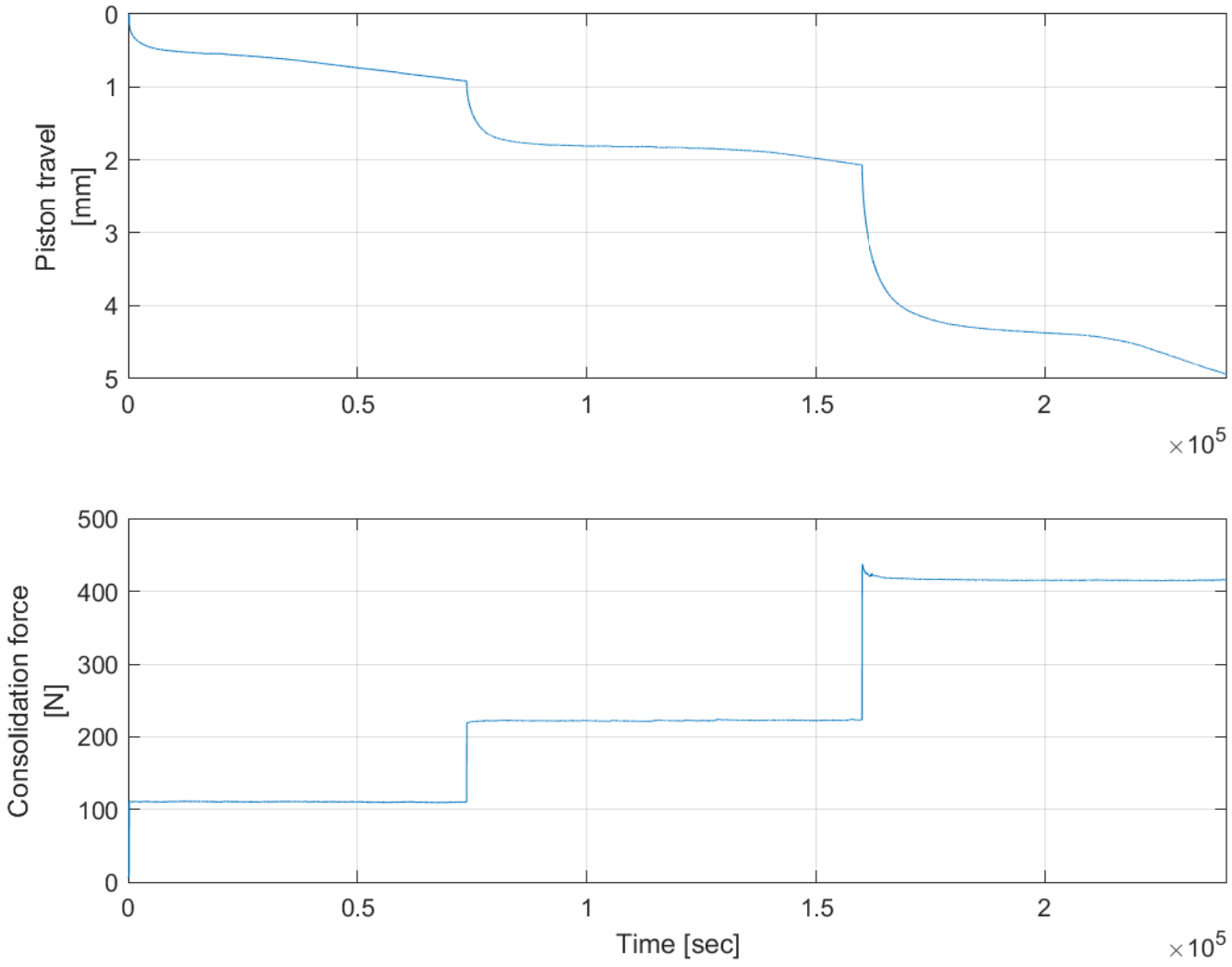
Piston travel
[mm]
0
1
2
3
4
5
0
0.5
1
1.5
2
×10^5
Consolidation force
[N]
500
400
300
200
100
0
0
0.5
1
1.5
2
Time [sec]
×10^5

Test 5

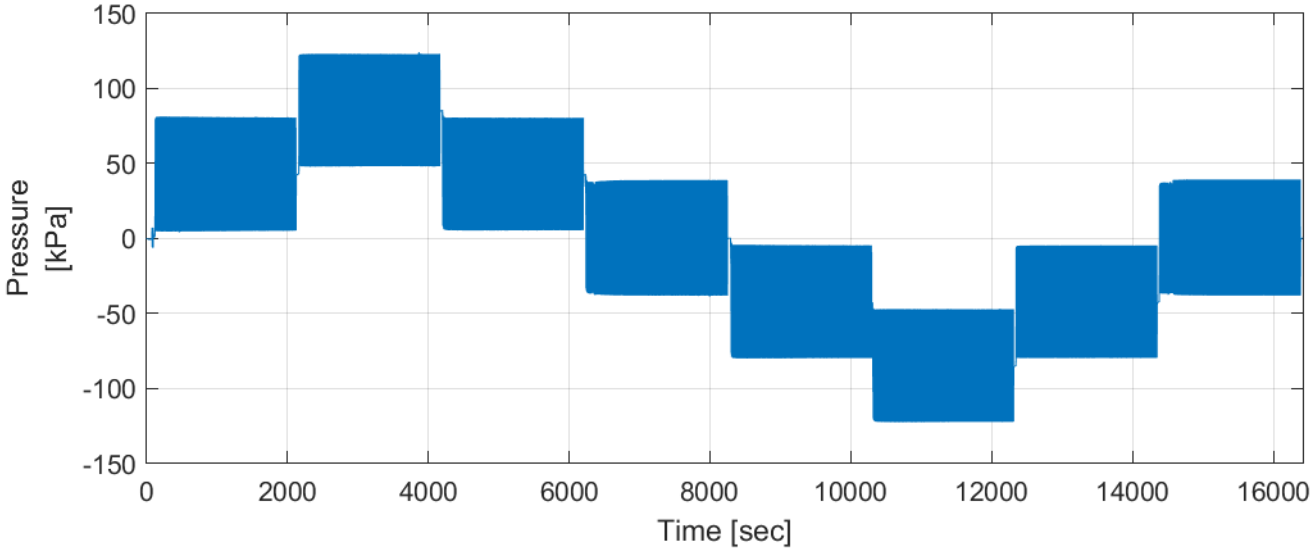
Pressure [kPa]
150
100
50
0
-50
-100
-150
0
2000
4000
6000
8000
10000
12000
14000
16000
Time [sec]

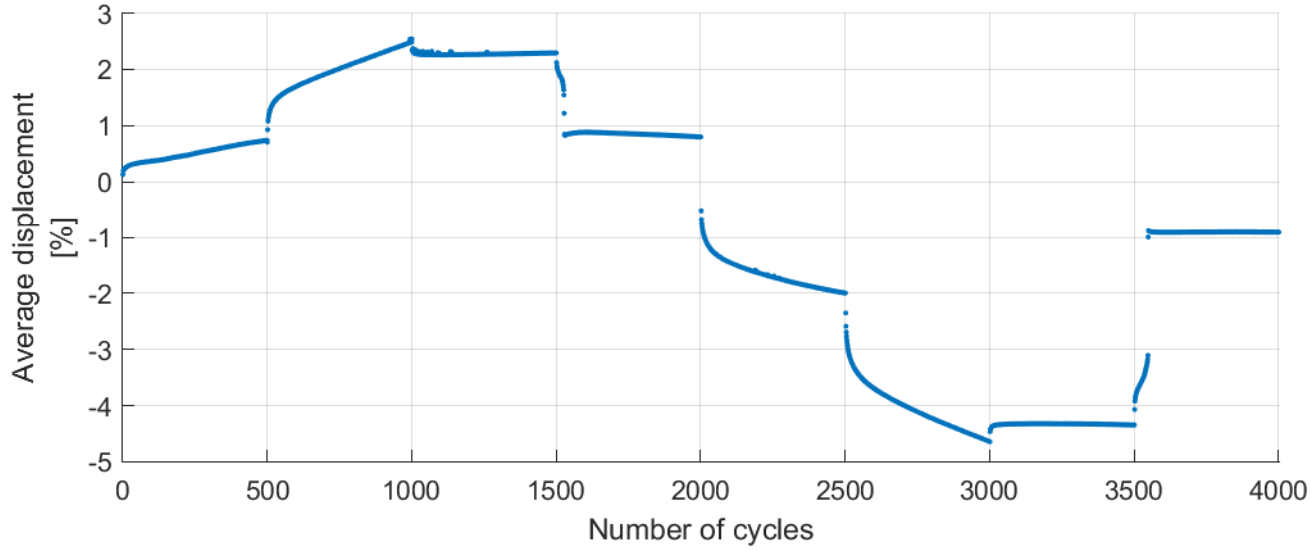
Average displacement [%]
3
2
1
0
-1
-2
-3
-4
-5
0
500
1000
1500
2000
2500
3000
3500
4000
Number of cycles

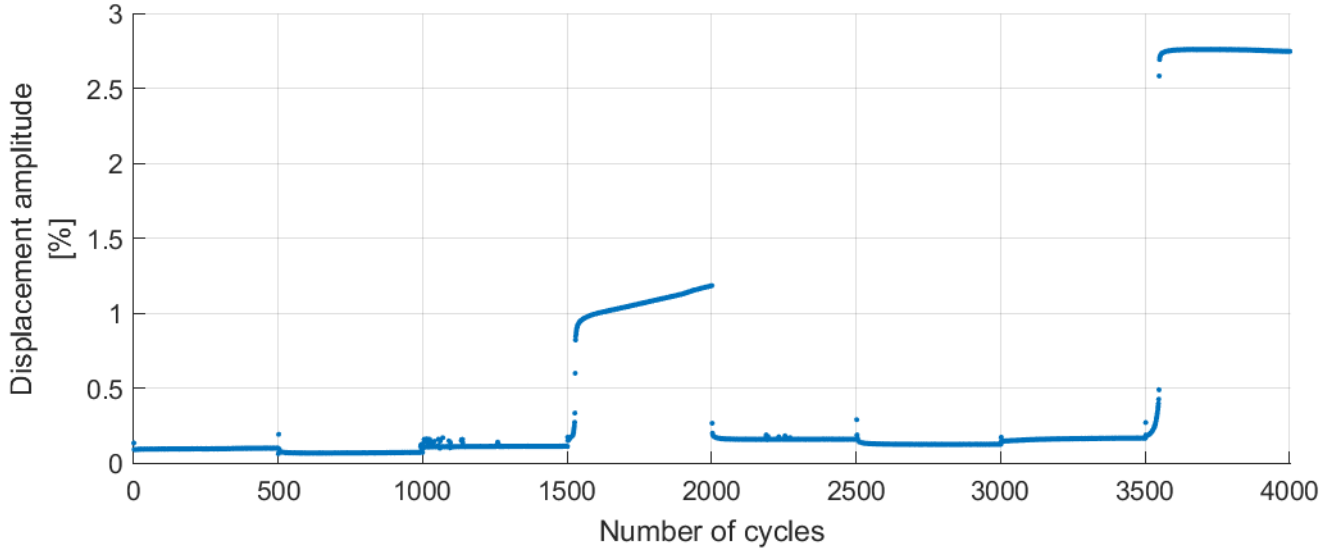
Displacement amplitude [%]
3
2.5
2
1.5
1
0.5
0
0
500
1000
1500
2000
2500
3000
3500
4000
Number of cycles

Test 5

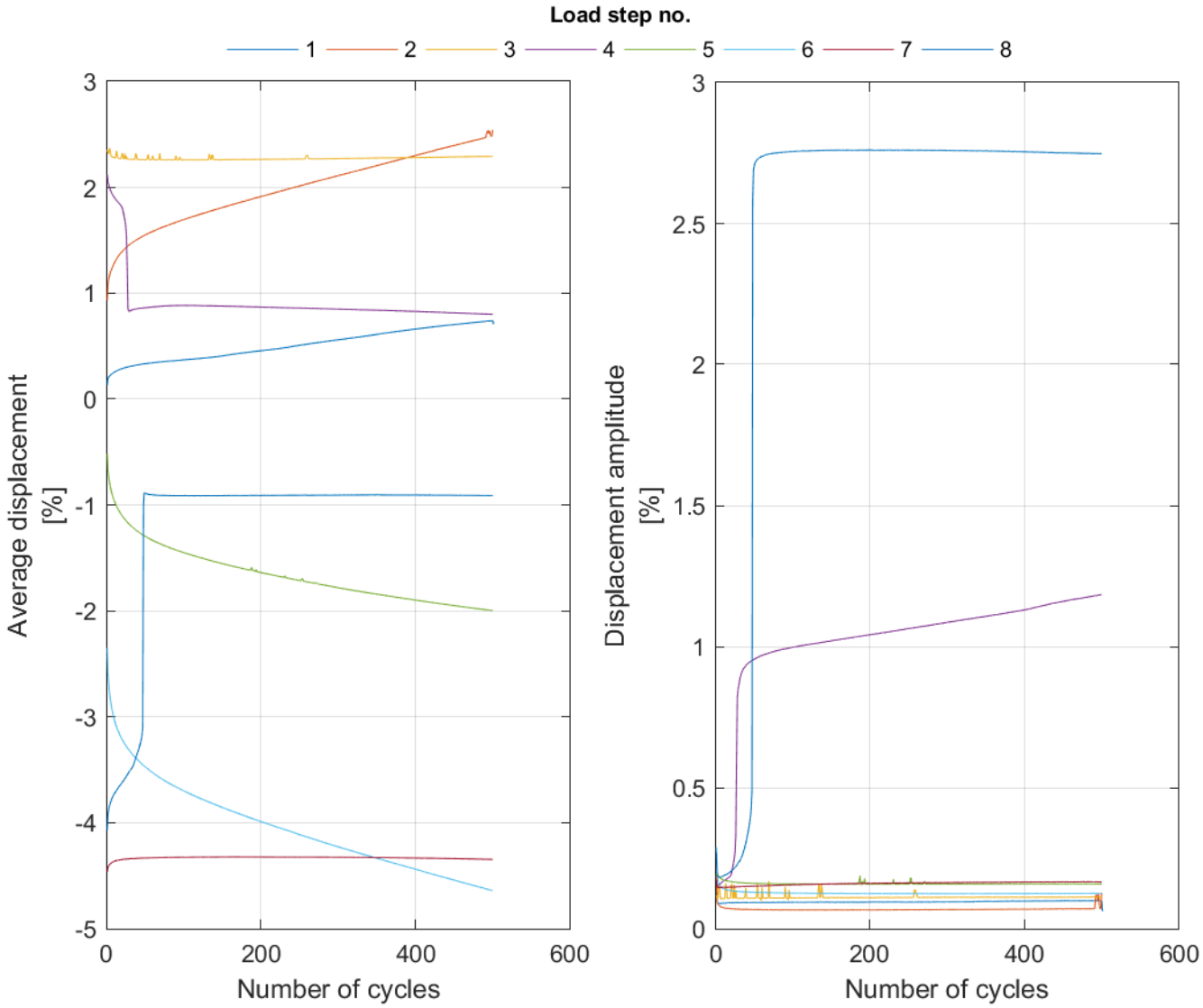
Load step no.
1
2
3
4
5
6
7
8
Average displacement [%]
Number of cycles
Displacement amplitude [%]
Number of cycles

Test 5

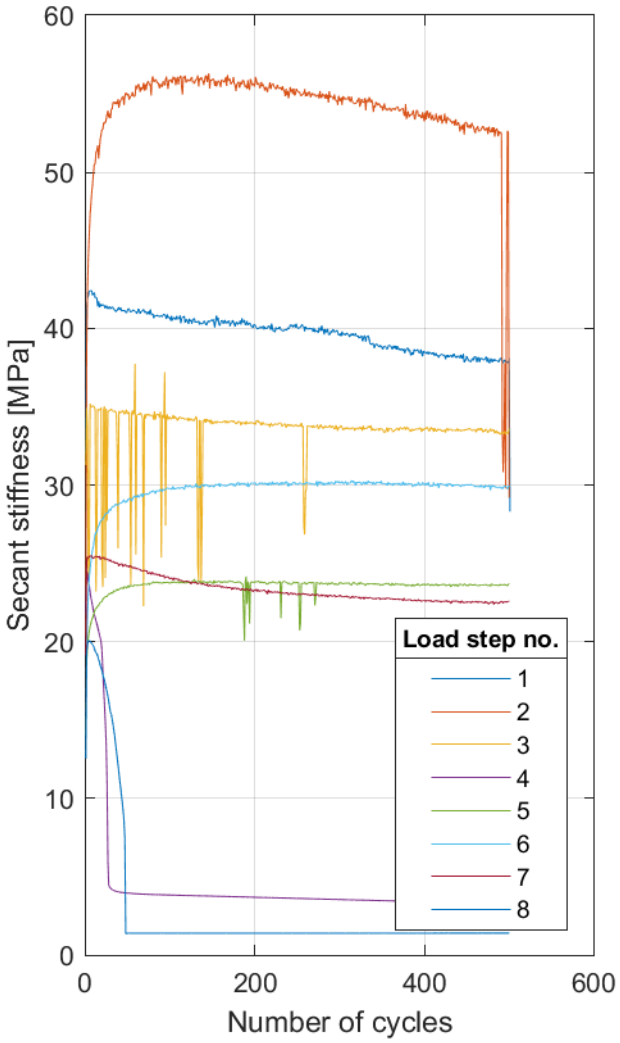
Secant stiffness [MPa]
Number of cycles
Load step no.
1
2
3
4
5
6
7
8

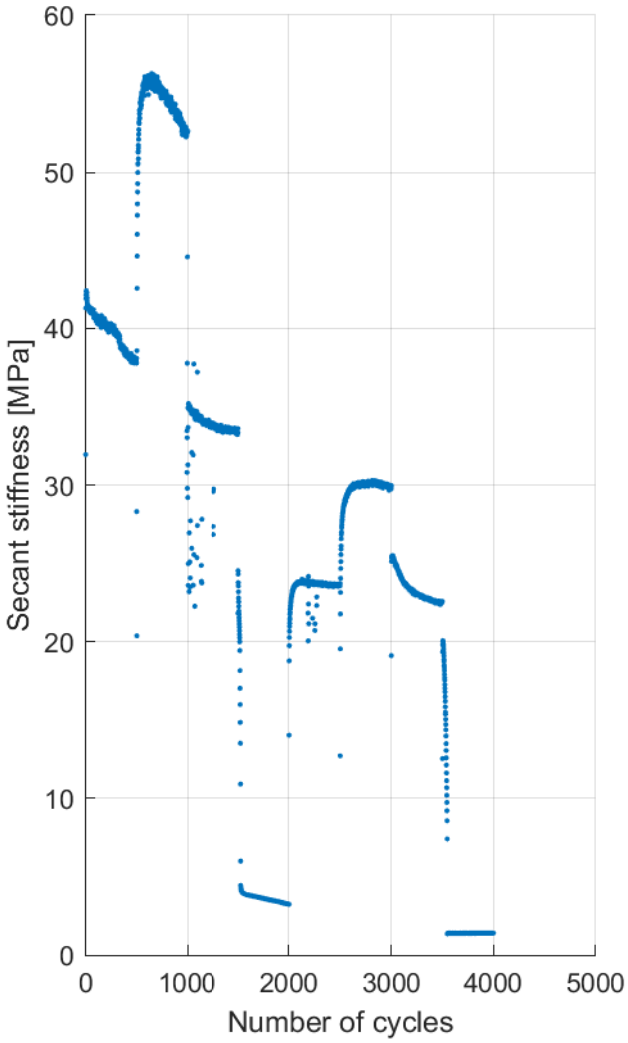
Secant stiffness [MPa]
Number of cycles

Test 5

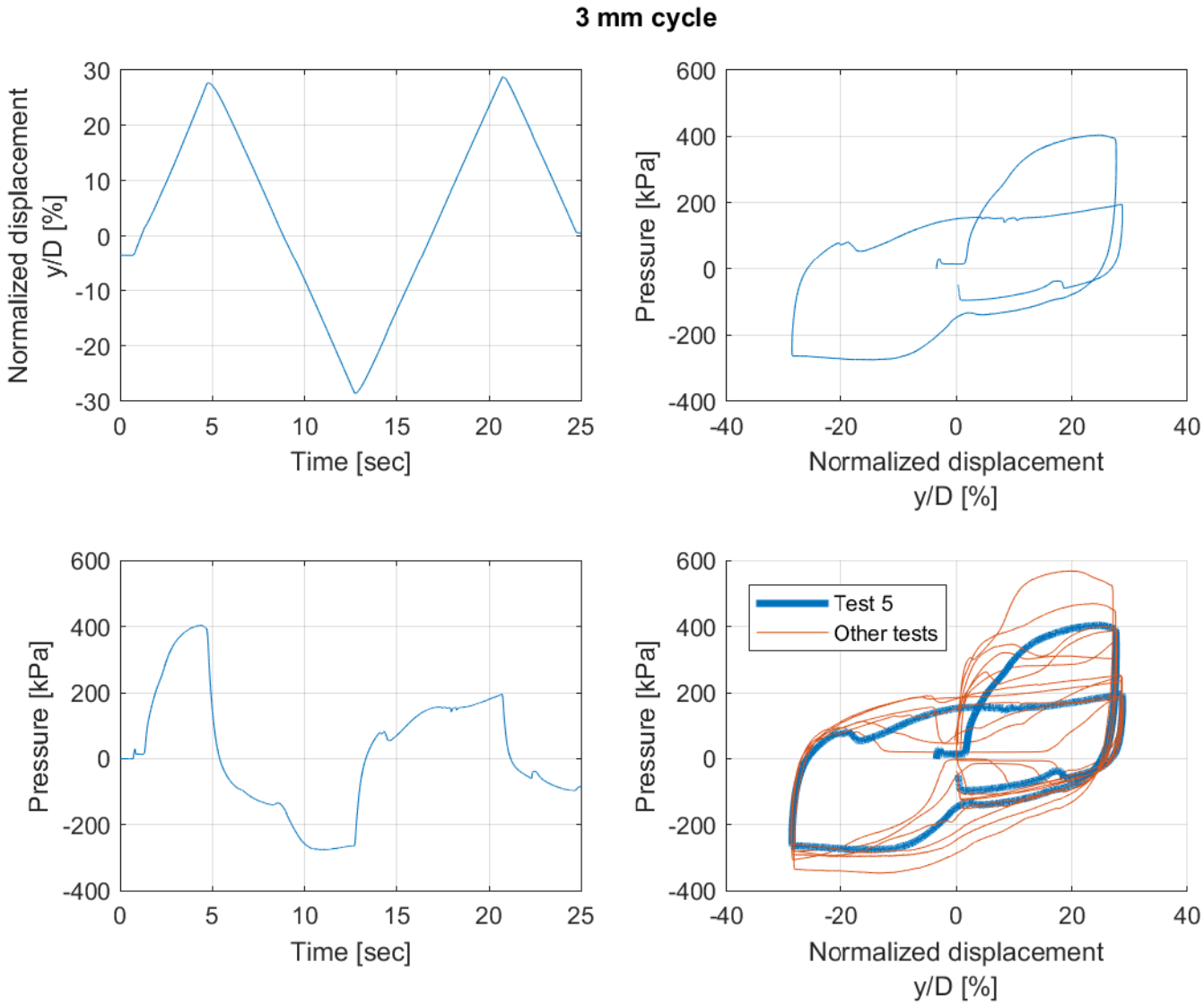
3 mm cycle
Normalized displacement y/D [%]
Time [sec]
Pressure [kPa]
Normalized displacement y/D [%]
Pressure [kPa]
Time [sec]
Test 5
Other tests
Pressure [kPa]
Normalized displacement y/D [%]

Test 5

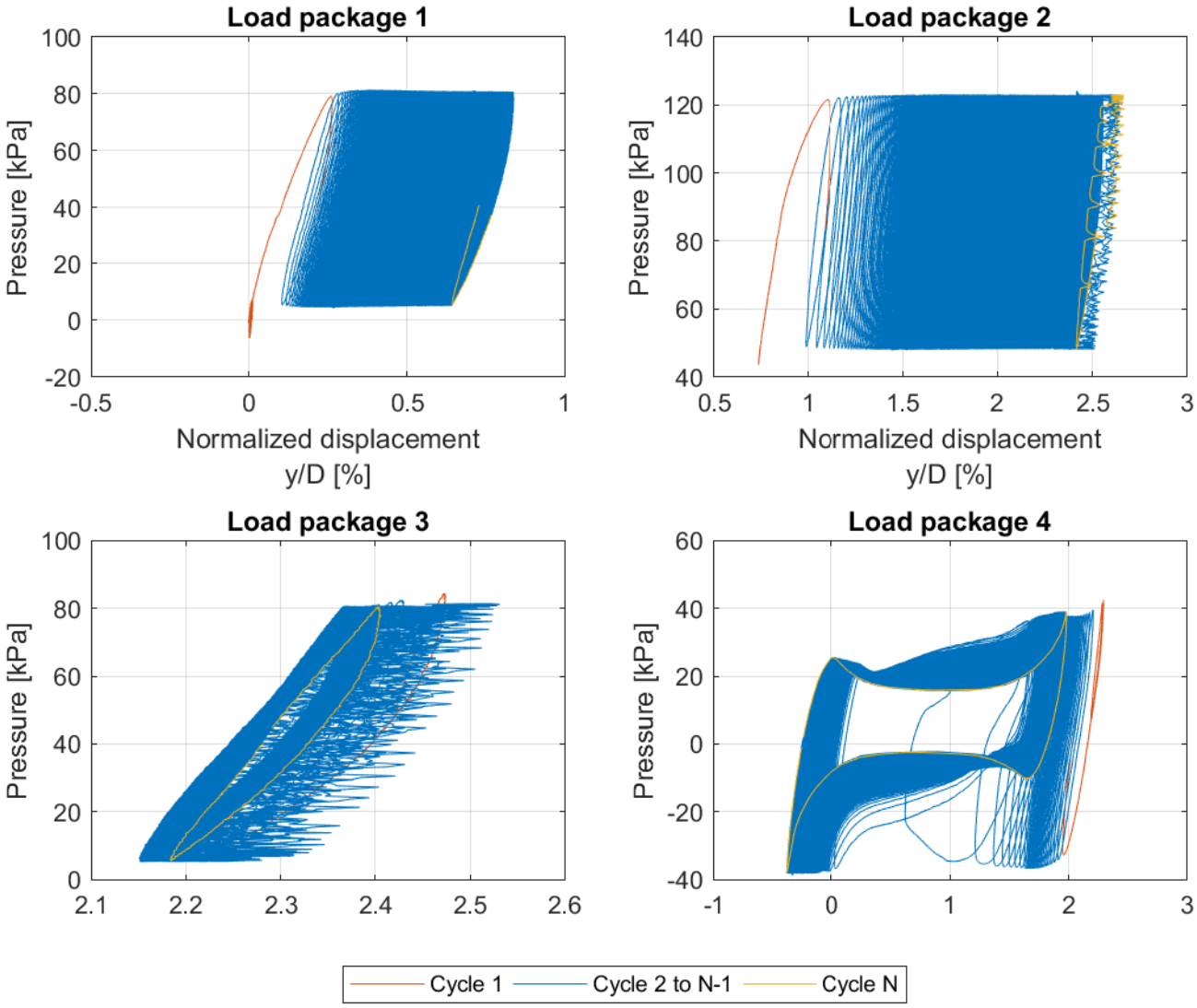
Load package 1
Pressure [kPa]
Normalized displacement
y/D [%]
Load package 2
Pressure [kPa]
Normalized displacement
y/D [%]
Load package 3
Pressure [kPa]
Load package 4
Pressure [kPa]
Cycle 1
Cycle 2 to N-1
Cycle N

Test 5

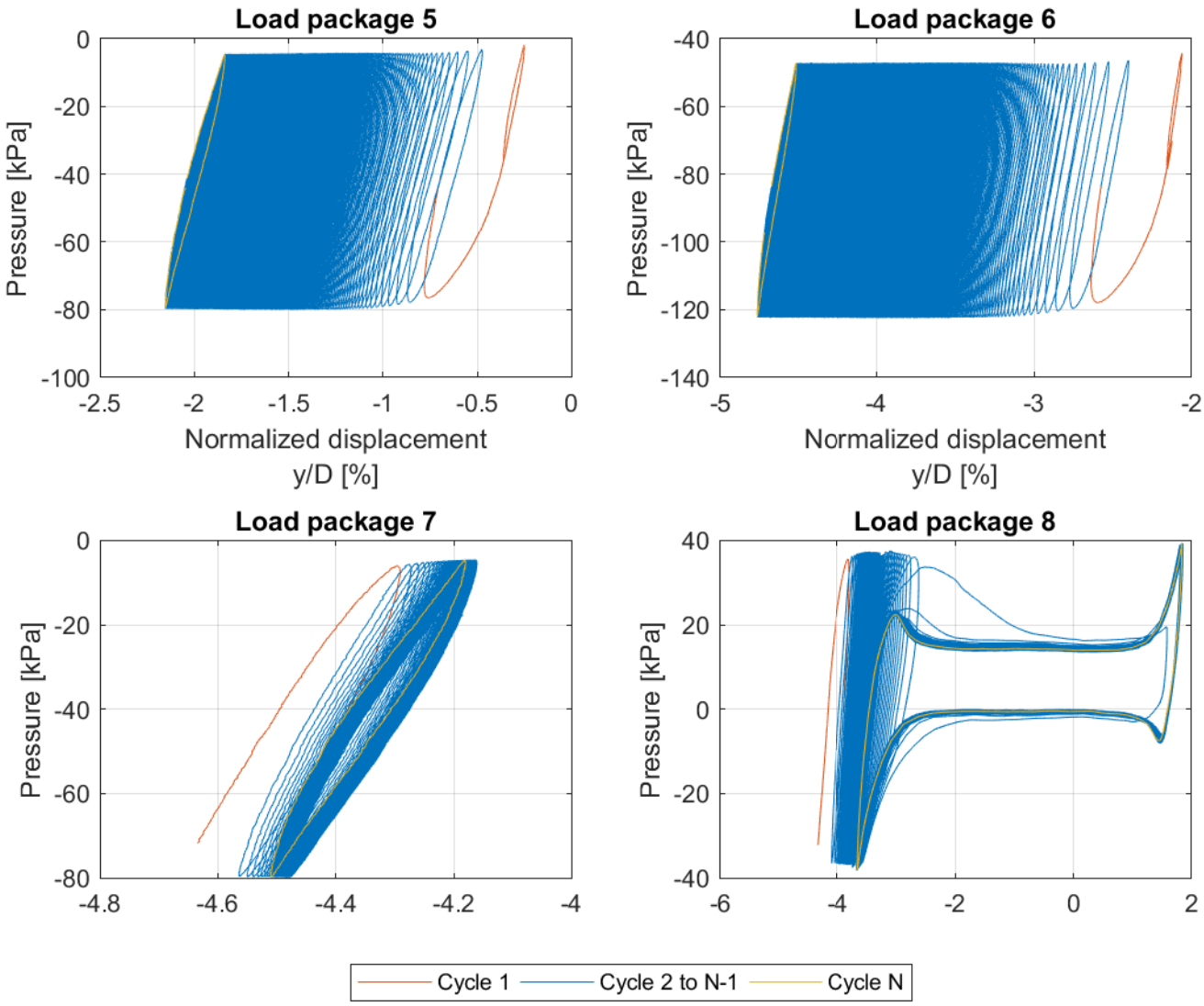
Load package 5
Pressure [kPa]
0
-20
-40
-60
-80
-100
-2.5
-2
-1.5
-1
-0.5
0
Normalized displacement
y/D [%]
Load package 6
Pressure [kPa]
-40
-60
-80
-100
-120
-140
-5
-4
-3
-2
Normalized displacement
y/D [%]
Load package 7
Pressure [kPa]
0
-20
-40
-60
-80
-4.8
-4.6
-4.4
-4.2
-4
Load package 8
Pressure [kPa]
40
20
0
-20
-40
-6
-4
-2
0
2
Cycle 1
Cycle 2 to N-1
Cycle N

Test 5

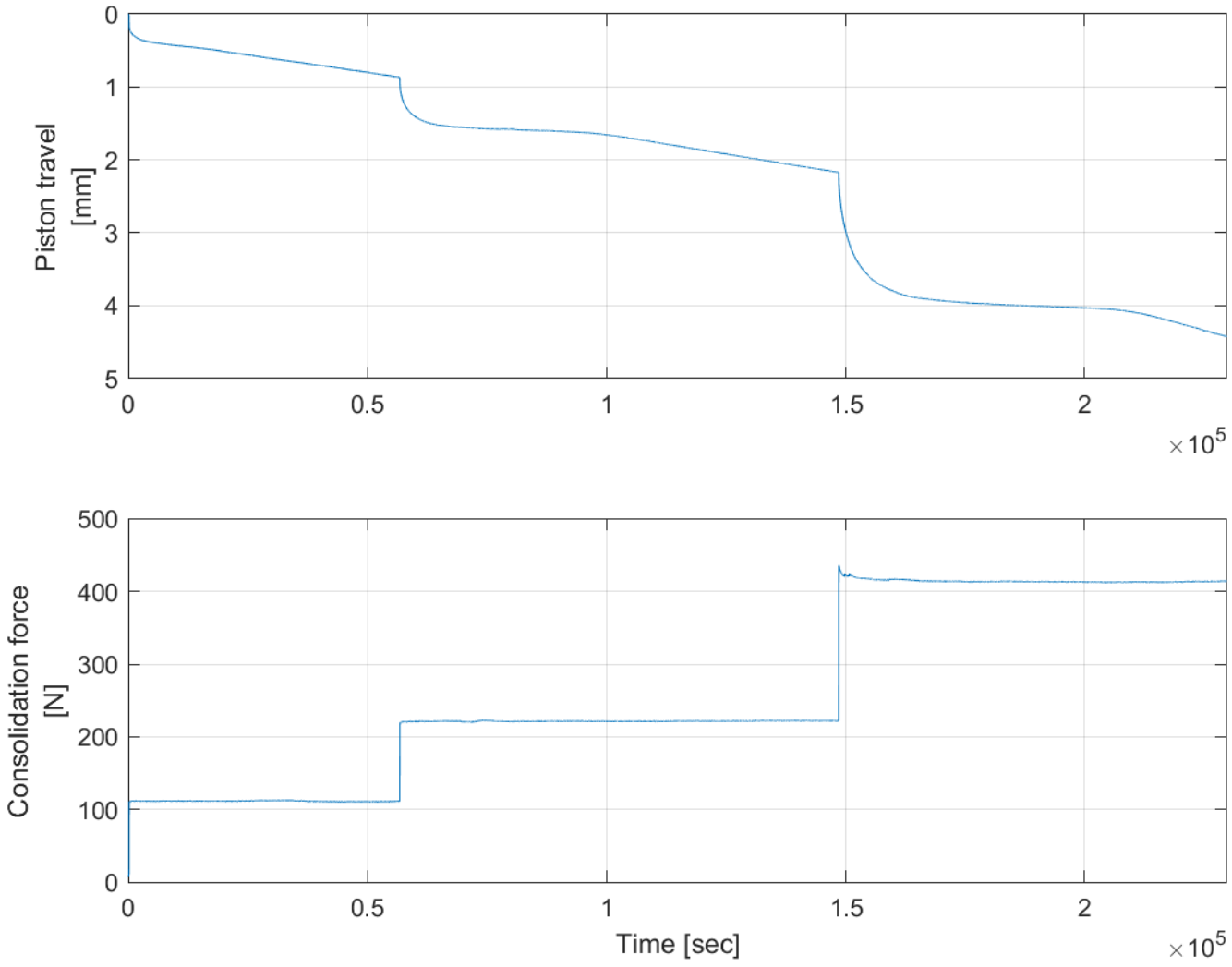
Piston travel [mm]
0
1
2
3
4
5
0
0.5
1
1.5
2
×10^5
Consolidation force [N]
500
400
300
200
100
0
0
0.5
1
1.5
2
Time [sec]
×10^5

Test 6

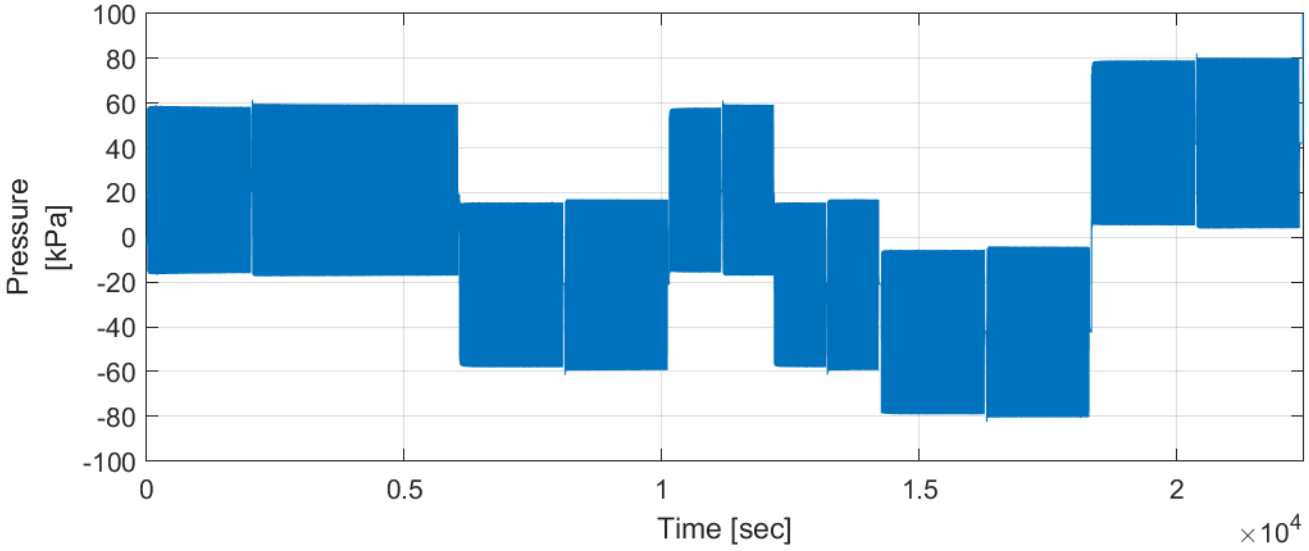
Pressure [kPa]
100
80
60
40
20
0
-20
-40
-60
-80
-100
0
0.5
1
1.5
2
Time [sec]
×10^4

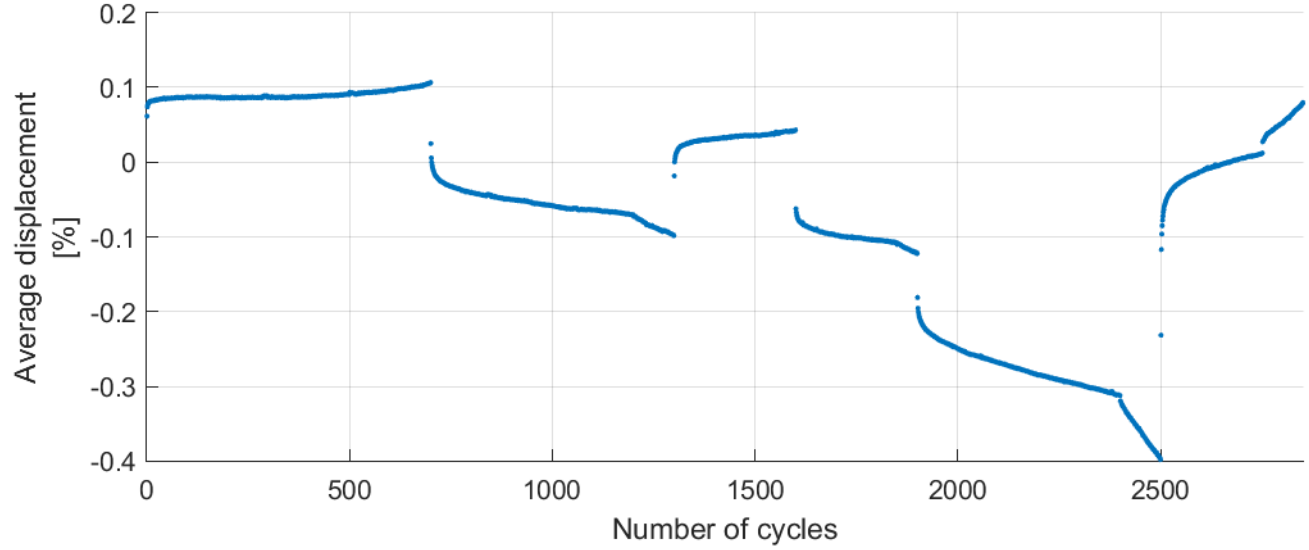
Average displacement [%]
0.2
0.1
0
-0.1
-0.2
-0.3
-0.4
0
500
1000
1500
2000
2500
Number of cycles

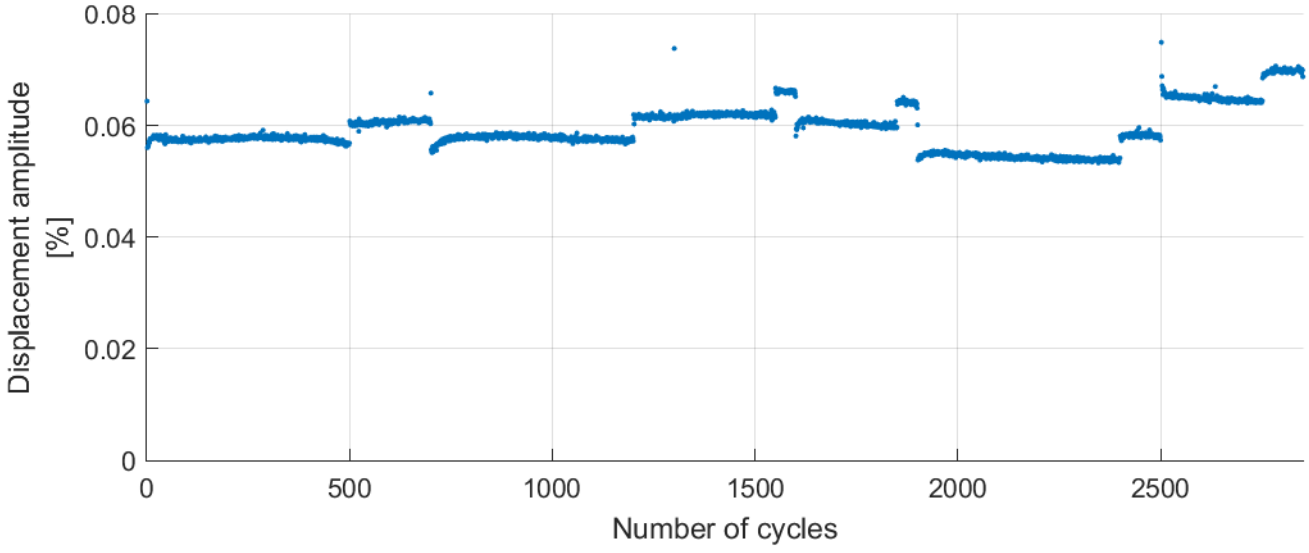
Displacement amplitude [%]
0.08
0.06
0.04
0.02
0
0
500
1000
1500
2000
2500
Number of cycles

Test 6

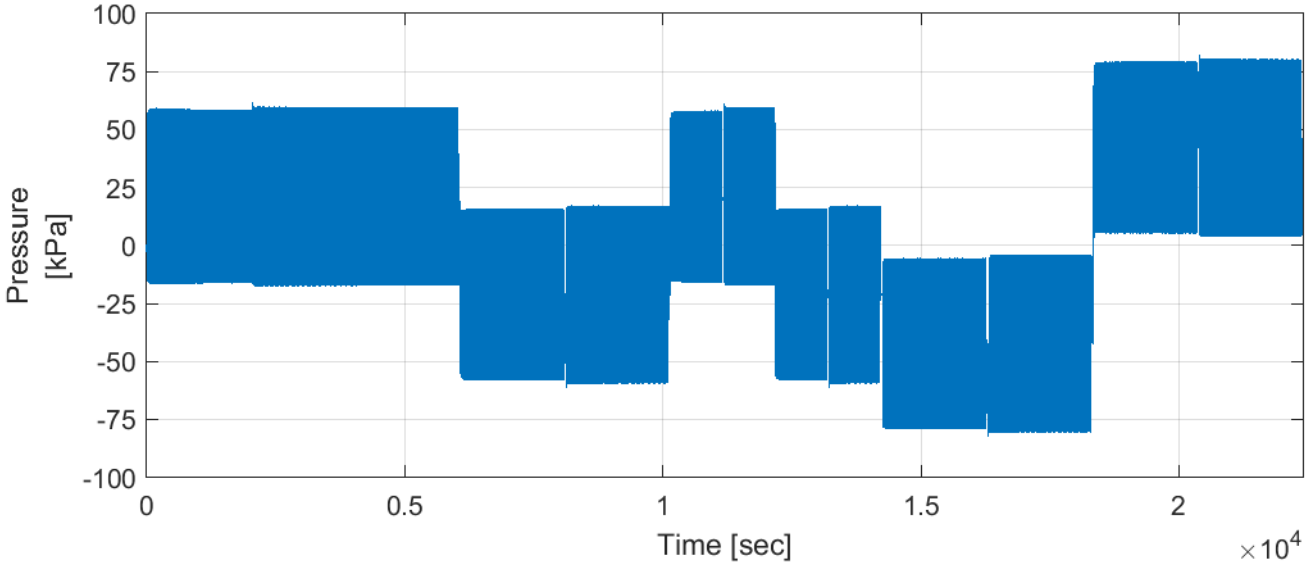
Pressure [kPa]
100
75
50
25
0
-25
-50
-75
-100
0
0.5
1
1.5
2
Time [sec]
×10^4

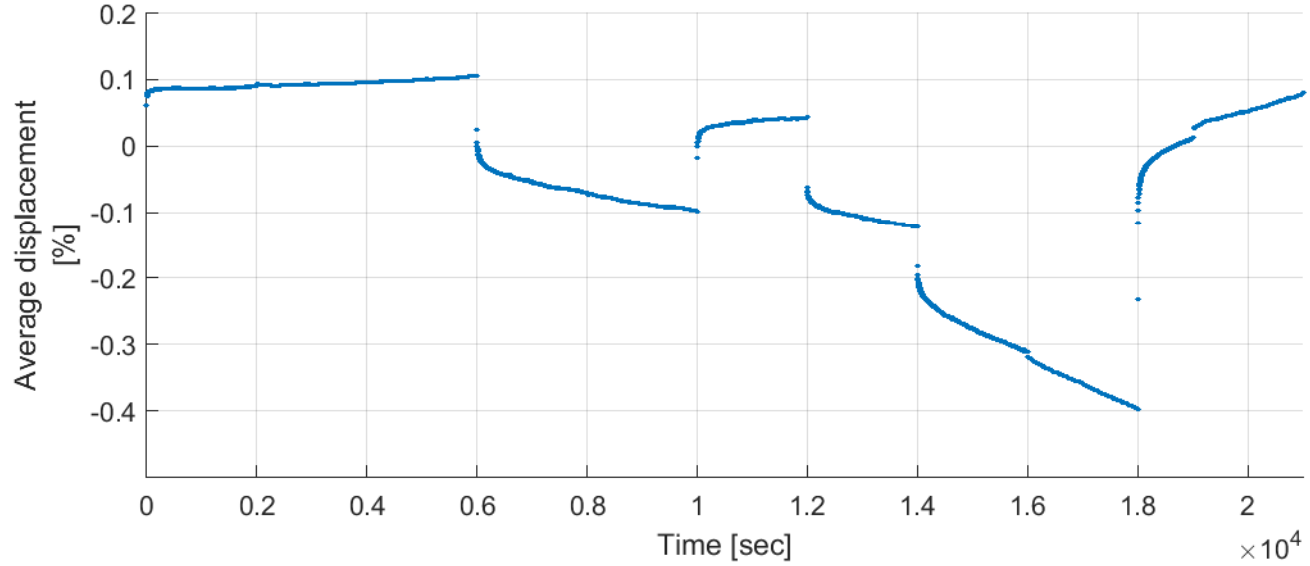
Average displacement [%]
0.2
0.1
0
-0.1
-0.2
-0.3
-0.4
0
0.2
0.4
0.6
0.8
1
1.2
1.4
1.6
1.8
2
Time [sec]
×10^4

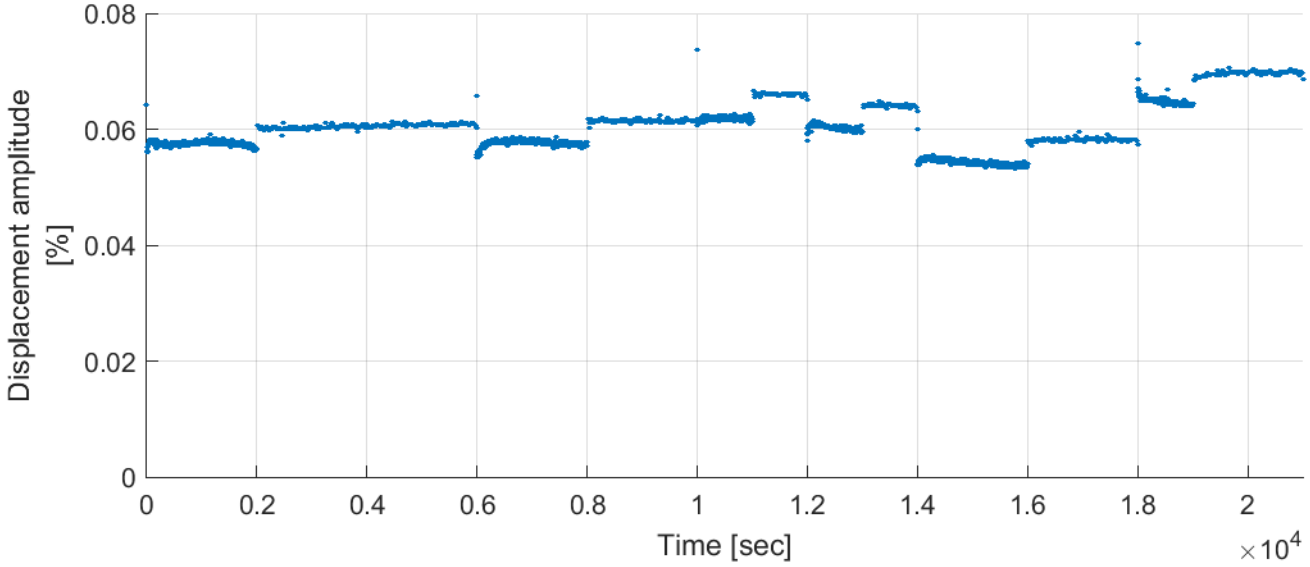
Displacement amplitude [%]
0.08
0.06
0.04
0.02
0
0
0.2
0.4
0.6
0.8
1
1.2
1.4
1.6
1.8
2
Time [sec]
×10^4

Test 6

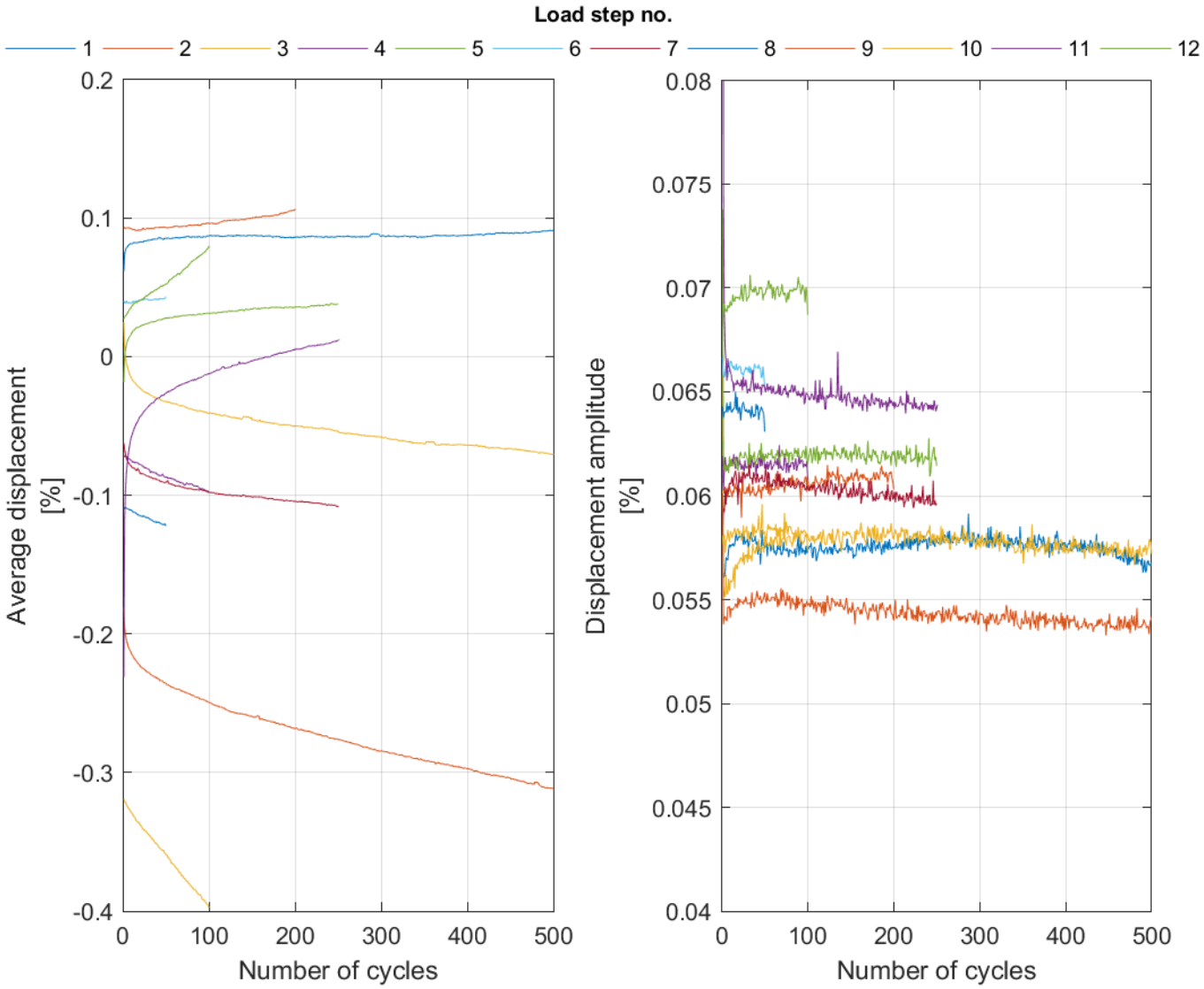
Load step no.
1
2
3
4
5
6
7
8
9
10
11
12
Average displacement [%]
0.2
0.1
0
-0.1
-0.2
-0.3
-0.4
0
100
200
300
400
500
Number of cycles
Displacement amplitude [%]
0.08
0.075
0.07
0.065
0.06
0.055
0.05
0.045
0.04
0
100
200
300
400
500
Number of cycles

Test 6

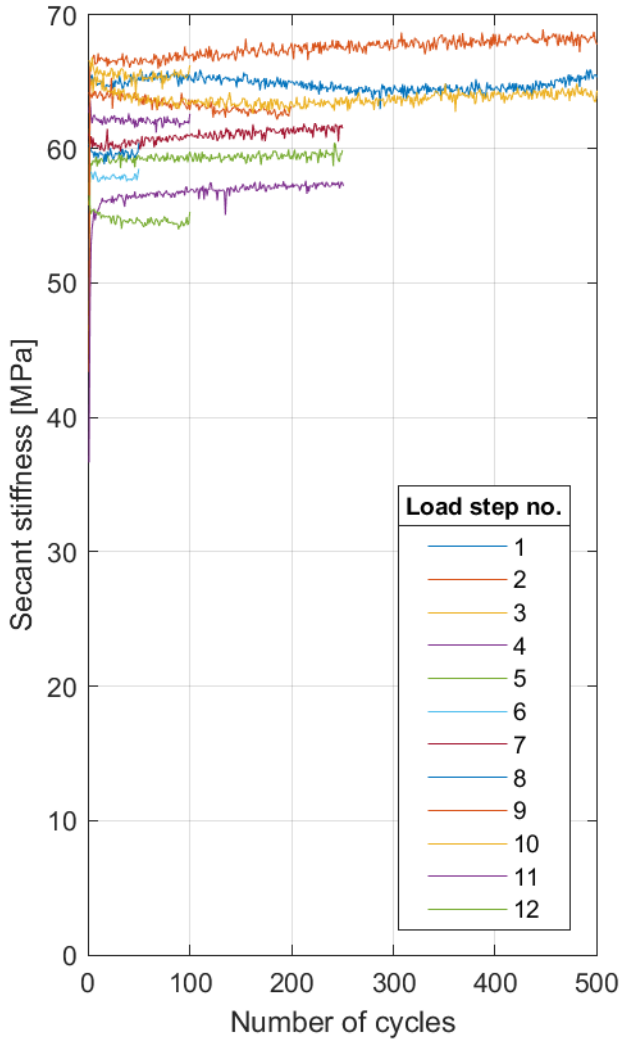
Secant stiffness [MPa]
Number of cycles
Load step no.
1
2
3
4
5
6
7
8
9
10
11
12

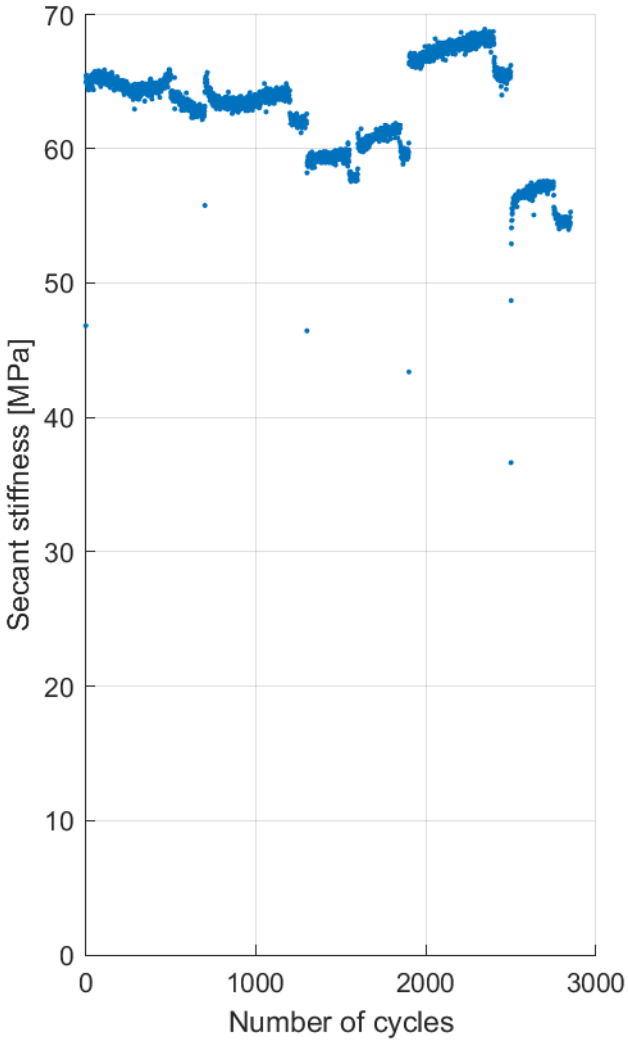
Secant stiffness [MPa]
Number of cycles

Test 6

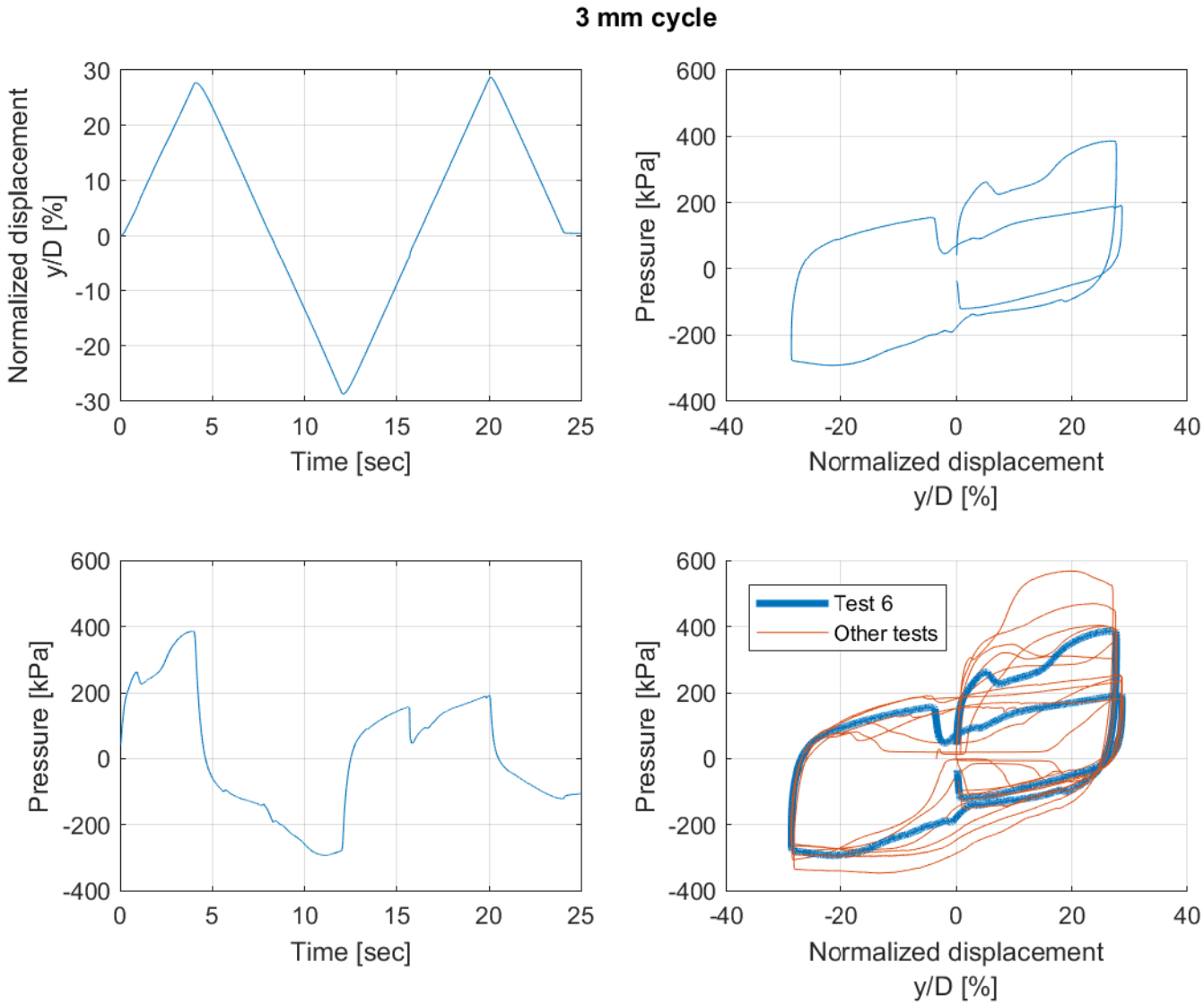
3 mm cycle
Normalized displacement y/D [%]
Time [sec]
Pressure [kPa]
Normalized displacement y/D [%]
Pressure [kPa]
Time [sec]
Test 6
Other tests
Pressure [kPa]
Normalized displacement y/D [%]

Test 6

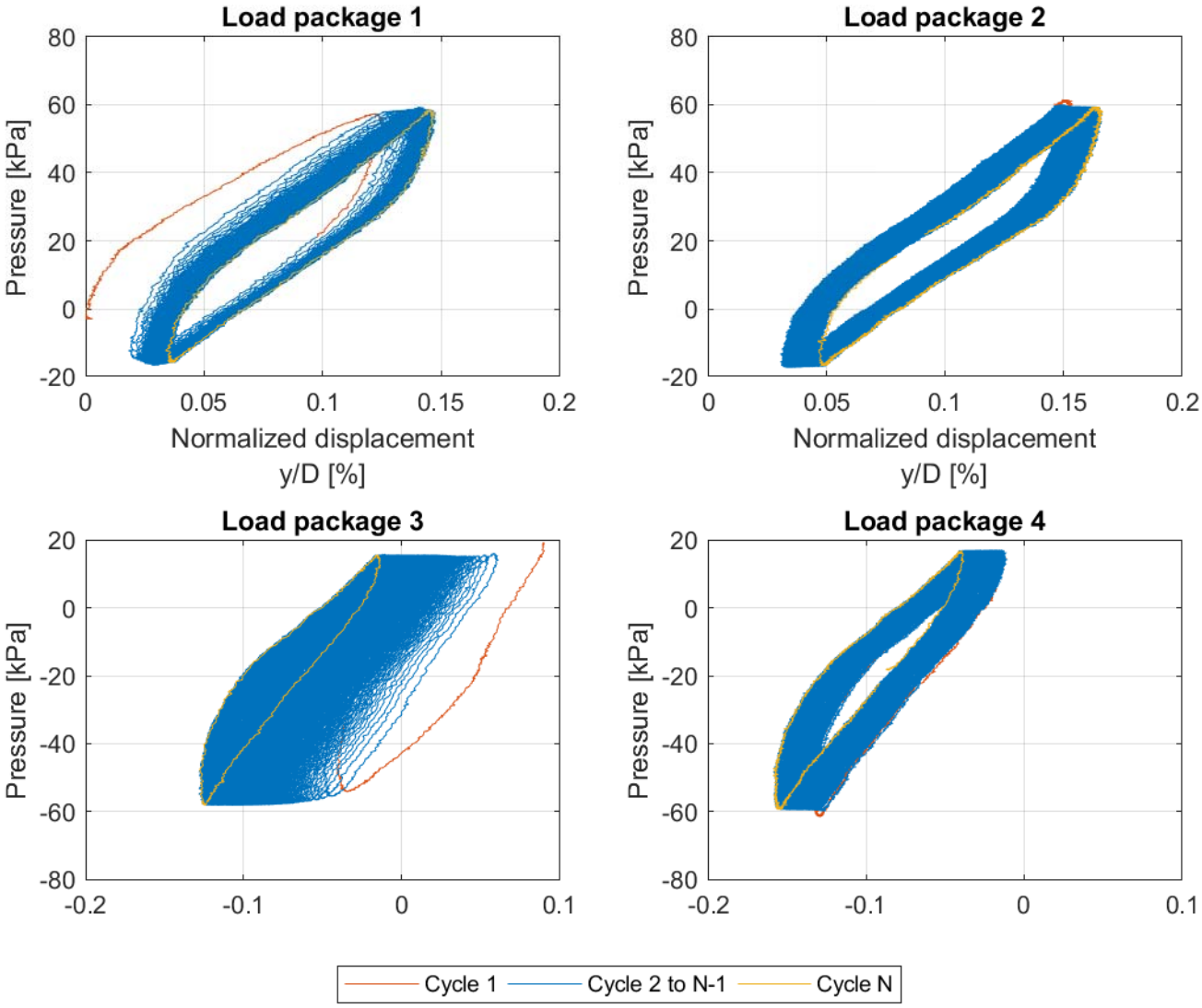
Load package 1
Load package 2
Load package 3
Load package 4
Pressure [kPa]
Normalized displacement
y/D [%]
Cycle 1
Cycle 2 to N-1
Cycle N

Test 6

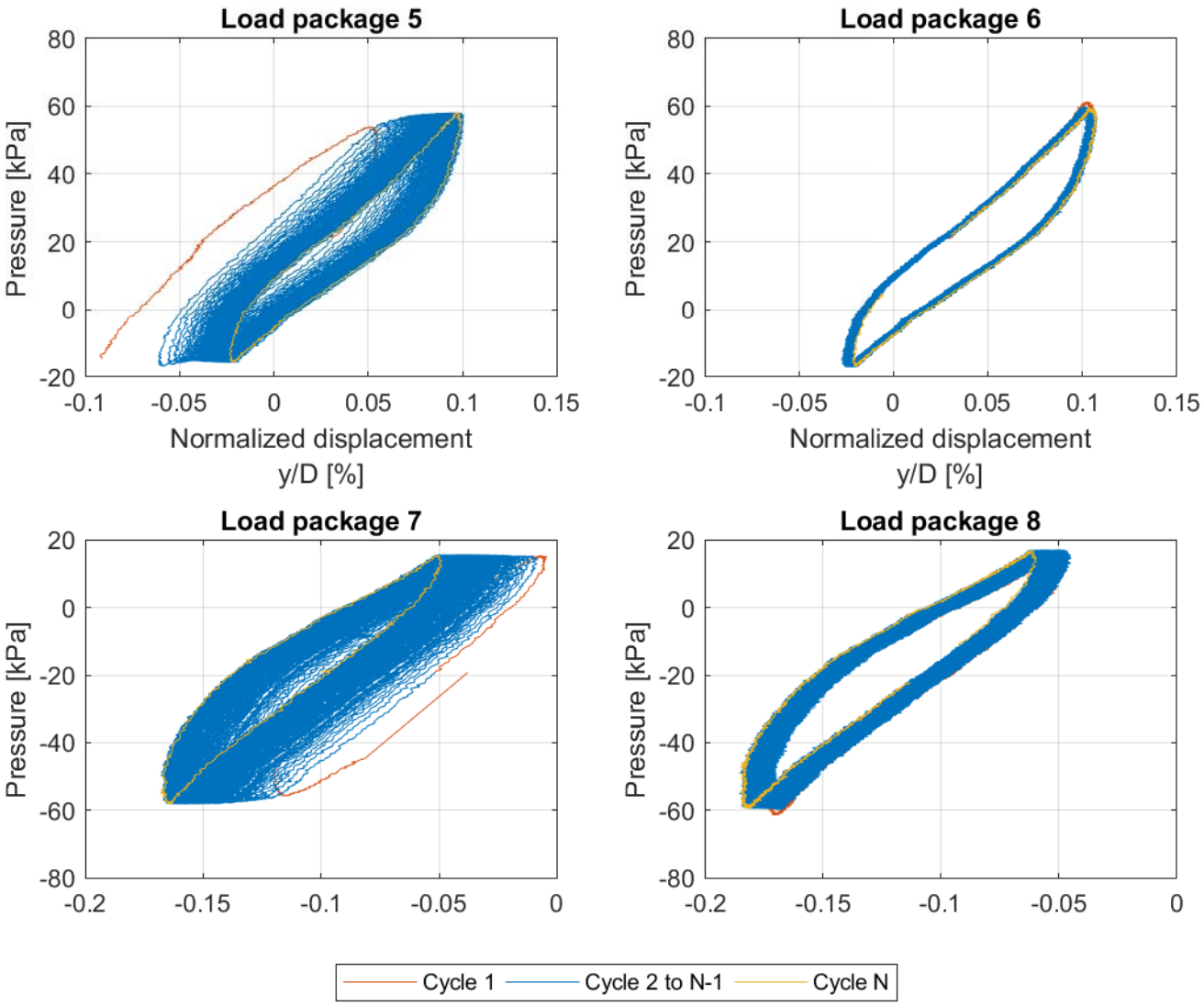
Load package 5
Load package 6
Load package 7
Load package 8
Pressure [kPa]
Normalized displacement
y/D [%]
Cycle 1
Cycle 2 to N-1
Cycle N

Test 6

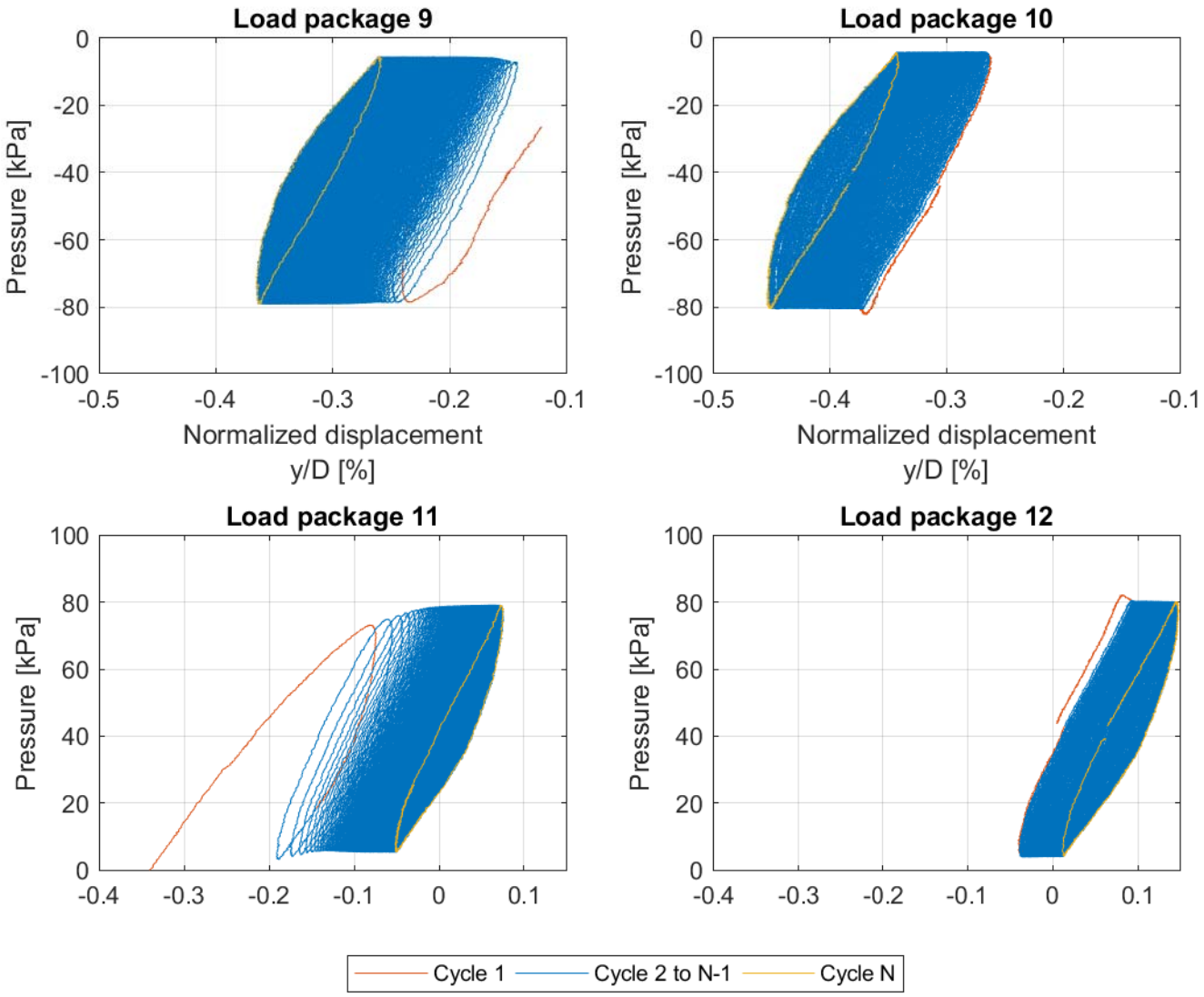
Load package 9
Load package 10
Load package 11
Load package 12
Pressure [kPa]
Normalized displacement
y/D [%]
Cycle 1
Cycle 2 to N-1
Cycle N

Test 6

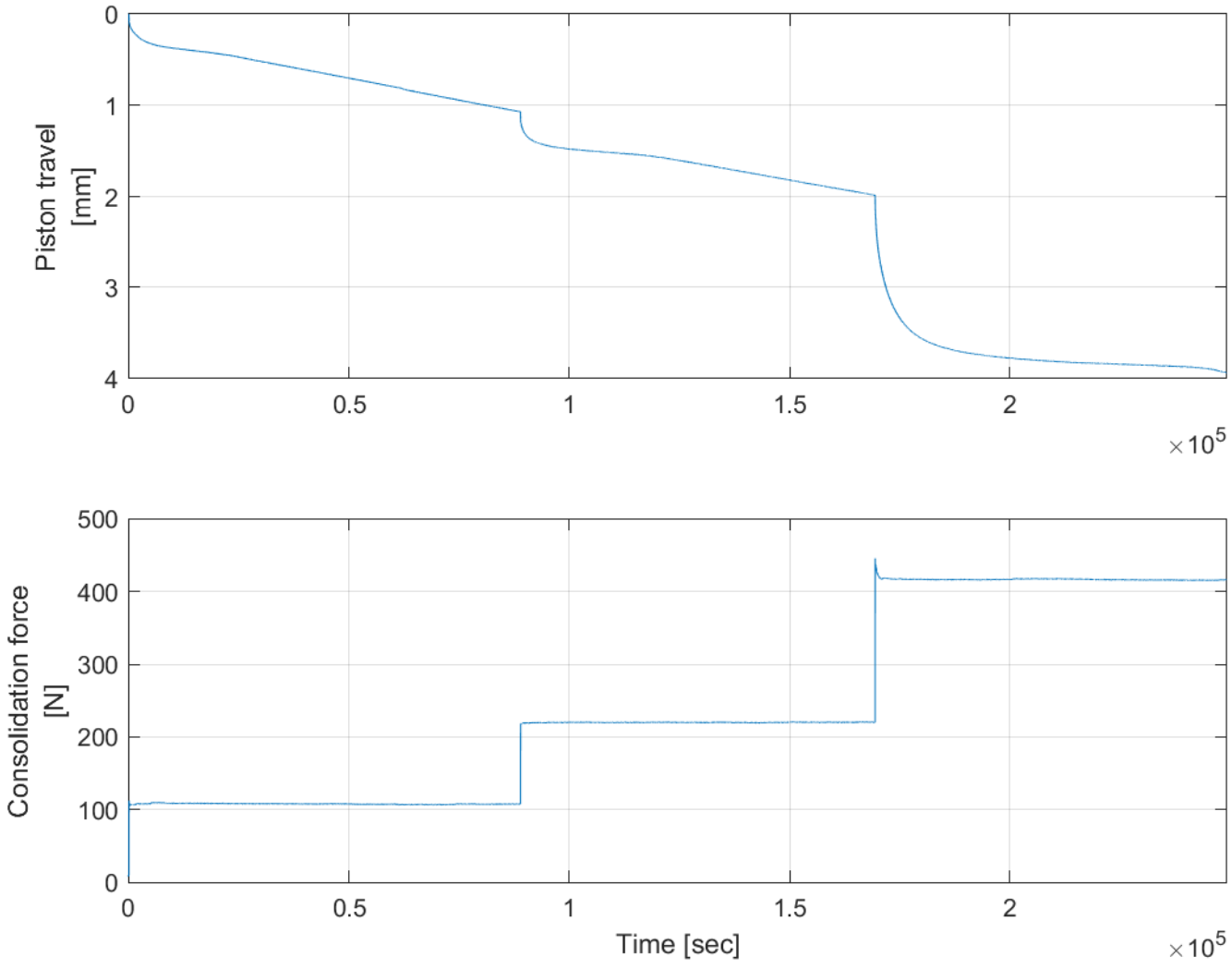
Piston travel
[mm]
0
1
2
3
4
0
0.5
1
1.5
2
×10^5
Consolidation force
[N]
500
400
300
200
100
0
0
0.5
1
1.5
2
Time [sec]
×10^5

Test 7

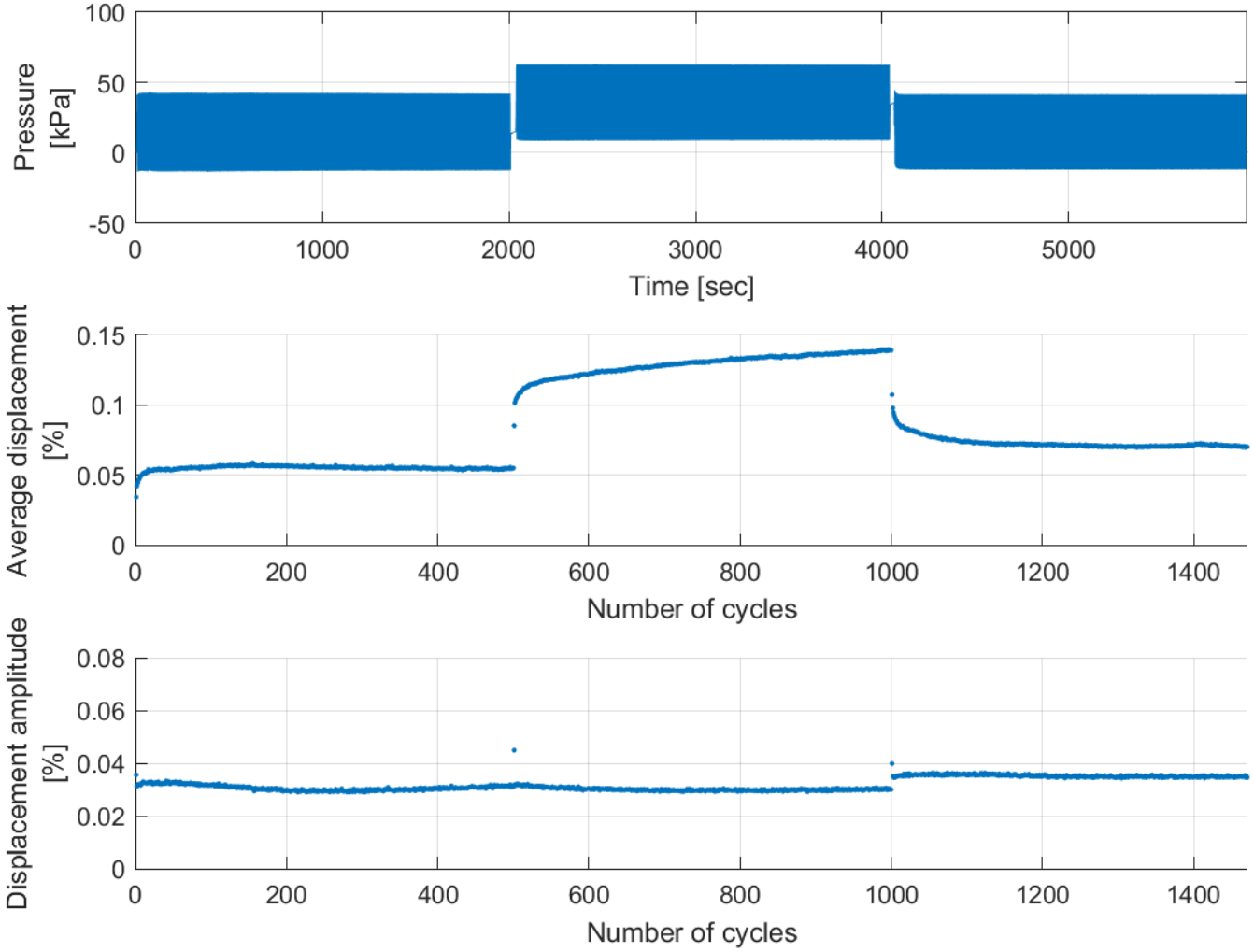
Pressure [kPa]
100
50
0
-50
0
1000
2000
3000
4000
5000
Time [sec]
Average displacement [%]
0.15
0.1
0.05
0
0
200
400
600
800
1000
1200
1400
Number of cycles
Displacement amplitude [%]
0.08
0.06
0.04
0.02
0
0
200
400
600
800
1000
1200
1400
Number of cycles

Test 7

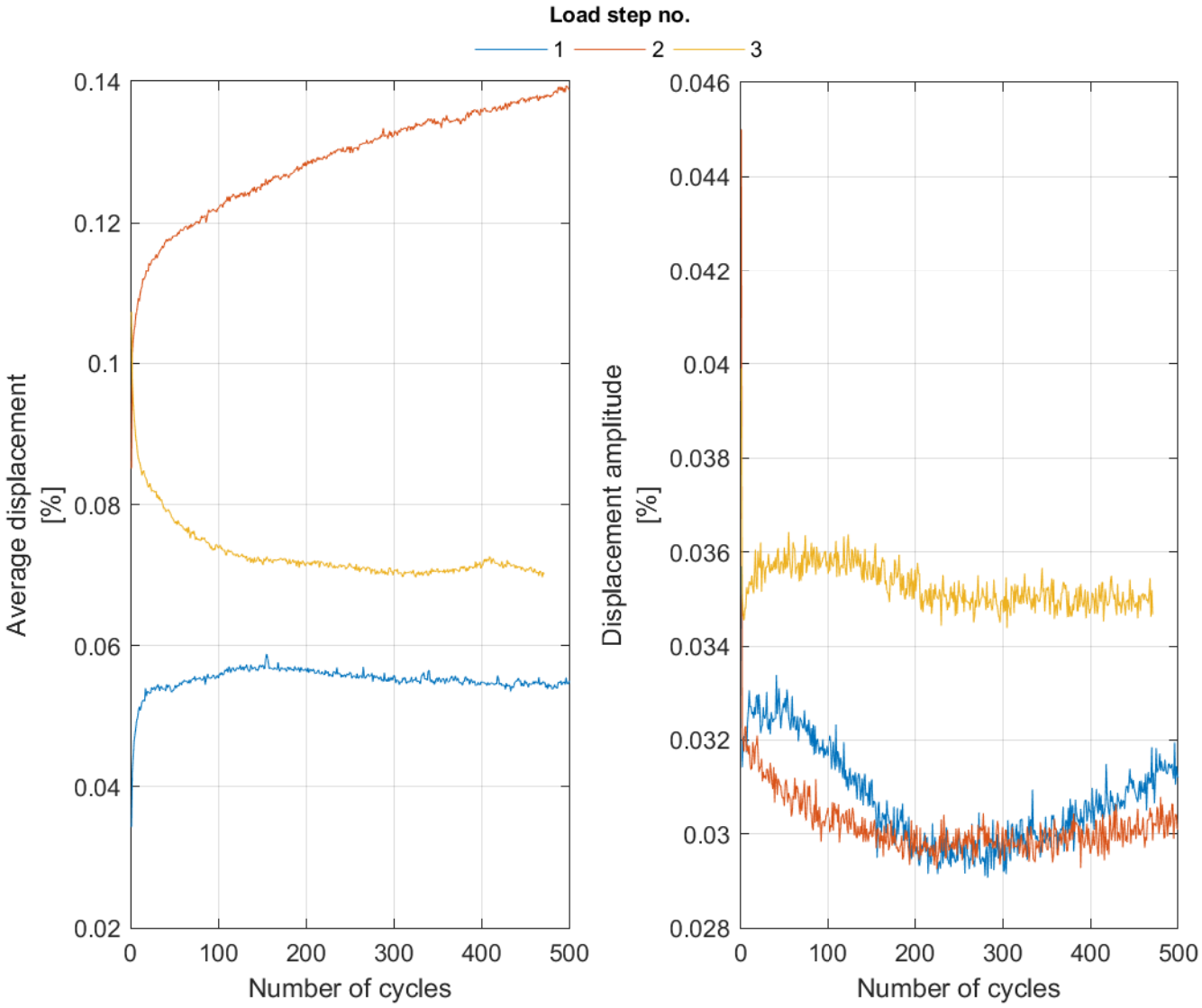
Load step no.
1
2
3
Average displacement [%]
0.14
0.12
0.1
0.08
0.06
0.04
0.02
0
100
200
300
400
500
Number of cycles
Displacement amplitude [%]
0.046
0.044
0.042
0.04
0.038
0.036
0.034
0.032
0.03
0.028
0
100
200
300
400
500
Number of cycles

Test 7

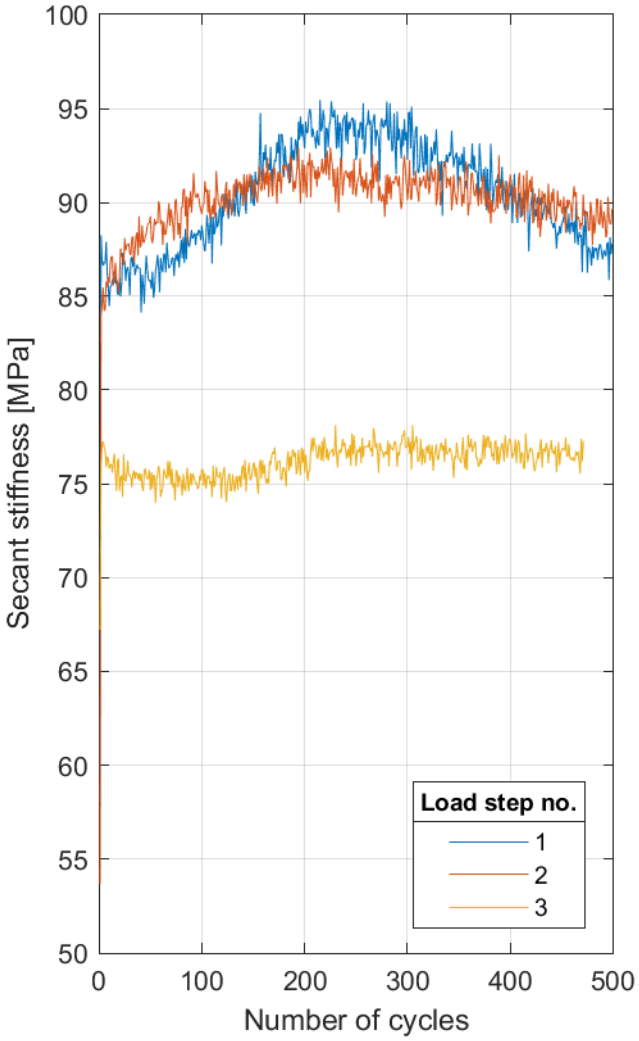
Secant stiffness [MPa]
Number of cycles
Load step no.
1
2
3

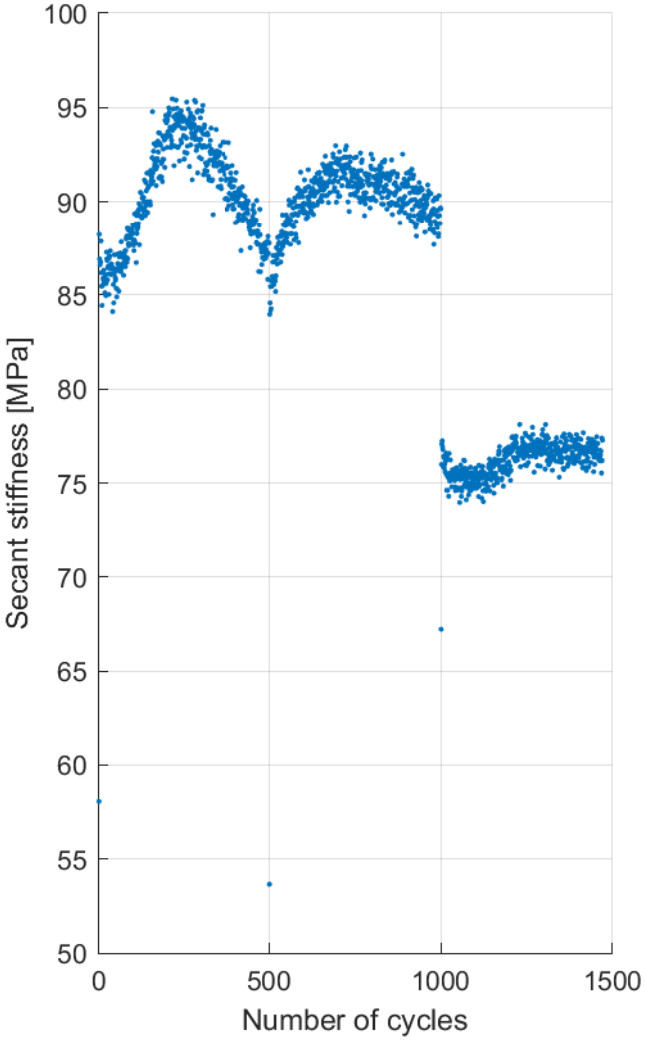
Secant stiffness [MPa]
Number of cycles

Test 7

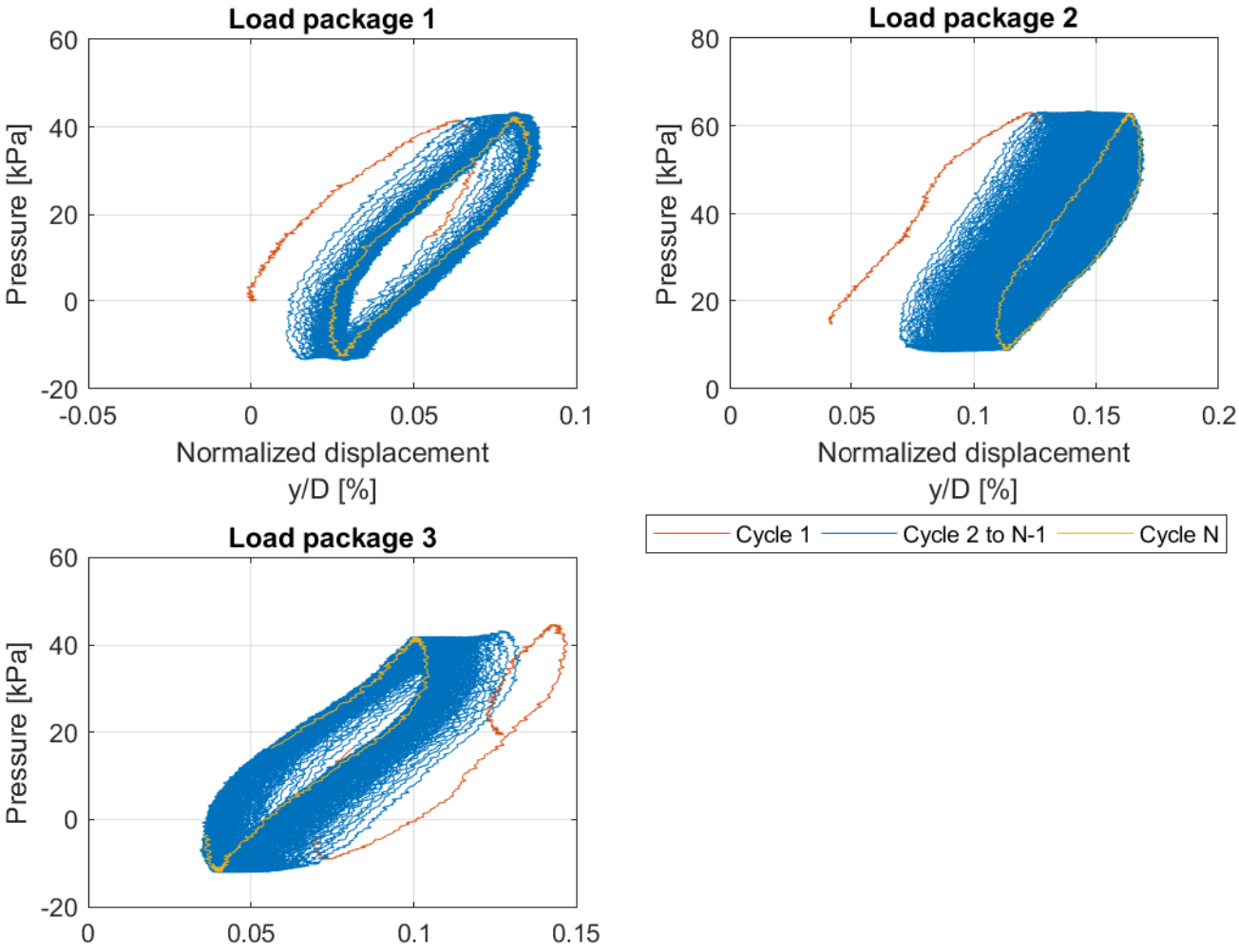
Load package 1
Pressure [kPa]
Normalized displacement
y/D [%]
Load package 2
Pressure [kPa]
Normalized displacement
y/D [%]
Load package 3
Pressure [kPa]
Cycle 1
Cycle 2 to N-1
Cycle N

Test 7

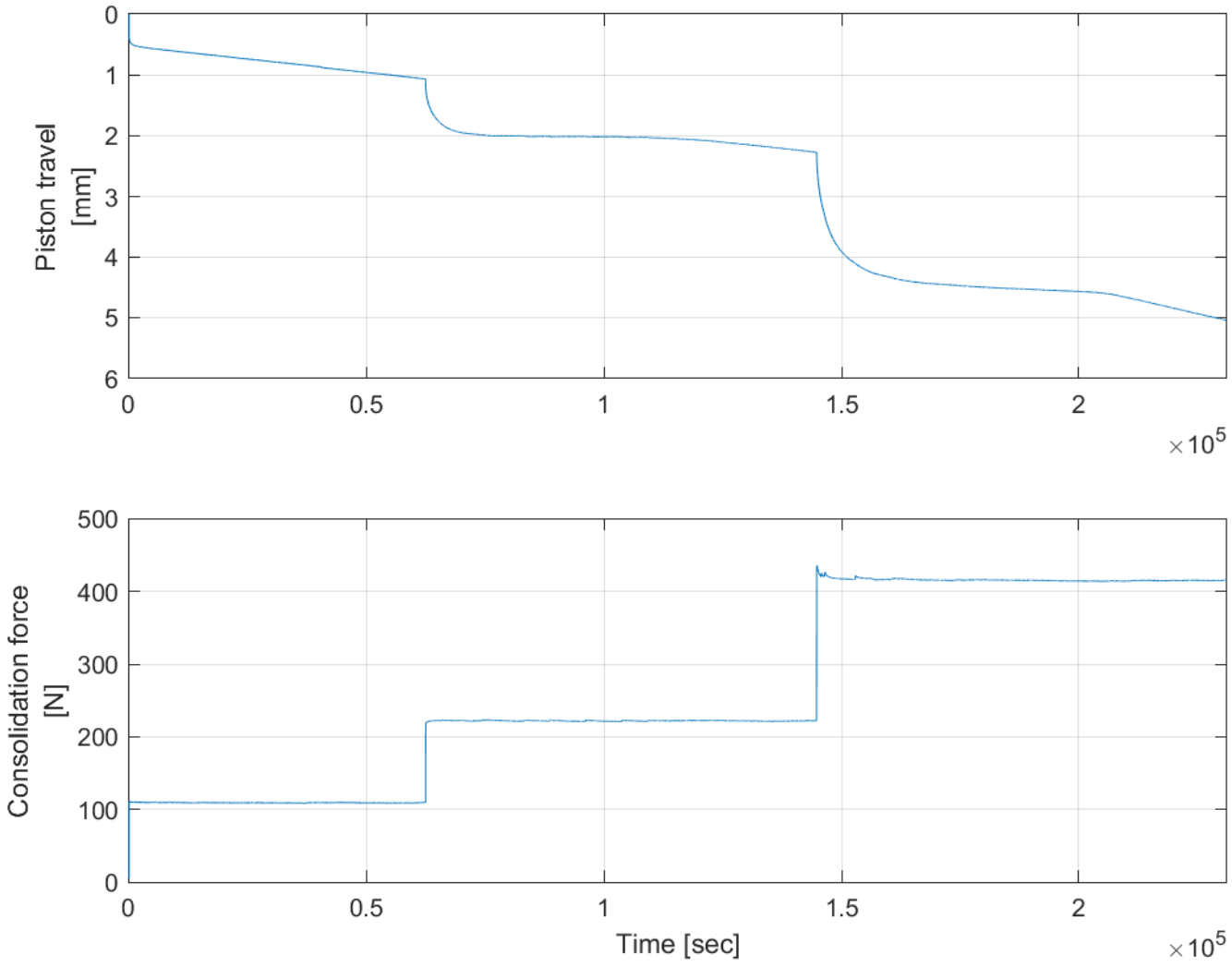
Piston travel [mm]
0
1
2
3
4
5
6
0
0.5
1
1.5
2
×10^5
Consolidation force [N]
500
400
300
200
100
0
0
0.5
1
1.5
2
Time [sec]
×10^5

Test 8

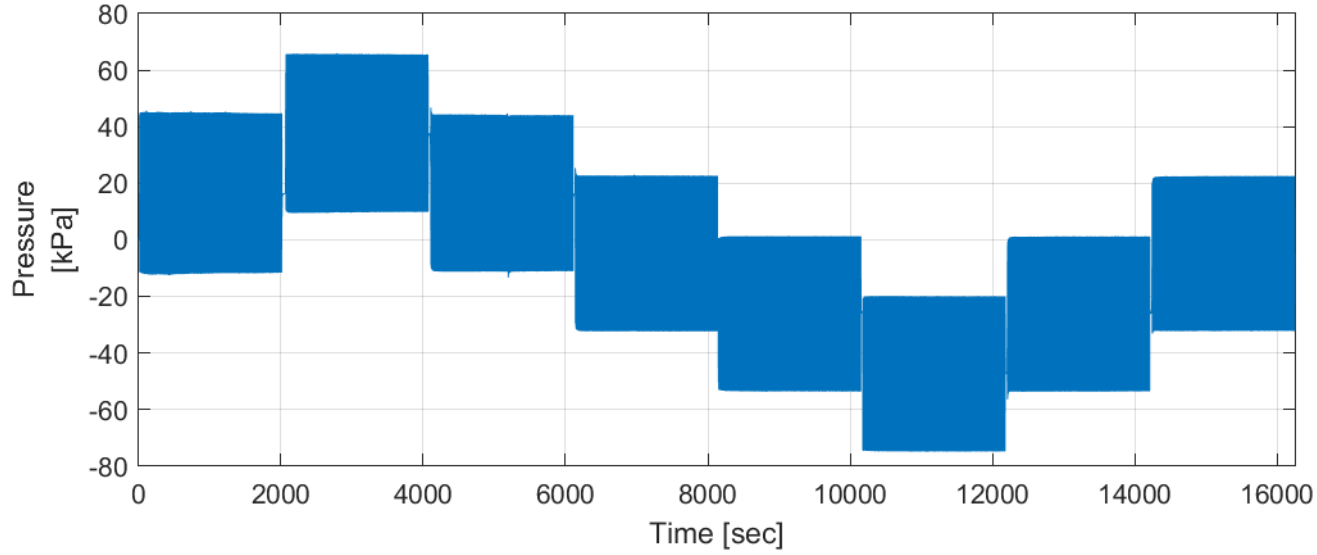
Pressure [kPa]
80
60
40
20
0
-20
-40
-60
-80
0
2000
4000
6000
8000
10000
12000
14000
16000
Time [sec]

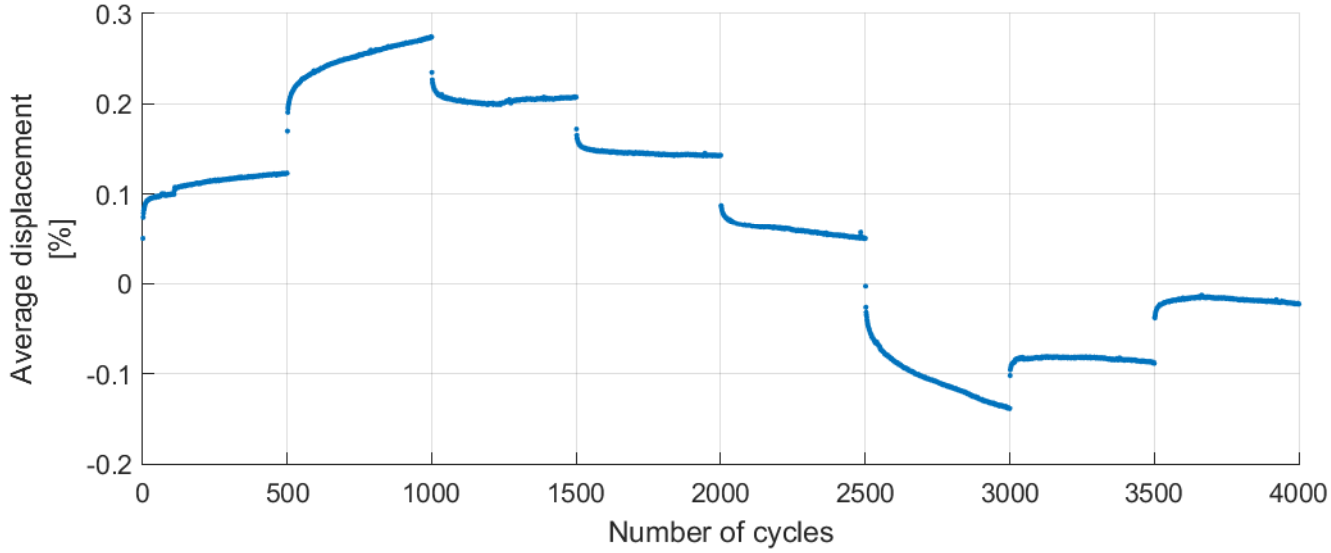
Average displacement [%]
0.3
0.2
0.1
0
-0.1
-0.2
0
500
1000
1500
2000
2500
3000
3500
4000
Number of cycles

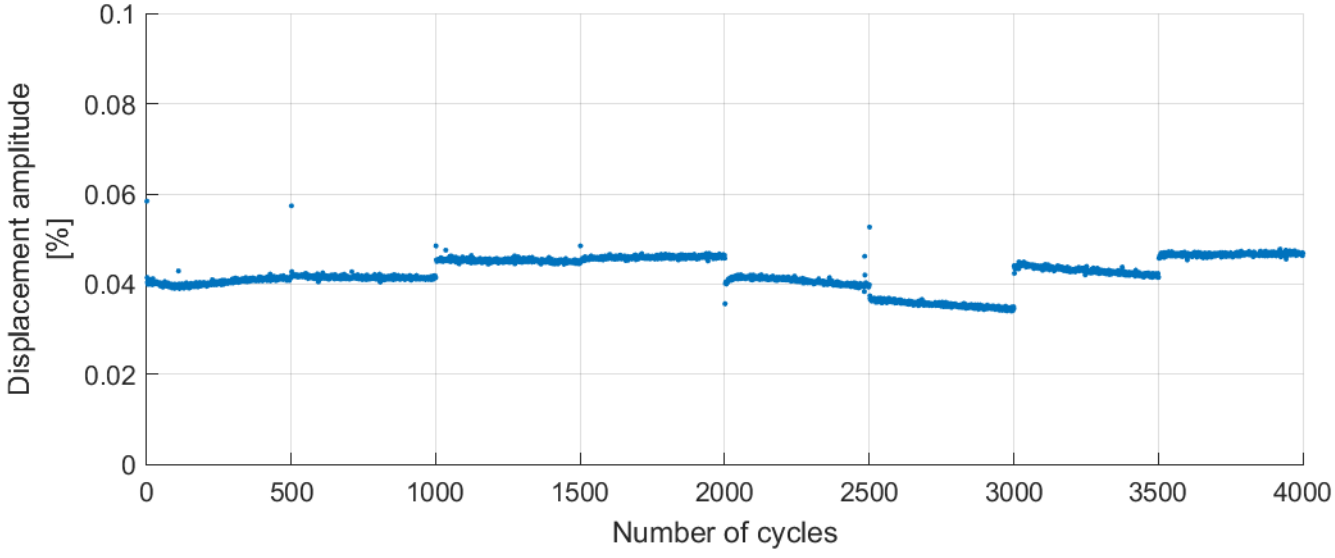
Displacement amplitude [%]
0.1
0.08
0.06
0.04
0.02
0
0
500
1000
1500
2000
2500
3000
3500
4000
Number of cycles

Test 8

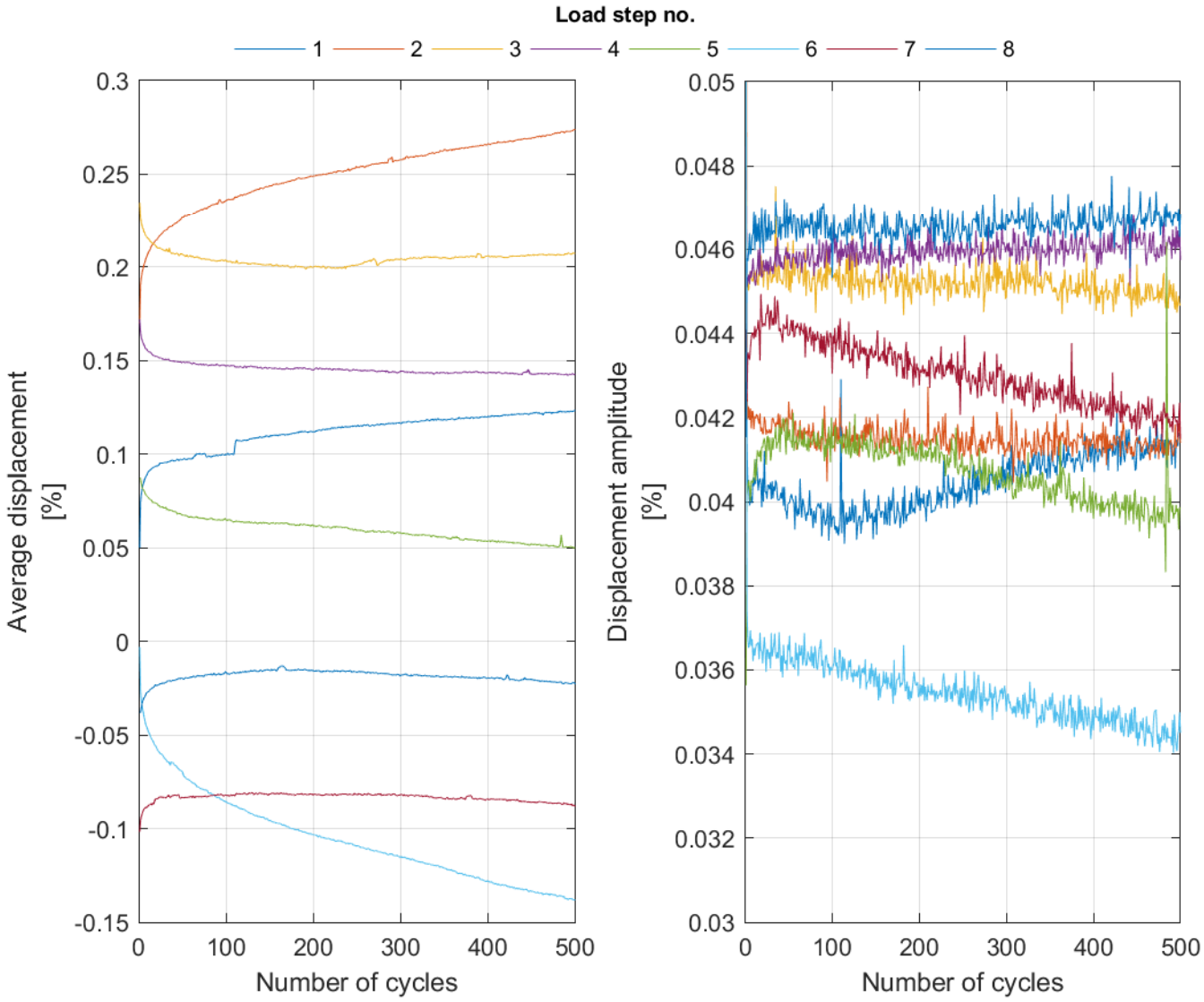
Load step no.
1
2
3
4
5
6
7
8
Average displacement [%]
Number of cycles
Displacement amplitude [%]
Number of cycles

Test 8

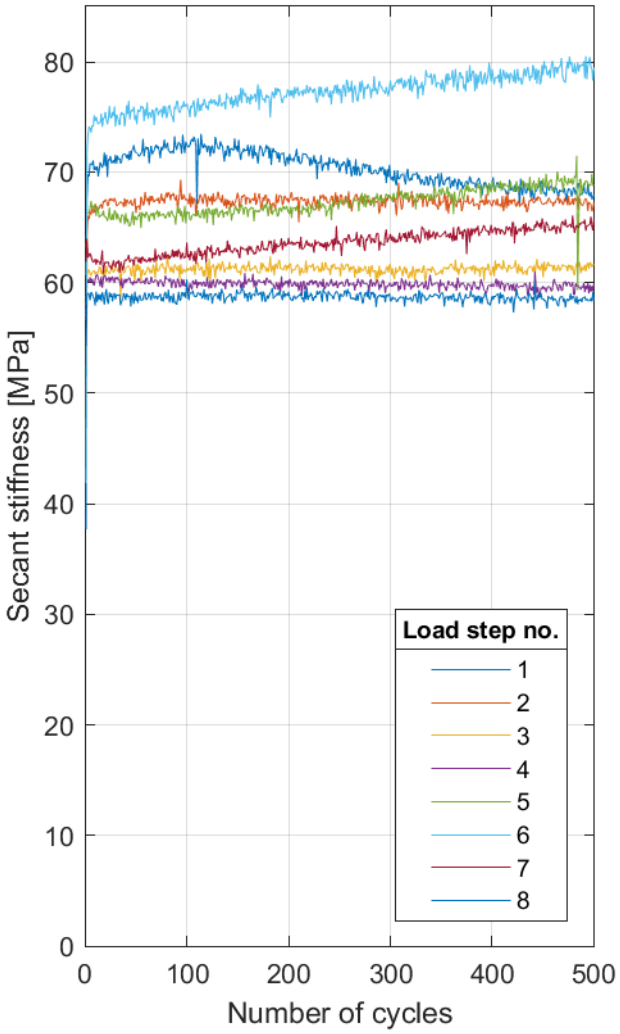
Secant stiffness [MPa]
Number of cycles
Load step no.
1
2
3
4
5
6
7
8

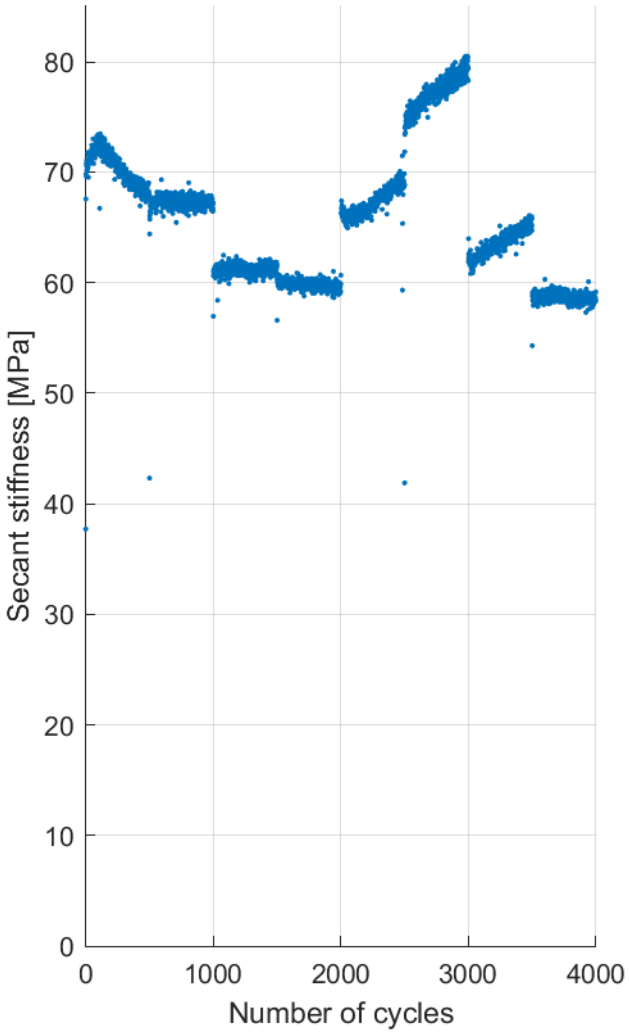
Secant stiffness [MPa]
Number of cycles

Test 8

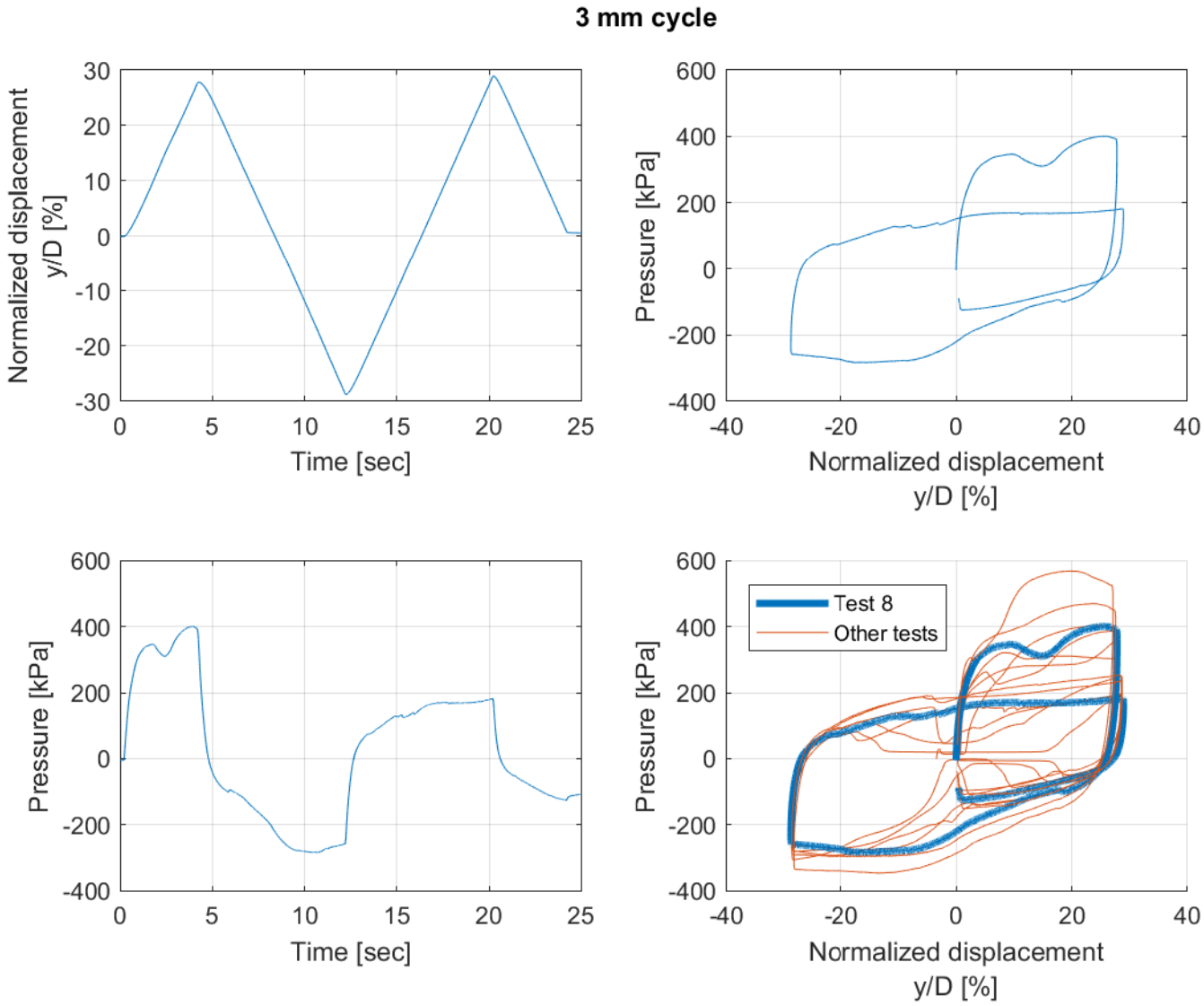
3 mm cycle
Normalized displacement y/D [%]
Time [sec]
Pressure [kPa]
Normalized displacement y/D [%]
Pressure [kPa]
Time [sec]
Test 8
Other tests
Pressure [kPa]
Normalized displacement y/D [%]

Test 8

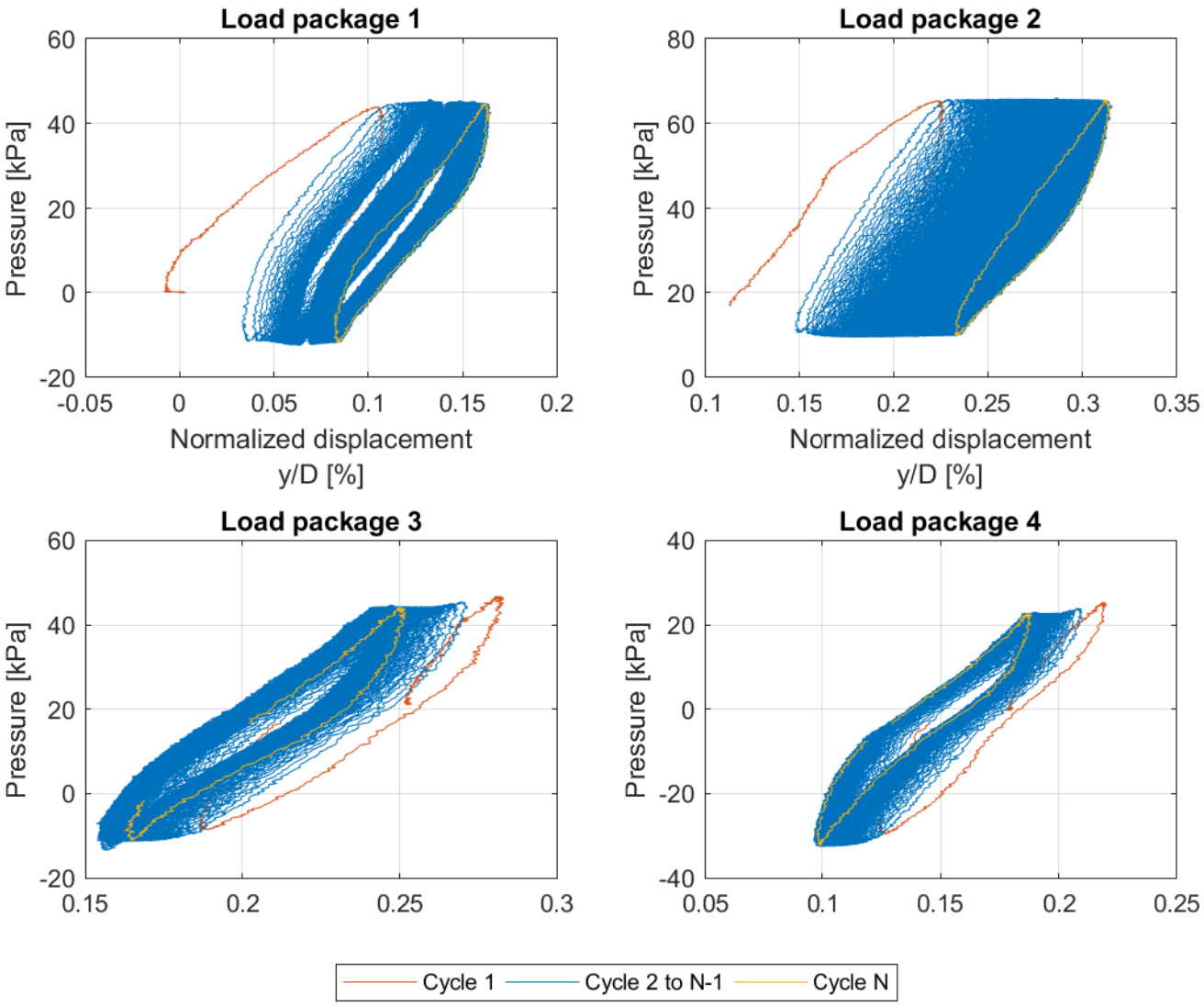
Load package 1
Pressure [kPa]
Normalized displacement
y/D [%]
Load package 2
Pressure [kPa]
Normalized displacement
y/D [%]
Load package 3
Pressure [kPa]
Load package 4
Pressure [kPa]
Cycle 1
Cycle 2 to N-1
Cycle N

Test 8

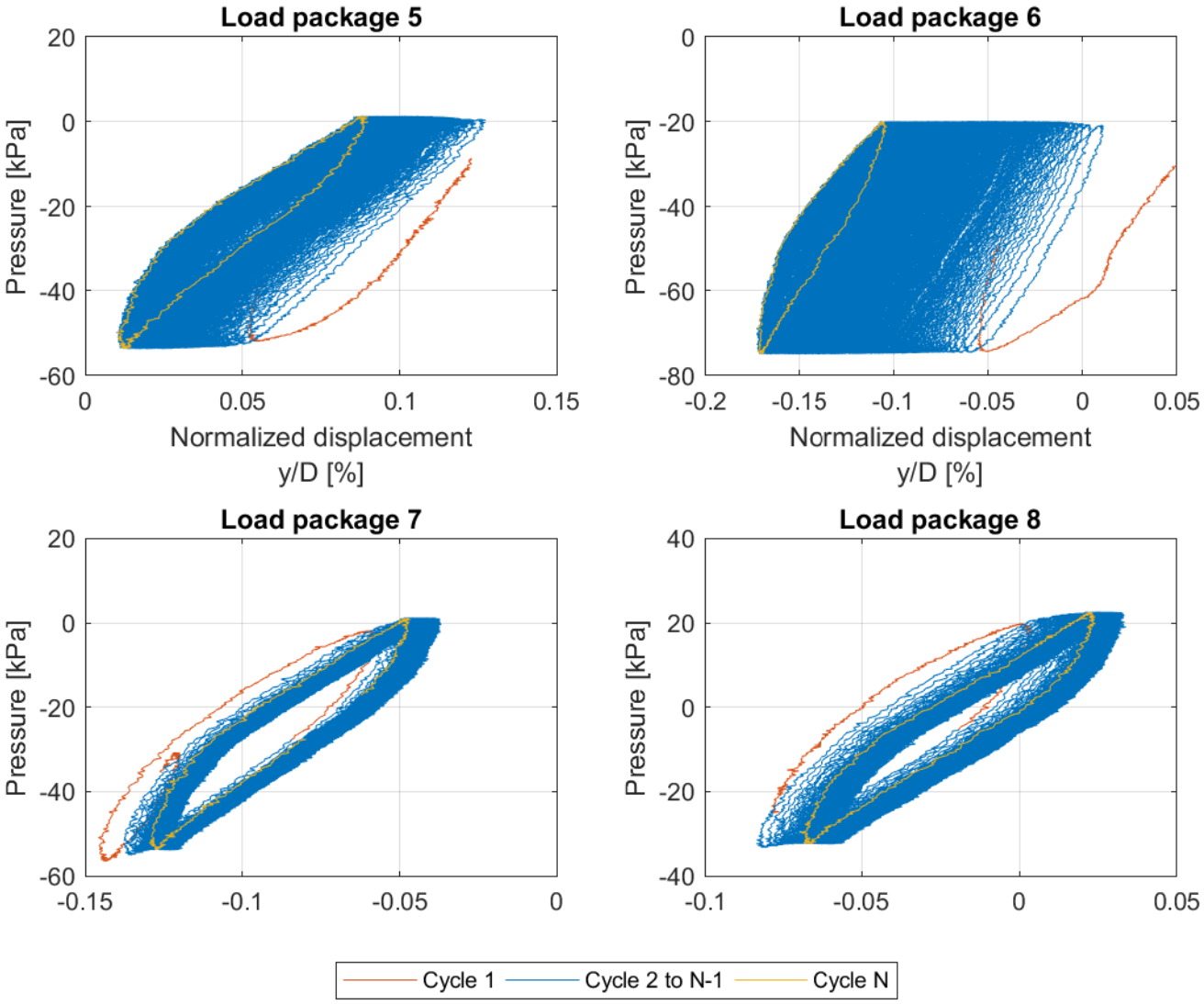
Load package 5
Pressure [kPa]
Normalized displacement
y/D [%]
Load package 6
Pressure [kPa]
Normalized displacement
y/D [%]
Load package 7
Pressure [kPa]
Load package 8
Pressure [kPa]
Cycle 1
Cycle 2 to N-1
Cycle N

Test 8

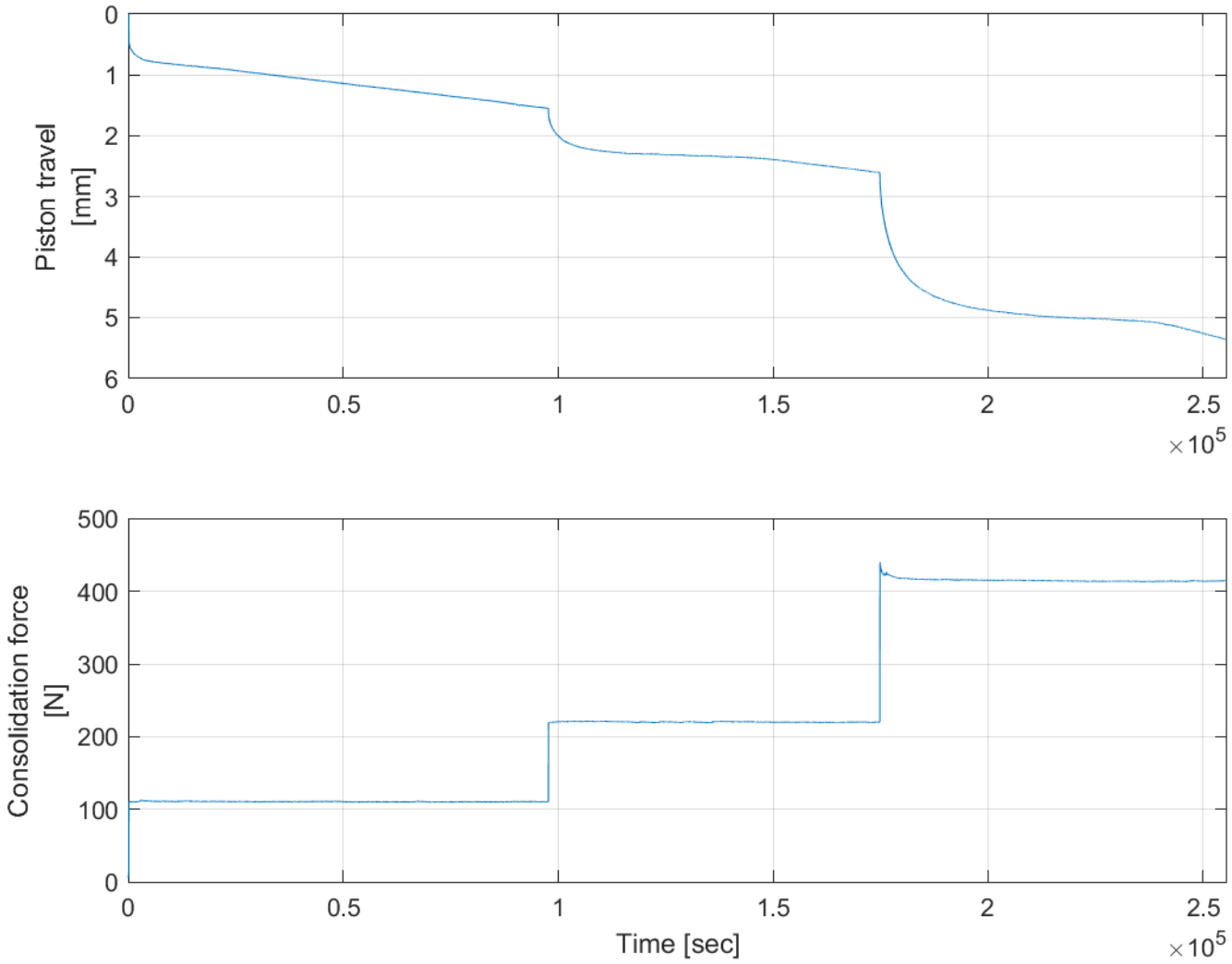
Piston travel [mm]
0
1
2
3
4
5
6
0
0.5
1
1.5
2
2.5
×10^5
Consolidation force [N]
500
400
300
200
100
0
0
0.5
1
1.5
2
2.5
Time [sec]
×10^5

Test 9

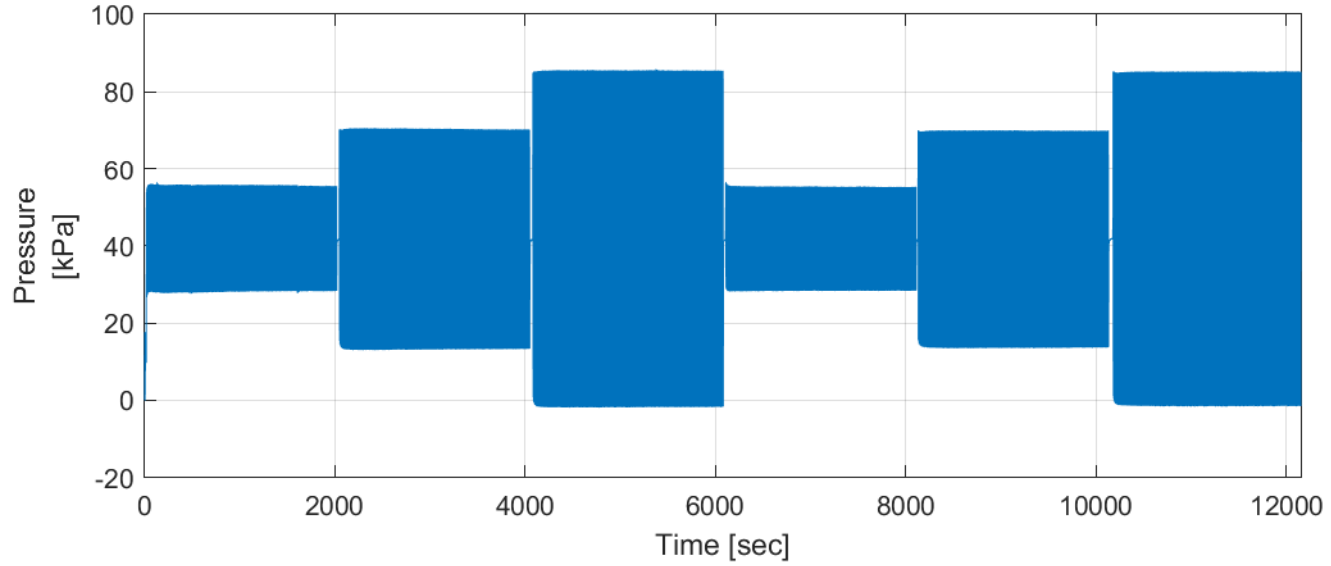
Pressure [kPa]
100
80
60
40
20
0
-20
0
2000
4000
6000
8000
10000
12000
Time [sec]

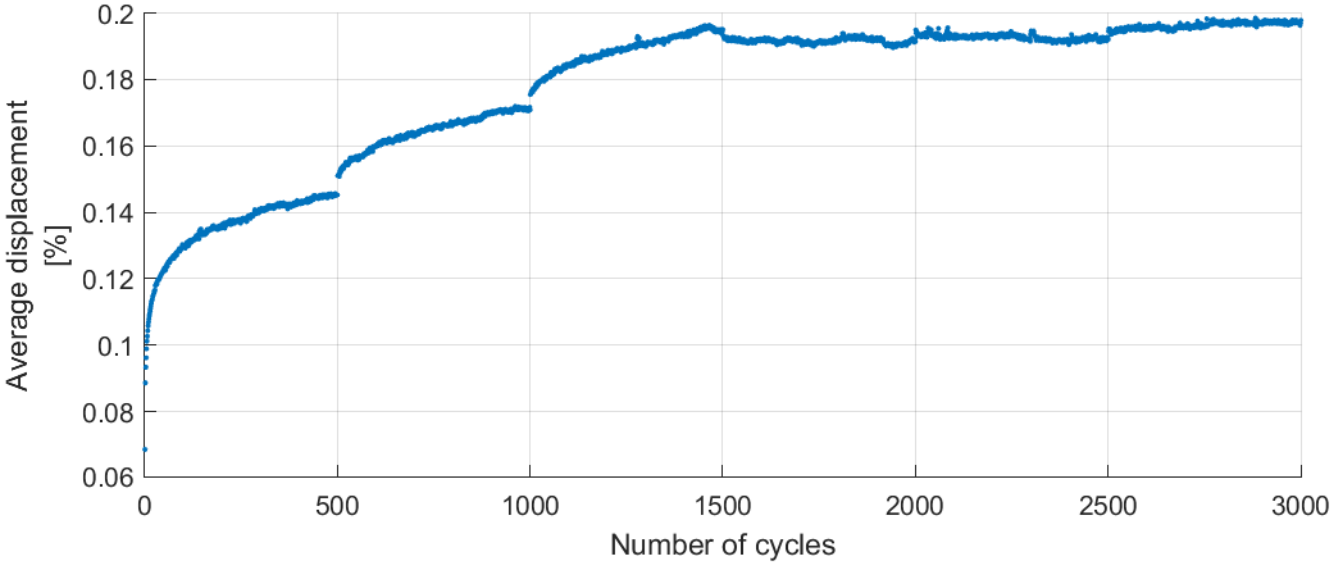
Average displacement [%]
0.2
0.18
0.16
0.14
0.12
0.1
0.08
0.06
0
500
1000
1500
2000
2500
3000
Number of cycles

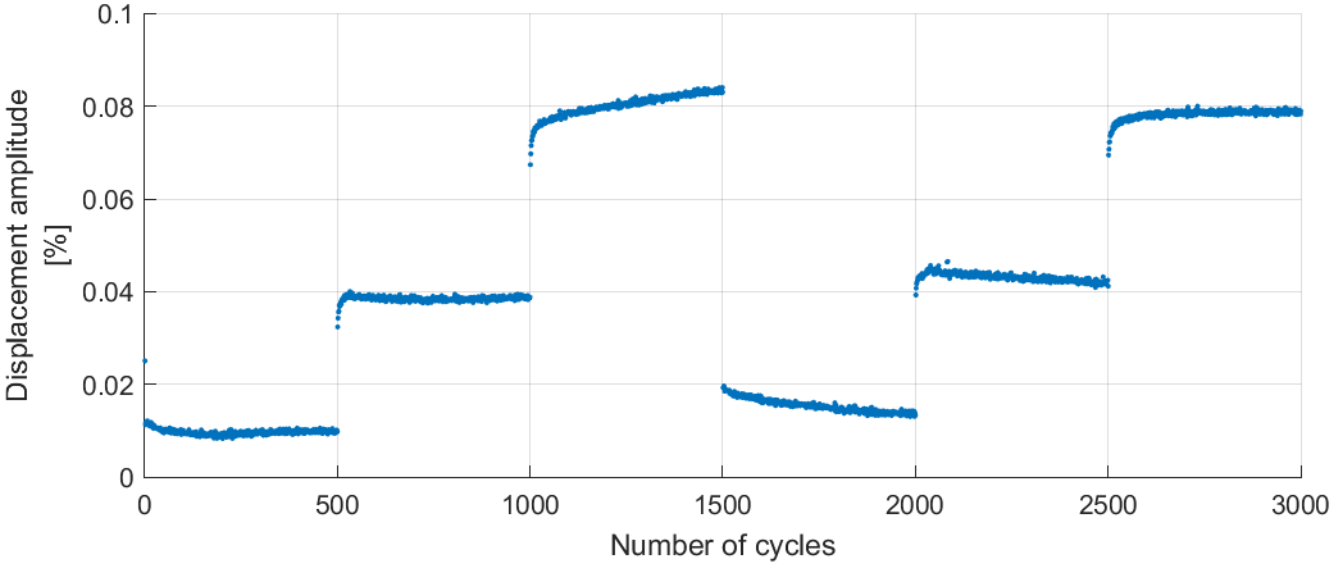
Displacement amplitude [%]
0.1
0.08
0.06
0.04
0.02
0
0
500
1000
1500
2000
2500
3000
Number of cycles

Test 9

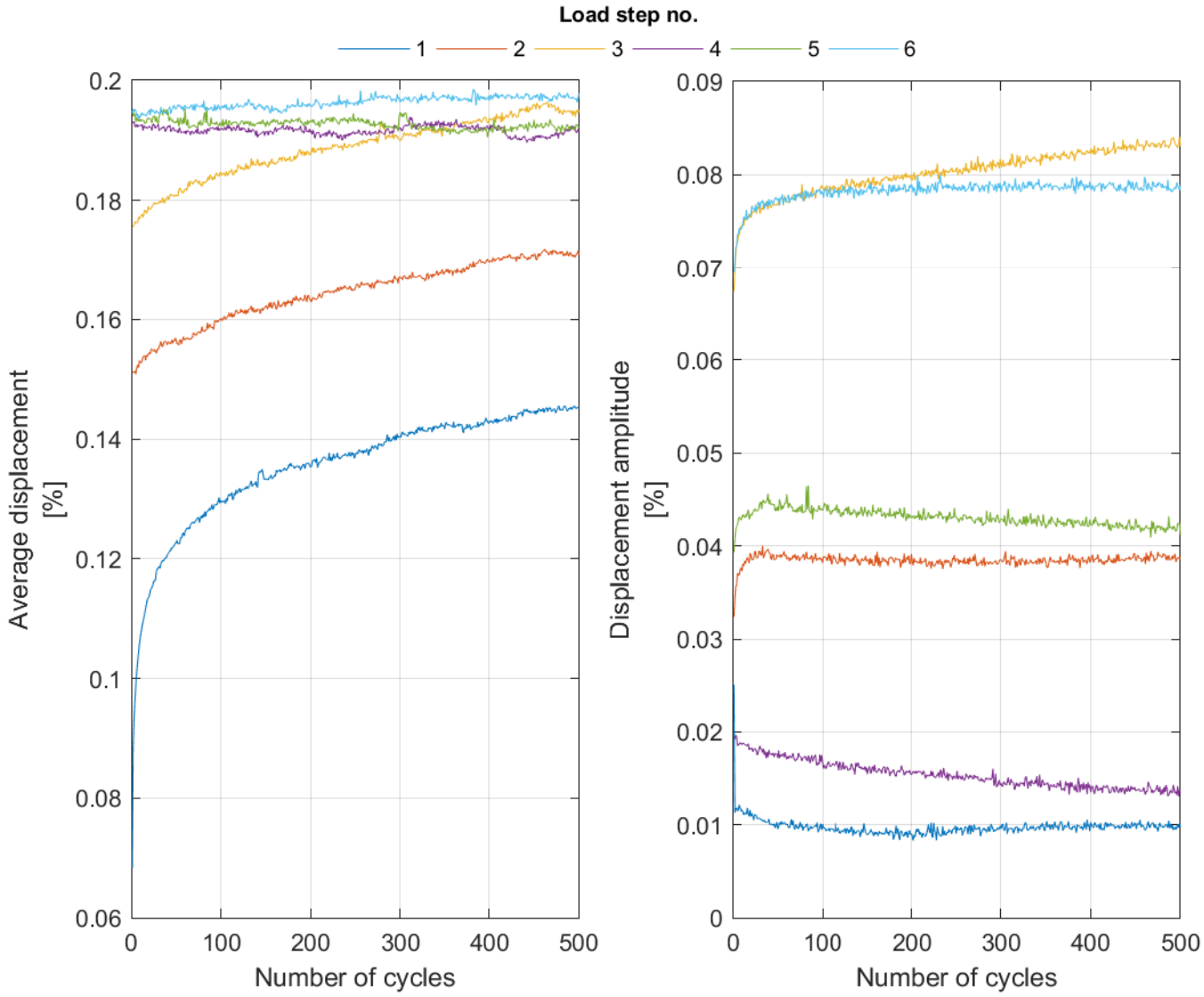
Load step no.
1
2
3
4
5
6
Average displacement [%]
Number of cycles
Displacement amplitude [%]
Number of cycles

Test 9

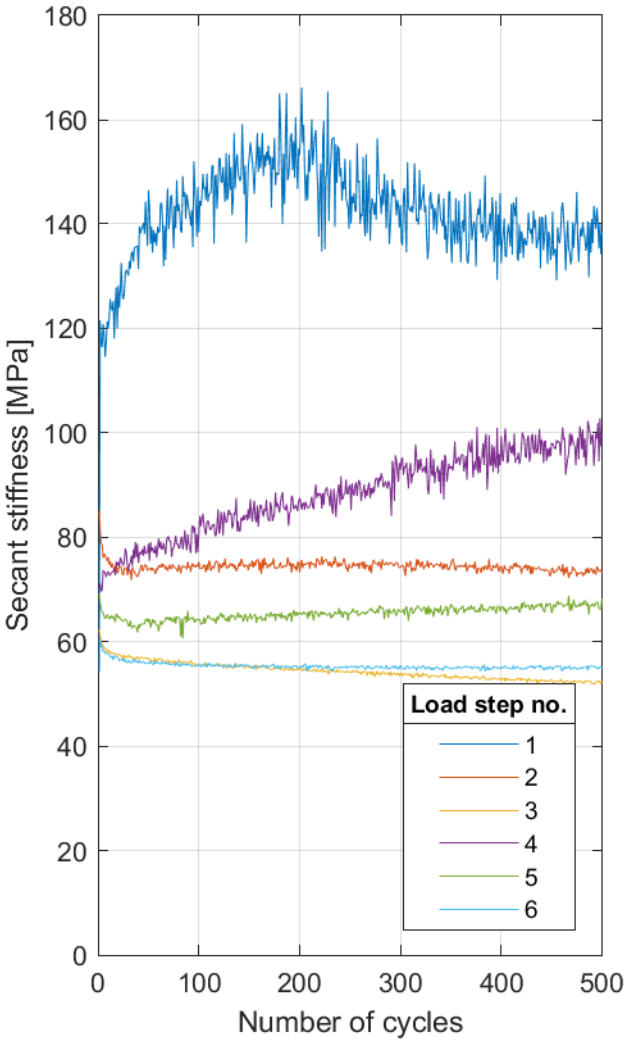
Secant stiffness [MPa]
Number of cycles
Load step no.
1
2
3
4
5
6

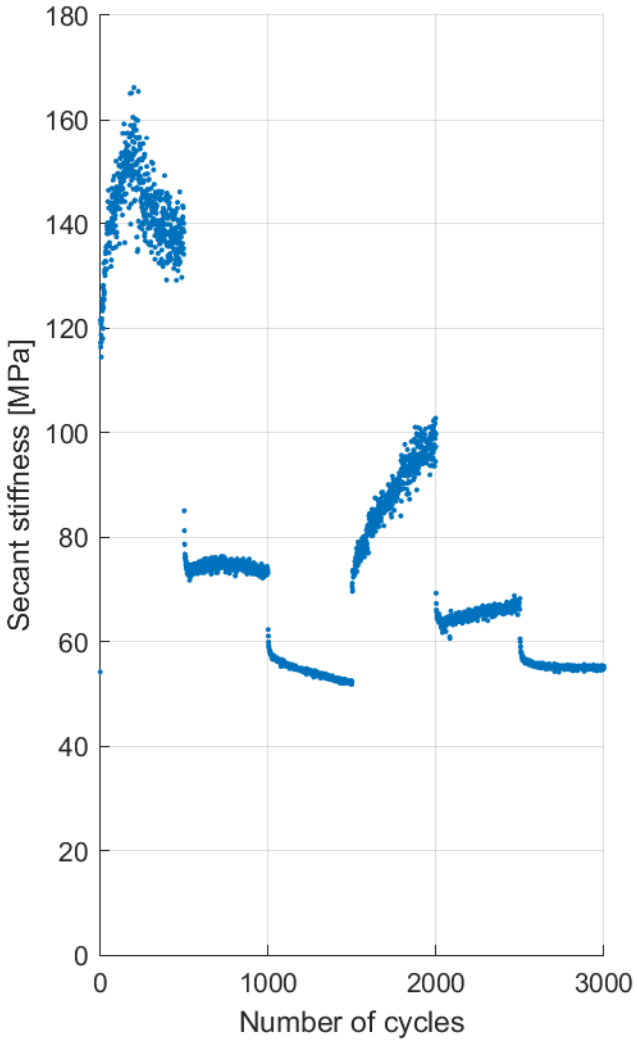
Secant stiffness [MPa]
Number of cycles

Test 9

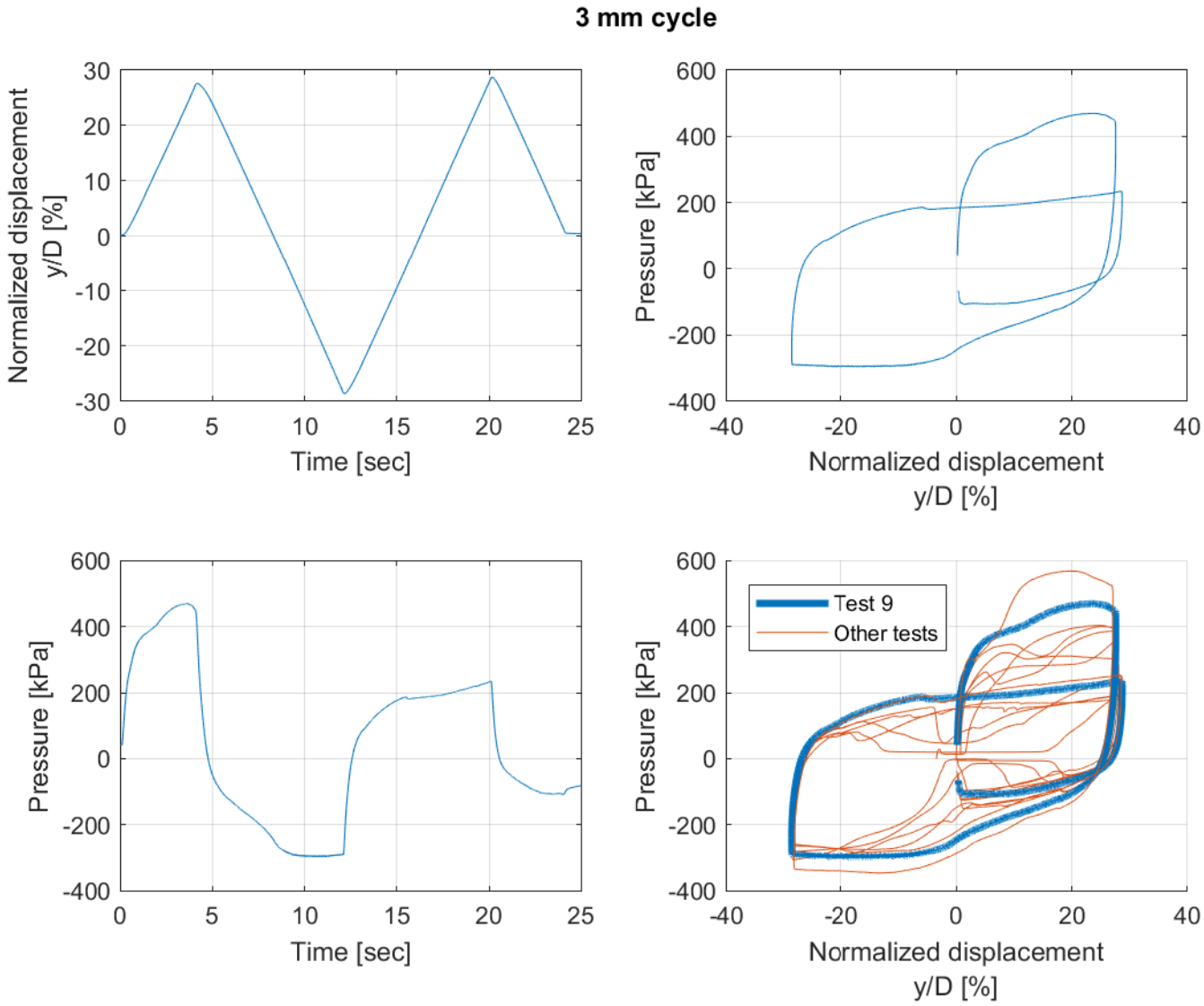
3 mm cycle
Normalized displacement y/D [%]
Time [sec]
Pressure [kPa]
Normalized displacement y/D [%]
Pressure [kPa]
Time [sec]
Test 9
Other tests
Pressure [kPa]
Normalized displacement y/D [%]

Test 9

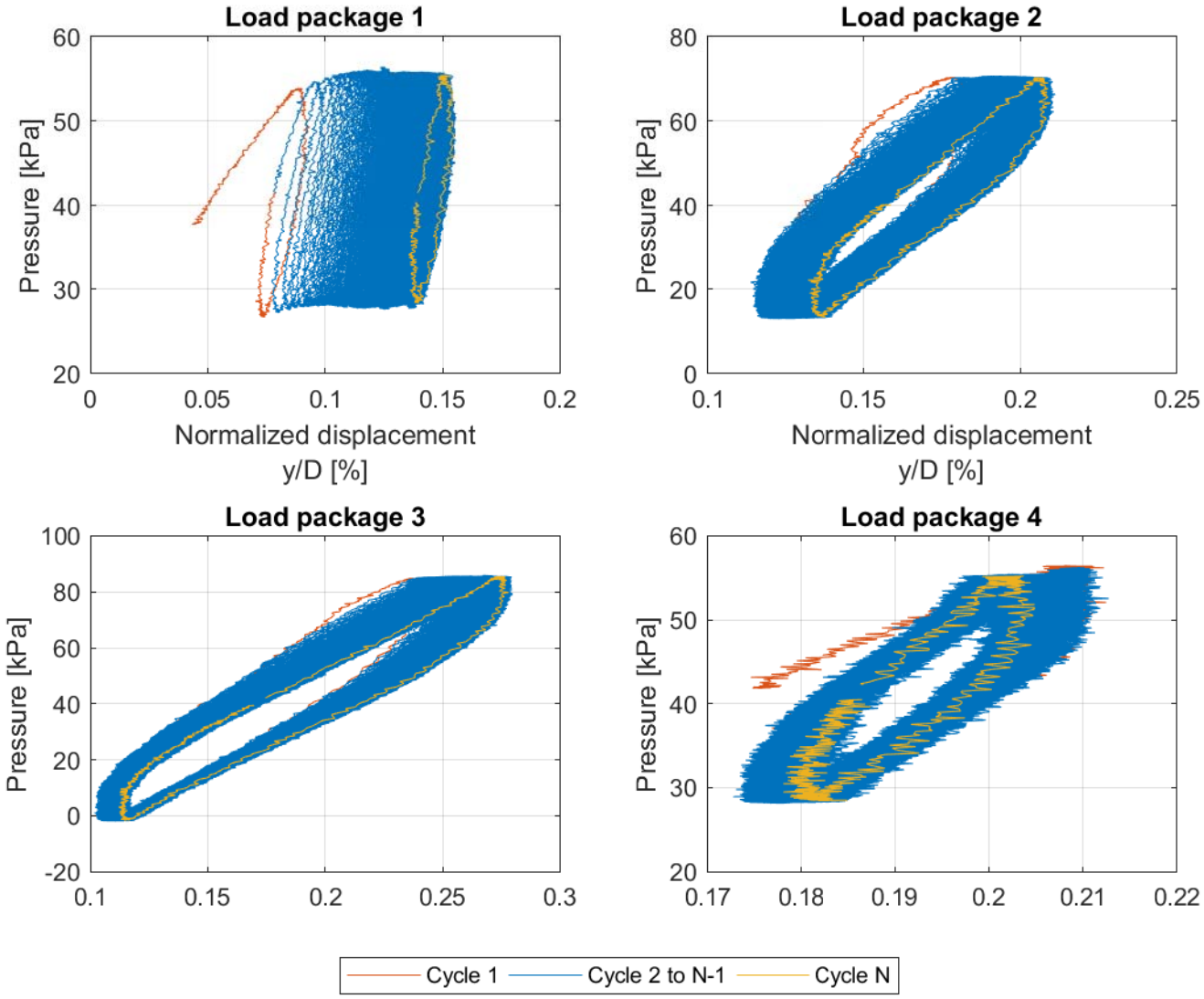
Load package 1
Pressure [kPa]
Normalized displacement
y/D [%]
Load package 2
Pressure [kPa]
Normalized displacement
y/D [%]
Load package 3
Pressure [kPa]
Load package 4
Pressure [kPa]
Cycle 1
Cycle 2 to N-1
Cycle N

Test 9

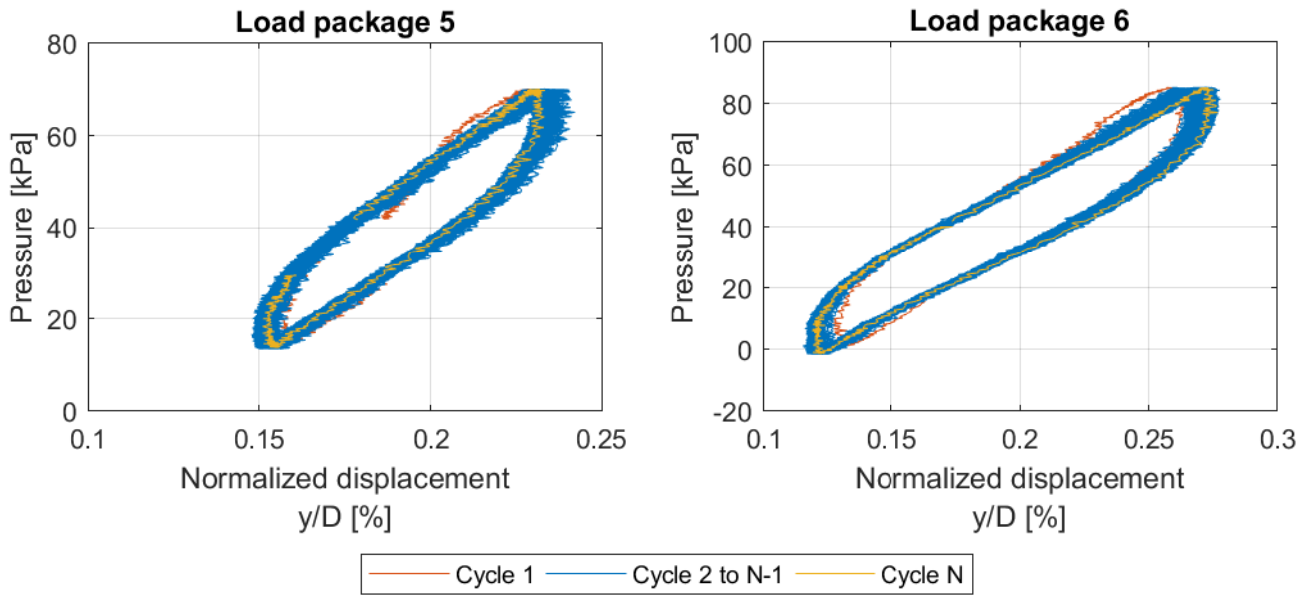
Load package 5
Pressure [kPa]
Normalized displacement
y/D [%]
Load package 6
Pressure [kPa]
Normalized displacement
y/D [%]
Cycle 1
Cycle 2 to N-1
Cycle N

Test 9

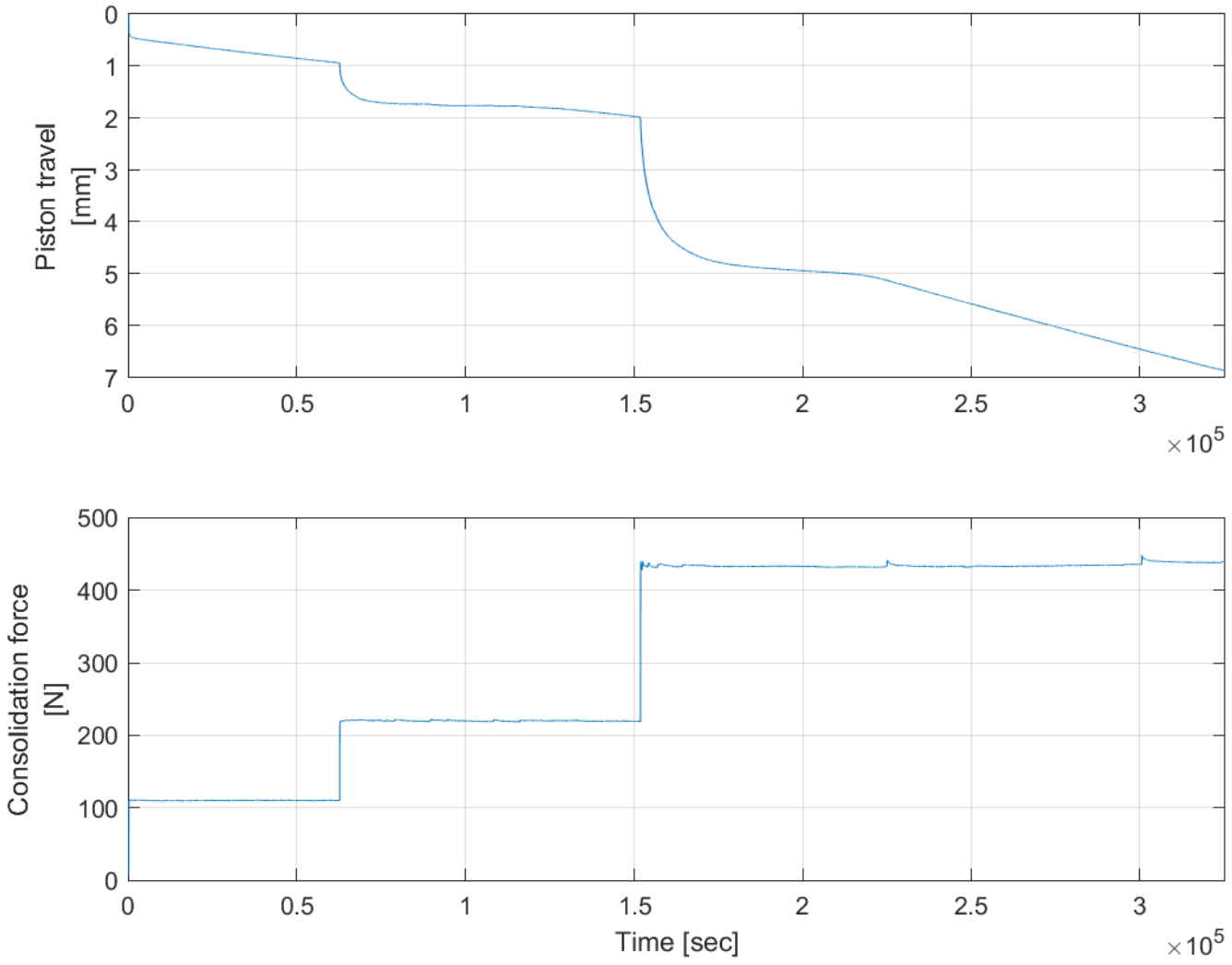
Piston travel [mm]
0
1
2
3
4
5
6
7
0
0.5
1
1.5
2
2.5
3
×10^5
Consolidation force [N]
500
400
300
200
100
0
0
0.5
1
1.5
2
2.5
3
Time [sec]
×10^5

Test 10

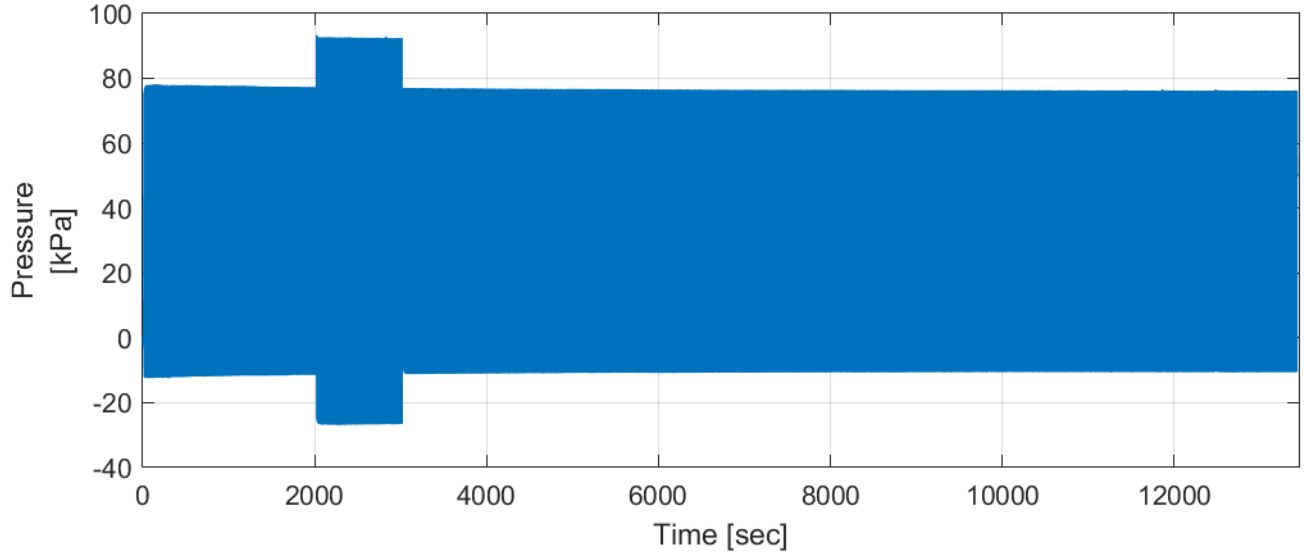
Pressure [kPa]
100
80
60
40
20
0
-20
-40
0
2000
4000
6000
8000
10000
12000
Time [sec]

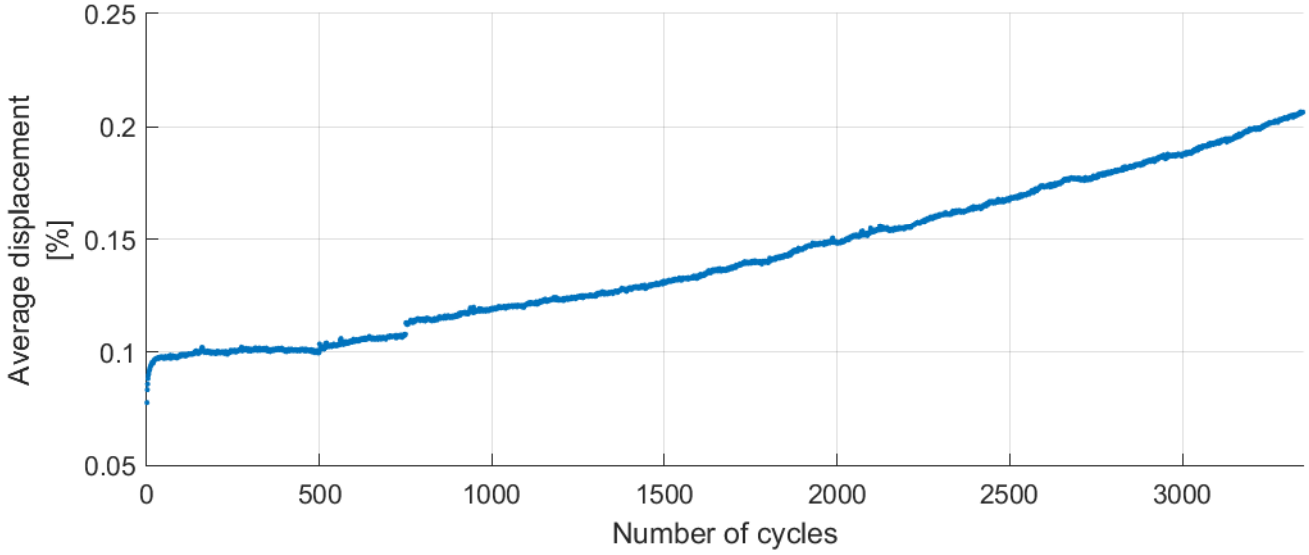
Average displacement [%]
0.25
0.2
0.15
0.1
0.05
0
500
1000
1500
2000
2500
3000
Number of cycles

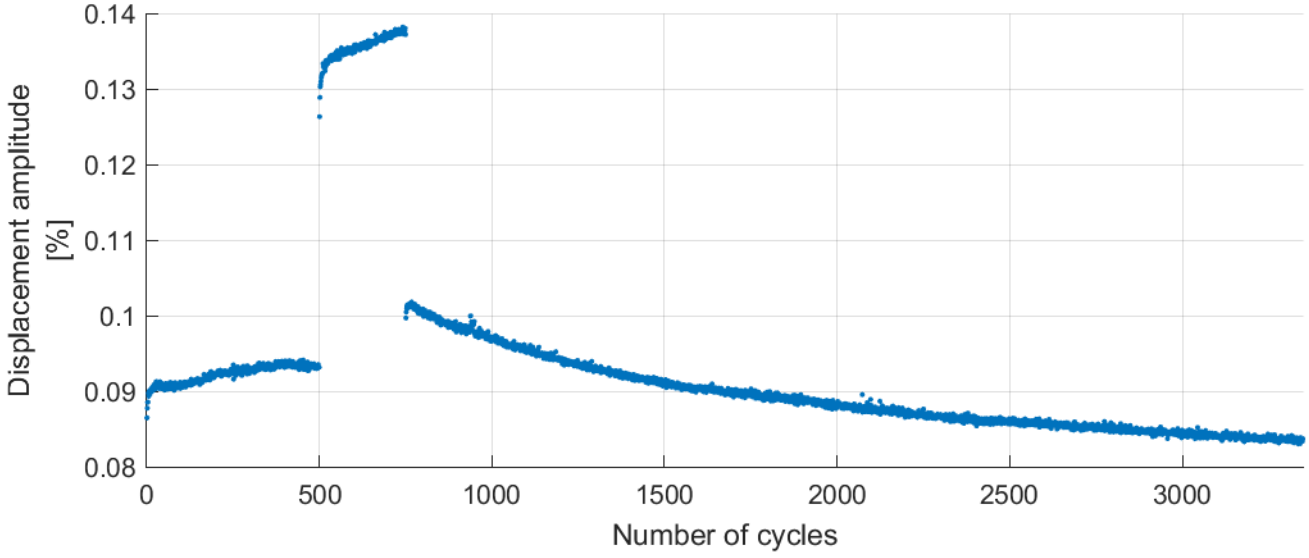
Displacement amplitude [%]
0.14
0.13
0.12
0.11
0.1
0.09
0.08
0
500
1000
1500
2000
2500
3000
Number of cycles

Test 10

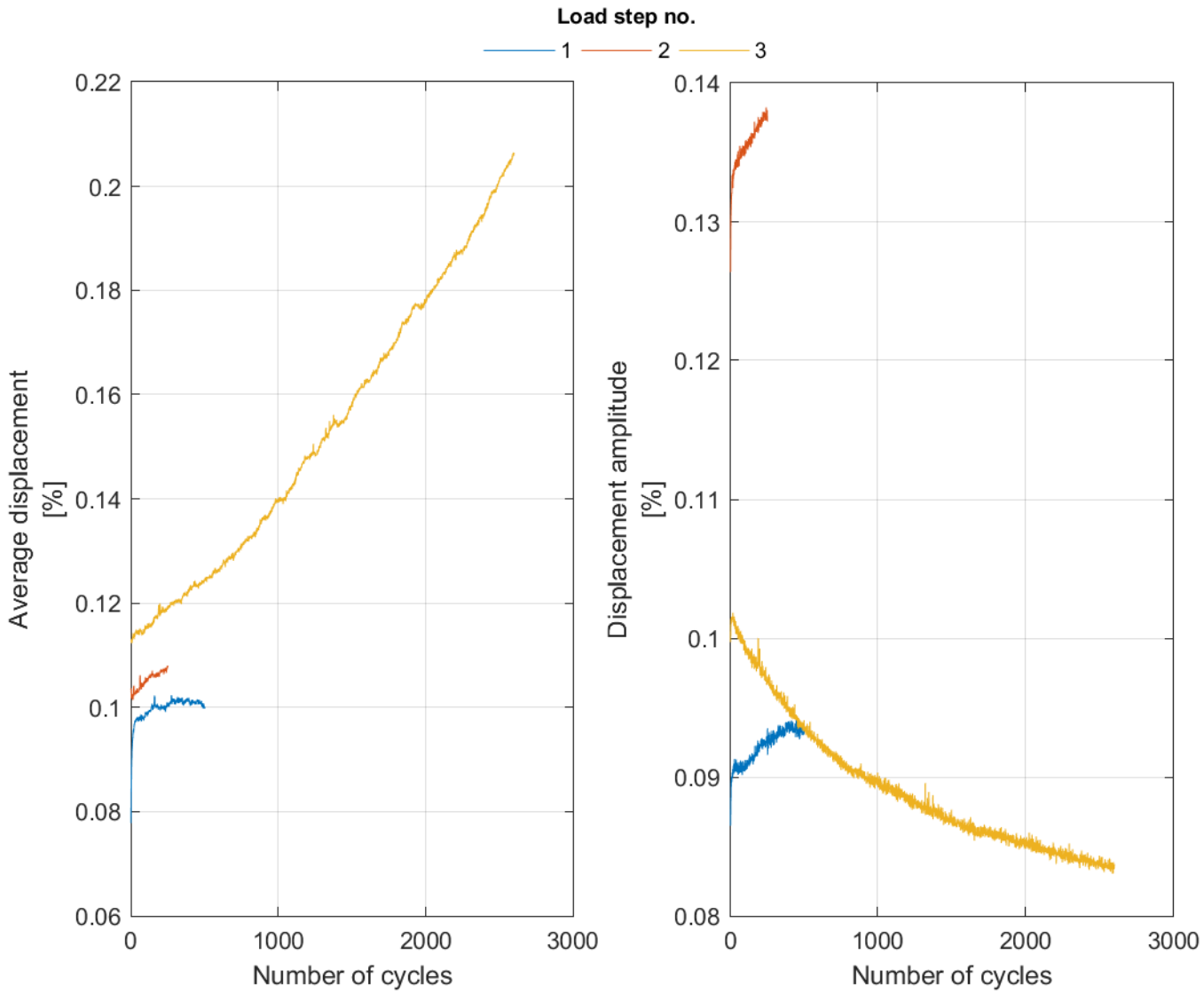
Load step no.
1
2
3
Average displacement [%]
0.22
0.2
0.18
0.16
0.14
0.12
0.1
0.08
0.06
0
1000
2000
3000
Number of cycles
Displacement amplitude [%]
0.14
0.13
0.12
0.11
0.1
0.09
0.08
0
1000
2000
3000
Number of cycles

Test 10

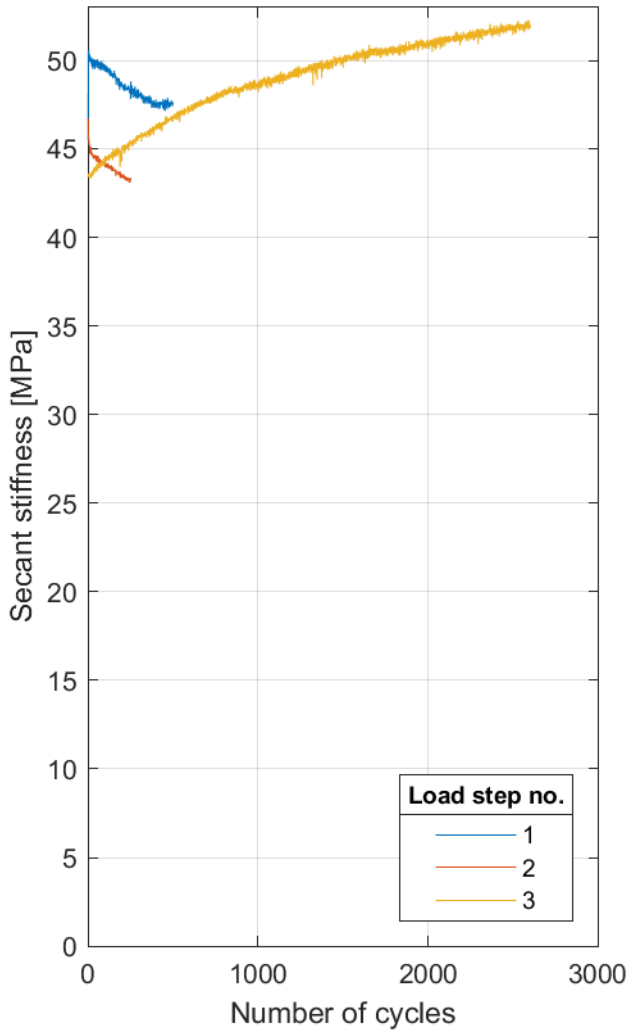
Secant stiffness [MPa]
Number of cycles
Load step no.
1
2
3

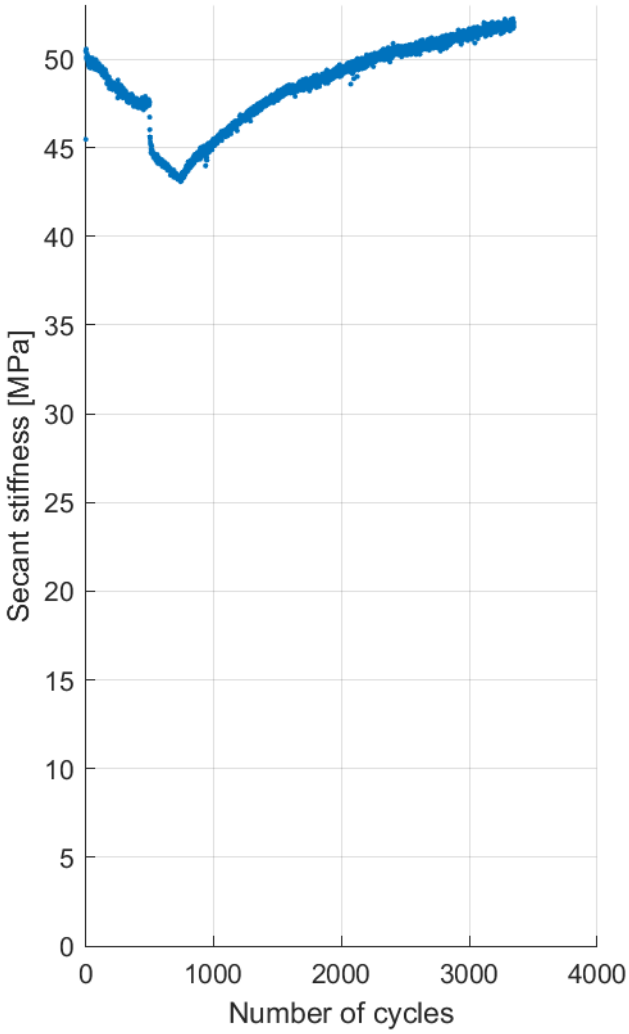
Secant stiffness [MPa]
Number of cycles

Test 10

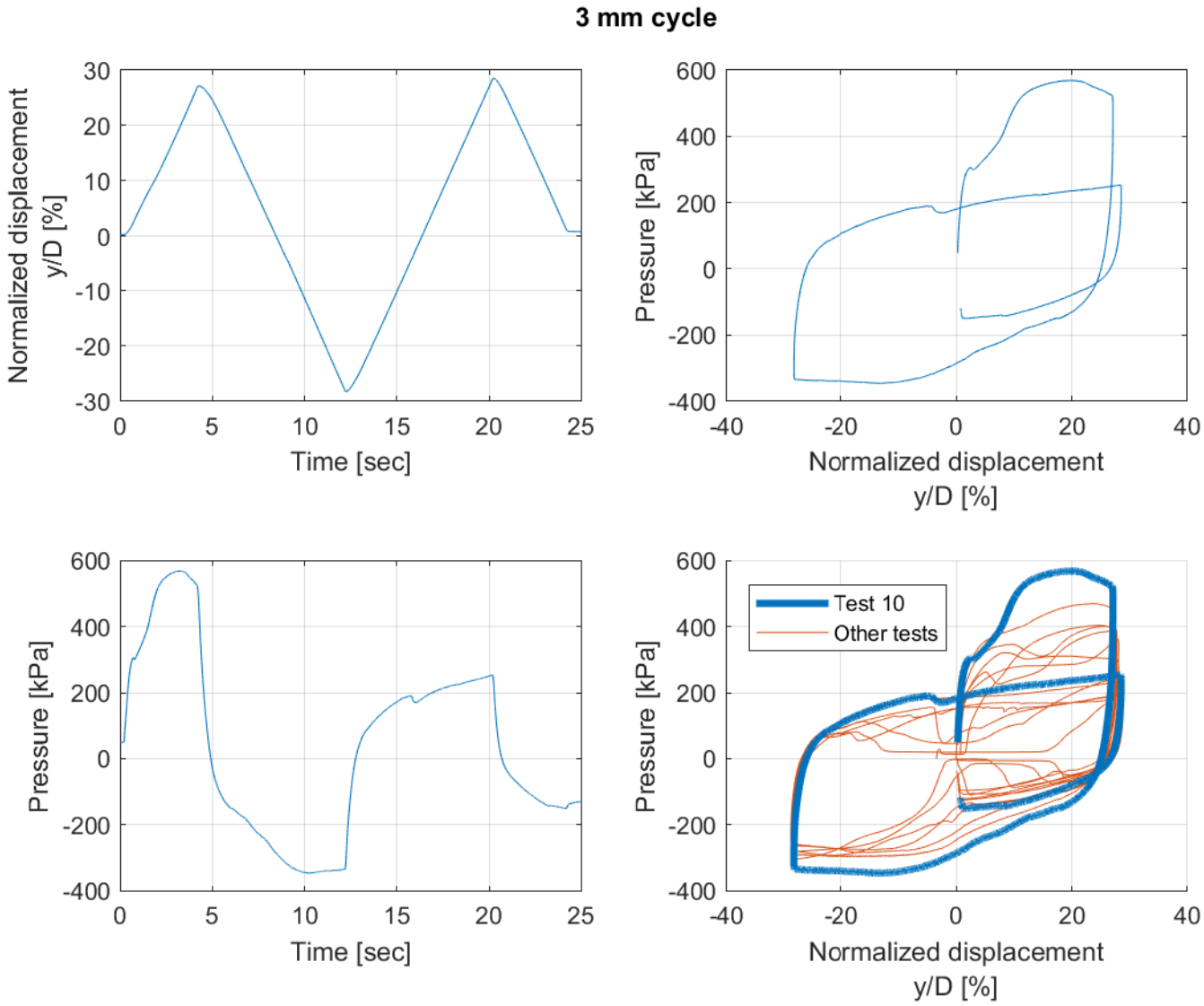
3 mm cycle
Normalized displacement y/D [%]
Time [sec]
Pressure [kPa]
Normalized displacement y/D [%]
Pressure [kPa]
Time [sec]
Test 10
Other tests
Pressure [kPa]
Normalized displacement y/D [%]

Test 10

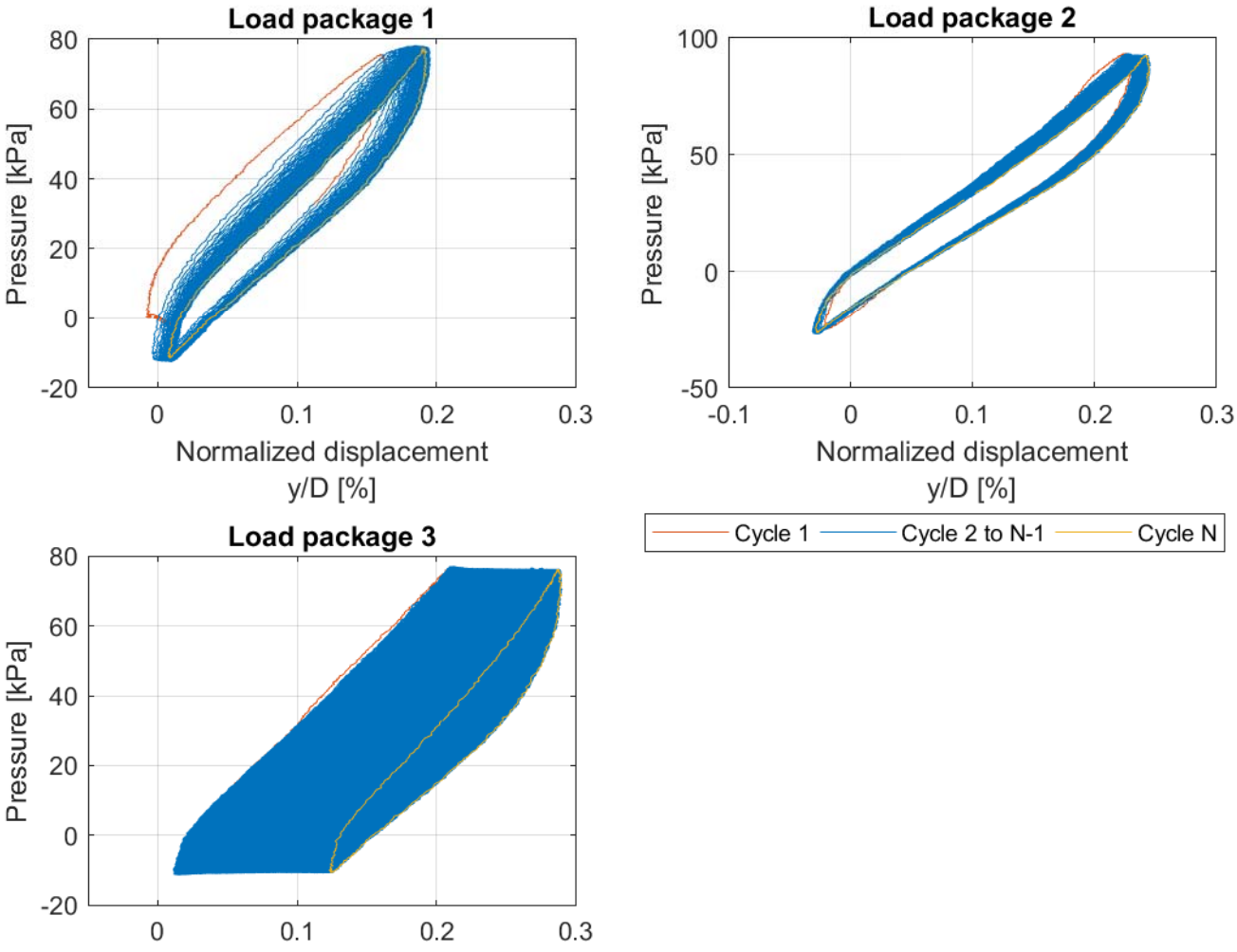
Load package 1
Pressure [kPa]
Normalized displacement
y/D [%]
Load package 2
Pressure [kPa]
Normalized displacement
y/D [%]
Load package 3
Pressure [kPa]
Cycle 1
Cycle 2 to N-1
Cycle N

Test 10

B.2 Tests on North Sea samples

Test results of tests 11 and 12 are given in this section.

The results of each test are presented in the following order:

Test 11:

- Consolidation force, piston travel
- Pressure, normalized displacement

Test 12:

- Consolidation force, piston travel
- Pressure, normalized displacement

Tests 11 and 12:

- 270 N cycles
- 3 mm cycle

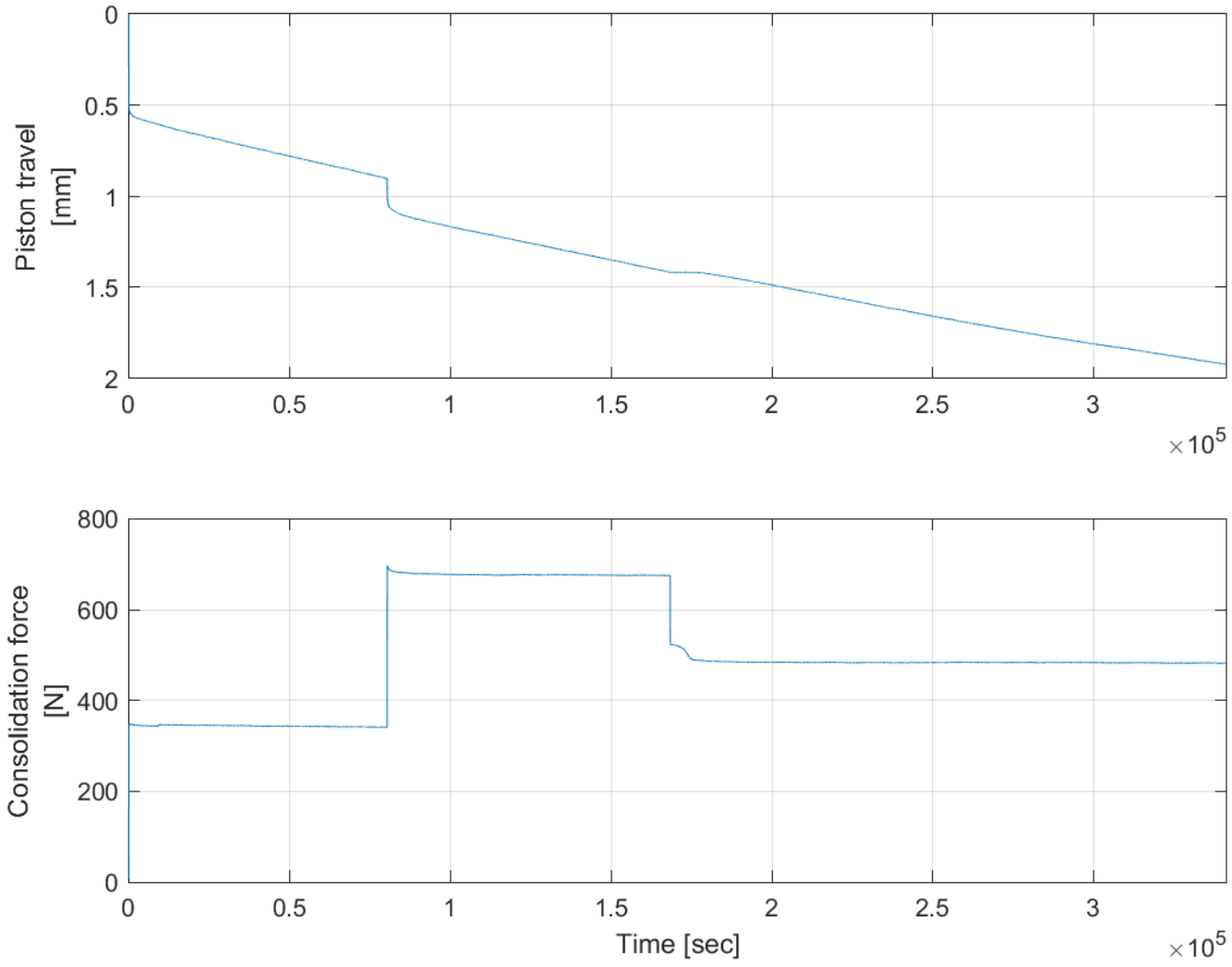
Piston travel
[mm]
0
0.5
1
1.5
2
0
0.5
1
1.5
2
2.5
3
×10^5
Consolidation force
[N]
800
600
400
200
0
0
0.5
1
1.5
2
2.5
3
Time [sec]
×10^5

Test 11

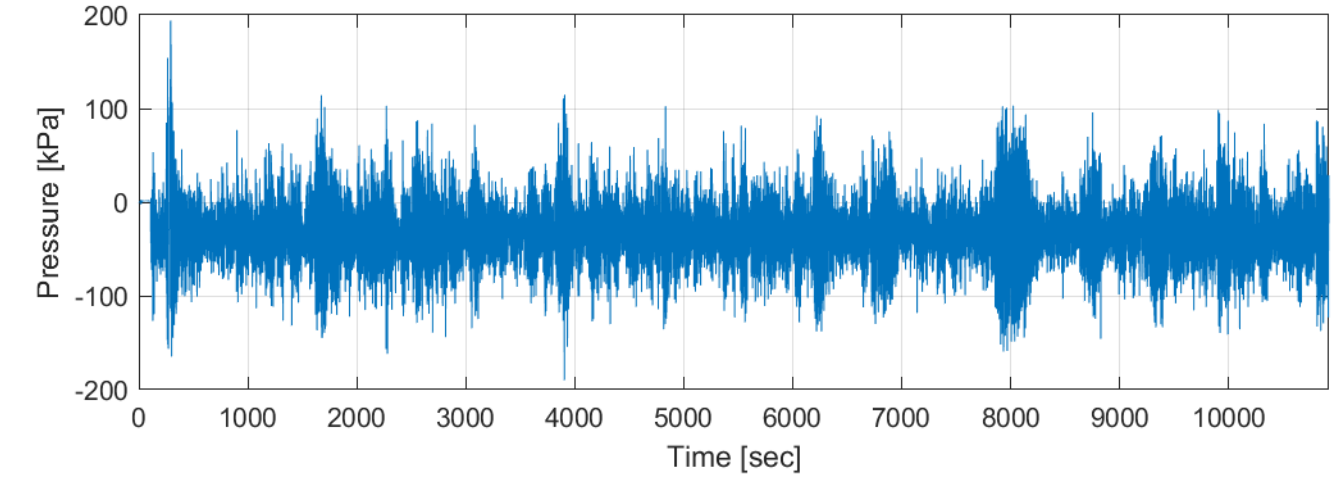
Pressure [kPa]
200
100
0
-100
-200
0
1000
2000
3000
4000
5000
6000
7000
8000
9000
10000
Time [sec]

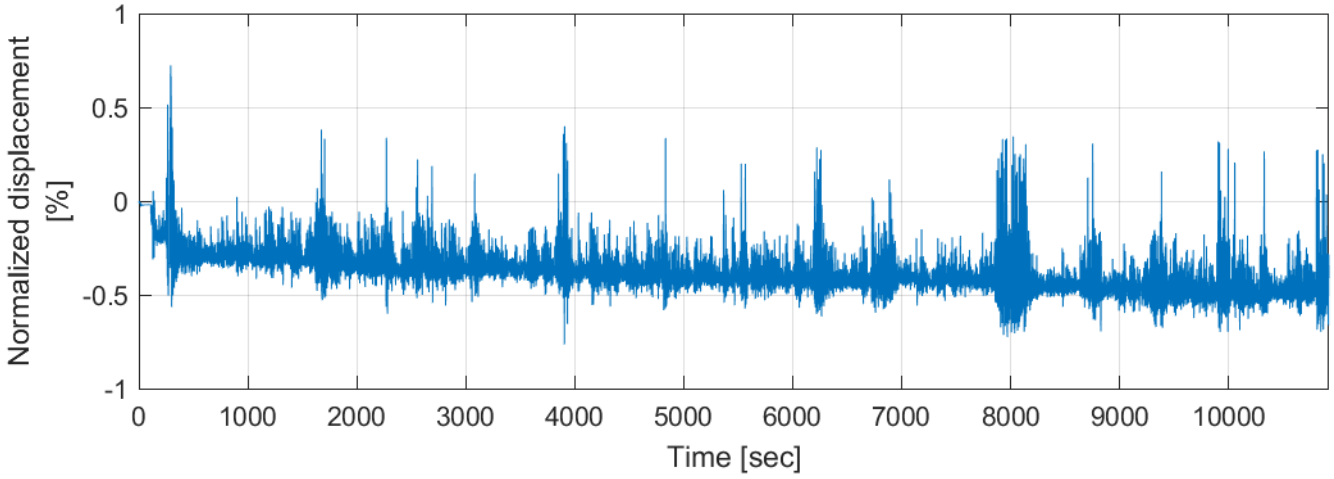
Normalized displacement [%]
1
0.5
0
-0.5
-1
0
1000
2000
3000
4000
5000
6000
7000
8000
9000
10000
Time [sec]

Test 11

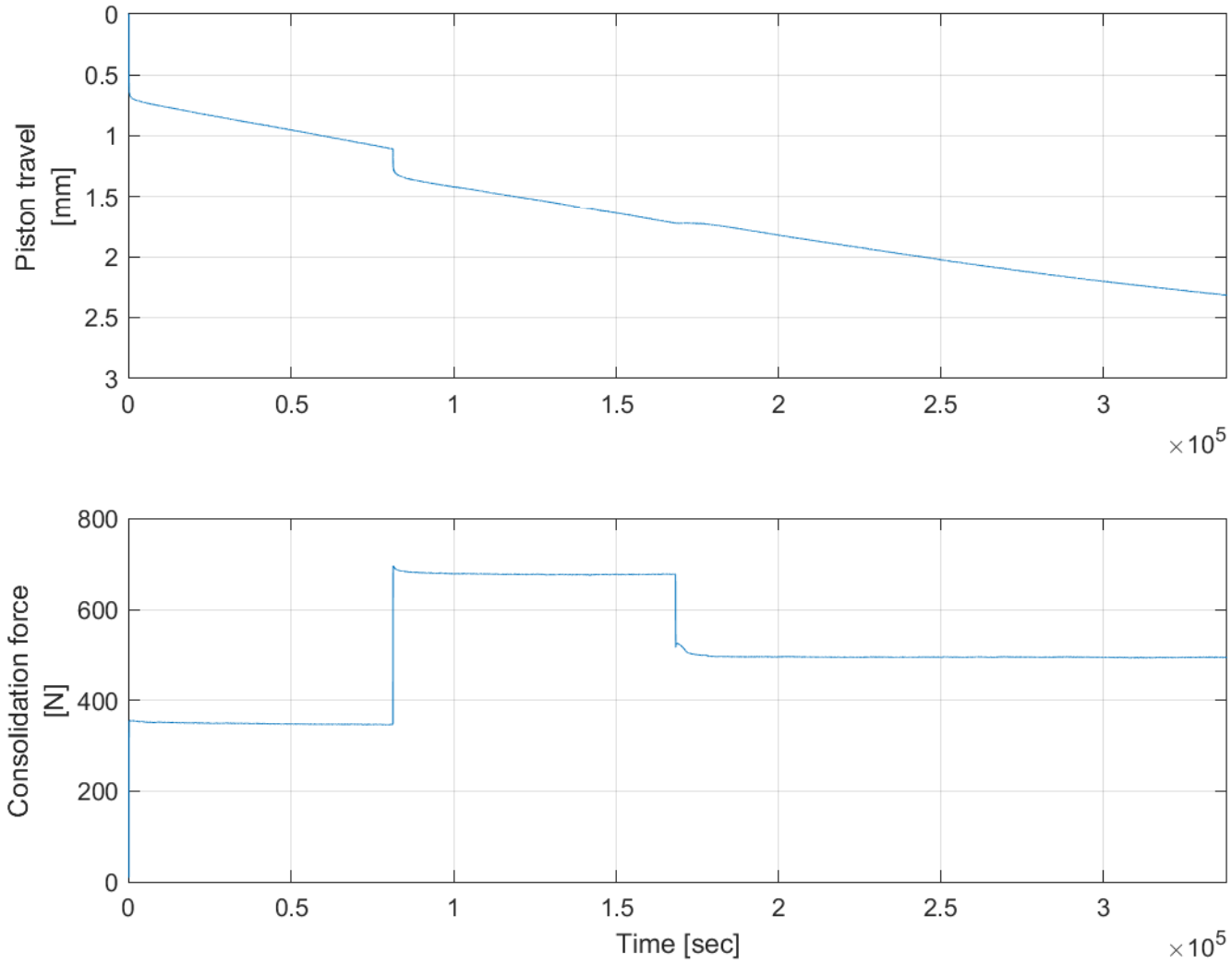
Piston travel
[mm]
0
0.5
1
1.5
2
2.5
3
0
0.5
1
1.5
2
2.5
3
×10^5
Consolidation force
[N]
800
600
400
200
0
0
0.5
1
1.5
2
2.5
3
Time [sec]
×10^5

Test 12

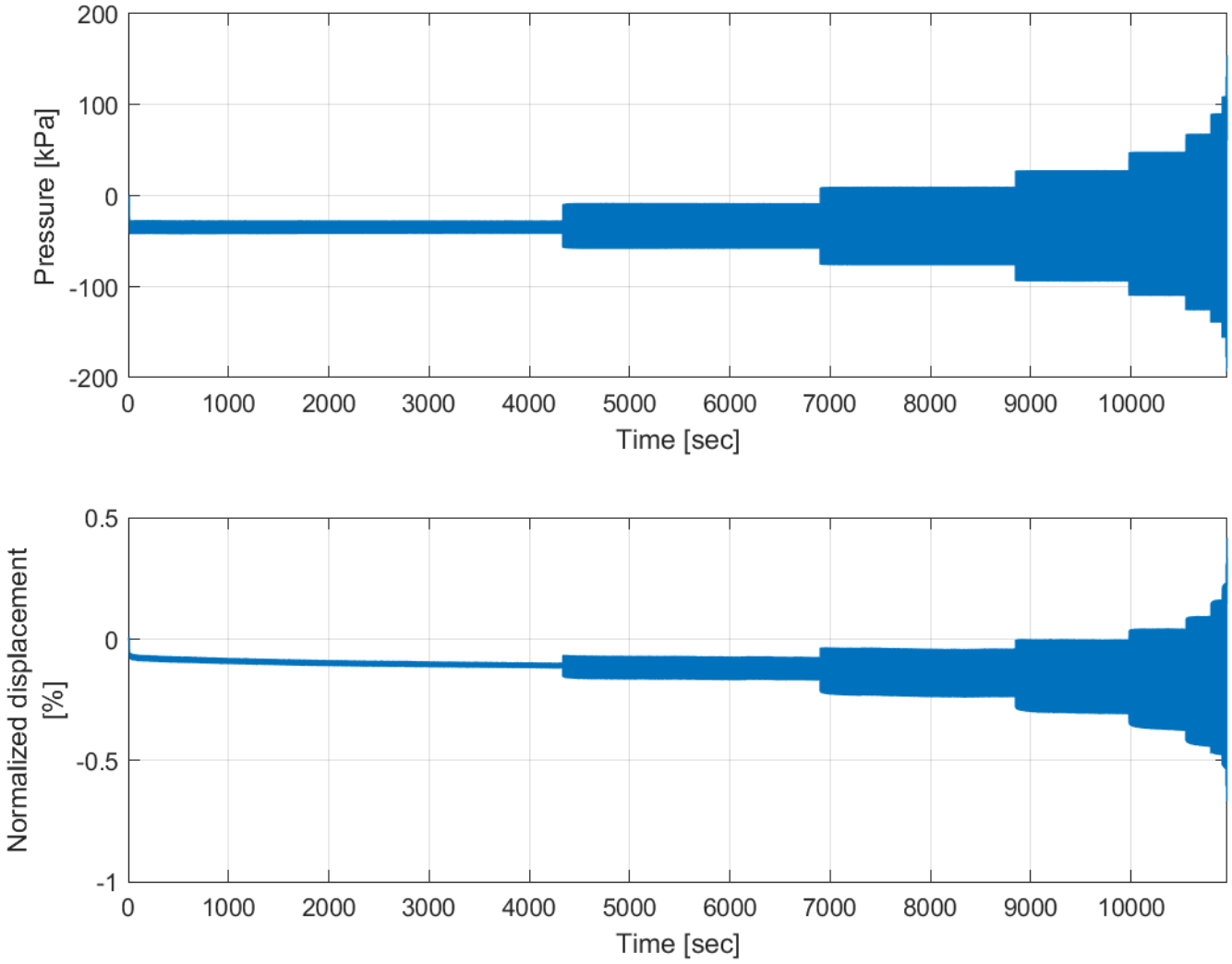
200
100
0
-100
-200
Pressure [kPa]
0
1000
2000
3000
4000
5000
6000
7000
8000
9000
10000
Time [sec]
0.5
0
-0.5
-1
Normalized displacement [%]
0
1000
2000
3000
4000
5000
6000
7000
8000
9000
10000
Time [sec]

Test 12

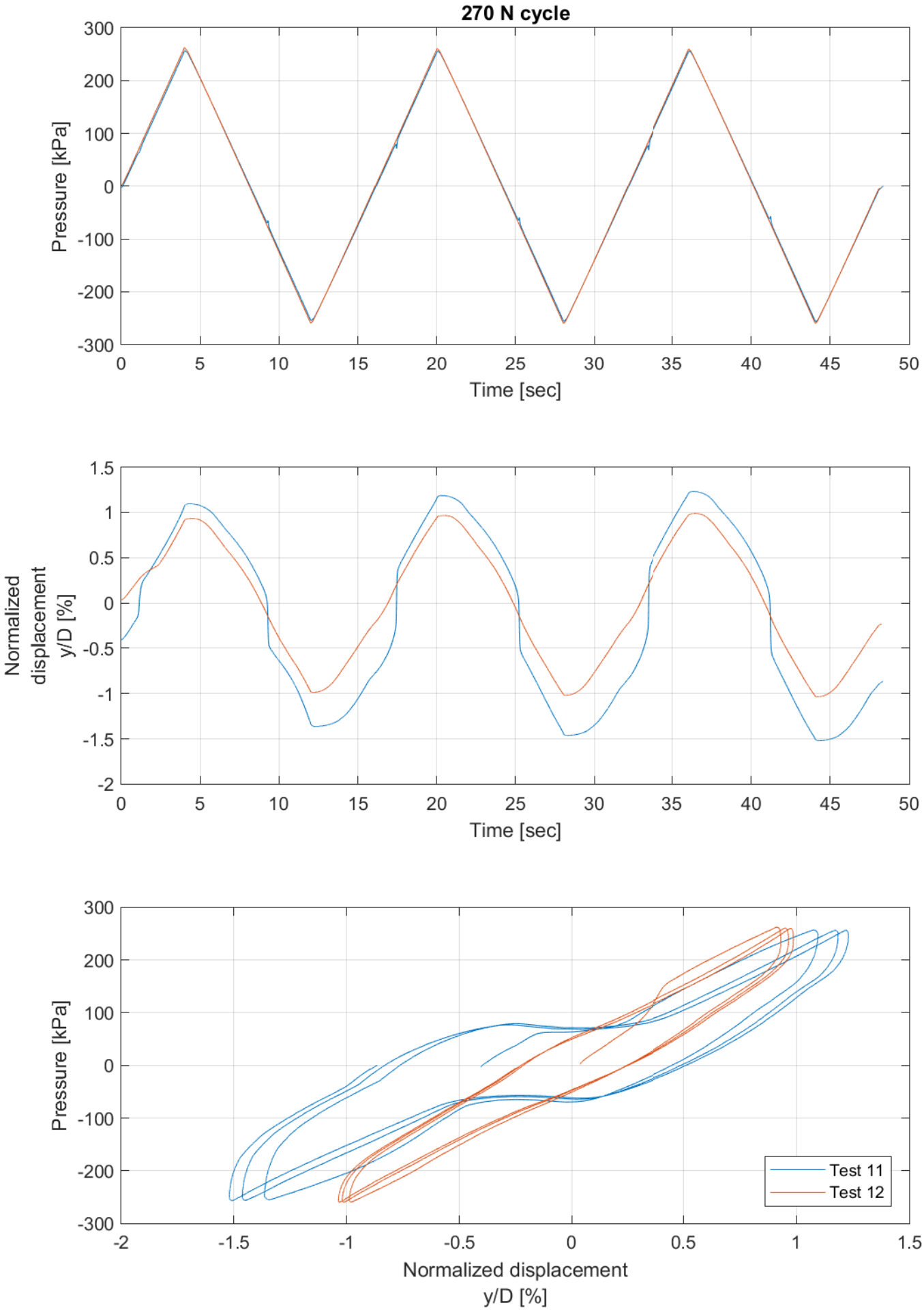
270 N cycle
Pressure [kPa]
Time [sec]
Normalized displacement y/D [%]
Time [sec]
Pressure [kPa]
Normalized displacement y/D [%]
Test 11
Test 12

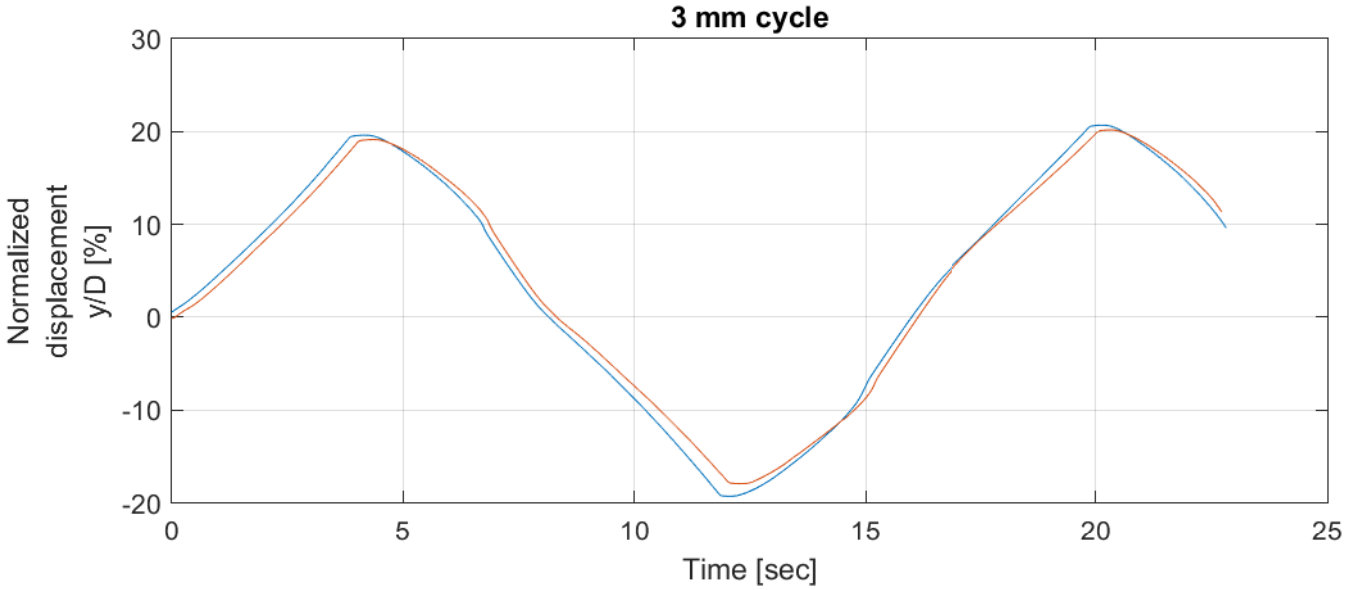
3 mm cycle
Normalized displacement y/D [%]
Time [sec]

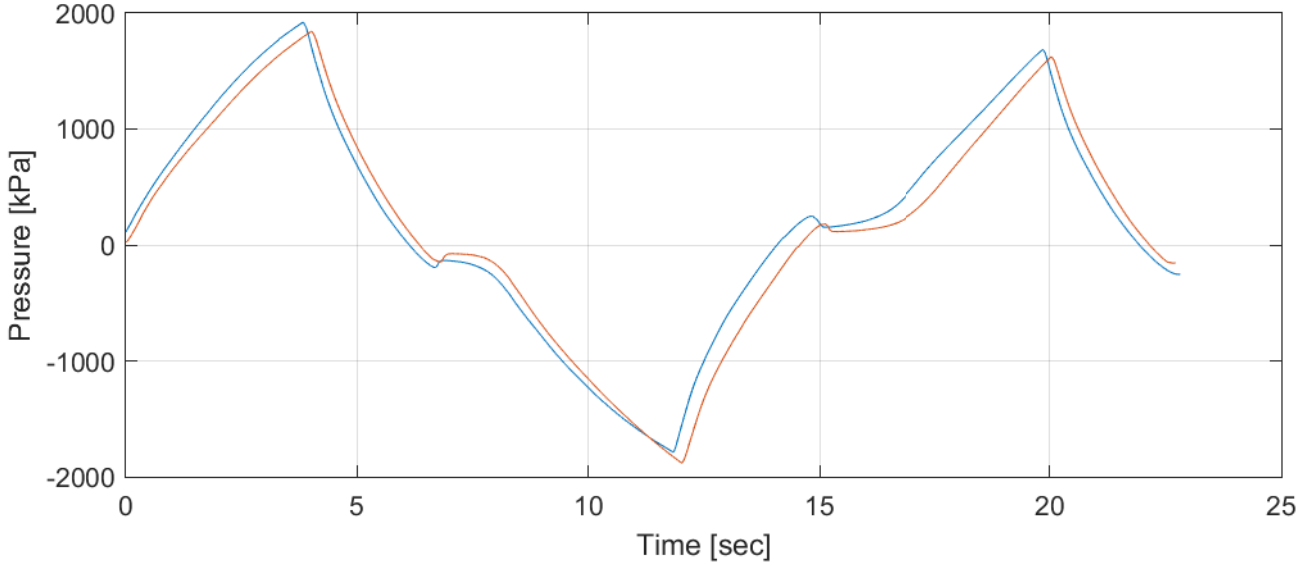
Pressure [kPa]
Time [sec]

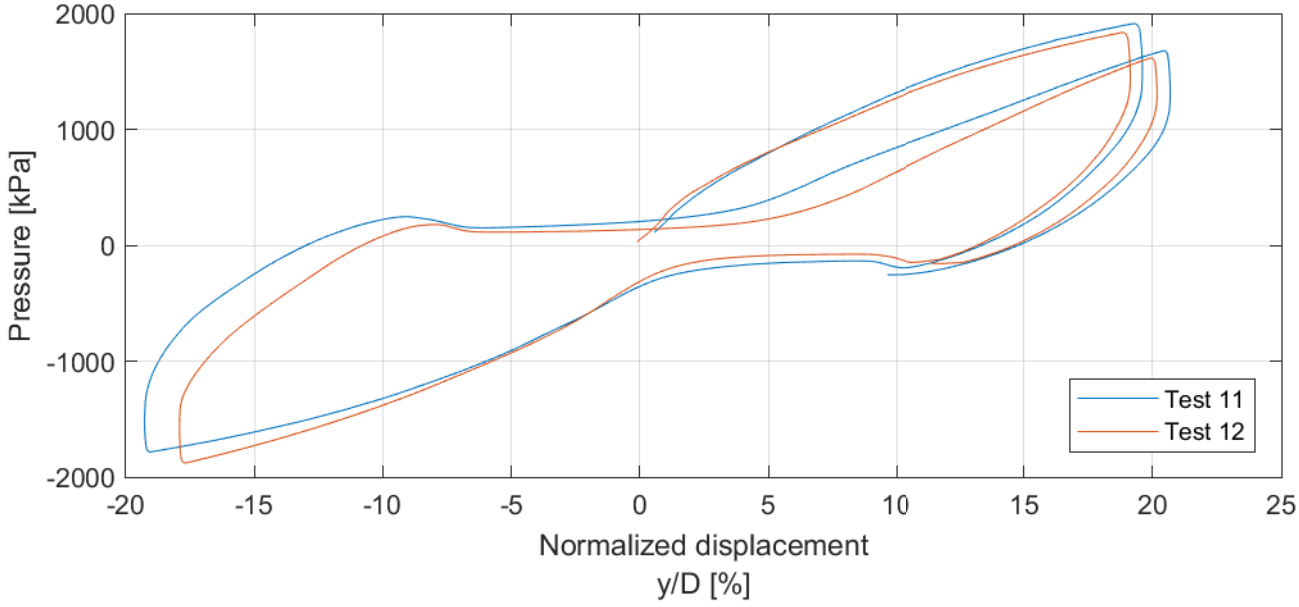
Pressure [kPa]
Normalized displacement y/D [%]
Test 11
Test 12

B.3 Dummy tests

Test results of tests D2, D3, D4 and D5 are given in this section.

The results of each test are presented in the following order:

Tests D2, D3 and D4:

- Consolidation force, piston travel
- Pressure, normalized displacements
- Normalized displacements
- Secant stiffness
- Hysteresis loops in pressure-displacement plots

Test D5:

- Consolidation force, piston travel
- Pressure, normalized displacement (Load history 1)
- Pressure, normalized displacement (Load history 2)

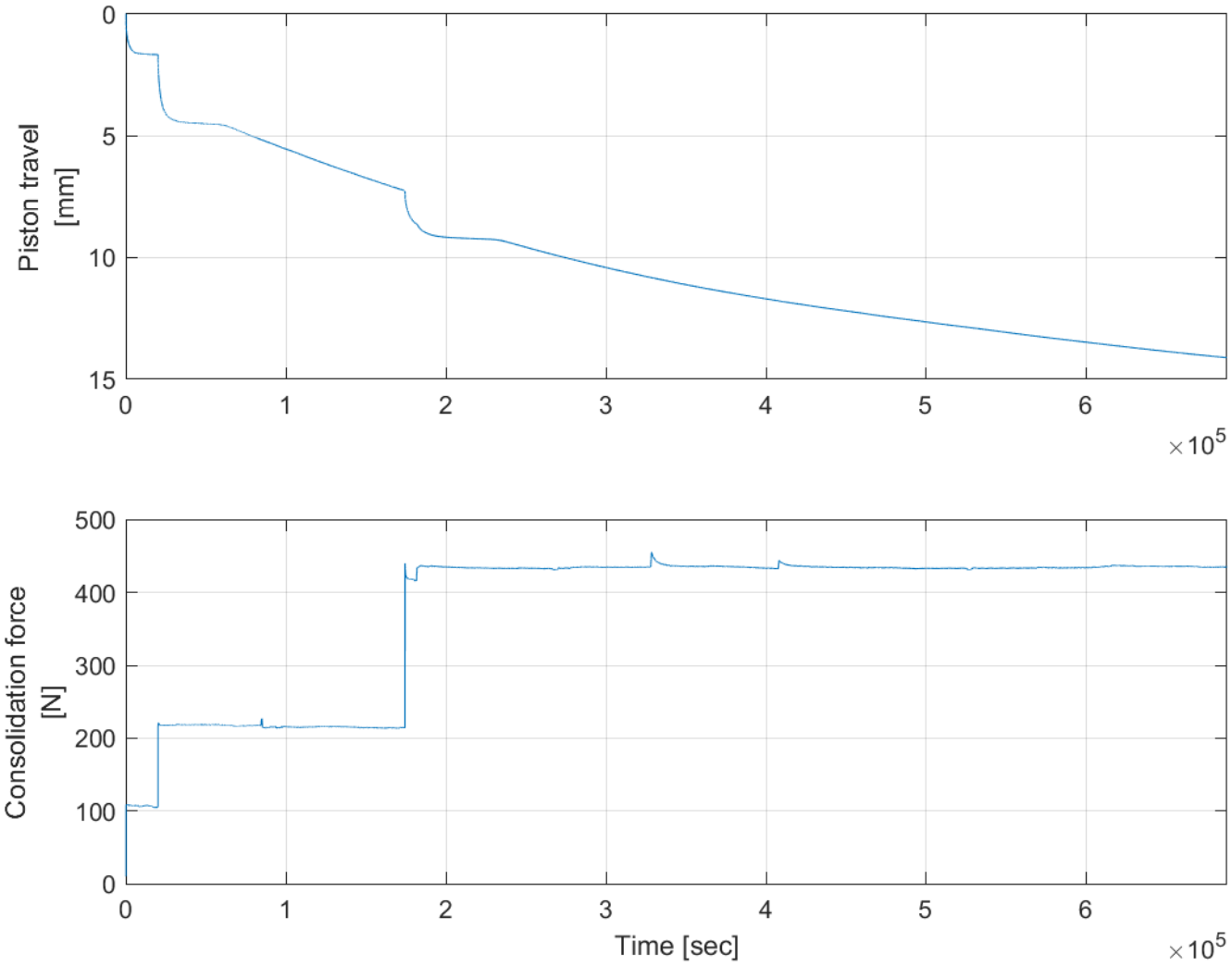
Piston travel
[mm]
0
5
10
15
0
1
2
3
4
5
6
×10^5
Consolidation force
[N]
500
400
300
200
100
0
0
1
2
3
4
5
6
Time [sec]
×10^5

Test D2

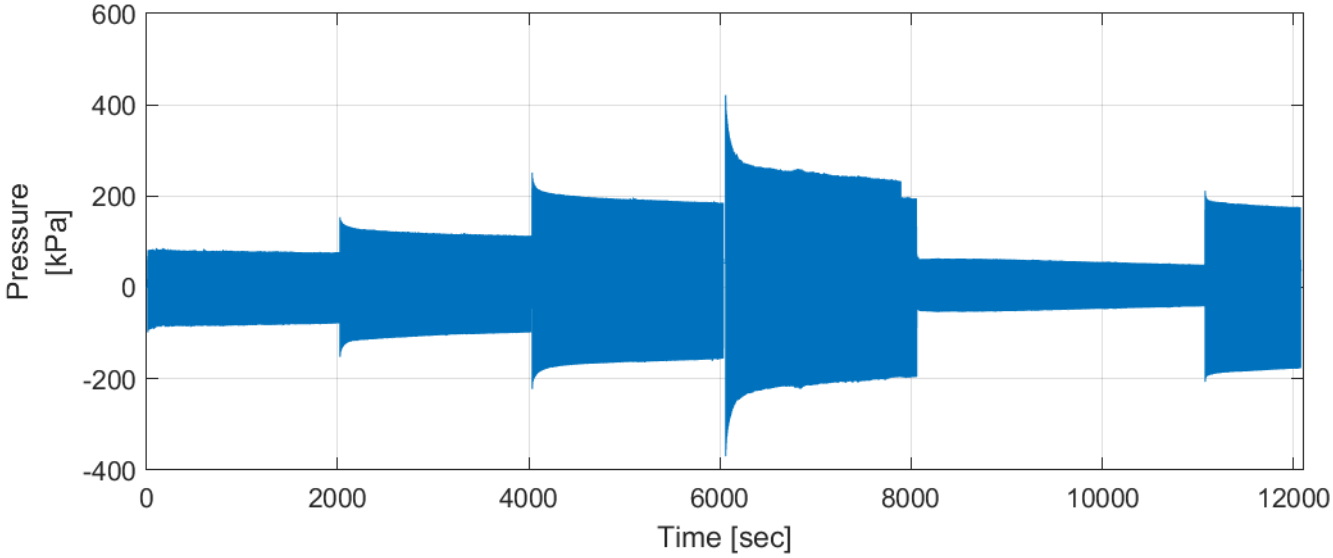
Pressure [kPa]
600
400
200
0
-200
-400
0
2000
4000
6000
8000
10000
12000
Time [sec]

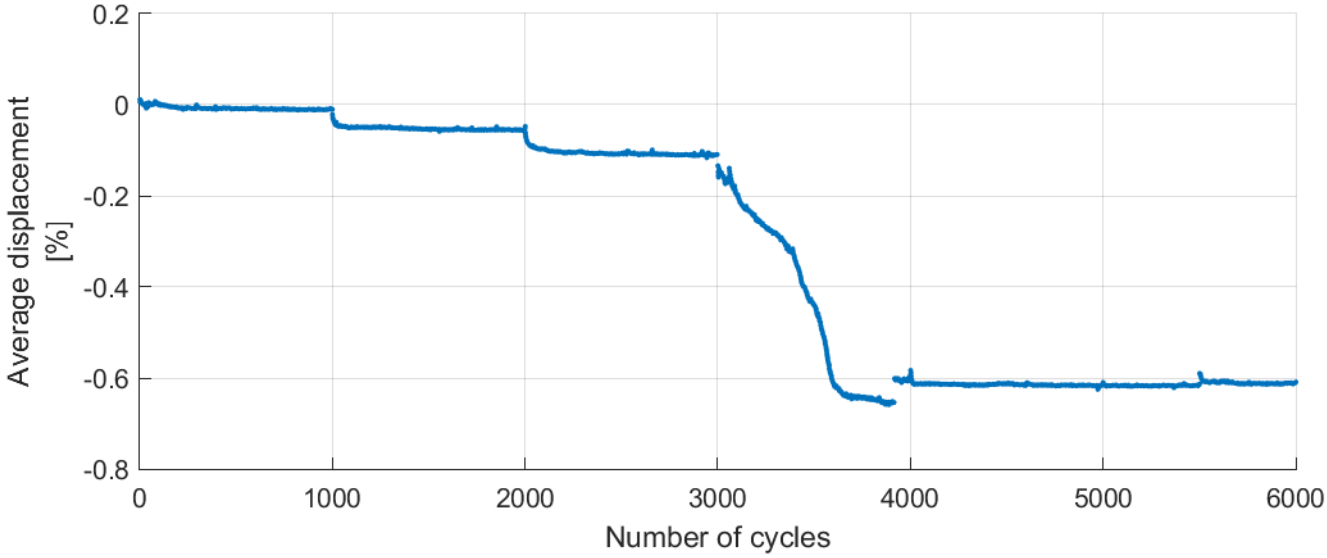
Average displacement [%]
0.2
0
-0.2
-0.4
-0.6
-0.8
0
1000
2000
3000
4000
5000
6000
Number of cycles

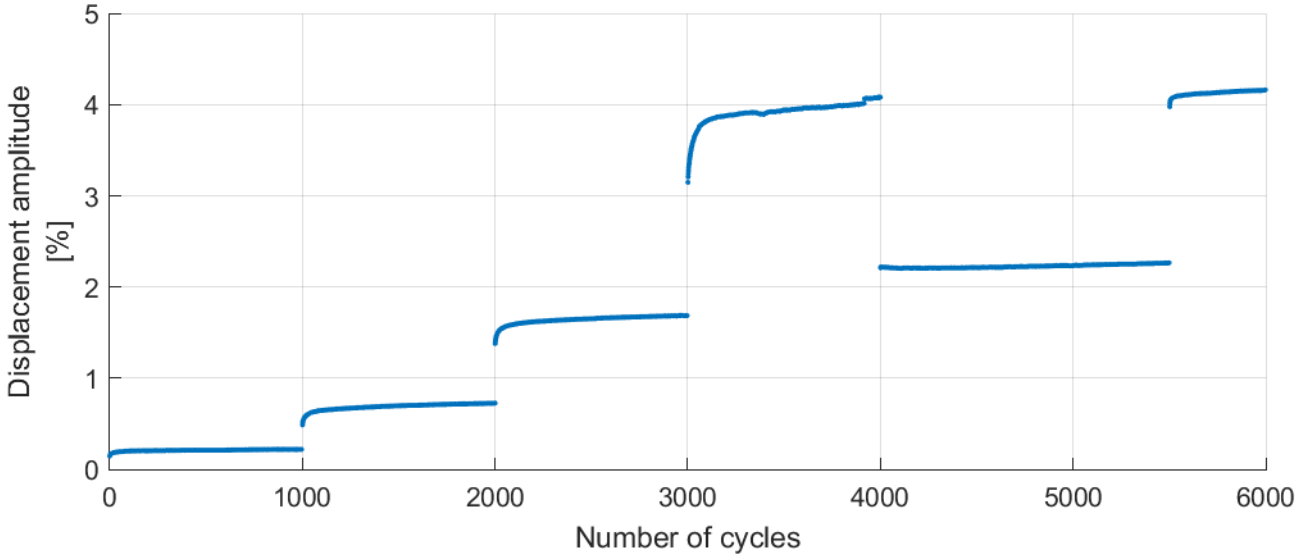
Displacement amplitude [%]
5
4
3
2
1
0
0
1000
2000
3000
4000
5000
6000
Number of cycles

Test D2

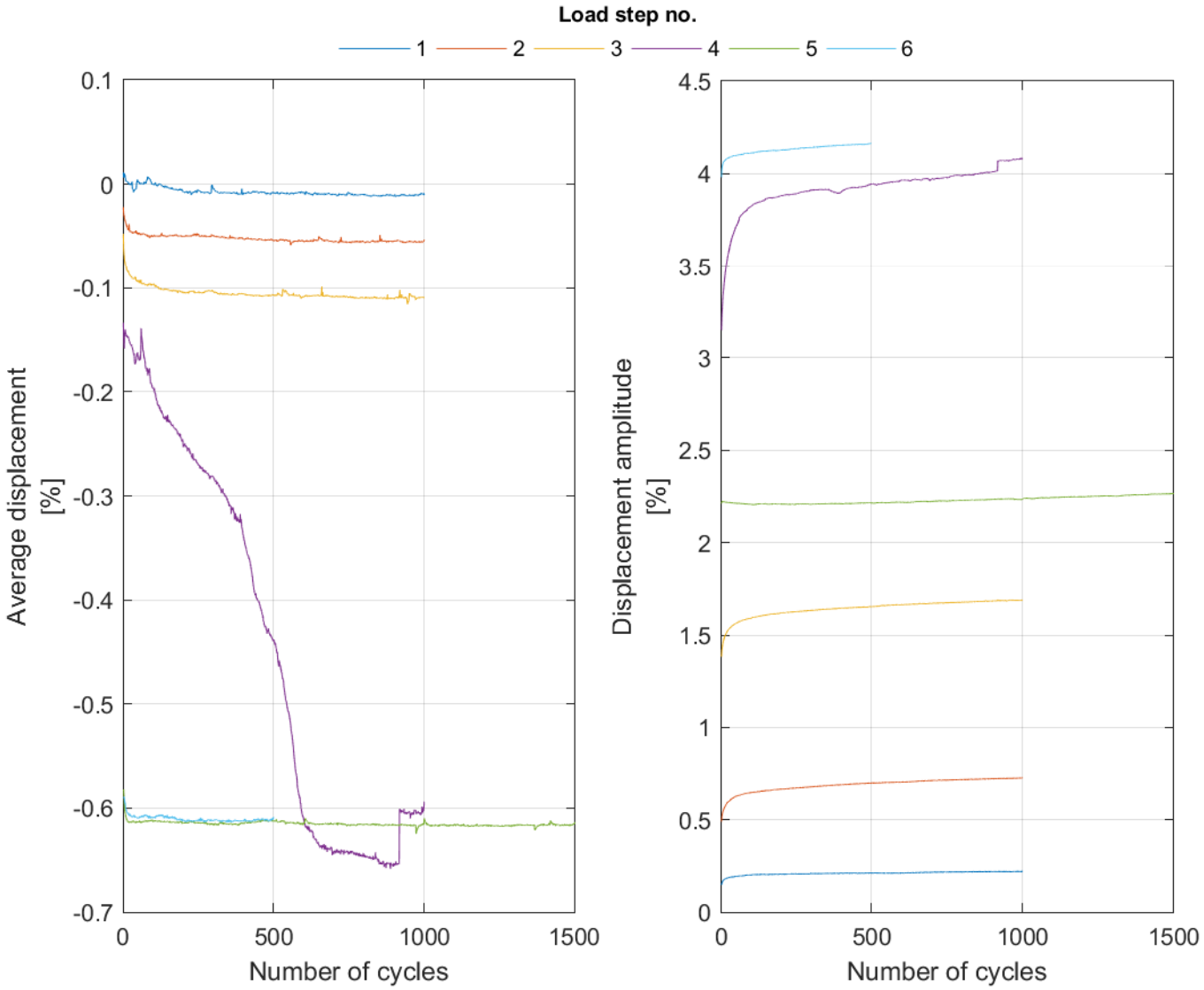
Load step no.
1
2
3
4
5
6
Average displacement [%]
Number of cycles
Displacement amplitude [%]
Number of cycles

Test D2

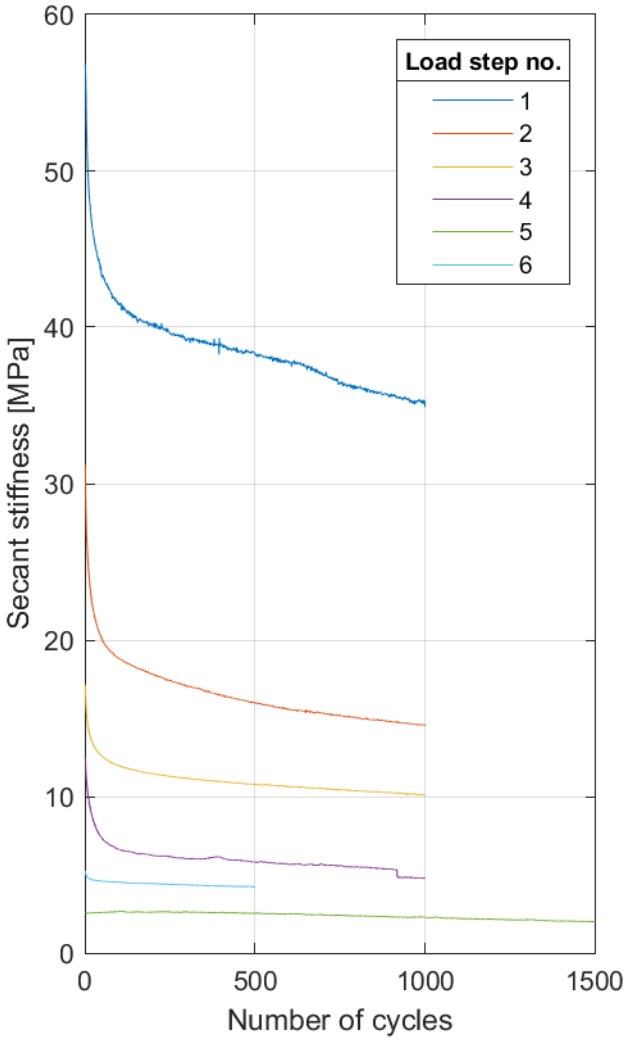
Load step no.
1
2
3
4
5
6
Secant stiffness [MPa]
Number of cycles
0
10
20
30
40
50
60
0
500
1000
1500

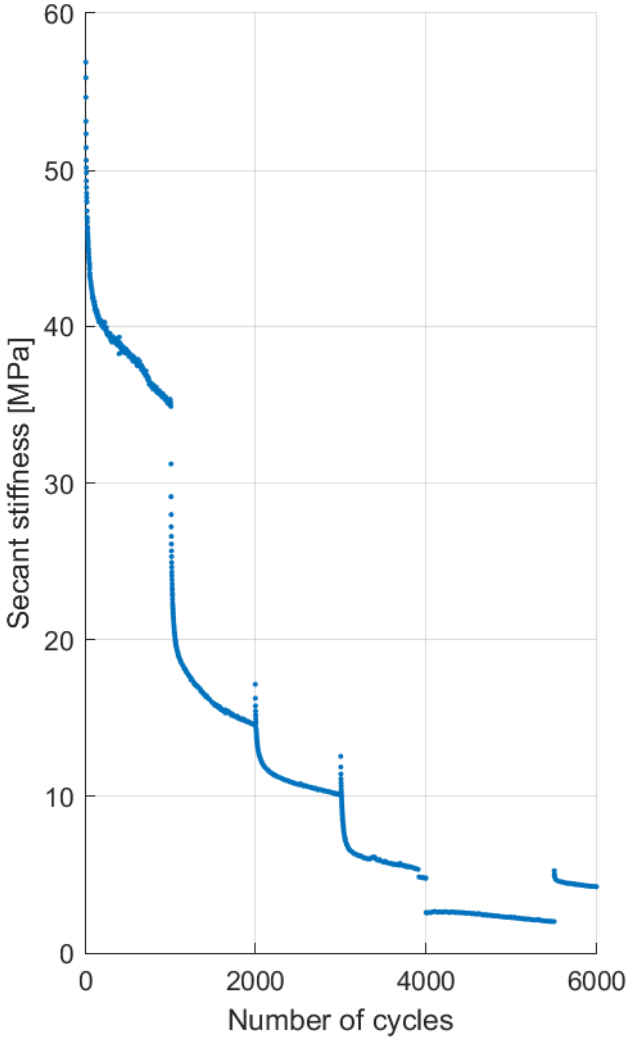
Secant stiffness [MPa]
Number of cycles
0
10
20
30
40
50
60
0
2000
4000
6000

Test D2

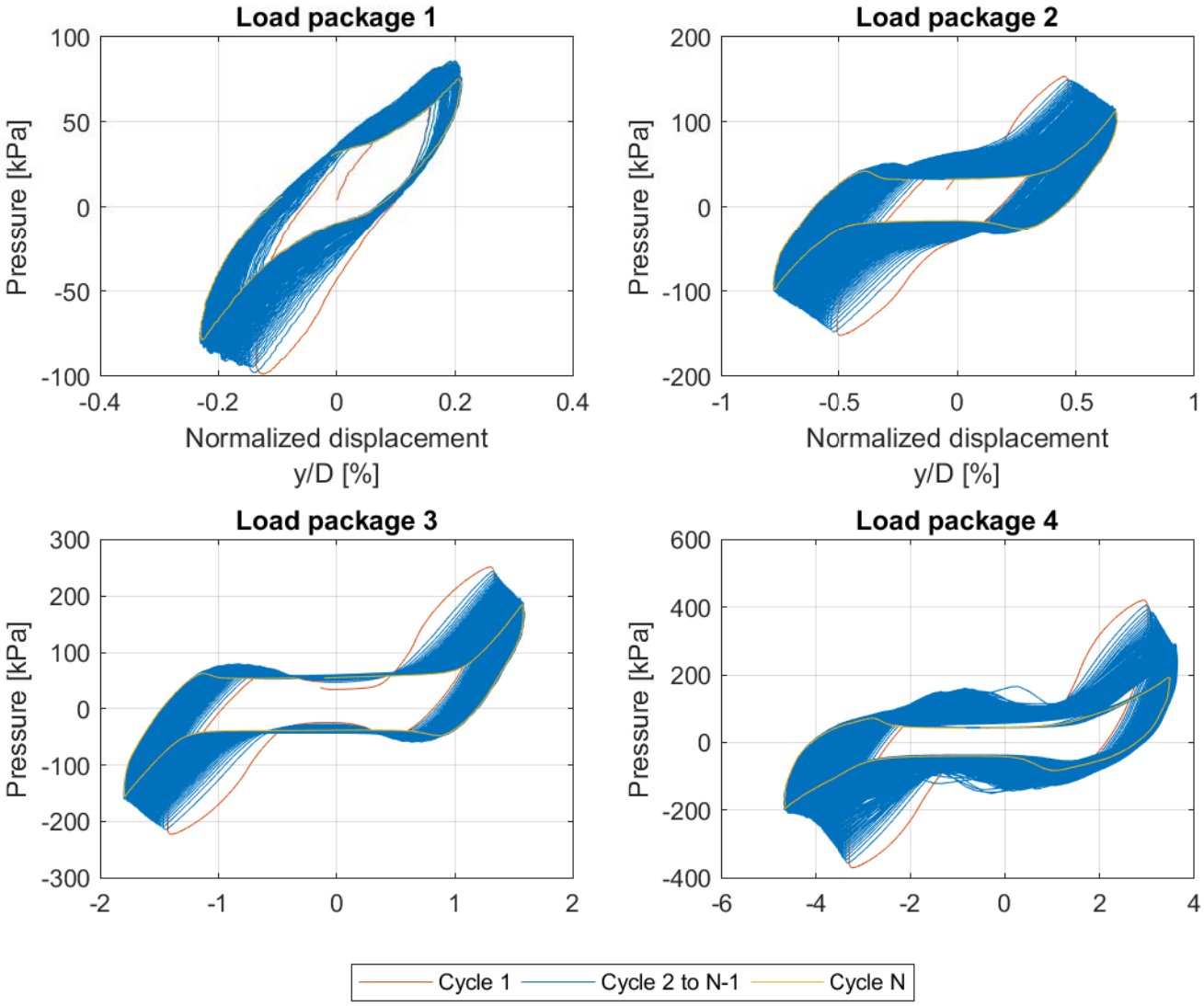
Load package 1
Pressure [kPa]
Normalized displacement
y/D [%]
Load package 2
Pressure [kPa]
Normalized displacement
y/D [%]
Load package 3
Pressure [kPa]
Load package 4
Pressure [kPa]
Cycle 1
Cycle 2 to N-1
Cycle N

Test D2

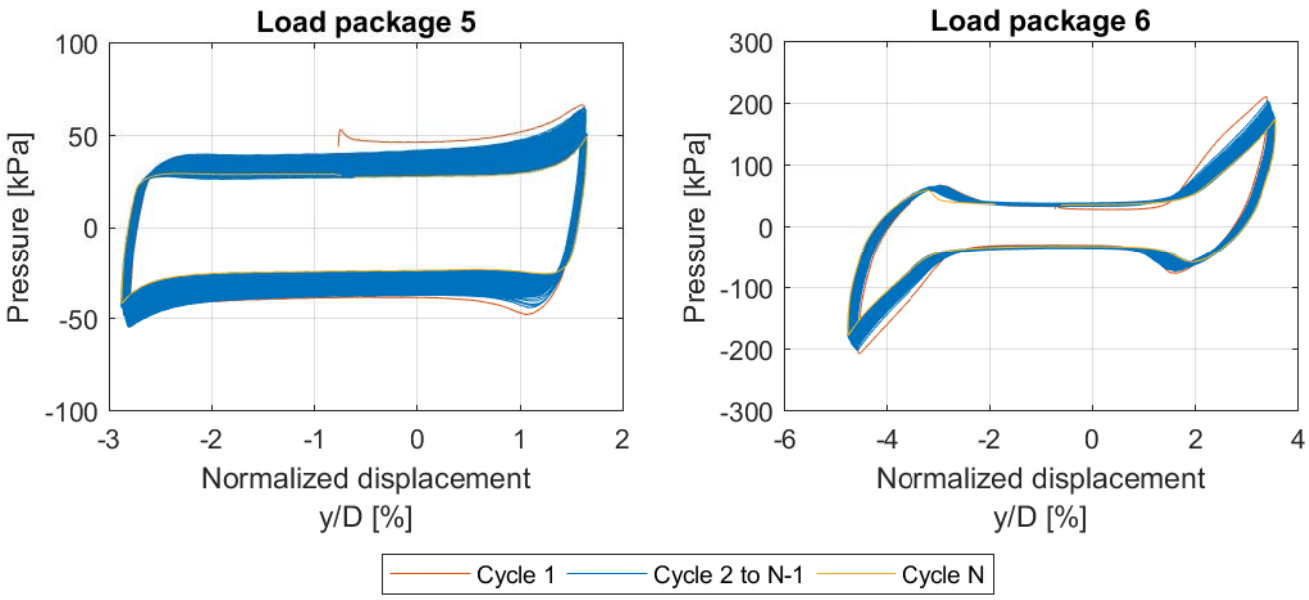
Load package 5
Pressure [kPa]
100
50
0
-50
-100
-3
-2
-1
0
1
2
Normalized displacement
y/D [%]
Load package 6
Pressure [kPa]
300
200
100
0
-100
-200
-300
-6
-4
-2
0
2
4
Normalized displacement
y/D [%]
Cycle 1
Cycle 2 to N-1
Cycle N

Test D2

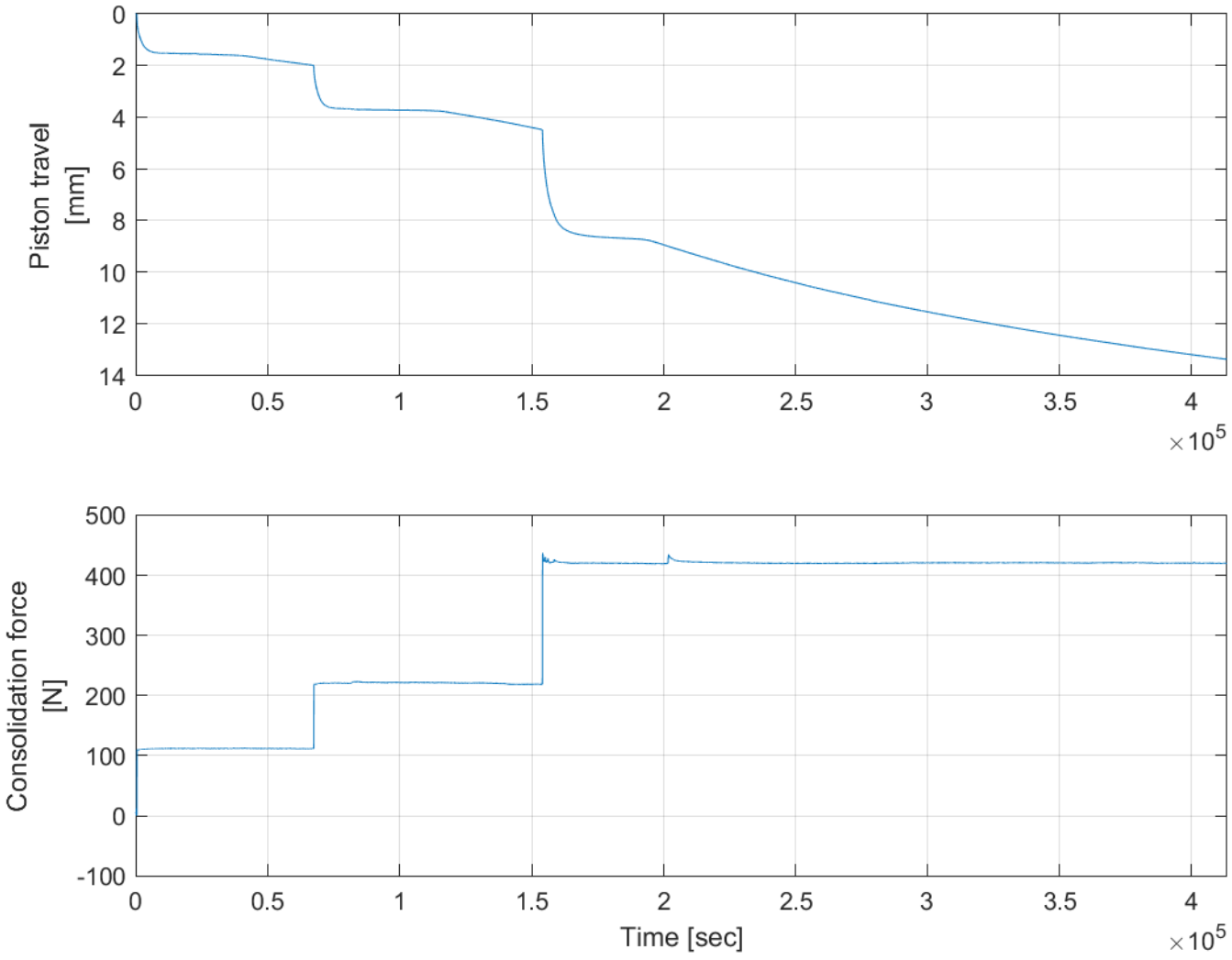

Test D3, part 1

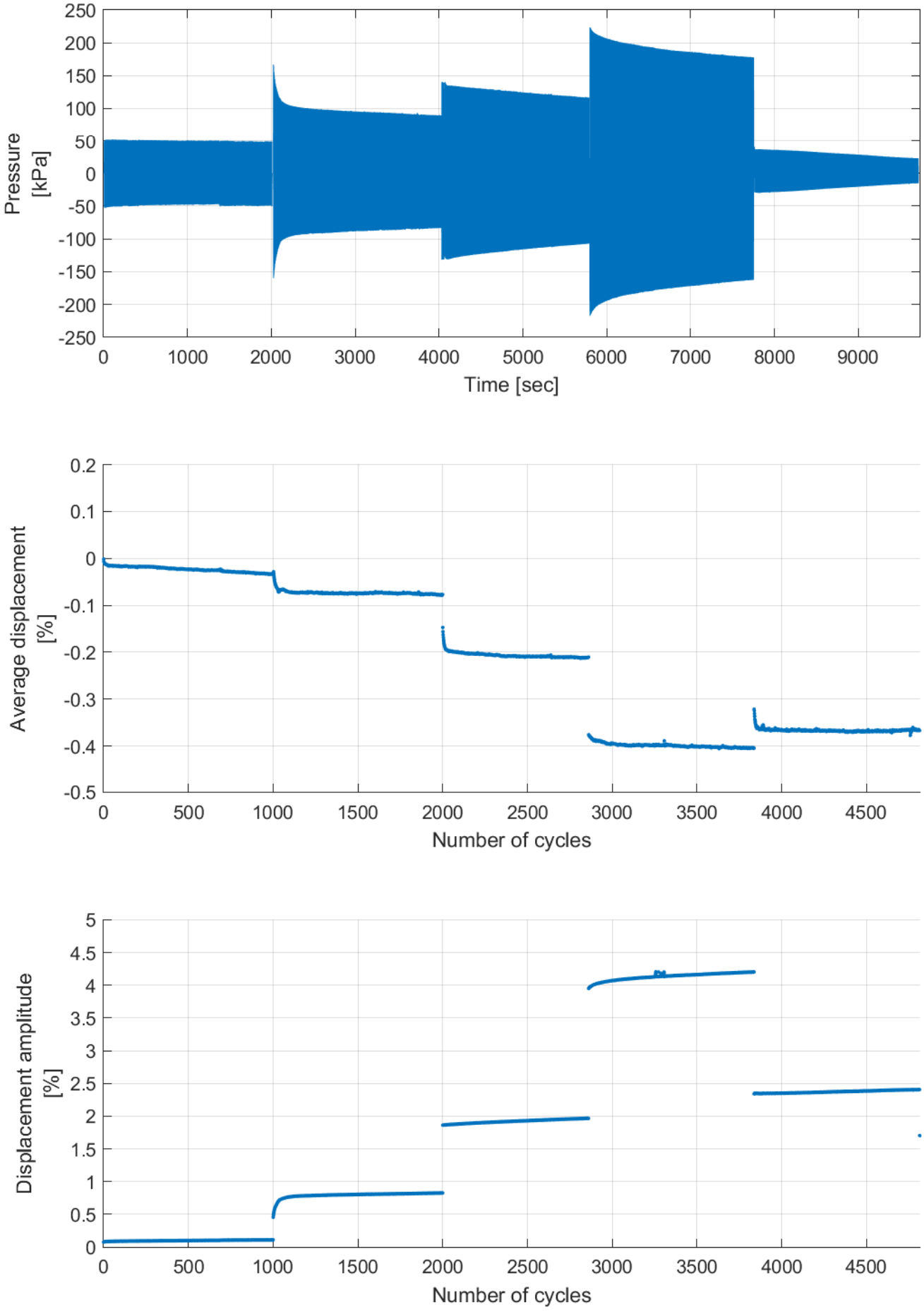

Test D3, part 1

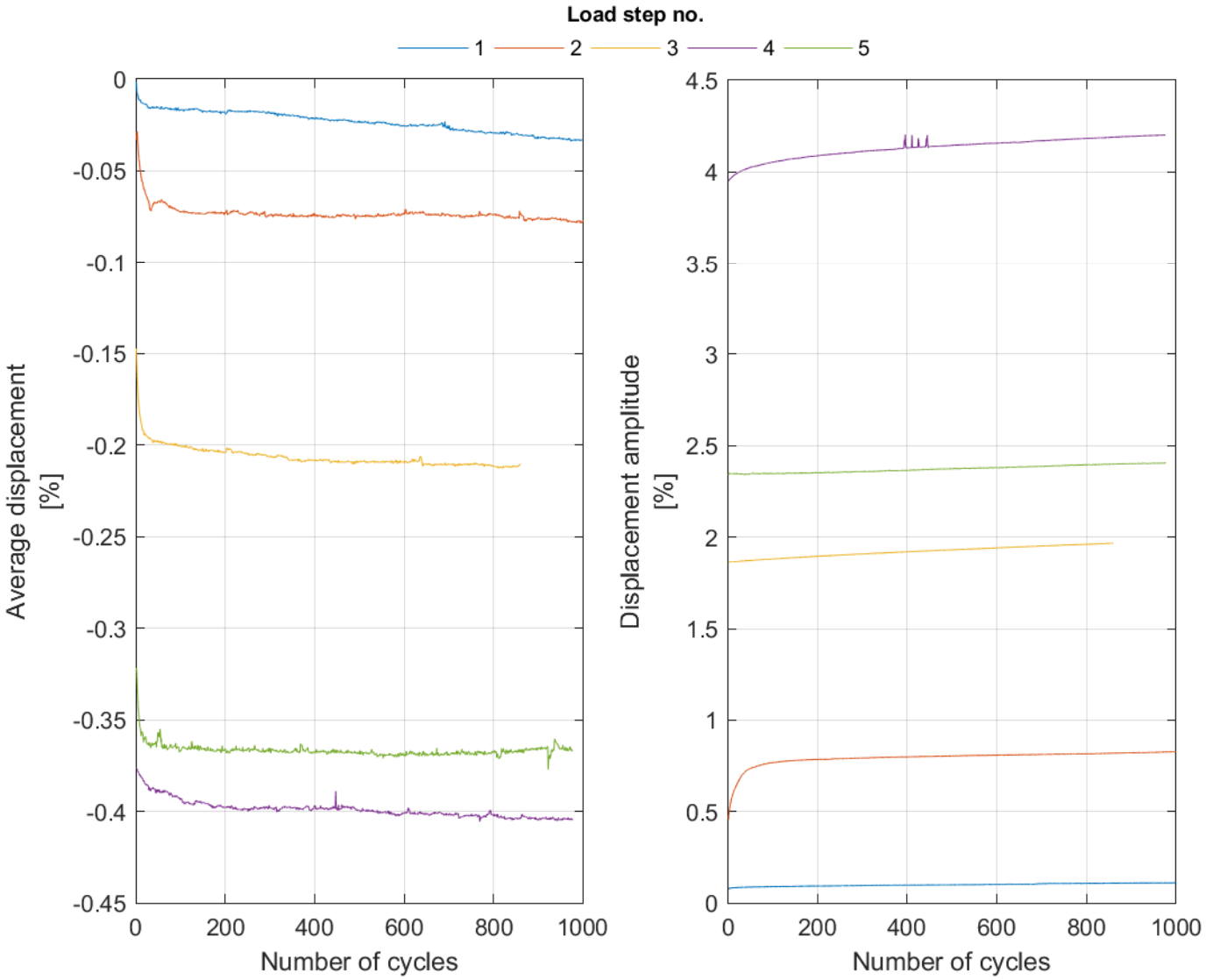

Test D3, part 1

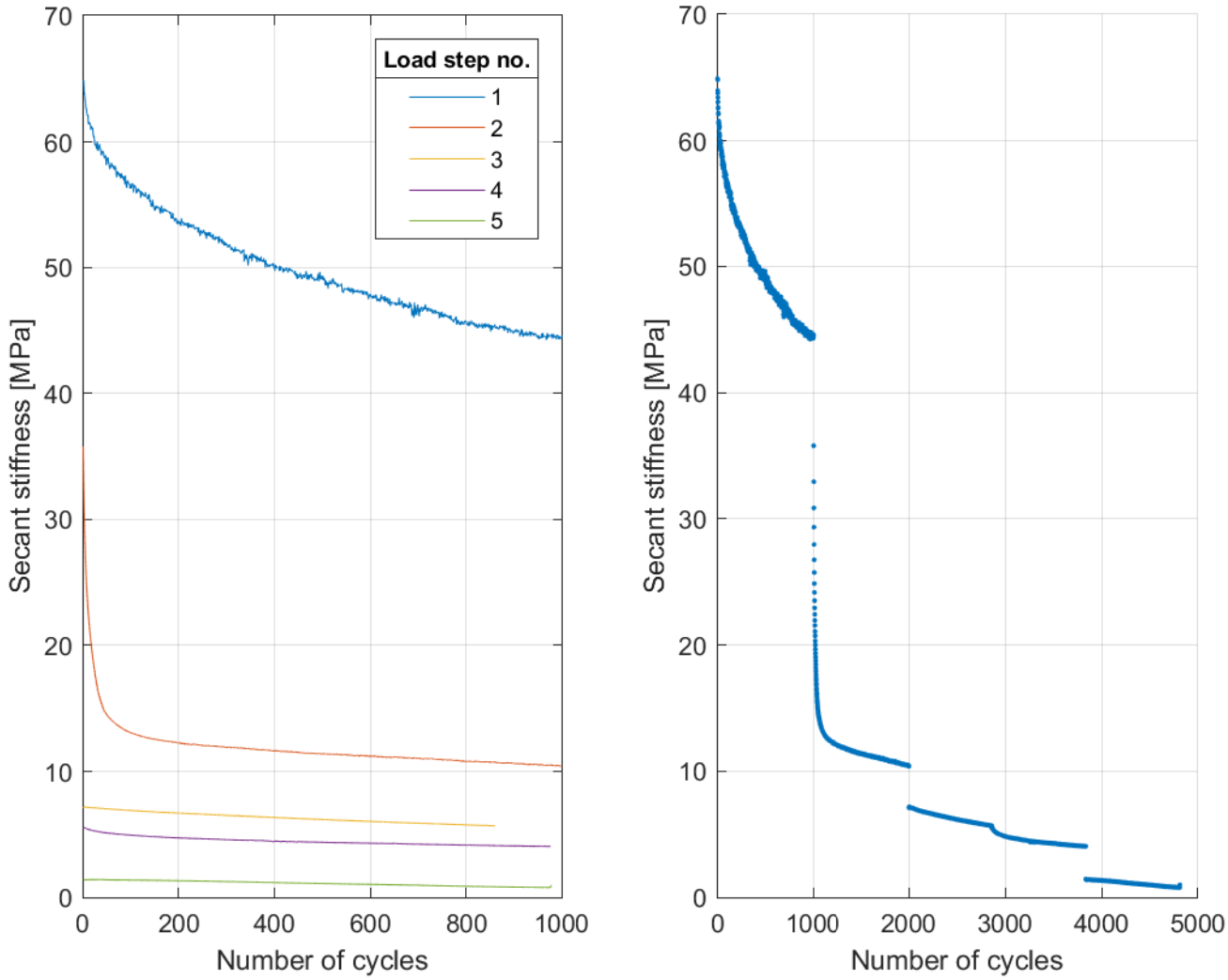

Test D3, part 1

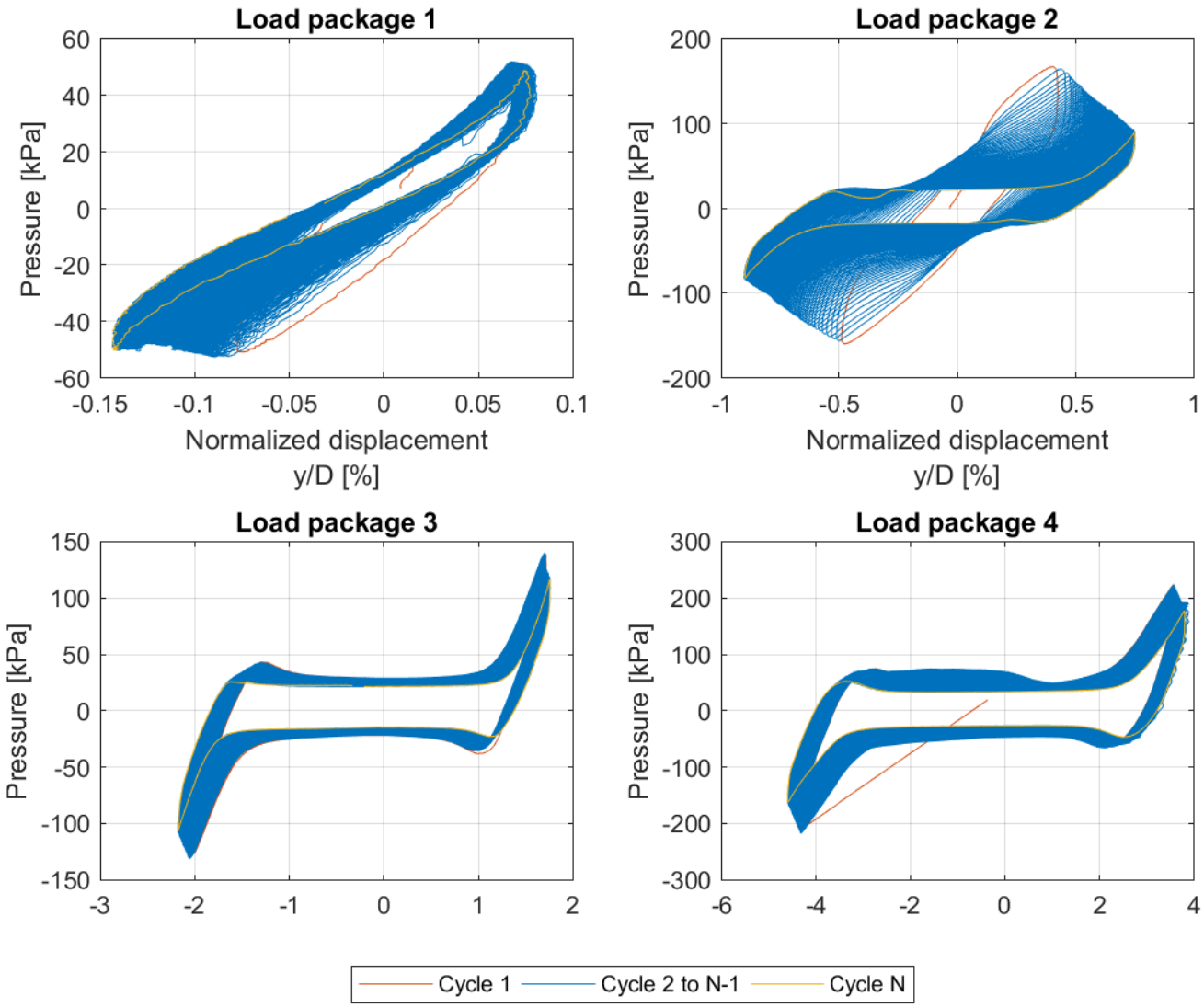

Test D3, part 1

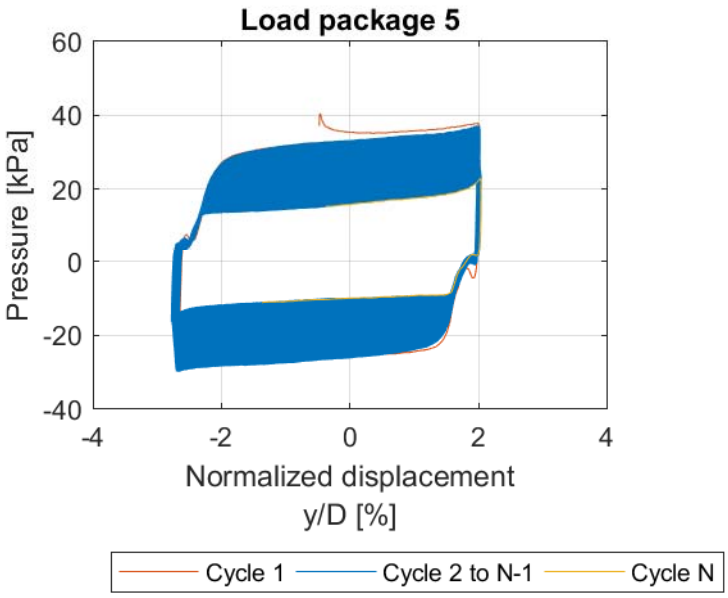

Test D3, part 1

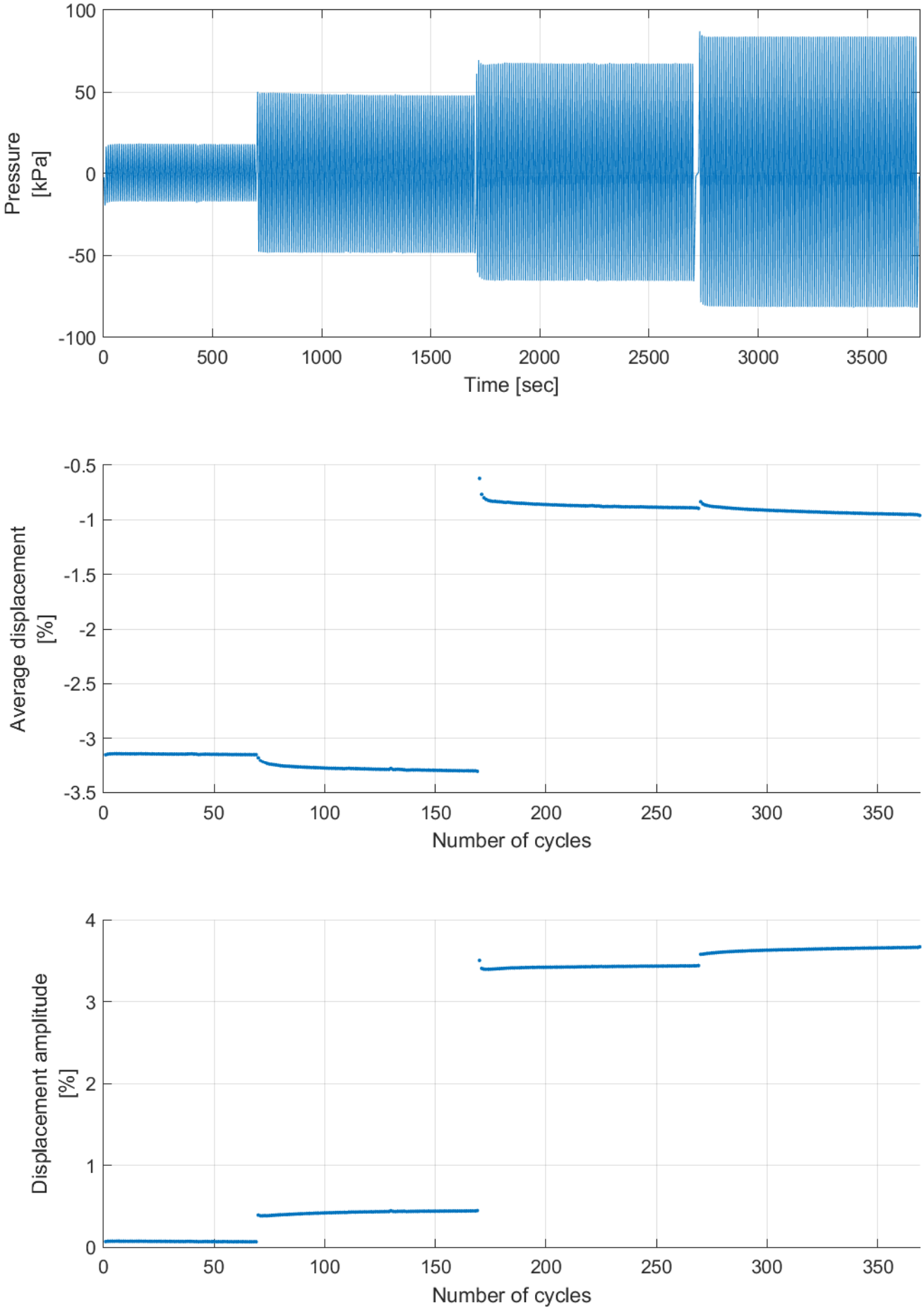

Test D3, part 2

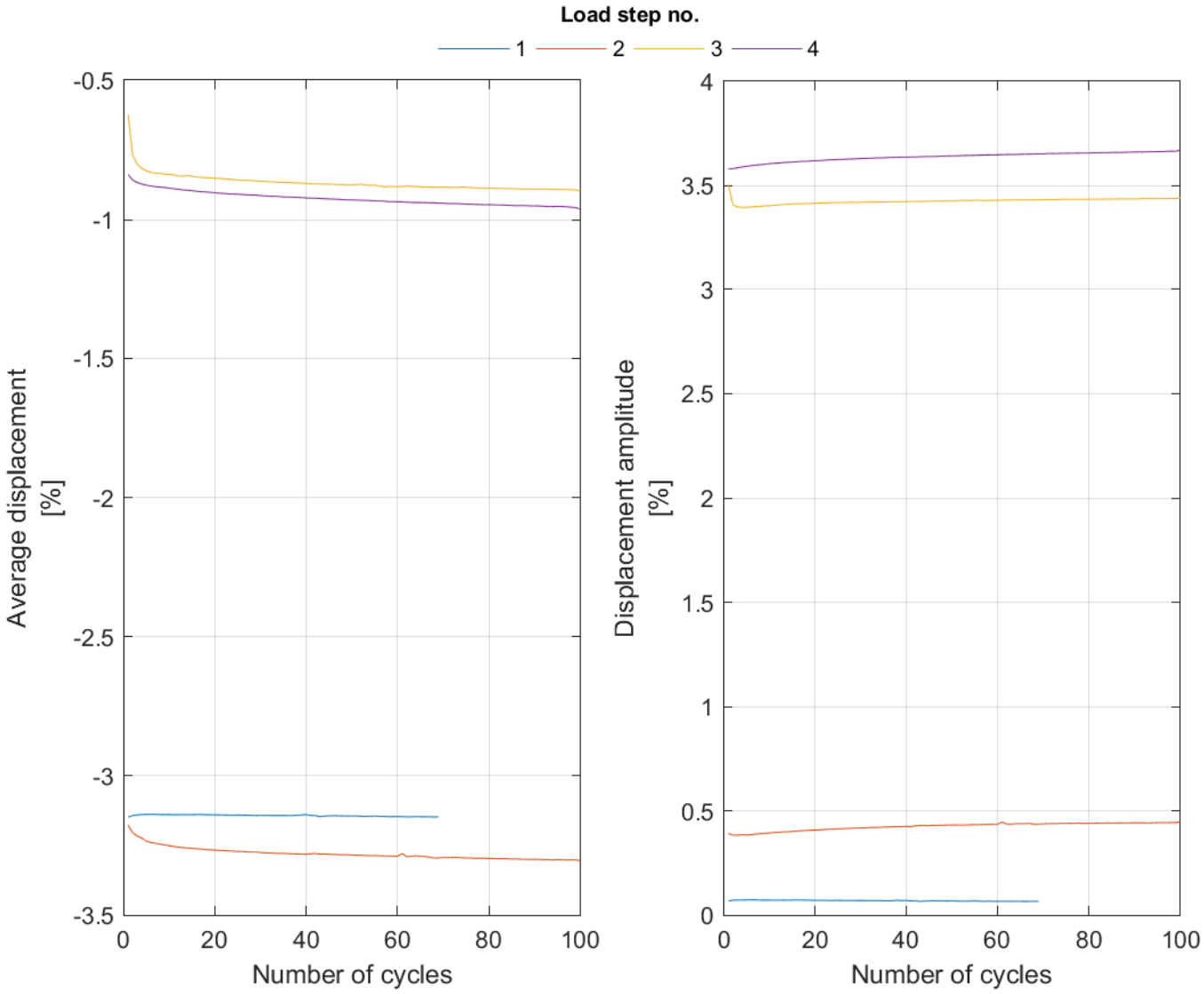

Test D3, part 2

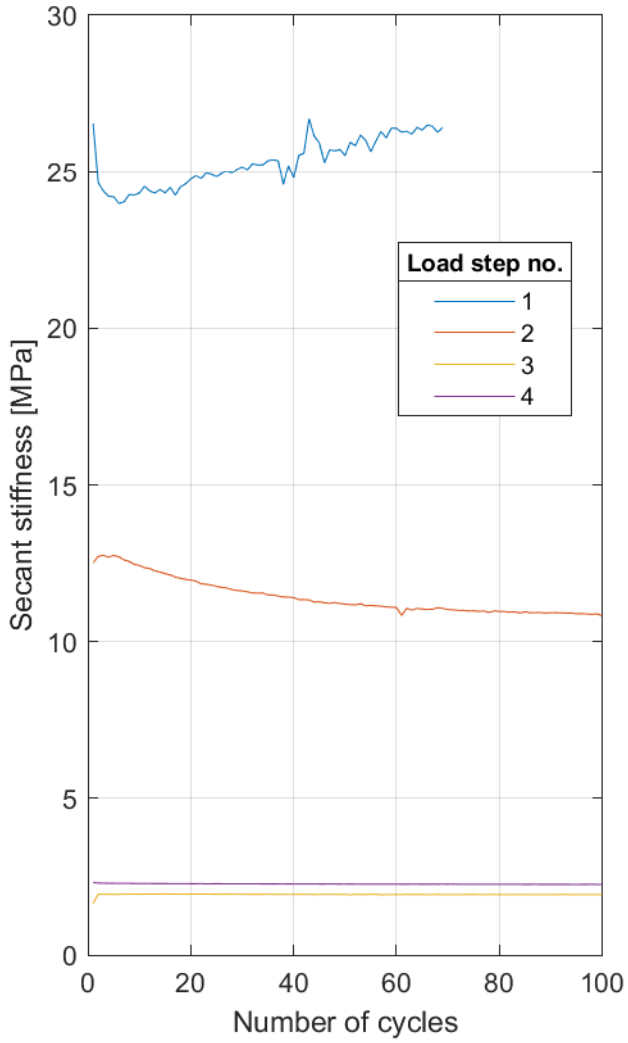

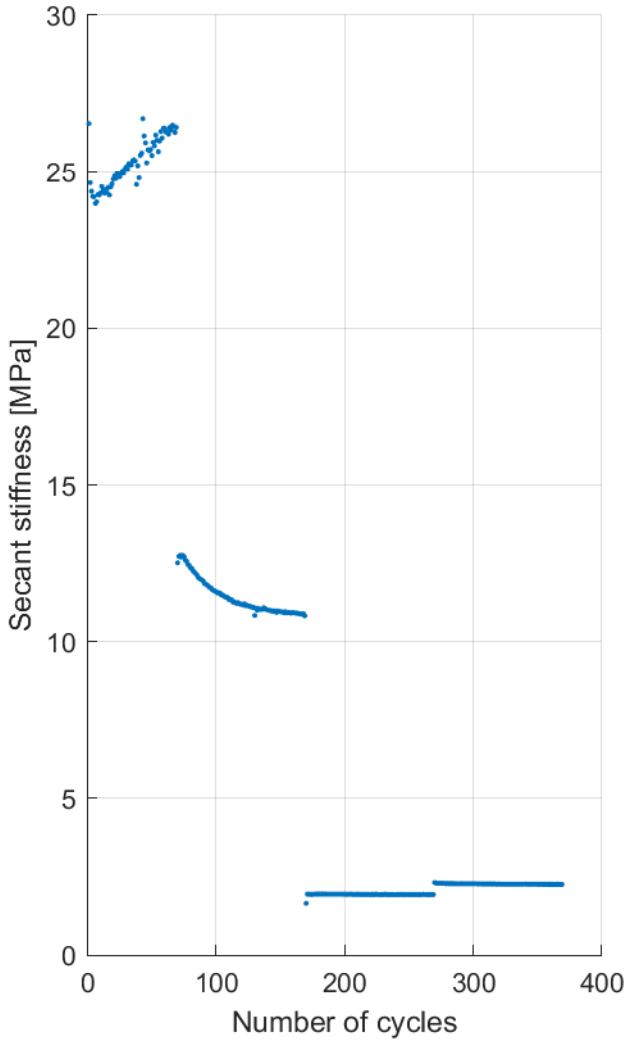

Test D3, part 2

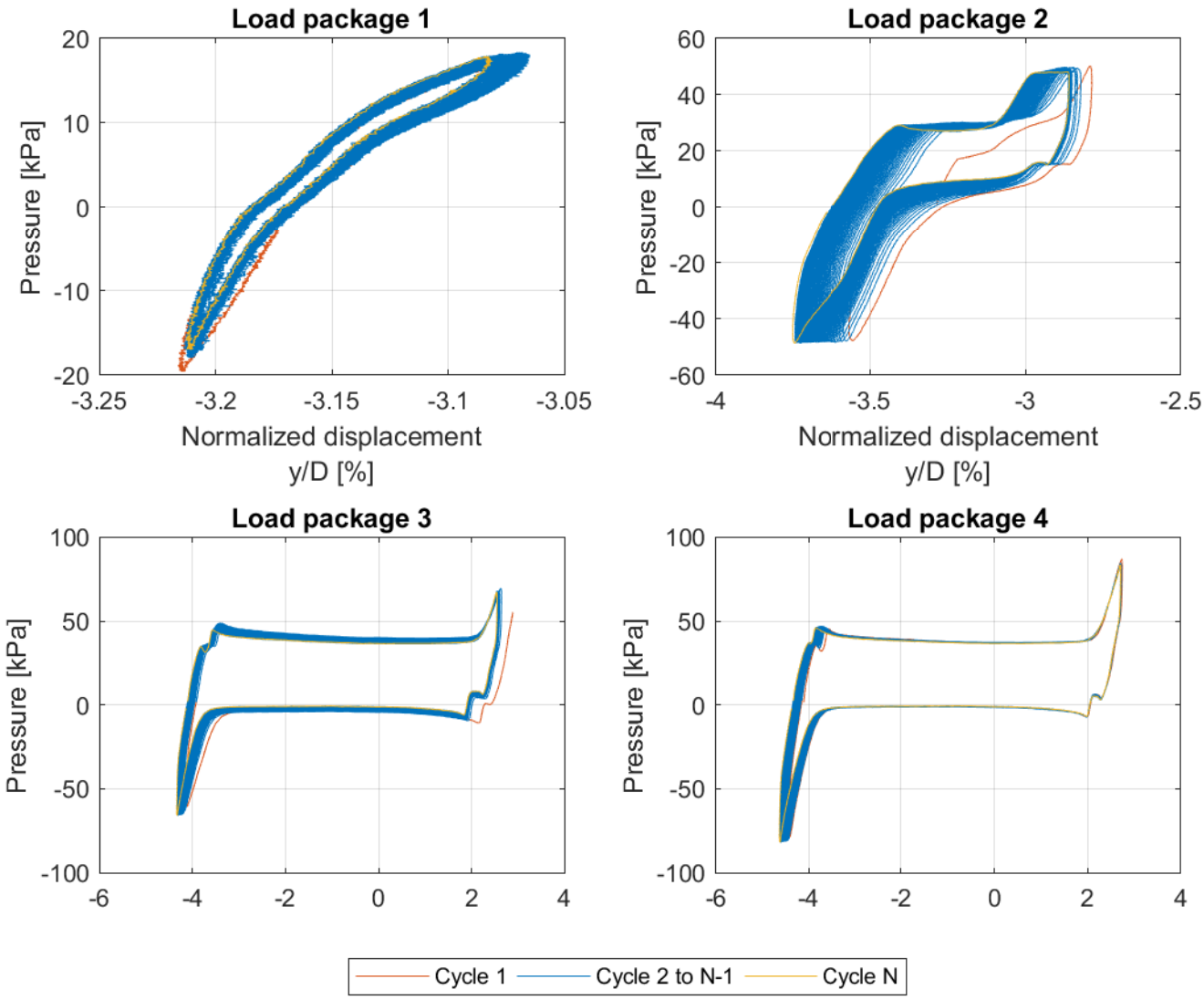

Test D3, part 2

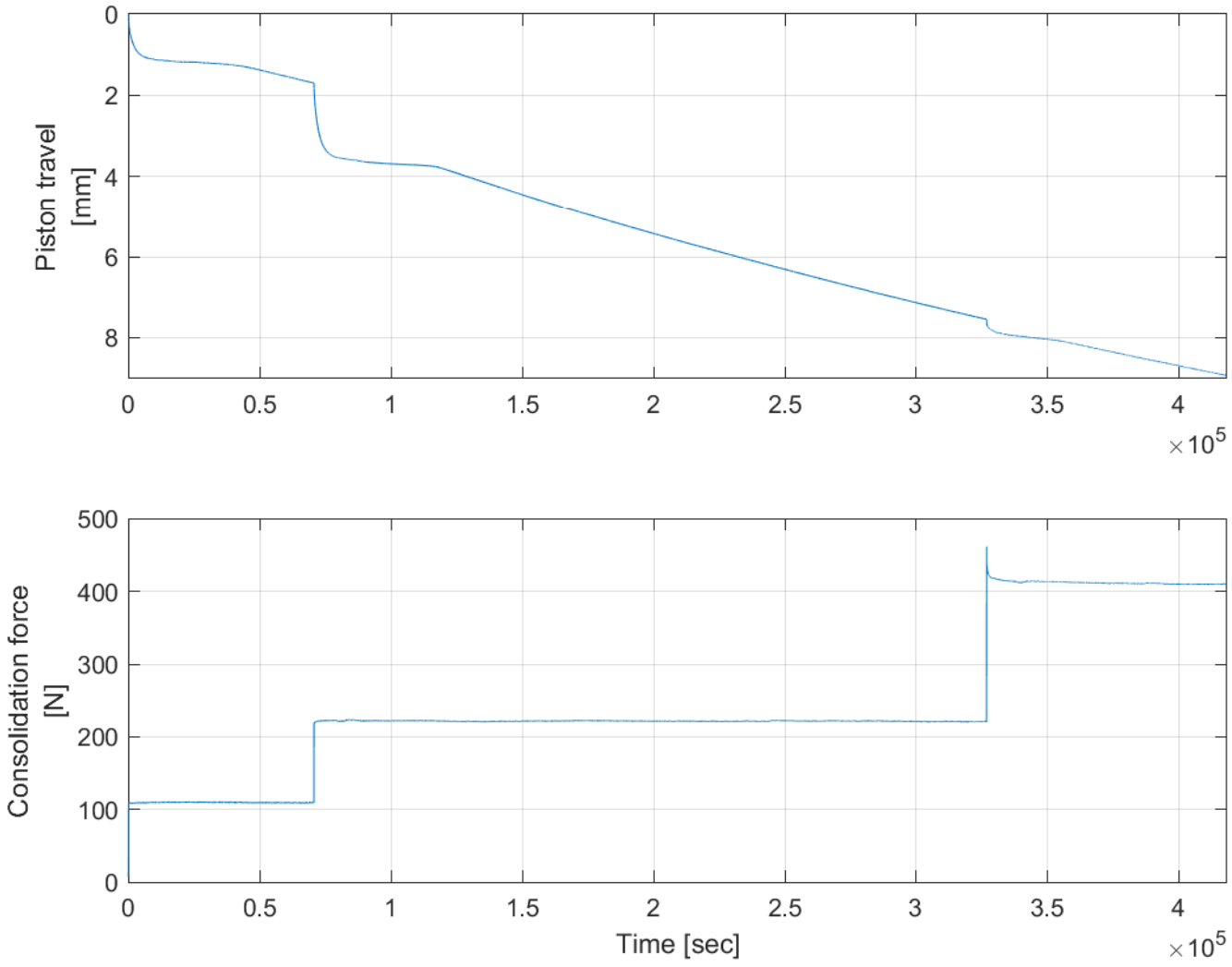
Piston travel [mm]
0
2
4
6
8
0
0.5
1
1.5
2
2.5
3
3.5
4
×10^5
Consolidation force [N]
500
400
300
200
100
0
Time [sec]

Test D4

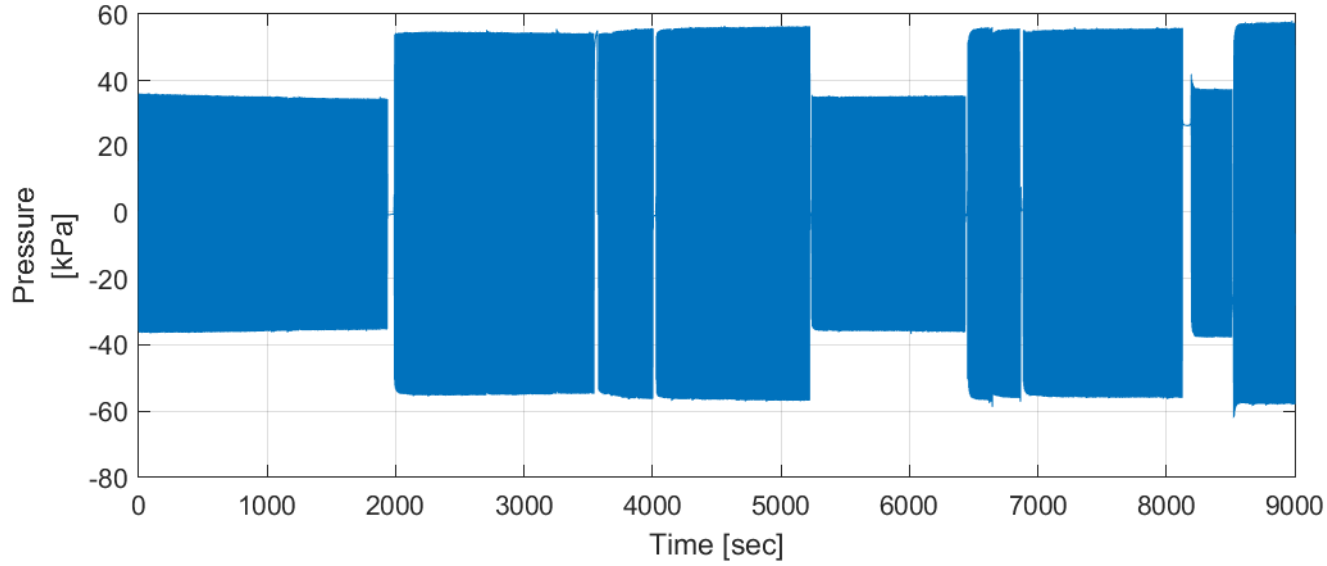
Pressure [kPa]
60
40
20
0
-20
-40
-60
-80
0
1000
2000
3000
4000
5000
6000
7000
8000
9000
Time [sec]

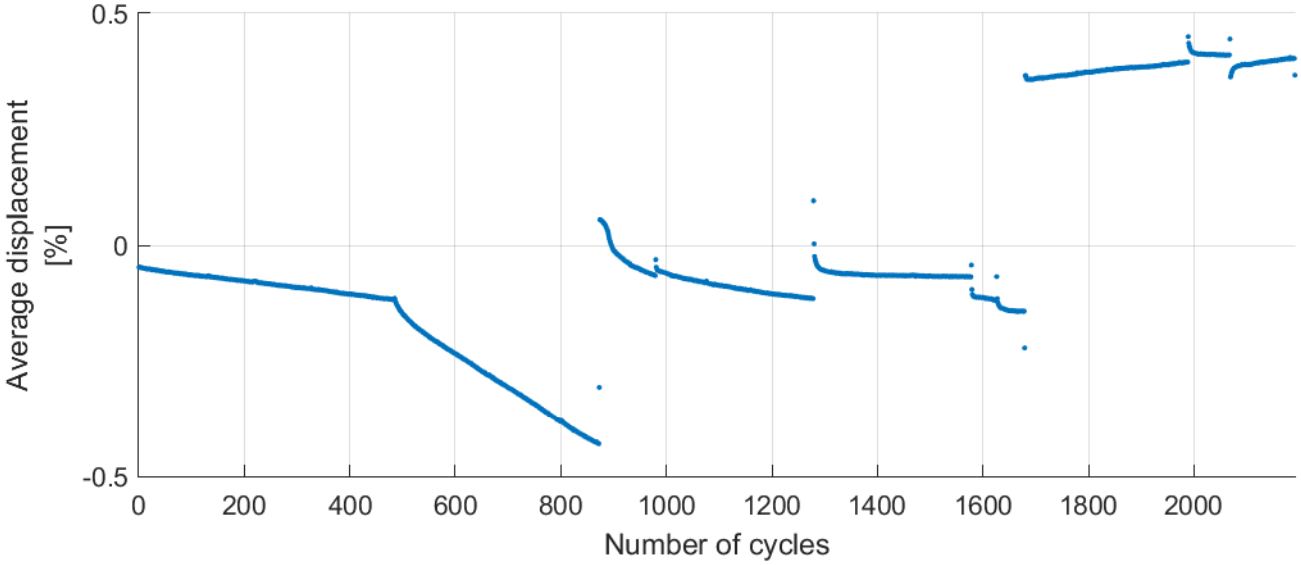
Average displacement [%]
0.5
0
-0.5
0
200
400
600
800
1000
1200
1400
1600
1800
2000
Number of cycles

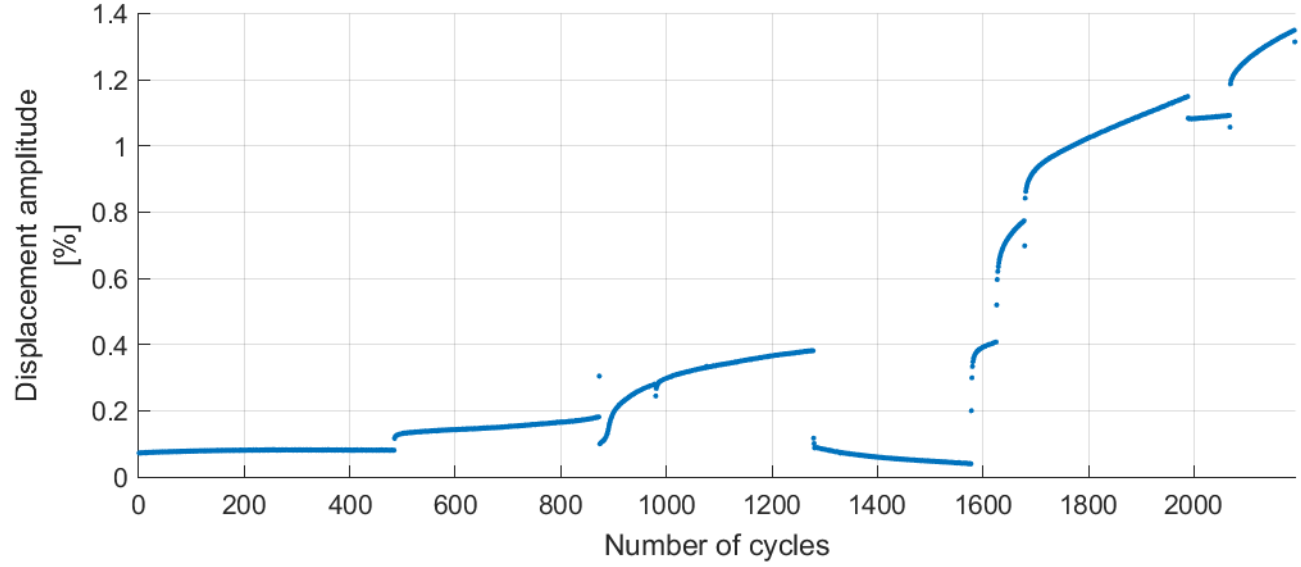
Displacement amplitude [%]
1.4
1.2
1
0.8
0.6
0.4
0.2
0
0
200
400
600
800
1000
1200
1400
1600
1800
2000
Number of cycles

Test D4

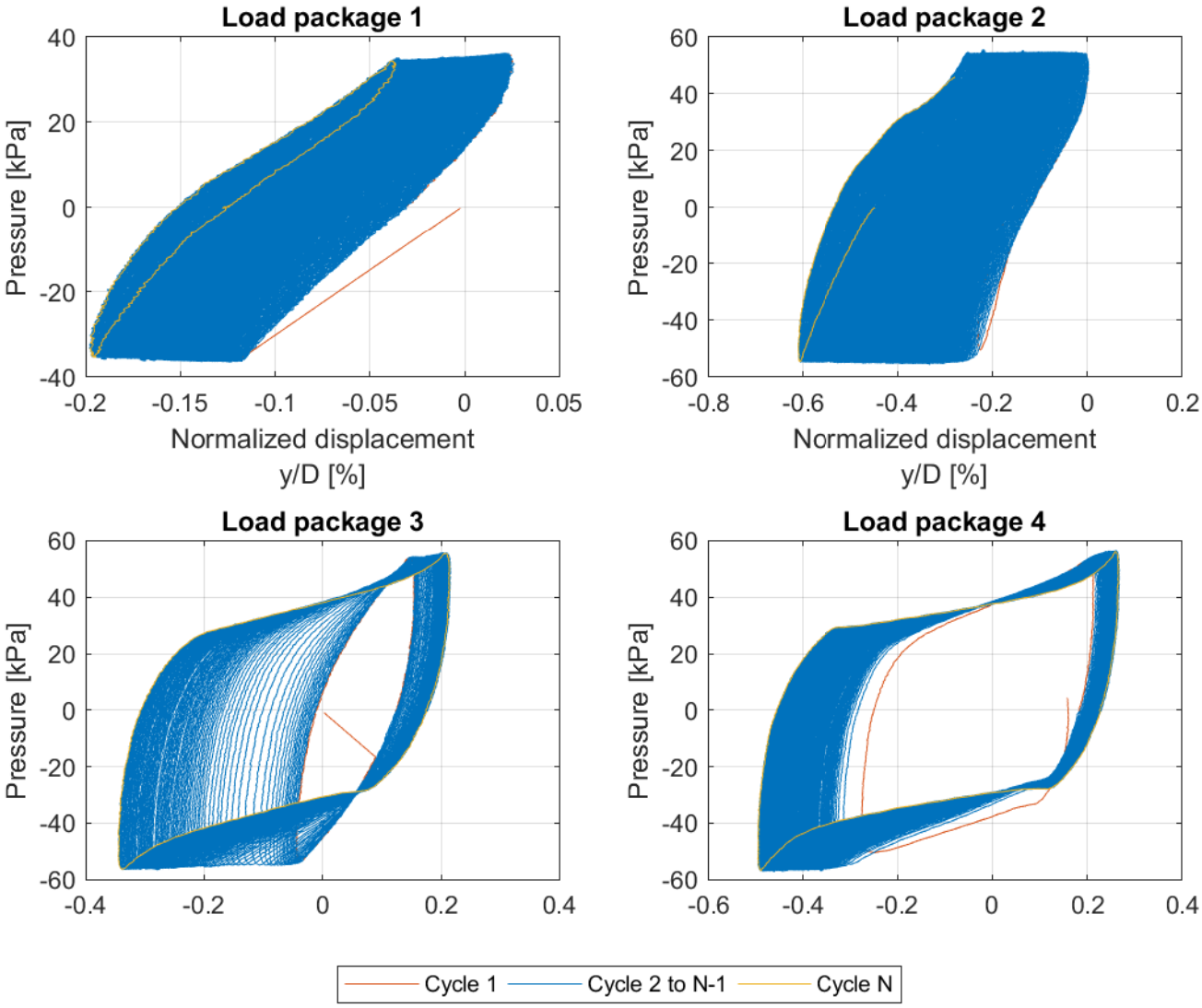
Load package 1
Pressure [kPa]
Normalized displacement
y/D [%]
Load package 2
Pressure [kPa]
Normalized displacement
y/D [%]
Load package 3
Pressure [kPa]
Load package 4
Pressure [kPa]
Cycle 1
Cycle 2 to N-1
Cycle N

Test D4

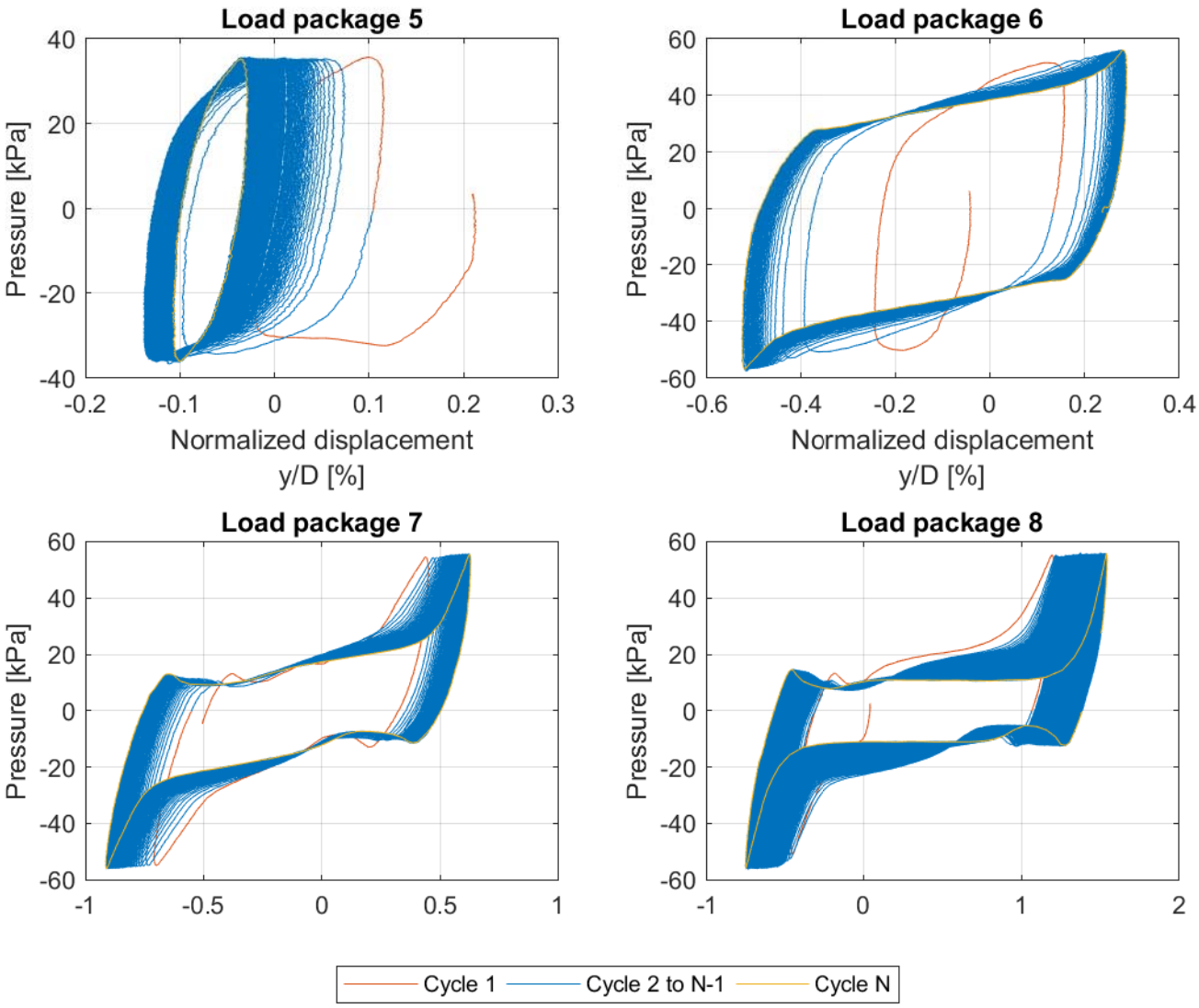
Load package 5
Load package 6
Load package 7
Load package 8
Pressure [kPa]
Normalized displacement
y/D [%]
Cycle 1
Cycle 2 to N-1
Cycle N

Test D4

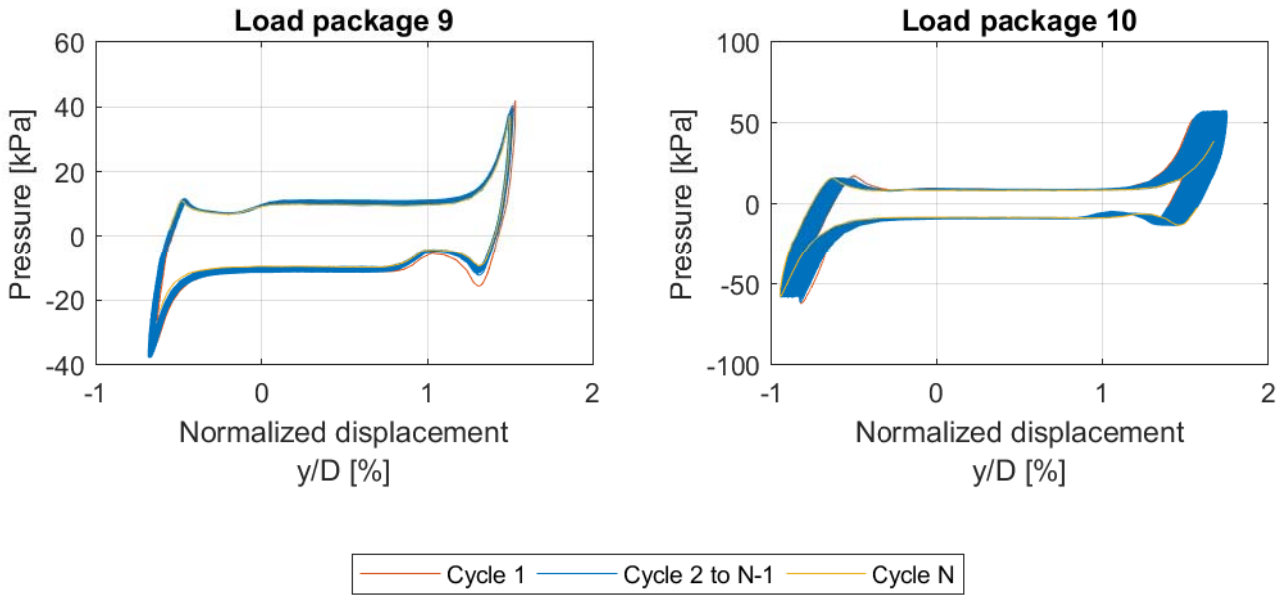
Load package 9
Pressure [kPa]
60
40
20
0
-20
-40
-1
0
1
2
Normalized displacement
y/D [%]
Load package 10
Pressure [kPa]
100
50
0
-50
-100
-1
0
1
2
Normalized displacement
y/D [%]
Cycle 1
Cycle 2 to N-1
Cycle N

Test D4

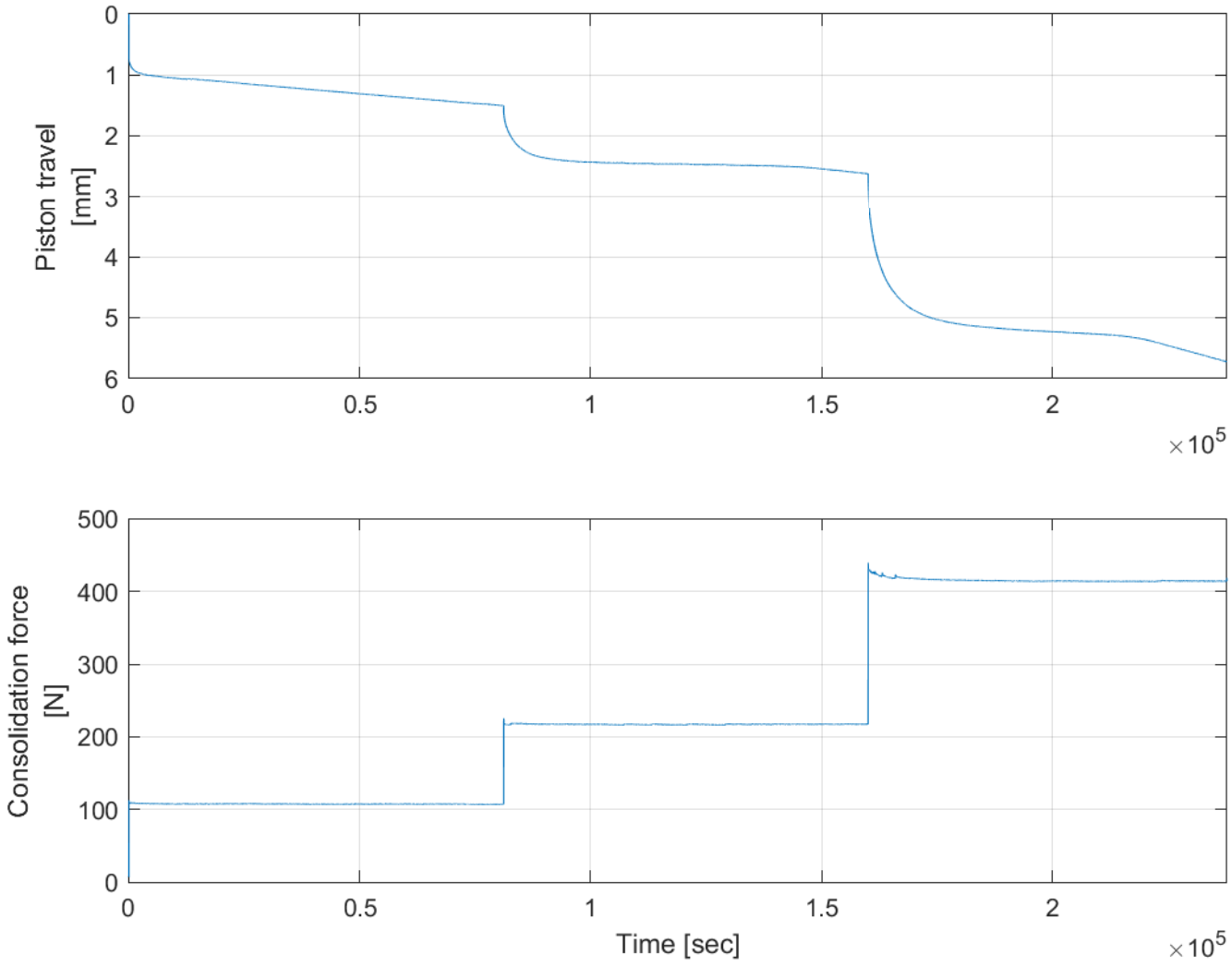
Piston travel [mm]
0
1
2
3
4
5
6
0
0.5
1
1.5
2
×10^5
Consolidation force [N]
500
400
300
200
100
0
0
0.5
1
1.5
2
Time [sec]
×10^5

Test D5

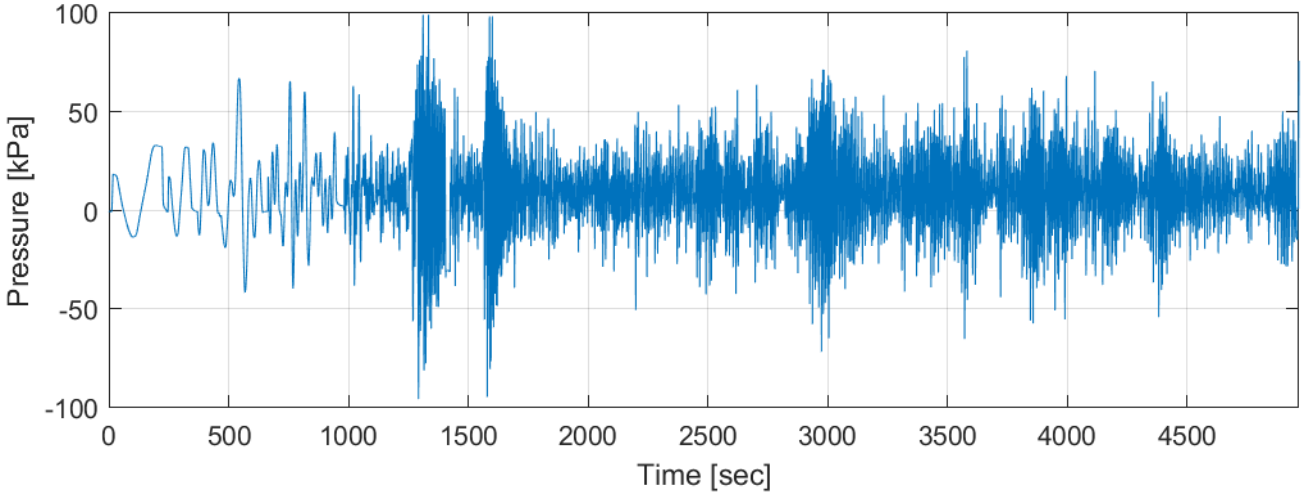

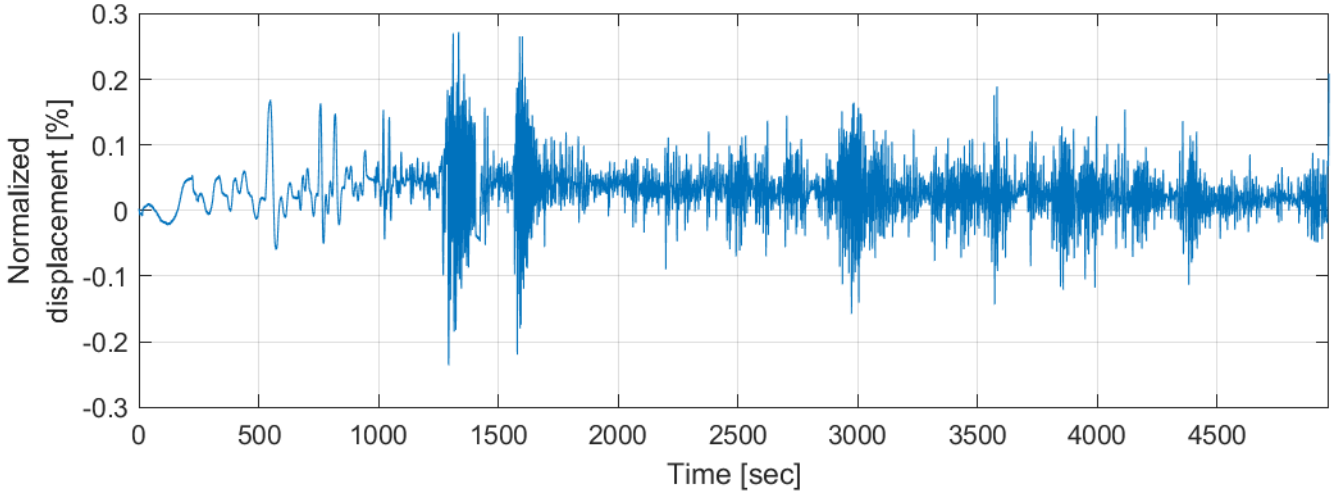

Load history 1 Test D5

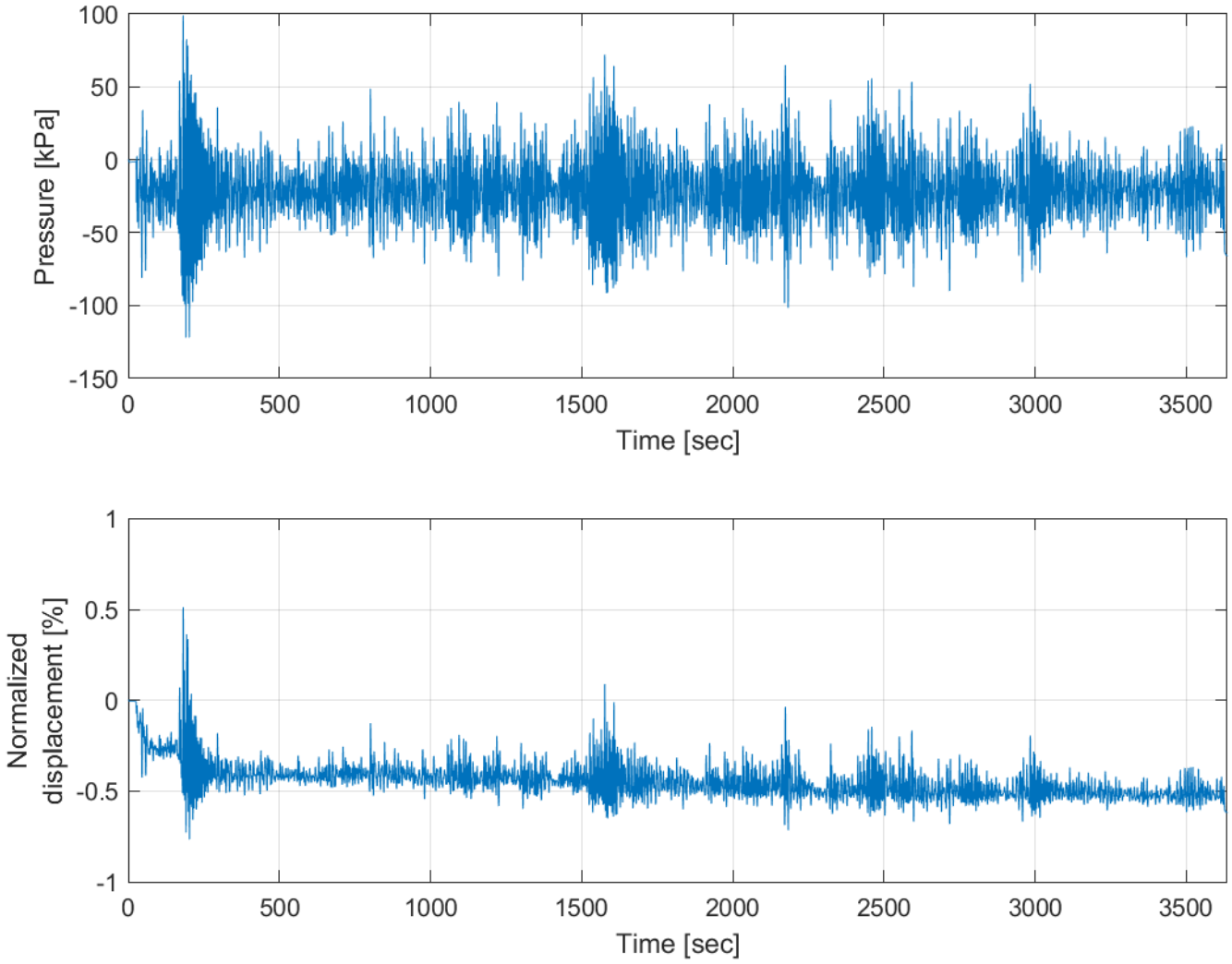

Load history 2 Test D5

Appendix C

Samples after testing

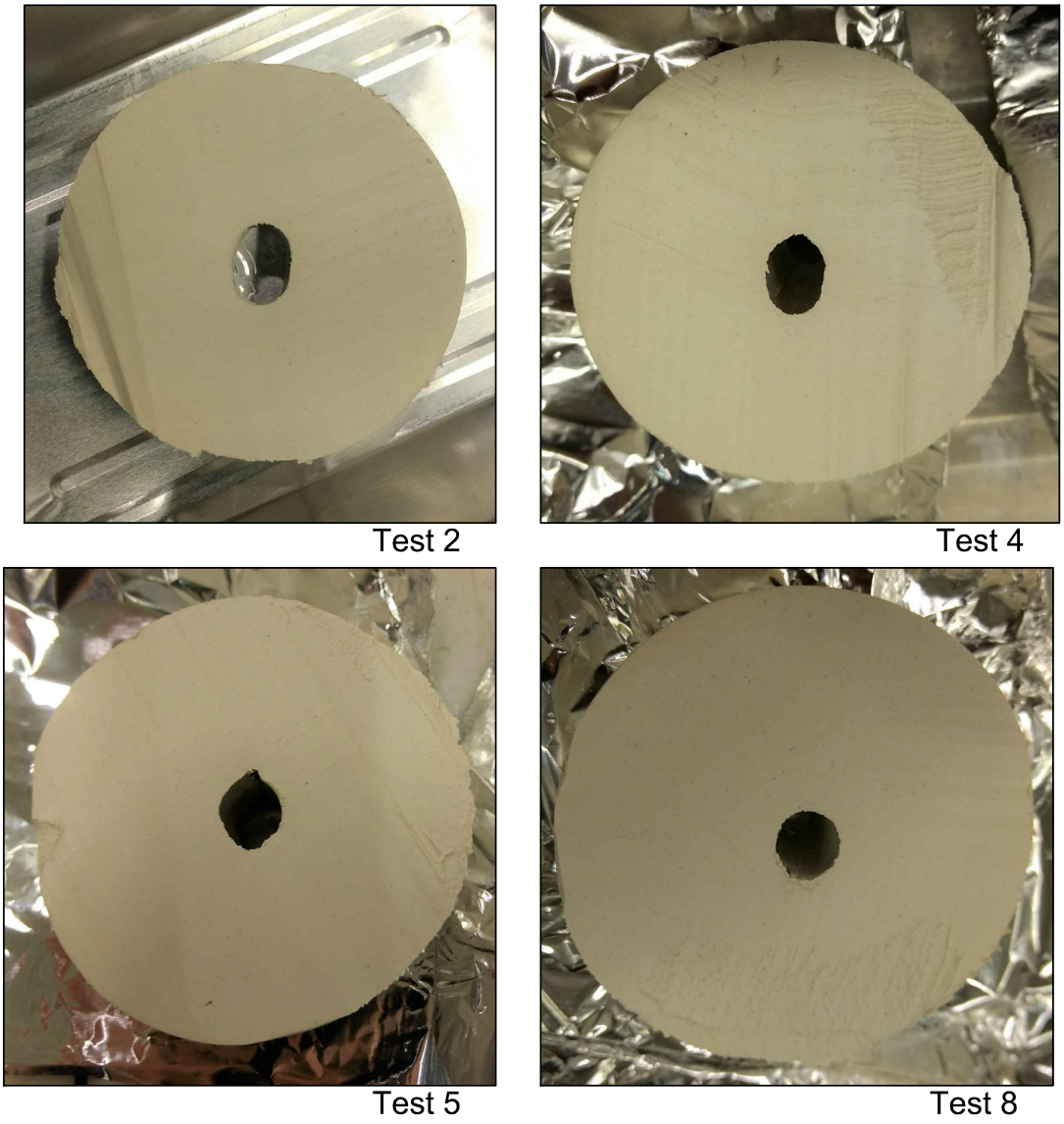

Figure C.1: Kaolin samples after testing

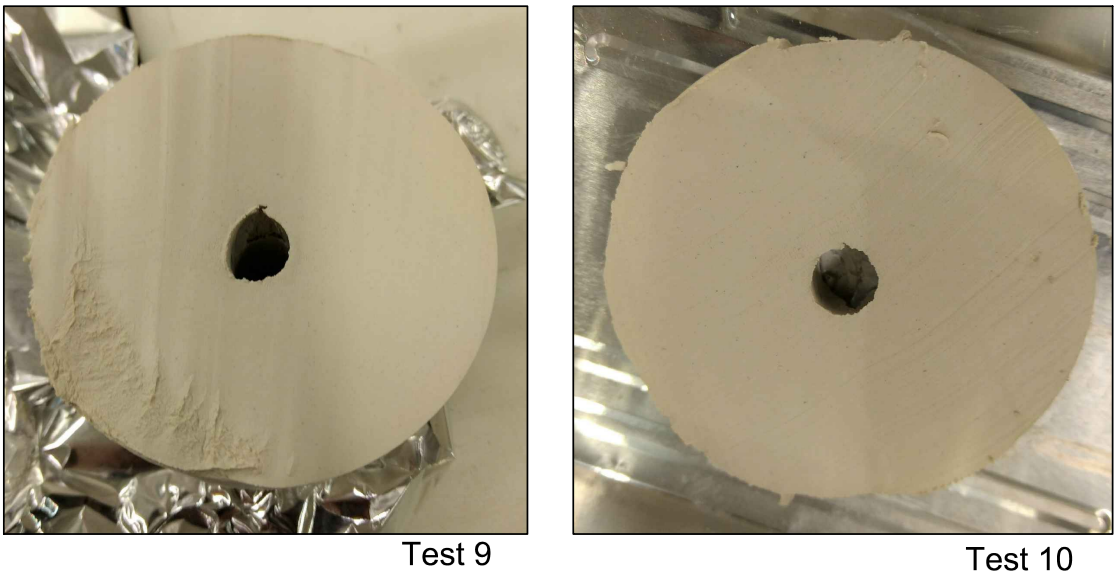

Figure C.2: Kaolin samples after testing

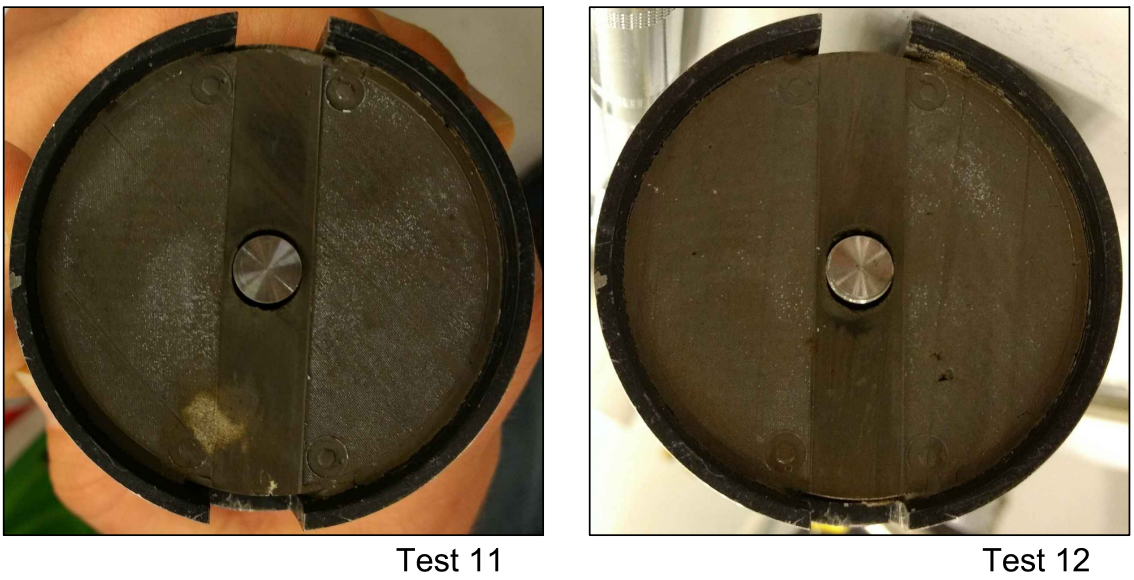

Figure C.3: North Sea samples after testing

Appendix D

Consolidation and water content

Table D.1: Consolidation and water content after testing

Test	Height before consolidation [mm]	Piston travel [mm]	Part	Water content [%]
	Kaolin samples			
1	102	4.1	Left Mid Right	44.7 46.2 42.8
2	100	5.5	Left Mid Right	42.8 44.0 42.0
3	101	4.7	Left Mid Right	44.7 45.8 43.1
4	102	4.7	Left Mid Right	44.0 45.3 42.6
5	101	4.9	Left Mid Right	44.1 45.6 44.1
6	102	4.4	Left Mid Right	44.6 46.0 43.9
7	100	3.9	Left Mid Right	44.8 46.6 44.1
8	101	5.1	Left Mid Right	43.7 45.7 44.6
9	102	5.4	Left Mid Right	44.3 45.3 42.0
			Left	43.1

10	100	6.9	Mid	44.1
			Right	42.5
	North Sea samples			
			Left	20.0
11	100	1.9	Mid	20.3
			Right	20.9
			Left	23.3
12	100	2.3	Mid	20.6
			Right	19.8

Appendix E

Contour diagrams

Contour diagrams of Prestige-NY kaolin clay consolidated to 125 kPa constructed from DSS test results reported by Carotenuto et al. (2018).

γ_{cy} = 0 - 0.05 - 0.1 - 0.25 - 0.5 - 1.0 - 2.5 - 15 %

γ_{a} = 0 - 0.1 - 0.25 - 0.5 - 1.0 - 2.5 - 5.0 - 15 %

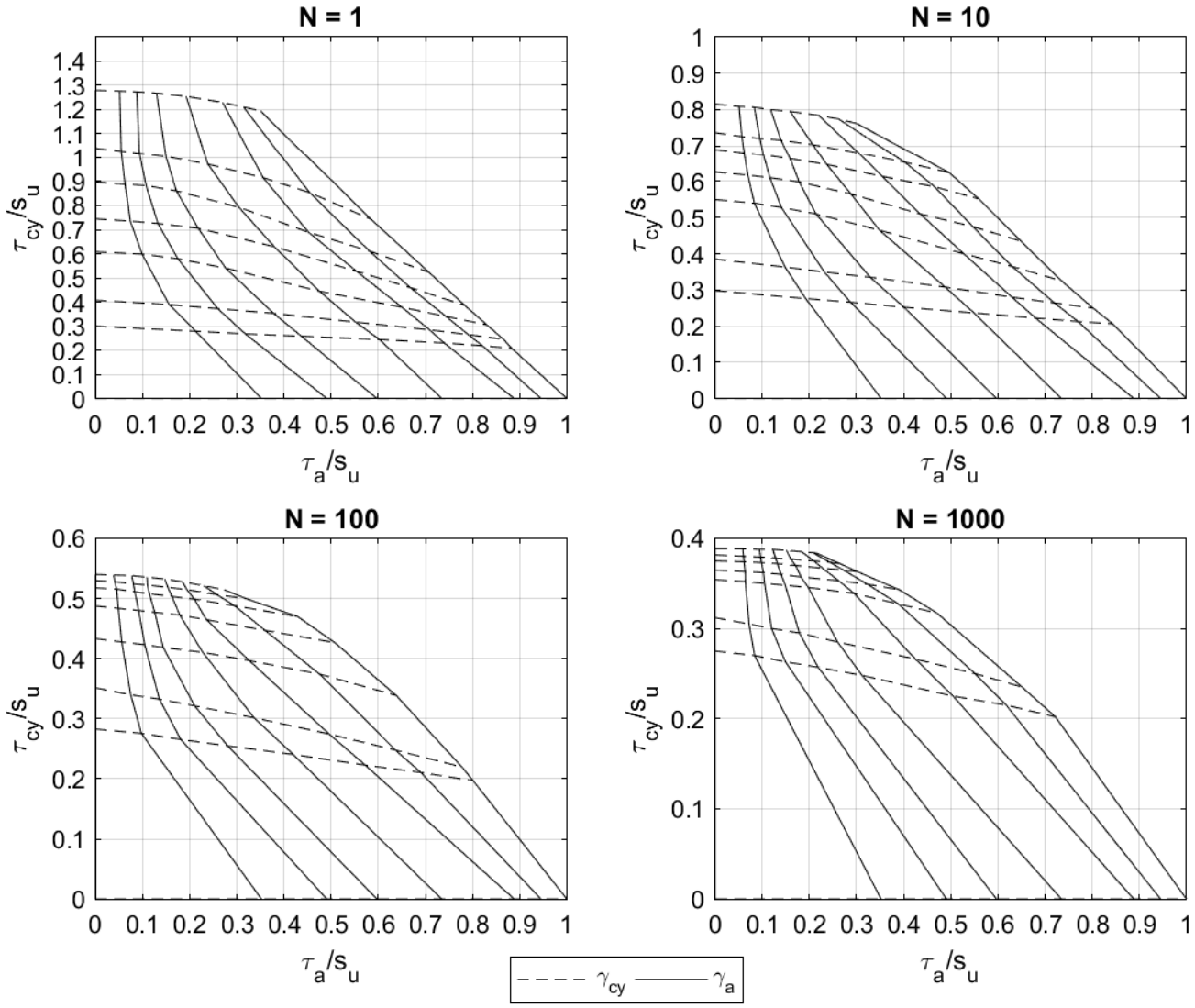
N = 1
N = 10
N = 100
N = 1000
τ_{cy}/s_u
τ_a/s_u
γ_{cy}
γ_a

Appendix F

Preparation and consolidation of reconstituted kaolin clay

The material used in this study is reconstituted Prestige-NY kaolin clay. The material was prepared and consolidated similar to the kaolin material used in a research project at NGI in 2015, to have access to material data and results from former laboratory tests. Index properties are presented in Table F.1.

Table F.1: Index properties (Carotenuto et al., 2018)

Specific density	ρ_s	$[g/cm^3]$	2.59
Clay content		[%]	55.7
Grain size distribution	D_{60}	[mm]	0.003
Plastic limit	w_p	[%]	28.0
Liquid limit	w_l	[%]	56.1
Plasticity index	I_p	[%]	28.1

F.1 Preparation procedure

Kaolin clay was reconstituted in the laboratory and preconsolidated to 80 kPa before divided into test samples to be used for model testing. The material was made in two batches and consolidated in two separate consolidation boxes. The amount was increased in the second batch to make sure the end height of the samples were sufficient. The amounts of natural mass and de-aired water is given in Table F.2. Natural mass denotes the clay powder which consists of 70% kaolinite, 22% quartz and 8% nordstrandite (Carotenuto et al., 2018).

Water and kaolin powder were mixed together manually into a slurry. The water content of

Table F.2: Kaolin clay

		Batch 1	Batch 2
Total natural mass	[g]	15 007	20 010
Water mass	[g]	13 867	18 490

the slurry is 92.4%. Next, the slurry was inserted into a concrete mixer and a suction of -0.6 atmosphere was applied before the mixing was continued. Suction was applied to reduce air voids in the slurry. The mixing continued for 16-24 hours until the material was homogeneous. The mixer and slurry is shown in Figure F.1.

Figure F.1: Slurry after mixing is completed (left) and concrete mixer (right)

The consolidation boxes had area 27x27 cm^2 and 15 mm thick side walls. Silicon grease was spread on all contact surfaces before the boxes were mounted to avoid leakage. Filters allowing drainage were placed under and over the slurry, and four drainage tubes were installed to transport water away from the bottom of the box. The material was carefully transferred into the box and any visible air voids were removed during the process. Next, the box was installed for consolidation. The installation rig with both boxes in place is shown in Figure F.2. A steel plate of thickness 15 mm was placed above the top filter and connected to the load actuator. Vertical load was applied using air pressure and a deformation sensor was applied to monitor the consolidation. Free de-aired water was added above the steel plate to avoid the sample's top surface to dry out. The box before attaching the load actuator is shown in Figure F.3.

Pressure and displacement at the end of each consolidation step are given in Table F.3. Diagrams of consolidation is given in Section F.2. During the consolidation level of 10 kPa for the first batch, there were some problems with leakage. Insufficient amount of silicon grease in

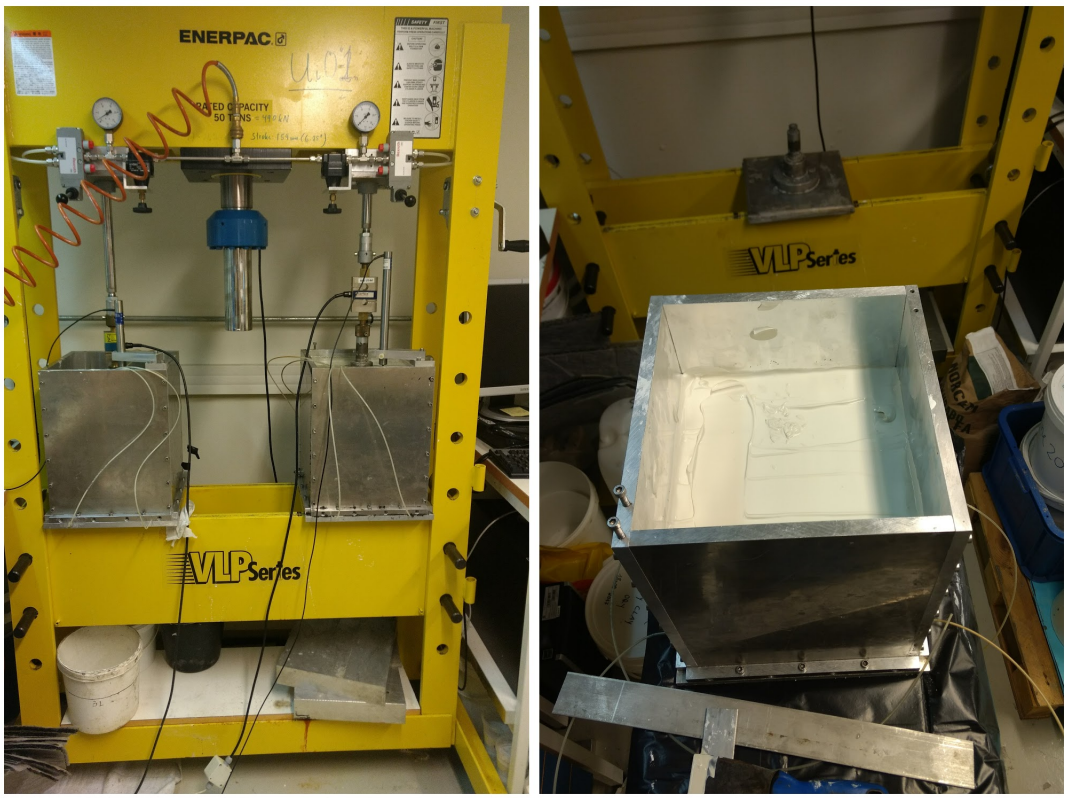

Figure F.2: Consolidation boxes installed (left) and slurry placed in consolidation box (right)

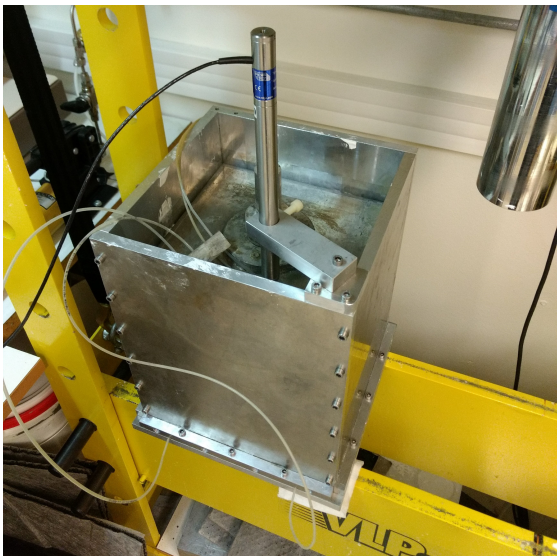

Figure F.3: Consolidation box before attaching the load actuator

the upper part caused water leaking from the sides of the box. As the material consolidated, water did not longer access the upper parts of the box, and the leakage was thus stopped.

After consolidation to 80 kPa was finished, the free water on top was removed and the load rapidly decreased to zero. The top plate and filter were also immidiately removed to avoid swelling. The box was dismounted and the material cut into nine samples of 9x9 cm^2. The

Table F.3: Consolidation

Pressure	Piston travel left box [mm]	Piston travel right box [mm]
0.5 kPa (self weight top plate)	17.70	10.67
10 kPa	69.45	81.14
20 kPa	81.51	99.89
40 kPa	94.29	117.42
80 kPa	105.94	132.90
Initial height	24.5 cm	33.0 cm
Height after consolidation	14.8 cm	21.5 cm

finished consolidated material before and after divided into test samples is shown in Figure F.4. Each sample was placed on a small plastic plate and sealed in two plastic bags. Both plastic bags were tied seperately aiming to remove excess air before sealing. Inside the outer bag there was added some paper soaked in water to preserve humidity. The samples were stored cold.

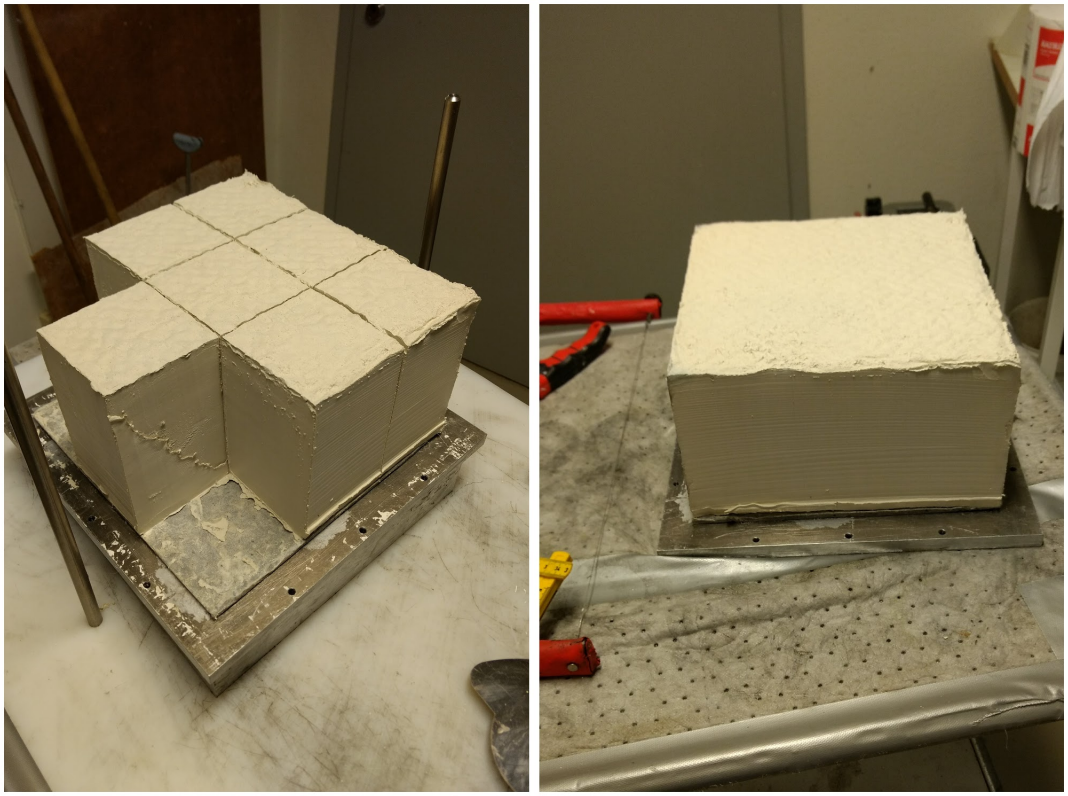

Figure F.4: Finished consolidated kaolin clay

F.2 Consolidation diagrams

Kaolin clay was reproduced as the material used in a research project at NGI in 2015 in order to utilize existing lab results. The clay used in this study was preconsolidated to 80 kPa instead of 50 kPa to simplify the process of building the material into the soil chamber used in the p-y apparatus. Vertical strain at the different consolidation steps is shown in Figure F.5 for the two batches of kaolin and three reference batches. The consolidation curves coincide reasonably well.

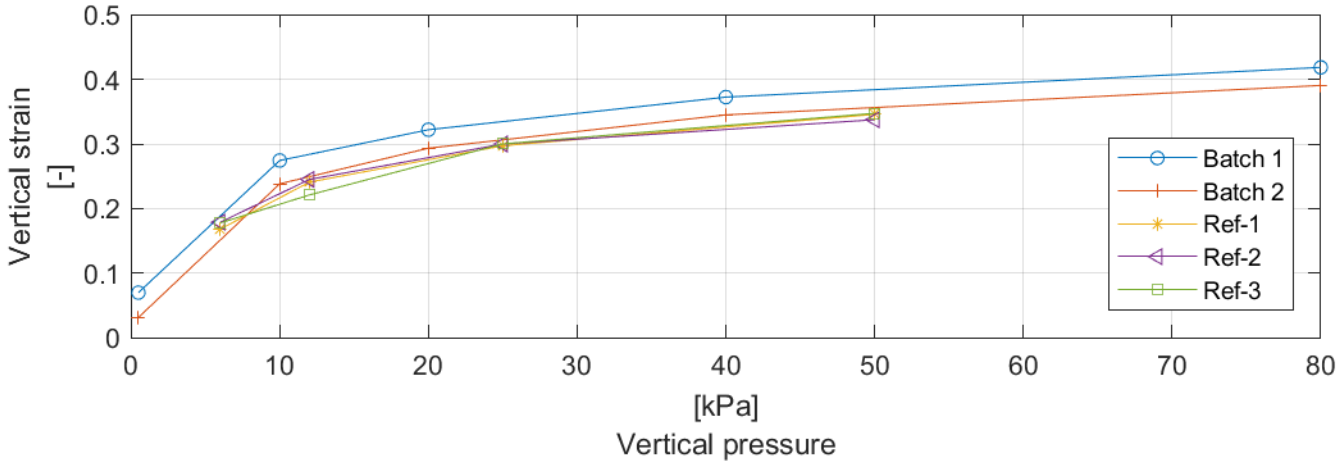

Figure F.5: Consolidation of batch 1 and 2 of kaolin clay compared to kaolin clay used in research project at NGI, denoted ref. 1, 2 and 3.

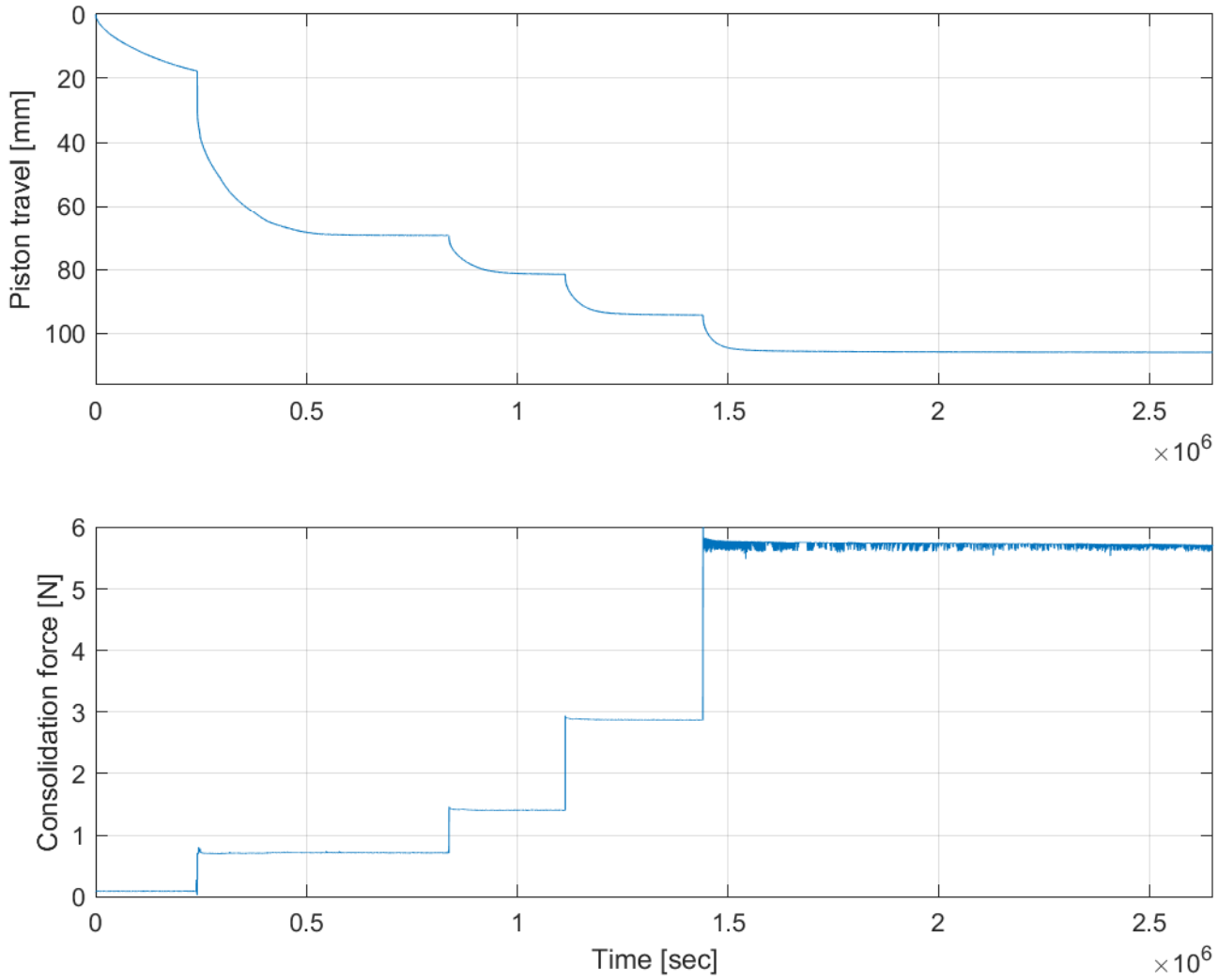
Piston travel [mm]
0
20
40
60
80
100
0
0.5
1
1.5
2
2.5
×10^6
Consolidation force [N]
0
1
2
3
4
5
6
0
0.5
1
1.5
2
2.5
Time [sec]
×10^6

Batch 1

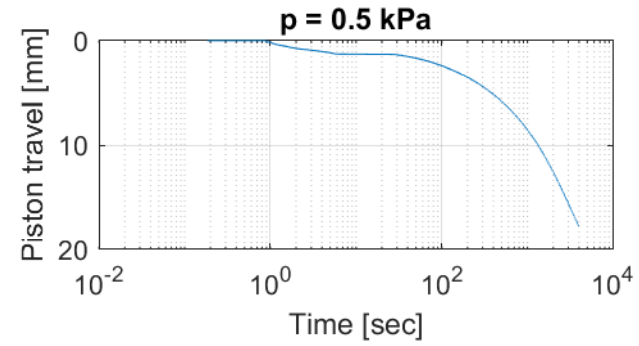
p = 0.5 kPa
Piston travel [mm]
0
10
20
10^{-2}
10^{0}
10^{2}
10^{4}
Time [sec]

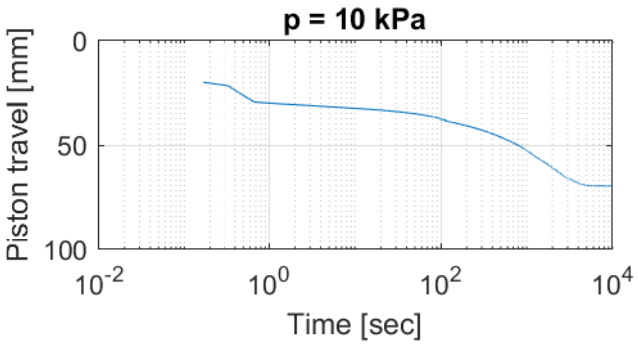
p = 10 kPa
Piston travel [mm]
0
50
100
10^{-2}
10^{0}
10^{2}
10^{4}
Time [sec]

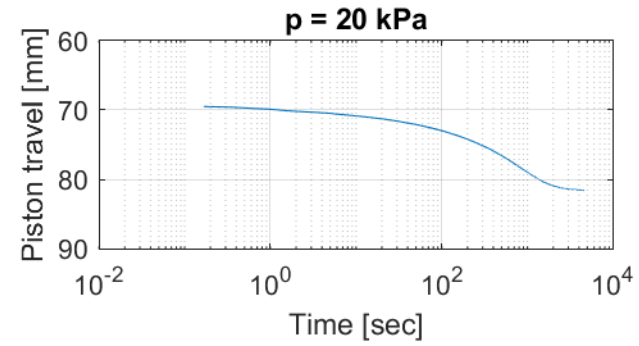
p = 20 kPa
Piston travel [mm]
60
70
80
90
10^{-2}
10^{0}
10^{2}
10^{4}
Time [sec]

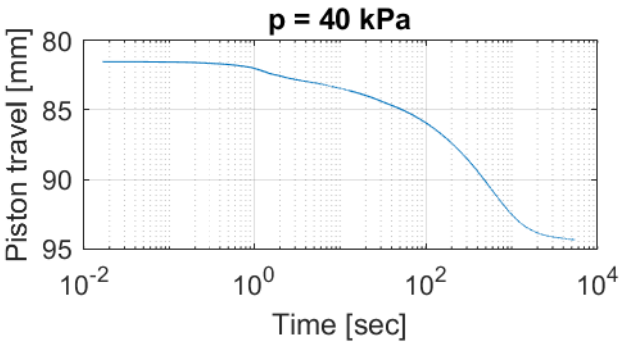
p = 40 kPa
Piston travel [mm]
80
85
90
95
10^{-2}
10^{0}
10^{2}
10^{4}
Time [sec]

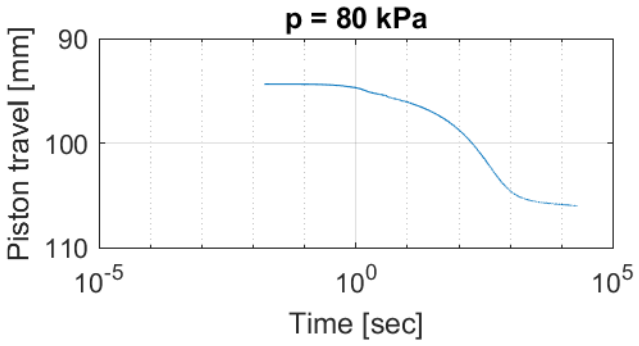
p = 80 kPa
Piston travel [mm]
90
100
110
10^{-5}
10^{0}
10^{5}
Time [sec]

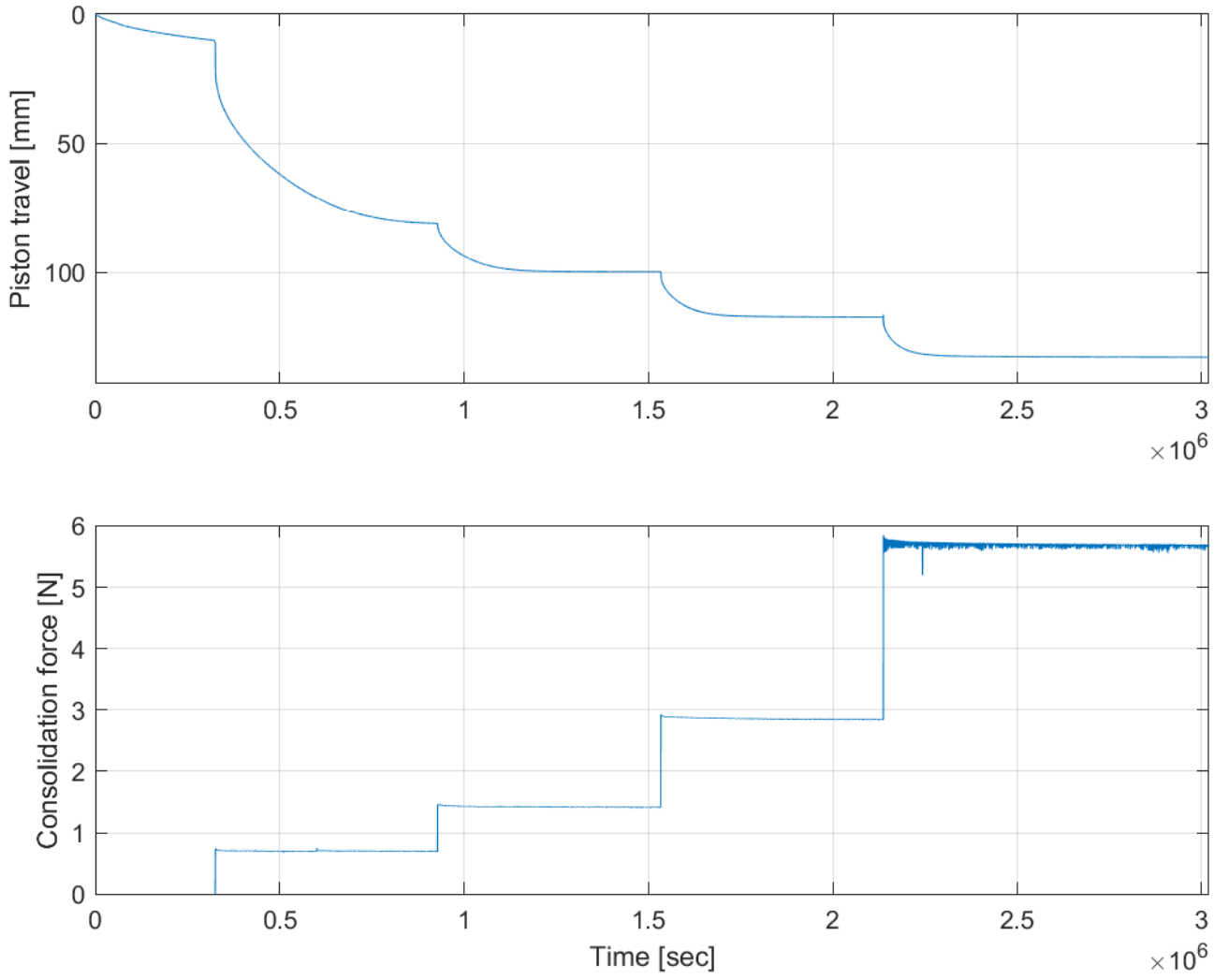
Piston travel [mm]
0
50
100
0
0.5
1
1.5
2
2.5
3
×10^6
Consolidation force [N]
0
1
2
3
4
5
6
0
0.5
1
1.5
2
2.5
3
Time [sec]
×10^6

Batch 2

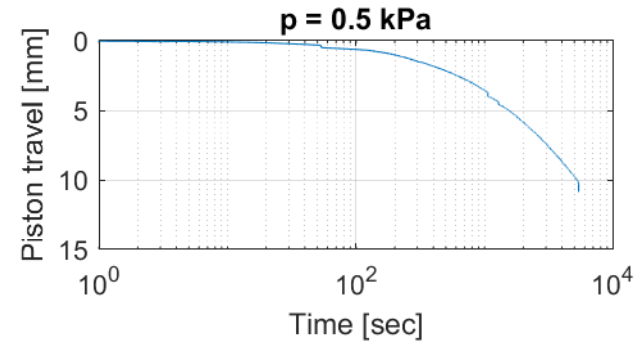
p = 0.5 kPa
Piston travel [mm]
0
5
10
15
10^0
10^2
10^4
Time [sec]

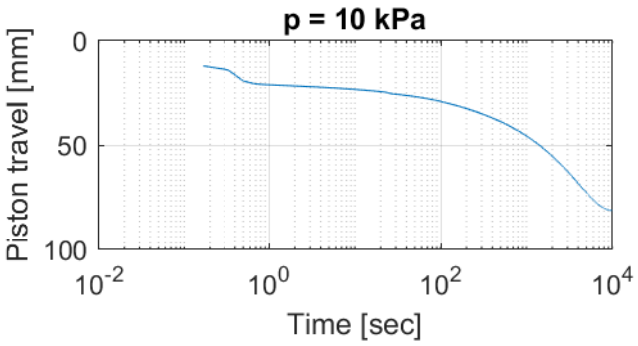
p = 10 kPa
Piston travel [mm]
0
50
100
10^{-2}
10^0
10^2
10^4
Time [sec]

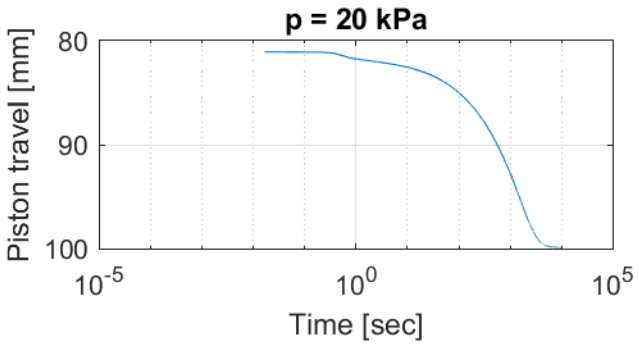
p = 20 kPa
Piston travel [mm]
80
90
100
10^{-5}
10^0
10^5
Time [sec]

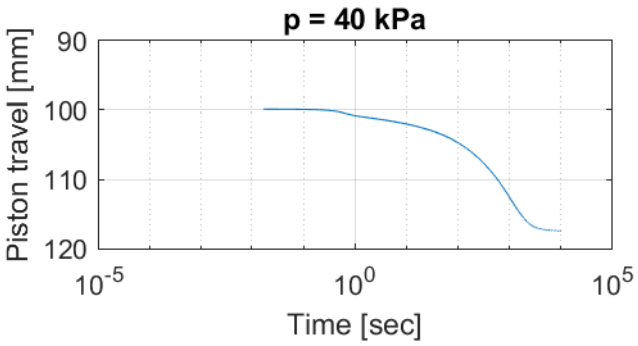
p = 40 kPa
Piston travel [mm]
90
100
110
120
10^{-5}
10^0
10^5
Time [sec]

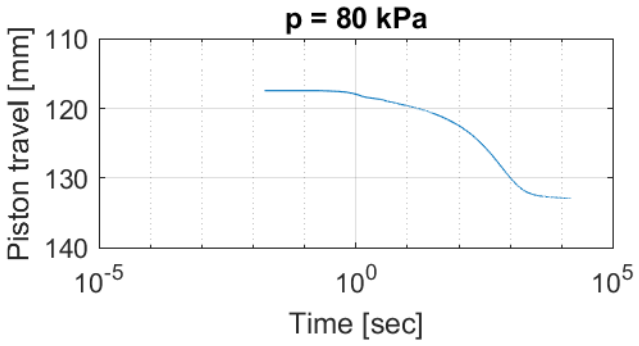
p = 80 kPa
Piston travel [mm]
110
120
130
140
10^{-5}
10^0
10^5
Time [sec]

Batch 2

Appendix G

P-y apparatus

Specifications and detailed figures of the p-y device are given in this appendix.

Figures G.1 and G.2 show the different parts of the device. The soil specimen is situated in the soil chamber, which is held in place by the fastening block in front and the end supports by the specimen's ends. During installation of the steel rod, the end supports and bar clamps are fixed. Before consolidation can begin, the reaction support for consolidation is installed at the right hand side and fixed. Consolidation pressure is applied by the air pressure piston. The bar clamps and right end support are unlocked during consolidation to allow the specimen to deform.

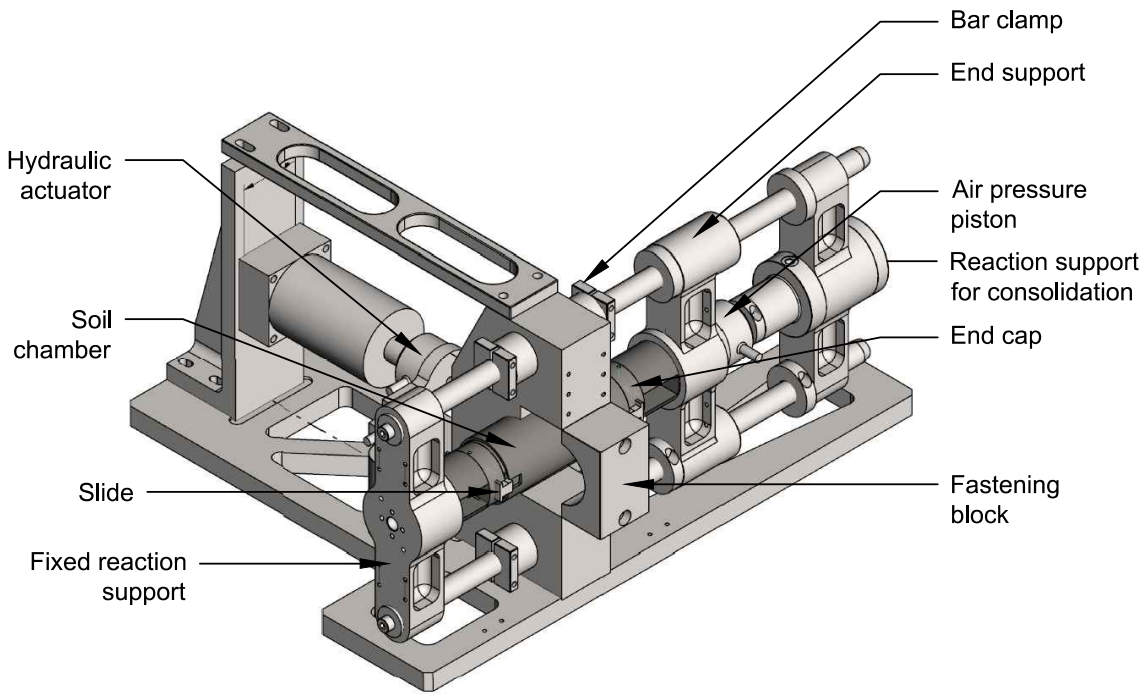

Figure G.1: P-y apparatus

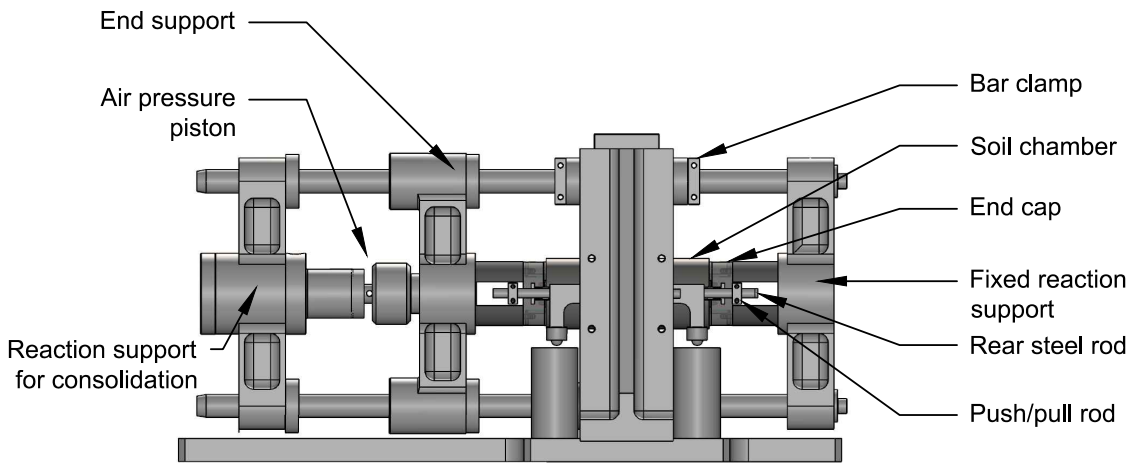

Figure G.2: Back view of the p-y apparatus

After consolidation, the bar clamps and end supports are fixed and the consolidation piston removed. Cyclic loading is applied to the specimen by the hydraulic actuator through the two push/pull rods. The model pile is held parallell to the rear steel rod attached to the load actuator, as shown in Figure G.3. Cyclic loading is applied under constant soil height. Slides in the end caps make lateral movement possible. Figure G.4 shows the details of the soil sample parts.

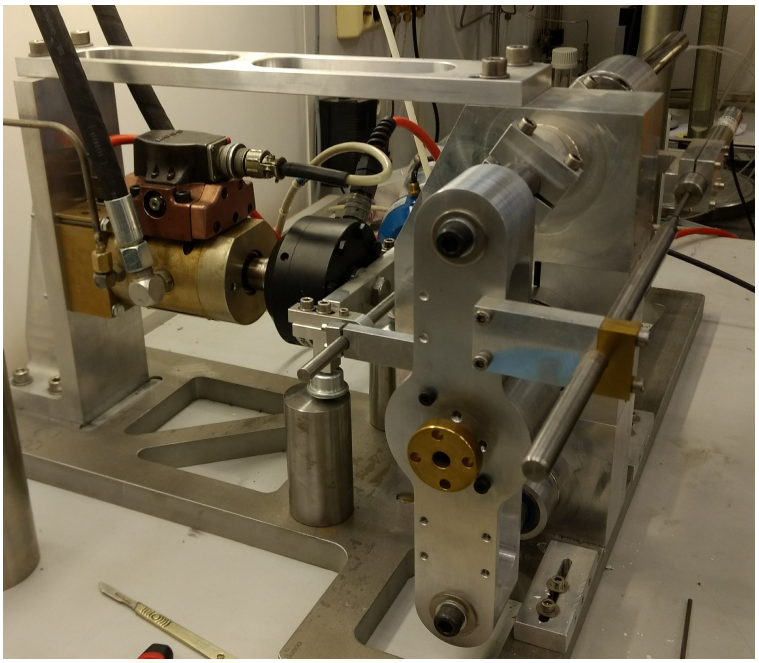

Figure G.3: Side view of the p-y apparatus

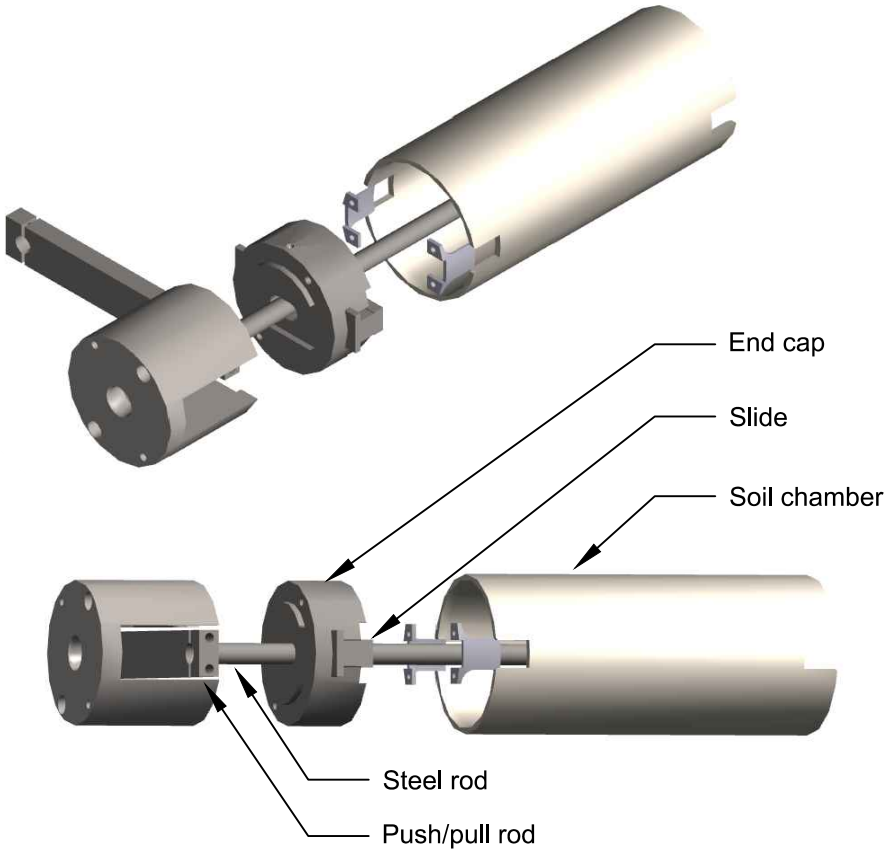

Figure G.4: Exploded view of sample parts

The device without the soil chamber installed is shown in Figures G.5 and G.6. In Figure G.5 the two available soil chambers with corresponding steel rods are placed left to the device. In this study, only the chamber of height 100 mm have been used.

Specifications

Specifications of the apparatus is provided in the report by Zakeri et al. (2017).

Consolidation frame

- Constant stress applied to the specimen by the air pressure piston
- Applies pressures up to 800 kPa
- All tests in this study have been loaded under constant soil height, but loading under constant pressure is possible

Soil chamber

- Cylindrical tube

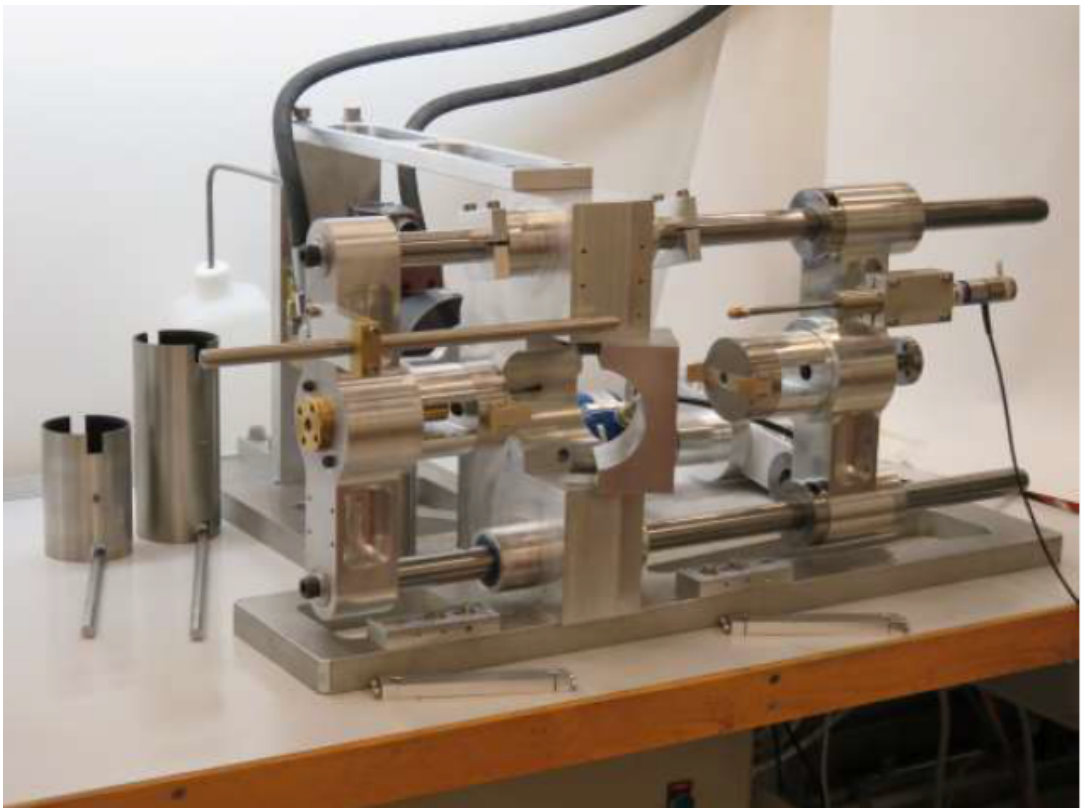

Figure G.5: P-y apparatus (NGI, 2018)

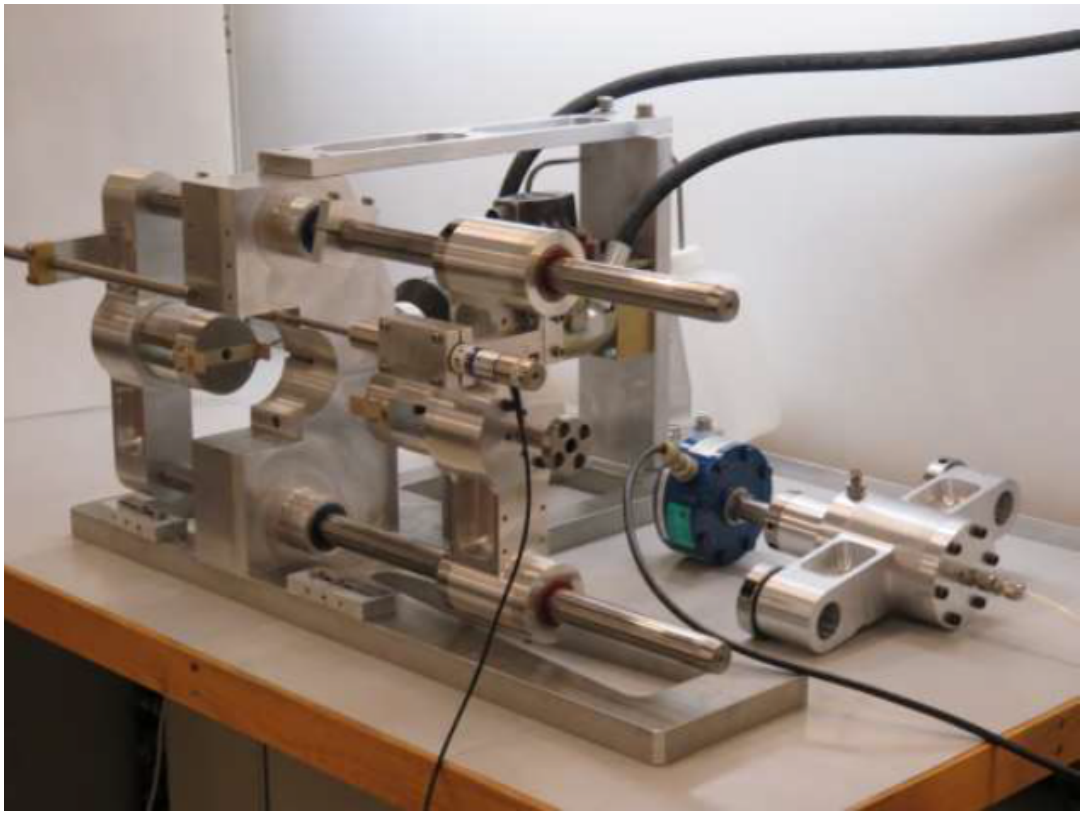

Figure G.6: P-y apparatus (NGI, 2018)

- Inner diameter: 68 mm
- Height of soil chamber: 100 mm
- Diameter steel rod: 10 mm

MTS and hydraulic actuator

- Displacement range from +/- 0.001 to 4 mm
- Frequencies vary from 0.01 to 4 Hz
- Control modes: displacement and force
- Multiple loading events can be applied, such as cyclic loading with different waveforms (sinusoidal/ramp/square), irregular load histories, constant displacement or load, or monotonic tests.

Limitations of the device:

- The device can only be used for clay specimens, but can be adjusted for sand if required.
- The apparatus does not have back pressure.
- The apparatus does not have sealing.
- Pore pressure is not measured during testing.
- The device is suited for samples with soil strength less than 100 kPa.